Investigating the role of the cardiac apelin receptor using human embryonic stem cell derived-cardiomyocytes.

by

Robyn Grace Campbell Macrae

St Catharine's College

Experimental Medicine and Immunotherapeutics/Wellcome-MRC Cambridge Stem Cell Institute

Research Supervisors: Professor Anthony P. Davenport and Professor Sanjay Sinha

December 2021

This thesis is submitted for the degree of

Doctor of Philosophy

Declaration

This thesis is the result of my own work and includes nothing which is the outcome of work done in collaboration except as declared in the Preface and specified in the text.

I further state that no substantial part of my thesis has already been submitted, or, is being concurrently submitted for any such degree, diploma or other qualification at the University of Cambridge or any other University or similar institution except as declared in the Preface and specified in the text.

The length of this thesis does not exceed the prescribed word limit for the Clinical Medicine and Clinical Veterinary Medicine Degree Committee (60,000 words).

Robyn G.C. Macrae

Investigating the role of the cardiac apelin receptor using human embryonic stem cell derived-cardiomyocytes.

Robyn G.C. Macrae

Abstract

The G-protein coupled apelin receptor and its two endogenous peptide ligands, apelin and Elabela, have emerged as key regulators of cardiovascular development, physiology and disease. It has therefore been suggested that targeting the apelin receptor therapeutically may be beneficial for the treatment of a range of cardiovascular pathophysiologies. Despite this, there is a lack of a suitable human based *in vitro* system to investigate the cardiac apelin receptor. Human embryonic stem cells (hESCs) represent a powerful tool for modelling as they are amenable to genetic editing and can be induced to differentiate to any cell type. This study aimed to use hESC-derived cardiomyocytes to examine the role of the apelin receptor in cardiomyocyte development and function.

For the first time, hESC-derived cardiomyocytes were found to express the apelin receptor at similar levels to human hearts, indicating suitability for use as a model for investigating the apelin receptor. A novel apelin receptor inducible knockdown system was generated in hESCs. Inducing apelin receptor knockdown throughout differentiation reduced cardiomyocyte differentiation efficiency, and had functional consequences, including disrupted beating pattern and prolonged voltage sensing. Moreover, apelin receptor knockdown in differentiated cardiomyocytes, combined into 3D engineered heart tissues had detrimental effects on contractility, with decreased force generation and increased stiffness observed, accompanied by an increase in collagen deposition. An apelin receptor variant identified from the NIHR BioResource BRIDGE project and previously shown to affect ligand binding was also introduced into hESCs. Again, detrimental effects on hESC-derived cardiomyocyte differentiation and function were observed, similar to that seen with apelin receptor knockdown.

This thesis has characterised the expression of the apelin receptor in hESC-derived cardiomyocytes, and utilised genetic engineering to manipulate apelin receptor expression, identifying a key role for the apelin receptor in hESC-derived

cardiomyocyte differentiation and function. This recapitulates what has previously been shown in animal models but in a more clinically relevant model, and offers a potential platform for further characterisation of apelin receptor function. It also offers a system for screening of novel pharmacological compounds for the treatment of heart failure and other cardiovascular diseases.

For Grandad.

Table of Contents

Acknowledgements

Firstly, my sincerest thanks to Professor Anthony Davenport and Professor Sanjay Sinha for giving me the opportunity to undertake my PhD in their research groups. It has been a brilliant experience, and I am so grateful for their continued time, support and intellectual input.

My thanks to the British Heart Foundation for funding my PhD research. I am very grateful, and I am proud to have represented such an important charity.

Being part of both the Davenport and Sinha research groups over the past few years has been a pleasure – I have learnt so much and have had the privilege of working with fantastic people. I send my thanks to all members and collaborators (past and present) of both groups, and in particular thank the following people: my day-to-day supervisor Dr Maria Colzani for her continued support and encouragement, and for being the font of knowledge for all things cardiomyocyte. I have learnt so much from her, and have thoroughly enjoyed spending time working alongside her. I thank Dr Janet Maguire for her constant support, advice and kindness, coupled with her ability to solve any problem you might have and her quick wit and brilliant sense of humour. I would also like to thank Mrs Rhoda Kuc for all her help and for teaching me various techniques over the years. Aside from the science, I have always enjoyed our Bake Off and Strictly chats, and I will always remember the delicious birthday cakes she made for us all! My sincerest thanks to Mr Semih Bayraktar for his help with MATLAB, without whom I would still be analysing my data now! I would also like to thank Dr Laure Gambardella for her positivity, support and input throughout the entirety of my PhD. I also thank her for her brilliant fitness classes through lockdown, which were so important to me during a difficult time.

All members of both groups have been so supportive and I thank them all for their valuable insights and helpful feedback. I would like to thank my fellow students in both groups for their help and friendship over the years, and I wish them all the best for the future. Particular thanks to Tom Williams for his knowledge and assistance with imaging techniques. He has been the most brilliant friend throughout my PhD, and I will greatly miss our long experimental days and the laughs we had together.

Thanks also go to Dr Emma Davenport and Dr Emma Robinson, for their assistance and expertise with RNA sequencing; the NIHR Phenotyping Hub, for their flow cytometry support; and Darren Clements and Peter Humphreys, for their imaging advice.

I am extremely grateful to my fellow countryman Dr William Bernard for his constant support, encouragement and advice throughout. Despite leaving the Sinha group at the end of my first year, he has always been available to help and I am thankful for his continued expertise and technical guidance on genetic engineering. I also thank him for helping me find a Scottish contingent with which to watch the rugby and complain about missing hills and empire biscuits!

Thanks also to my fellow British Heart Foundation PhD students, Jen, Matt and Anna, affectionately known as the Lunch Laddies, for their friendship and support over the years. I am so grateful for the many friends I have made through St Catharine's College MCR, whom I have shared many great times with and hope to keep in touch with for years to come – Laura, Soph, Stephen, Putu, Casper, Fynn and Toby to name but a few. Thank you for all the laughs.

My time at Cambridge has allowed me to meet some of the most wonderful people through the equestrian community, giving me the chance to escape the Cambridge bubble. To Kate and Aeisha, my brilliant fellow polo team members, I will be forever grateful for your love and support through both the amazing times and the challenging times. To Francis, my friend and polo coach, I am so thankful for all that you have done for me. I also thank Kerry, Steph, Louis, Tim, Jo and all the Dean and Dean/Gally's Farm polo teams for being like a family to me – our summers spent out on the polo grounds have provided welcome relief from the daily grind and I will always look back on this time fondly. I am also so grateful to all at CUDH, for providing me with the most incredibly riding opportunities, and for their kindness and support. Particular thanks to Cathy, for allowing me to ride her wonderful horses, which has been so important for me.

To my college sister, Jen, thank you for always being there. Thank you for your support, friendship and love, and for all the laughter we have shared. Our Toast to the Laddies will never be replicated! A huge thank you also to Dan, for his helpfulness, friendship and for always keeping us well fed!

I am, of course, extremely grateful to my family and friends at home. Thank you to my dear friend Mollie, and all the horse girls for their irrepressible energy and incomparable sense of humour.

I would particularly like to thank my lovely boyfriend Alex, who has been a source of constant support and kindness – thank you for always believing in me.

Finally, I thank my parents for their unwavering support and encouragement and for all that they have done for me – without them I would not be here and I hope I have made them proud.

Publications

Macrae R.G.C, Colzani M.T, Williams T.L., Bayraktar S, Kuc R.E., A.L. Pullinger, Bernard W.G., Robinson E.L., Maguire J.J., Sinha S. and Davenport A.P. Knockdown of apelin receptor reduces cardiomyocyte differentiation efficiency and contractility of human embryonic stem cell-derived cardiomyocytes. ***In Submission.***

Davaapil H., McNamara M., Granata A., **Macrae R.G.C.**, Hirano M., Smith D.M., Bhattacharya S. & Sinha S. A phenotypic screen of Marfan syndrome iPSC-derived VSMCs uncovers GSK3β as a new target. ***In Submission.***

Williams, T.L., Strachan G., **Macrae R.G.C.**, Kuc R.E, Nyimanu D., Paterson A.L., Sinha S., Maguire J.J. and Davenport A.P. (2021). Differential expression in humans of the viral entry receptor ACE2 compared with the short deltaACE2 isoform lacking SARS-CoV-2 binding sites. *Scientific Reports* 11(1), 24336.

Williams T.L., Colzani M.T., **Macrae R.G.C**, Robinson E.L., Bloor S., Greenwood E.J.D, Zhan R.U., Strachan G., Kuc R.E., Nyimanu D., Maguire J.J., Lehner P.J, Sinha S. and Davenport A.P (2021). Human embryonic stem cell-derived cardiomyocytes express SARS-CoV-2 host entry proteins: screen to identify inhibitors of infection. *Communications Biology* 4, 926.

Read C., Nyimanu D., Williams T.L., Huggins D.J., Sulentic P., **Macrae R.G.C**, Yang P., Glen R.C., Maguire J.J. and Davenport A.P. (2019). International Union of Basic and Clinical Pharmacology. CVII. Structure and Pharmacology of the Apelin Receptor with a Recommendation that Elabela/Toddler Is a Second Endogenous Peptide Ligand. *Pharmacological Reviews* 71(4): 467-502.

Presentations

Investigating the critical role of the cardiac apelin receptor for contractility in hESC-derived cardiomyocytes using a novel inducible knockdown system.

Oral Communication, British Pharmacological Society (BPS) Pharmacology 2021, *online.*

Oral Communication, British Heart Foundation (BHF) Centre for Excellence Research Symposium 2021, *online.*

Oral Communication, BHF Student Symposium 2021, *online*. **Runner up prize** for best oral communication.

Flash Talk, British Atherosclerosis Society/British Society for Cardiovascular Research (BSCR/BAS) Joint Spring Meeting 2021, *online*.

Angiotensin-converting enzyme 2 (ACE2) is rate-limiting for severe acute respiratory syndrome coronavirus 2 (SARS-CoV-2) viral infection in beating stem cell-derived cardiomyocytes.

Poster, American Heart Association Scientific Sessions 2021, *online.*

Novel strategy using hESC-derived cardiomyocytes to explore the critical importance of the apelin receptor in the cardiovascular system.

Poster, BPS Pharmacology 2020, *online.*

Development and characterisation of tools to pharmacologically characterise the apelin receptor in cardiovascular development and physiology.

Oral Communication, BPS Pharmacology 2019, *Edinburgh, UK.*

Generation of a novel inducible knockdown system to characterise the role of the apelin receptor in human embryonic stem cell derived-cardiomyocytes.

Poster, British Society for Cardiovascular Research (BSCR) Autumn Meeting 2019, *Cambridge, UK.* **Runner up prize** for best poster.

Poster, Cambridge Stem Cell Institute Annual PhD Symposium 2019, *Cambridge, UK.*

Characterisation of the apelin receptor protein from beating human embryonic stem cell derived cardiomyocytes.

Poster, BSCR/BAS Joint Spring Meeting 2019, *Manchester, UK*.

Poster, BHF Student Symposium 2019, *London, UK.*

Poster, The Physiological Society, Biochemical Society and British Pharmacological Society Life Sciences 2019: Post-Translational Modifications and Cell Signalling Meeting, *Nottingham, UK.*

Poster, Milner Therapeutics Symposium 2019, *Cambridge, UK*.

Characterising the apelin/Elabela signalling pathway in human embryonic stem cell derived cardiomyocytes, endothelial and smooth muscle cells.

Poster, BPS 7th Focused Meeting on Cell Signalling 2018, *Nottingham, UK.*

Poster, Department of Medicine Research Day 2018, *Cambridge*, *UK.*

Training Record

Lab Training

Mar 2021	Extracting Biological Information from Gene Lists Course
June 2020	BRC Phenotyping Hub Flow Cytometry Induction and Training
May 2020	Analysis of Bulk RNA-seq Data Course
May 2020	Medicine: The 'Big Four' Databases For Your Literature Search
Dec 2018	An Introduction to Solving Biological Problems with R
Nov 2018	Department of Medicine: Using Containment Facilities and Microbiological Safety Cabinets
Nov 2018	Chemical Safety Course
Nov 2018	CRUK: Image Analysis with Fiji
Oct 2018	Laboratory for Regenerative Medicine Confocal Microscopy (LSM 700) Training

GSLS Core Skills Training Programme (CSTP) + Advanced Skills Training Programme (ASTP)

July 2019	ASTP The Art of Negotiation and Influence
May 2019	ASTP Making the Most of Conferences Course
Feb 2018	CSTP Writing an Academic Report Course
Dec 2017	CSTP Introduction to Scientific Writing
Nov 2017	CSTP Presentation and Performance Toolkit
Nov 2017	ASTP Planning and Managing a Research Project
Nov 2017	CSTP Time Management Toolkit

Oct 2017	CSTP Development Plan
Oct 2017	CSTP Skills Analysis Survey

Other

Dec 2020-Mar 2021	Judge Business School EnterpriseTECH Postgraduate programme for scientific entrepreneurship
Aug 2020	RD Live: Career planning post-COVID
April 2020	Understanding Unconscious Bias
April 2020	Minute Taking: An Introduction Online
Nov 2019	Judge Business School Wo+Men's Leadership Centre Women in Tech Challenge 2019
Oct 2019	Effective Undergraduate Supervision (Life Sciences)
Mar 2019	Equality & Diversity Essentials
Oct 2018	Anti-Bribery & Corruption Training

Outreach

April-Sep 2020	Volunteer for 'I'm a Scientist, Stay at Home!' scheme
Mar 2019	Volunteer at Cambridge Cardiovascular 'The Heart: a Sensational Phenomenon' Stand at Cambridge Science Festival
Jun 2018	Registered BHF Volunteer (ongoing)
May 2018	Organiser for Pint of Science Cambridge
Mar 2018	Volunteer at Cambridge Cardiovascular 'The Heart: a Sensational Phenomenon' Stand at Cambridge Science Festival

Abbreviations

2D, Two dimensional

3D, Three dimensional

ACE2, Angiotensin converting enzyme 2

ACh, Acetylcholine

ALS, Amyotrophic lateral sclerosis

AngII, Angiotensin II

APELA, Gene encoding Elabela Apelin Receptor Early Endogenous Ligand

APLN, Gene encoding apelin

APLNR, Gene encoding apelin receptor

APLNR KD, Apelin receptor gene knockdown

AT1, Angiotensin II receptor type 1

ATP, Adenosine triphosphate

B2M, β2 microglobulin

B_{Max}, Receptor density

BMP, Bone morphogenetic protein

bp, Base pair

BSA, Bovine serum albumin

cAMP, Cyclic adenosine monophosphate

CBE, Cytosine base editor

CDM-BSA, Complete defined medium with bovine serum albumin

cDNA, Complementary DNA

CHO, Chinese hamster ovary

CICR, Calcium induced calcium release

CRISPR, Clustered Regularly Interspaced Short Palindromic Repeats

CT, Cycle threshold

DAG, Diacylglycerol

DCM, Dilated cardiomyopathy

DEG, Differentially expressed gene

DMD, Duchenne Muscular Dystrophy

DSB, Double stranded break

DTT, Dithiothreitol

E8, Essential 8

Early KD, Apelin receptor knockdown throughout cardiomyocyte differentiation

ECG, Electrocardiogram

EDTA, Ethylenediaminetetraacetic acid

eGFP, Enhanced Green Fluorescent Protein

EHT, Engineered heart tissue

EIA, Enzyme immunoassay

ELA, Elabela/Toddler

ELISA, Enzyme-linked immunoassay

ER, Endoplasmic reticulum

ERK1/2, Extracellular signal-regulated kinase 1/2

ESC, Embryonic stem cell

EthD-1, Ethidium Homodimer-1

FAK, Focal adhesion kinase

FBS, Foetal bovine serum

FCB, Fixed concentration binding

FDR, False discovery rate

FGF, Fibroblast growth factor

FPD, Field potential duration

GDP, Guanosine diphosphate

GO, Gene ontology

GPCR, G-protein coupled receptor

GRK, G-protein coupled receptor kinase

gRNA, Guide RNA

GTP, Guanosine triphosphate

HAR, Homology arm

HBSS, Hanks' Balanced Salt Solution

HDR, Homology directed repair

HEK, Human embryonic kidney

hESC, Human embryonic stem cell

hESC-CM, Human embryonic stem cell-derived cardiomyocyte

hiPSC, Human induced pluripotent stem cell

hiPSC-CM, Human induced pluripotent stem cell-derived cardiomyocyte

HTS, High throughput screening

iKD, Inducible knockdown

IP_3, Inositol trisphosphate

IP_3R, Inositol trisphosphate receptor

iPSC, Induced pluripotent stem cell

KD, Knockdown

K_D, Receptor affinity

KO, Knockout

KSR, Knockout serum replacer

LAA, L-Ascorbic acid 2-phosphate

Late KD, Apelin receptor knockdown upon completion of cardiomyocyte differentiation

LB, Lysogeny broth

MCT, Monocrotaline

MEF2, Myocyte enhancer factor 2

MLCK, Myosin light chain kinase

mRNA, Messenger RNA

MYH6, Myosin heavy chain 6

MYL7, Myosin light chain 7

NCX, Sodium calcium exchanger

NGS, Next generation sequencing

NHE, Sodium hydrogen exchanger

NHEJ, Non-homologous end joining

NHS, National Health Service

NIHR, National Institute for Health Research

NO, Nitric oxide

NSB, Non-specific binding

OCT, Optimal cutting temperature

pA, Polyadenylation signal

PAH, Pulmonary arterial hypertension

PAI-1, Plasminogen activator inhibitor-1

PAM, Protospacer adjacent motif

PBE, Phosphate buffered saline with bovine serum albumin and EDTA

PBS, Phosphate buffered saline

PBS/T, Phosphate buffered saline with Tween

PCR, Polymerase chain reaction

PD, Parkinson's Disease

PDGF, Platelet derived growth factor

PDMS, Polydimethylsiloxane

PFA, Paraformaldehyde

PIP_2, Phosphatidylinositol 4,5-bisphosphate

PKA, Protein kinase A

PKC, Protein kinase C

PLCβ, Phospholipase C β

pre-miRNA, Precursor microRNA

PSC, Pluripotent stem cell

PSC-CM, Pluripotent stem cell-derived cardiomyocyte

Puro, Puromycin

qRT-PCR, Quantitative real time polymerase chain reaction

R168H, Apelin receptor variant with arginine 168 exchanged for histidine

RIN^e, RNA integrity numbers

RISC, RNA silencing complex

RLC, Myosin II regulatory light chain

RNA-Seq, RNA sequencing

ROCKi, Rho-associated protein kinase inhibitor

RPM, Reads per million

rRNA, Ribosomal RNA

RT, Room temperature

RyR, Ryanodine receptor

SA, Splice acceptor

SA-HRP, Streptavidin-horseradish peroxidase

SDS, Sodium dodecyl sulphate

SERCA2A, Cardiac sarcoplasmic reticulum Ca^{2+}-ATPase 2A

shAPLNR, Short hairpin RNA targeting the apelin receptor gene

shB2M, Short hairpin RNA targeting the β2 microglobulin gene

SHIM, Second-harmonic imaging microscopy

shRNA, Short hairpin RNA

siAPLNR, Short interfering RNA targeting the apelin receptor gene

siRNA, Short interfering RNA

sOPTiKD, Single step optimised inducible knockdown

T2A, Self-cleaving T2A peptide

T90, Time to 90% decay

TALENs, Transcription activator-like effector nucleases

Tet, Tetracycline

tetR, Tetracycline-controlled repressor

TGF, Transforming growth factor

TnT, Troponin T

TO, Tet operon

TRC, The RNA Consortium

TTP, Time to peak

UMI, Unique molecular identifier

WGS, whole genome sequencing

WT, Wild-type

XGR, eXploring Genomic Relations

List of Figures and Tables

1. Introduction

2. Methods

3. Study of the Apelin Receptor in hESC-Derived Cardiomyocytes

4. Generation of an shRNA Inducible Apelin Receptor Knockdown System

5. Effect of Apelin Receptor Knockdown throughout hESC-Derived Cardiomyocyte Differentiation

6. Effect of Apelin Receptor Knockdown in hESC-Derived Cardiomyocytes

7. Generation of hESCs Carrying Apelin Receptor Genetic Variants and Effect of Apelin Receptor Genetic Variants in hESC-Derived Cardiomyocytes

1. Introduction

1.1 Background

In recent years, the apelinergic system has emerged as a key regulator of cardiovascular development, physiology and disease. The apelin receptor is a class A G-protein coupled receptor (GPCR), with the characteristic seven transmembrane domain structure (Pitkin *et al.*, 2010). Originally identified in 1993 (O'Dowd *et al.*, 1993), the apelin receptor remained an orphan receptor, until the identification of its cognate peptide ligand, apelin, which was isolated from bovine stomach extracts several years later (Tatemoto *et al.*, 1998). Since then, a second peptide ligand for the apelin receptor was identified from loss of function studies in zebrafish, known as Elabela/Toddler (referred to as ELA subsequently) (Chng *et al.*, 2013; Pauli *et al.*, 2014). The apelin receptor is expressed throughout the body, both centrally and peripherally (Medhurst *et al.*, 2003), but importantly expression is seen throughout the cardiovascular system, including in cardiomyocytes (Kleinz *et al.*, 2005). Correspondingly, expression of both peptides is found throughout the body (Kleinz and Davenport, 2004), with the ligands shown to act in an autocrine, paracrine and endocrine manner depending on the environment. Although the apelinergic system is expressed widely, this project has focussed on the role of the apelin receptor in the cardiovascular system, particularly in cardiomyocytes.

Activation of the apelin receptor has an important role in cardiovascular development, evidenced by the high embryonic lethality of apelin receptor knockout (KO) mice (Kang *et al.*, 2013). Furthermore, apelin receptor signalling in adult physiology has beneficial vasodilatory and positive inotropic effects (Pitkin *et al.*, 2010). In a number of cardiovascular pathologies, including heart failure, expression of apelin and ELA are reduced, with exogenous application of the ligands found to improve disease state (P. Yang *et al.*, 2015; Read *et al.*, 2019). Hence, targeting the apelin receptor has been proposed as a novel therapeutic strategy for the treatment of a range of cardiovascular conditions.

Despite the accumulating evidence for a key role of the apelin receptor in cardiovascular development and disease, thus far a suitable *in vitro* human model for investigating the role and mechanism of action of the apelin system in cardiomyocytes

has not been utilised. By inducing differentiation to cell types of interest, using human pluripotent stem cells (PSCs) for studying human development and disease is a powerful tool, which has become increasingly common in recent years (Avior *et al.*, 2016). However, PSCs have not yet been employed for the study of the apelin signalling system. In this project, human embryonic stem cell-derived cardiomyocytes (hESC-CMs) in combination with genetic and pharmacological manipulation were used to investigate the role of the apelin receptor in cardiomyocyte development and function.

In this introduction, I will discuss the isolation of PSCs, and how these have been utilised previously for the study of disease and development, as well as for drug screening. I will also introduce the key concepts relating to PSC-CMs, and explore the previous applications of this cell type. I will then discuss the apelinergic signalling system, including some of the identified roles of the apelin receptor in cardiovascular development, physiology and pathophysiology. I will also briefly discuss the therapeutic potential of targeting the apelin receptor pharmacologically. Finally, I will present the use of whole genome sequencing (WGS) in subjects with rare diseases to identify potential disease associated apelin receptor genetic variants.

1.2 Introduction to Stem Cells

1.2.1 Isolation of pluripotent stem cells

Stem cells are unspecialised cells which can self-renew indefinitely, and also have the unique ability to give rise to other cell types by a process of differentiation. Importantly, stem cells are found in both the embryo and the adult, with adult cells typically having a reduced differentiation potential (Zakrzewski *et al.*, 2019). Stem cells can be classified based on their potency (Figure 1.1). PSCs are capable of differentiating to all three germ layers of the embryo and therefore can give rise to any cell of the adult organism, while multipotent or unipotent stem cells are more restricted in their differentiation potential, only giving rise to cells of particular lineages *(*Singh *et al*., 2016). For example, haematopoietic stem cells of the bone marrow are multipotent and capable of giving rise to all cellular blood components which is essential for maintaining haematopoietic homeostasis (Pinho and Frenette, 2019).

In 1981, Evans and Kaufman demonstrated the first isolation and successful culture of PSCs directly from early preimplantation mouse embryos. When cultured in the absence of feeder cells, the isolated cells formed embryoid bodies and differentiated into complex tissues, and upon injection into mice formed teratocarcinomas, confirming pluripotency (M. J. Evans and Kaufman, 1981). In 1998, cells from the inner cell mass of human blastocysts capable of long term undifferentiated self-renewal and with the ability to differentiate to all three embryonic germ layers were isolated, and defined as human embryonic stem cells (hESCs) (Thomson *et al.*, 1998). The field was further progressed with the generation of induced pluripotent stem cells (iPSCs) from adult dermal fibroblasts. Here, a cocktail of four factors was introduced to fibroblasts, inducing reprogramming to produce cells with characteristics similar to hESCs, including the ability to differentiate to the three germ layers and the formation of teratocarcinomas upon *in vivo* injection (Takahashi *et al.*, 2007). The advent of this technology has facilitated the generation of patient and disease specific pluripotent cells. Together, the isolation of hESCs and hiPSCs has revolutionised the study of human development and has also provided a platform for progressing the study of human disease and therapeutics.

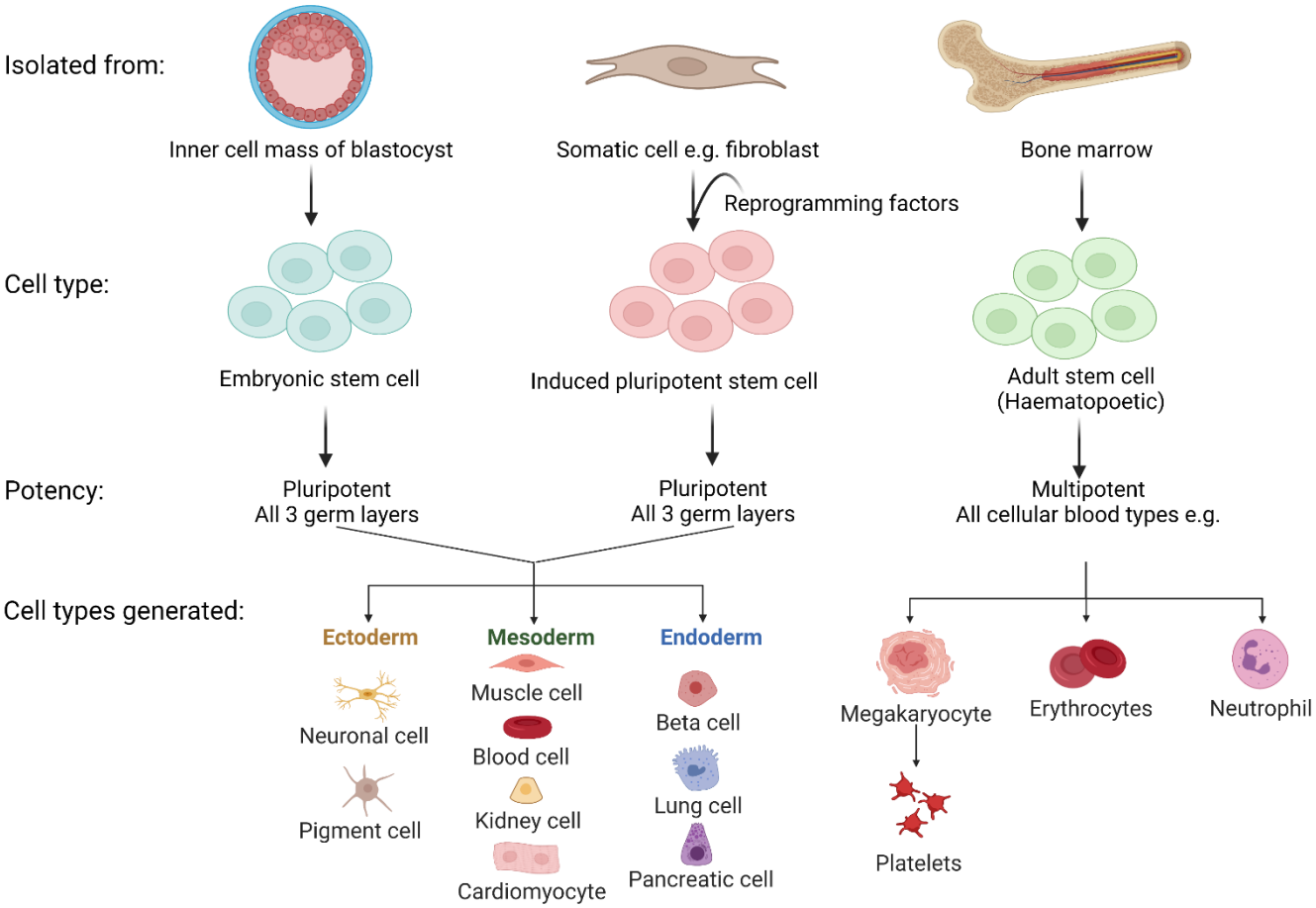

Figure 1.1: Types of stem cells, where they are isolated from and their differentiation potential. Created using Biorender.com.

1.2.2 Pluripotent stem cells for disease modelling

In recent years, there has been a dramatic increase in the use of human PSCs as platforms for modelling disease. Animal models have been essential for improving understanding of a large range of human physiology and pathophysiology, however there are a number of issues associated with using a non-human model, due to inherent physiological differences, often leading to untranslatable results (Sterneckert *et al.*, 2014). For example, when using a mouse model to study human cardiovascular disease, the large difference in the size of the human heart compared to mouse heart must be considered. Additionally, the heart of a mouse beats at an average rate of 500 beats per minute compared to a rate between 60 to 100 beats per minute in humans (Paik *et al.*, 2020), suggesting a mouse model would be unsuitable to study cardiac arrhythmias.

Mammalian genomes are highly conserved and the generation of KO mice have been invaluable in elucidating human gene function. However, it has been found that in mice, over 20% of human essential genes have nonessential orthologs (Liao and Zhang, 2008), and mutation or loss of the same gene can have differing effects. An extreme example of this is seen in Bloom's syndrome, where in humans mutation of the *BLM* gene causes dwarfism, immune deficiency and increased cancer risk, while mutation of the same gene in mice is embryonically lethal (Chester *et al.*, 1998). Furthermore, due to many years of inbreeding to generate well characterised lines, animal models have extremely similar genetic identity, in contrast to the huge genetic variation that exists within the human population (Libby, 2015). It is thought that genetic background has a large influence on disease manifestation and outcome. Additionally, animal models of disease often fail to incorporate complications induced by associated co-morbidities seen in humans (Libby, 2015). For instance, a patient with cardiovascular disease will often have associated conditions affecting disease progression such as diabetes mellitus or pulmonary disease (Buddeke *et al.*, 2019). Moreover, the methods used to generate animal models of disease may not replicate all components of the human condition. A mouse model of heart failure induced by surgical intervention is unlikely to have the associated chronic pressure overload or atherosclerosis seen in human patients (Riehle and Bauersachs, 2019), hence the mouse model is likely to respond better to therapeutic intervention. Pulmonary arterial hypertension (PAH) is an example of a complex condition in which a number of the animal models commonly used (e.g. monocrotaline treatment) do not fully recapitulate the condition (Maarman *et al.*, 2013). In PAH, remodelling of the pulmonary vasculature occurs, associated with high pulmonary pressures which develop over many years. In contrast, PAH is induced in animals over a period of a few weeks, hence it is difficult to generate the same level of disease severity (Das *et al.*, 2012). Furthermore, another indication that disease severity in animal models does not correlate with that seen in humans is that in animal models a range of treatments have been shown to improve PAH disease symptoms, which is not recapitulated in human patients (Maarman *et al.*, 2013). Because of the lack of appropriate models, a wide range of human conditions remain poorly understood, making it difficult to develop novel, effective therapeutic options.

Primary cells isolated from human donors can also be used as *in vitro* models. Although these are more likely to represent human physiology, access to samples is limited and they have only a limited lifespan in culture (Avior *et al.*, 2016). Immortalised cell lines present another option but their properties are altered, meaning they often do not function like native cells (Maqsood *et al.*, 2013). Hence, the use of PSCs induced to differentiate to cell types of interest for human disease modelling is increasing. PSCs have the advantages of a potentially unlimited lifespan in culture, many protocols existing to induce differentiation to any cell type of interest and the results generated are from a human background (Moradi *et al.*, 2019). Furthermore, by differentiating to multiple cell types and carrying out co-culture experiments, the influence of cellular interactions on physiology and pathophysiology can be interrogated (Bargehr *et al.*, 2019; Calejo *et al.*, 2020).

Crucially, PSCs are amenable to genetic editing (Avior *et al.*, 2016). The ability to measure the impact of the mutation of a single gene is a powerful technique to identify its contribution to pathology (Sterneckert *et al.*, 2014). It is possible to investigate gene or protein function within a cell type of interest, by utilising protocols to generate genetic knockout, knockdown or over expression systems (Bertero *et al.*, 2016; Ma *et al.*, 2018). Additionally, a range of methods are available to introduce specific genetic variants or mutations associated with disease into PSCs, for example using CRISPR/Cas9 based technology, before differentiating to a defined cell type and examining phenotypic effects (González *et al.*, 2014; Gupta *et al.*, 2018; Ma *et al.*, 2018; Hsu *et al.*, 2019). Importantly, a number of inducible systems have been developed, allowing manipulation of gene expression at specific time points. This enables investigation in cell types of interest of the role of a gene throughout differentiation (González *et al.*, 2014; Y. Chen *et al.*, 2015; Bertero *et al.*, 2016).

One of the main uses for genetic editing in PSCs is for the generation of isogenic lines with the same genetic background except for the variant being studied, allowing for the isolation of the effects of a mutation of interest (Avior *et al.*, 2016). In hESCs, disease-associated mutations can be introduced and compared with wild-type (WT) cells. The first example of this used hESCs to investigate Lesch-Nyhan syndrome, by introducing a mutation in the disease associated *HPRT1* gene and subsequently investigating its molecular effects (Urbach *et al.*, 2004). A further study successfully used TALEN-mediated genome editing to generate hESC lines carrying one of 15

mutations, identified to be linked to several disorders, including insulin resistance and motor neuron death, and found that the differentiated cells displayed independent disease linked phenotypes (Ding *et al.*, 2013). Similarly, hiPSCs derived from healthy donors can be used to introduce disease-causing mutations. Together, this demonstrates the potential of PSC genetic editing for the study of rare conditions, or for investigating genes for which the function in a cell type of interest is unknown.

Additionally, genetic engineering can be used to correct mutations in hiPSCs derived from patients, with the potential for use in cell therapy (Sterneckert *et al.*, 2014). This technique has been applied successfully in a range of conditions. The severe muscle wasting disease Duchenne Muscular Dystrophy (DMD) is caused by loss of function mutations in the dystrophin gene. CRISPR/Cas9 technology was used to successfully correct a mutation in DMD patient-derived iPSCs, which were then differentiated to skeletal muscle cells with restored dystrophin protein levels, which could potentially be transplanted back into the patient (H. L. Li *et al.*, 2015). Furthermore, CRISPR/Cas9 technology has been used to correct iPSCs derived from patients carrying mutations causing sickle cell diseases using a high efficiency adenoviral delivery system, with no off-target genetic modifications reported (C. Li *et al.*, 2016). It is hoped the corrected iPSCs could be differentiated to haematopoietic stem cells and used for autologous transplantation, meaning the patient would produce normal red blood cells, without risk of immunogenicity or need for immune suppression (C. Li *et al.*, 2016).

Isogenic iPSCs lines can also be used for *in vitro* study as a control line, which can be phenotypically compared to patient-derived cells carrying a mutation of interest thought to contribute to pathology. This offers a powerful tool to elucidate molecular mechanisms of disease pathogenesis. A study comparing an isogenic line created from the genetic manipulation of Parkinson's disease (PD) patient-derived iPSCs carrying a mutation in the *SNCA* gene revealed disruption of the MEF2C-PGC1α pathway contributes to neuronal damage, and also validated this pathway as a potential novel therapeutic target for PD (Ryan *et al.*, 2013). In complex disorders which may have a diverse genetic contribution, by isolating iPSCs from patients and correcting genetic variants at specific loci in turn, the cellular effects of each variant can be extrapolated and combined to gain insight into the condition (Sterneckert *et al.*, 2014). Furthermore, by generating PSCs carrying mutations of interest, by inducing

differentiation to different cell types, cell specific effects can be determined (Avior *et al.*, 2016).

1.2.3 Pluripotent stem cells for modelling development

PSCs can also be used to model human development by studying the molecular mechanisms involved throughout differentiation to cell type of interest. As mentioned above, a wide variety of protocols exist to induce differentiation towards a broad range of cell types, providing a relatively rapid and cost-effective strategy to study human development (Zhu and Huangfu, 2013). In order to induce differentiation, the temporal differentiation cues seen in embryonic development must be mimicked by exposing stem cells to defined concentrations of growth factors, signalling molecules or pharmacological compounds (Nostro *et al.*, 2011; Williams *et al.*, 2012; Burridge *et al.*, 2014). Thereafter, pathways which are involved in the differentiation process can be determined. Furthermore, by utilising inducible knockdown genetic engineering technologies, the stage-specific role of a gene of interest in development can be determined by inducing knockdown at defined time points and measuring effect on differentiation efficiency (Y. Chen *et al.*, 2015; Bertero *et al.*, 2016; M. Wu *et al.*, 2018). In this way, genes with previously unknown roles in development can be identified. Furthermore, genetic manipulation of PSCs can be used to allow modelling of abnormal development, particularly for conditions where gene mutation is embryonically lethal (Zhu and Huangfu, 2013). It is important to note that transgenes for genetic manipulation must be integrated at a genomic safe harbour, such as the *AAVS1* or *ROSA26* loci, in order to ensure expression is possible throughout all stages of differentiation (Smith *et al.*, 2008; Sadelain *et al.*, 2012).

For the use of PSCs in all modelling applications, it is important to consider a number of limitations in terms of their differentiation and development. Firstly, it has been shown that for both hESCs and hiPSCs, different cell lines possess differing abilities to differentiate to specific lineages (Osafune *et al.*, 2008; Hu *et al.*, 2010). When the differentiation potential of 17 different hESC lines was compared, it was found that the expression of standard pluripotency markers was similar in the undifferentiated cells. However, when differentiation was induced using both the embryoid body method and using protocols to induce differentiation to specific cell types, the different hESCs

displayed distinct differentiation propensities and tendencies to differentiate to the three germ layers and subsequent derivatives (Osafune *et al.*, 2008). It has been suggested that the heterogeneity in differentiation propensity is likely due to genetic variation, line derivation, culture conditions and epigenetic memory, particularly for iPSCs which show an increased tendency to differentiate to cell types of their tissue of origin (Zhu and Huangfu, 2013). For example, the chromatin structure of hiPSCs derived from pancreatic islet beta cells was shown to be more open at key beta-cell genes, and the hiPSCs more readily differentiated to beta-cells, compared to isogenic iPSCs derived from different tissues (Bar-Nur *et al.*, 2011). Furthermore, PSC-derived cell cultures can contain a mixture of cell types, including pluripotent cells and differentiation intermediates, as well as other lineages, which may influence results (Zhu and Huangfu, 2013). However, a number of techniques have been developed to isolate specific cell types, including metabolic selection for cardiomyocytes (Tohyama *et al.*, 2013) and enrichment of pancreatic progenitors using identified cell-surface markers (O. G. Kelly *et al.*, 2011). Differentiation efficiency could also be improved by modifications to differentiation protocols and more precisely controlled culture conditions.

In this thesis, strategies have been employed to mitigate these limitations, by performing characterisation of the cardiomyocytes generated from hESCs using a combination of techniques to ensure resultant cells express the standard cardiac markers.

1.2.4 Pluripotent stem cells for drug screening

Human PSC-derived cell types also have huge potential for use in drug development. Not only can they be used to identify novel drug targets and therapeutic compounds, but they can also be used for both safety and toxicology studies, providing more human relevant results (Sterneckert *et al.*, 2014). By generating an *in vitro* model, utilising PSCs carrying a disease-causing mutation differentiated to a cell type of interest, the disease phenotypes to be treated can be identified and drug screening carried out (Avior *et al.*, 2016). Firstly, it is possible to carry out a high-throughput screen (HTS) to identify compounds that can improve disease phenotype. Commonly used animal models such as mice can be used for this method of drug screening,

however there is associated high cost and limited throughput due to difficulty in quantifying improvement in phenotype quickly (Giacomotto and Ségalat, 2010). The first study to utilise iPSCs in a HTS identified five previously approved drugs capable of improving disease phenotype in iPSC-derived hepatocytes isolated from patients with alpha-1 antitrypsin deficiency, a common genetic cause of liver failure (Choi *et al.*, 2013). A limitation of HTS however, is that the assay output must be easily measured and quantified, for example with a fluorescent readout, and a high number of cells are needed which is not suitable when a lengthy differentiation process is necessary or yield of differentiation is low (Avior *et al.*, 2016). For disorders where the disease phenotype is more complex, PSC-based platforms can be used for the candidate drug approach, in which a relatively small number of compounds targeting a specific pathway thought to be involved in disease pathogenesis are screened for efficacy (Jhoti *et al.*, 2013). For example, Barmada *et al.* made use of an *in silico* drug screen to identify two molecules predicted to induce clearance of TDP43 via autophagy, which is thought to be important for the treatment of amyotrophic lateral sclerosis (ALS). The ability of the two identified compounds to reduce neurodegeneration was then tested in iPSC-derived motor neurons and astrocytes (Barmada *et al.*, 2014).

Secondly, PSC-derived cell types can be used for testing drug safety. Unpredicted drug toxicity accounts for many thousands of hospitalisations, with Onakpoya *et al*. (2016) reporting that for the post-market withdrawal of drugs between 1953 and 2013, the most commonly reported adverse reactions were hepatotoxicity (18%), immune-related reactions (17%) and cardiotoxicity (14%) (Onakpoya *et al.*, 2016). Cardiotoxic adverse drug responses are often accredited to unexpected effects on cardiac contractility and electrophysiology, particularly perturbing the QT interval of an electrocardiogram (ECG), inducing life-threatening arrhythmias (Braam *et al.*, 2010; Kraushaar *et al.*, 2012). Drug induced prolonged field potential duration values for hESC-CMs were shown to correlate well with serum drug concentrations with known effects on QT interval in human patients (Braam *et al.*, 2010). Hence, PSCs have been utilised as a model to screen for preclinical cardiotoxicity (Q. Zhao *et al.*, 2017; Kopljar *et al.*, 2018), which is further discussed below. Furthermore, a range of high-throughput and automated assays have been developed using iPSC-derived hepatocytes to test potential therapeutic compounds for effects on standard markers

of hepatotoxicity, such as cell viability and morphology, cytoskeleton integrity and phospholipid accumulation (Sirenko *et al.*, 2014).

A further advantage of using iPSC-based disease models is the ability to investigate genotype-phenotype variability. For a range of human conditions, a 'one treatment cures all' approach is not appropriate, and patients are often subjected to a long trial and error process to find a suitable therapy (Sterneckert *et al.*, 2014). Different patients may respond differently to drugs due to genetic variants modulating the drug's pharmacodynamics or pharmacokinetics. Identification of these variants is known as pharmacogenomics, and it presents an opportunity to revolutionise the way medicines are prescribed, potentially resulting in vastly improved healthcare (Relling and Evans, 2015).

By utilising patient-derived iPSCs prior to drug administration, a large number of potential treatments can be tested in parallel to identify the most effective drug (Avior *et al.*, 2016). For example, for the prevention of adverse cardiovascular events related to atherosclerosis, the current standard of care recommends the use of lipid lowering statins in those assessed to be at moderate to high risk (Stone *et al.*, 2014). However, a recent study found that more than 50% of patients in the general population display sub-optimal lipid lowering, meaning there is significantly increased risk of future cardiovascular disease (Akyea *et al.*, 2019). Investigating the responsiveness of iPSCs carrying specific common genetic signatures would allow patient stratification, meaning administered treatment is likely to have a positive effect (Paik *et al.*, 2020). This could also improve the productivity of the pharmaceutical industry developing therapeutics for complex disorders, by allowing potential novel compounds which show beneficial effects in a subset of patients to proceed to approval, while removing subsets of non-responders within trials (Sterneckert *et al.*, 2014; Hnatiuk *et al.*, 2021).

Furthermore, drug induced toxic effects can manifest in only a small population of patients, leading to market withdrawal (Thiel *et al.*, 2017). iPSC-based models could be used to identify patients who develop side effects such as cardiotoxicity *in vitro* (Sharma *et al.*, 2017), meaning a beneficial, efficacious drug can continue to be used in those patients identified as not being at risk (Liang *et al.*, 2013). For example, Liang *et al.* (2013) generated cardiomyocytes from hiPSCs derived from healthy subjects and patients with various cardiovascular morbidities including long QT syndrome and

familial hypertrophic cardiomyopathy, which were then treated with known cardiotoxic drugs. By comparing action potential duration and frequency of arrhythmia, they found the disease-specific hiPSC-derived cardiomyocytes possessed distinct adverse responses to pharmacological stimulation, contributing to the differences in susceptibility to drug-induced cardiotoxicity seen in the patient population (Liang *et al.*, 2013). Together, it is hoped that these strategies to test patient responsiveness and safety will contribute to the development of precision medicine, providing much improved treatments and outcomes for patients.

1.2.5 Pluripotent stem cells for modelling molecular pathways

Finally, PSC-based models can be used to investigate molecular signalling pathways and the effect of their activation at a cellular level. By interfering with the specific target pathway, for example by knocking down a receptor, the importance of the receptor and its associated signalling pathway to cellular function can be determined (Y. Chen *et al.*, 2015). It can also give novel insight into the signalling cascade induced following activation of a particular pathway, and subsequently the role of the identified signalling pathway components can be interrogated. Furthermore, it can be used to investigate the potential role of the pathway in disease pathogenesis. In this way, PSC models can allow identification of novel targets, and subsequent *in silico* modelling or medicinal chemistry strategies can facilitate rapid development of novel compounds. The novel compounds could then be tested in the PSC model, and resulting effects on overall cell phenotype determined (Sterneckert *et al.*, 2014). For example, siRNA screening could be used to induce knockdown of a range of genes in a PSC-derived cell type to identify molecular components involved in a specific process, or in a PSC-based disease model to determine if using a small molecule inhibitor of the gene's protein could be an effective therapeutic strategy (Mercola *et al.*, 2013).

1.3 Stem Cell-Derived Cardiomyocytes

1.3.1 Production of stem cell derived-cardiomyocytes

Human cardiomyocytes can be produced from PSCs. Both hESCs and hiPSCs were originally shown to form spontaneously contracting cardiomyocytes via embryoid body

production, expressing standard cardiac-specific genetic markers and proteins associated with contractility including cardiac troponin I and alpha-actinin, similar to those expressed in primary cardiomyocytes (Kehat *et al.*, 2001; Mummery *et al.*, 2002; J. Zhang *et al.*, 2009; Zwi *et al.*, 2009). A large number of studies investigated the electrophysiological, calcium handling and pharmacological properties of hESC- and hiPSC-derived cardiomyocytes (hESC-CM and hiPSC-CM) produced via embryoid bodies and found these were again reminiscent of those recorded for human cardiomyocytes *in vivo* (Kehat *et al.*, 2001; He *et al.*, 2003; Reppel *et al.*, 2004, 2005; S. E. Harding *et al.*, 2007; J. Zhang *et al.*, 2009; Yokoo *et al.*, 2009; Itzhaki *et al.*, 2011).

More recently, a number of high yield differentiation protocols have been developed to efficiently and reproducibly generate cardiomyocytes from both hESCs and hiPSCs in a monolayer culture, utilising growth factors, small molecules or a combination of both (Kattman *et al.*, 2011; Lian *et al.*, 2013; Burridge *et al.*, 2014).

In development, the heart is one of the first organs to develop, arising from the mesoderm soon after gastrulation, with the formation of cardiac mesoderm induced in response to signals from adjacent cells (Mummery *et al.*, 2012). From studies of model organisms, it is thought that four families of growth factors are essential for directing early cardiogenesis – bone morphogenetic proteins (BMPs), fibroblast growth factors (FGF), the Activin/Nodal/transforming growth factor β (TGFβ) pathway and the WNT signalling family (S. M. Evans *et al.*, 2010). As such, the majority of successful differentiation protocols act to target these identified pathways at defined time points, in attempt to mimic the developmental stages seen during *in vivo* embryogenesis (Kattman *et al.*, 2011; Lian *et al.*, 2013; Burridge *et al.*, 2014). Commonly used differentiation protocols typically produce a cardiomyocyte yield of ~70-80%, as evidenced by the cardiac troponin T positive percentage measured by flow cytometry. However, cardiomyocyte culture purity can be improved further by employing metabolic lactate selection as, unlike other cell types, cardiomyocytes can utilise lactate as an energy source via oxidative phosphorylation when cultured in glucose free medium (Tohyama *et al.*, 2013). Again, the cardiomyocytes produced via these methods display characteristics similar to that of primary cardiomyocytes (Kattman *et al.*, 2011; Ren *et al.*, 2011; Burridge *et al.*, 2014; Mendjan *et al.*, 2014). It is important to note that PSC-CMs display a more foetal phenotype (Sterneckert *et al.*, 2014), but

a number of strategies including 3D culture methods, mechanical strain and electrical pacing have been utilised to induce maturation (Ruan *et al.*, 2015; Uzun *et al.*, 2016; Mills *et al.*, 2017; Ronaldson-Bouchard *et al.*, 2018). Furthermore, PSC-CM cell populations represent a diverse mix of atrial-, ventricular- and nodal-like cells, with each subset possessing distinct molecular signatures and functional properties (Karakikes *et al.*, 2014). Hence, differentiation protocols are being adapted and developed in order to produce subtype specific cardiomyocytes. It is thought that this could be dependent on modulation of the WNT or retinoic acid signalling pathways (Q. Zhang *et al.*, 2011; Karakikes *et al.*, 2014; Y. Zhao *et al.*, 2019), but further work is needed to refine protocols for lineage-specific differentiation. Recently, CRISPR/Cas9 was used to generate a double hiPSC fluorescent reporter line, which specifically marked ventricular-like and atrial-like hiPSC-CMs with different colours. The mixed population was then separated using flow cytometry, with the hope that this system could be used to generate cardiomyocytes for modelling chamber-specific diseases (Chirikian *et al.*, 2021).

1.3.2 Uses of stem cell derived-cardiomyocytes

Subsequently, there has been substantial interest in the use of PSC-CMs as a source of cells for transplantation in regenerative medicine following injury, such as myocardial infarction. There is a severe shortfall in the number of organs available versus the number of patients requiring a heart transplant, hence utilising PSC-CMs could address a major unmet need. Originally, transplantation of undifferentiated hESCs was shown to improve cardiac function in a rat model of myocardial infarction (Min *et al.*, 2003). However, due to the associated risks of transplanting pluripotent cells (Caspi *et al.*, 2007), in more recent studies, PSCs have been differentiated to cardiomyocytes prior to transplantation, and often incorporated into a scaffold structure comprising multiple cell types to promote cell engraftment and retention (Ye *et al.*, 2014; Q. Wang *et al.*, 2016). The Sinha group recently demonstrated that co-transplantation of hESC-derived epicardium promoted hESC-CM graft retention and function in a rat model of myocardial infarction, suggesting that a supportive cell type may be essential for hESC-CM maturation and survival (Bargehr *et al.*, 2019). Although there has been substantial advances in the field, there are still a number of hurdles to overcome, for example how to produce the vast number of cells needed at

a clinical grade (Kishino *et al.*, 2020). It has also been reported that transplantation of PSC-CMs can induce ventricular arrhythmias within the first weeks of transplantation in both porcine and non-human primate models of myocardial ischaemia (J. J. H. Chong *et al.*, 2014; Romagnuolo *et al.*, 2019).

PSC-CMs have also been used extensively as a model to investigate human development and physiology, as well as cardiovascular pathologies (Földes *et al.*, 2011; Ebert *et al.*, 2012). Using PSC-CMs has the advantage over standard animal models or primary cell types in that they offer a potentially unlimited source of cardiomyocytes, whilst facilitating the generation of more human relevant results (Paik *et al.*, 2020). Additionally, cardiomyocytes derived from PSCs have been used as a platform to screen novel compounds for efficacy but also to investigate cardiotoxicity and drug-induced arrhythmia as described above, using both candidate and HTS approaches (Braam *et al.*, 2010; del Álamo *et al.*, 2016). Lee *et al.* (2019) demonstrated that iPSC-CMs generated from dilated cardiomyopathy (DCM) patient-specific cells carrying a mutation in the *LMNA* gene were prone to arrhythmias due to aberrant calcium signalling. The *LMNA* gene encodes lamin A/C and mutations in this gene account for 5-10% of DCMs (Hershberger *et al.*, 2013). Furthermore, by comparing to generated isogenic control iPSC-CMs, they found increased activity of the platelet derived growth factor (PDGF) signalling pathway, and demonstrated decreased frequency of arrhythmia when the PDGF pathway was inhibited pharmacologically or molecularly in mutant iPSC-CMs (J. Lee *et al.*, 2019). Another study utilised hiPSCs isolated from a DCM patient carrying a previously uncharacterised variant of the RBM20 splicing factor (Briganti *et al.*, 2020). By differentiating to cardiomyocytes, the RBM20 variant was confirmed to be disease causing, and was associated with dysregulated calcium signalling and decreased hiPSC-CM contractility. Furthermore, RBM20 upregulation improved cellular phenotype, suggesting this as a potential therapeutic strategy (Briganti *et al.*, 2020). These studies demonstrate the potential of PSC-derived cardiomyocytes for the elucidation of mechanisms involved in disease pathogenesis and for the discovery of novel therapeutic targets.

There is also increasing use of PSC-CMs in automated and high-throughput drug screening. For example, a recent study made use of hiPSC-CMs generated from long QT syndrome patients, carrying mutations in the cardiac sodium channel $Na_{V1.5}$

(McKeithan *et al.*, 2020). By using a combination of iterative cycles of medicinal chemistry and HTS to measure electrophysiological properties, including action potential duration and sodium current, four mexiletine (a known anti-arrhythmic drug) analogues with improved potency and enhanced anti-arrhythmic effects were identified (McKeithan *et al.*, 2020).

PSC-CMs can also be incorporated into scaffolds made of biomaterials to produce 3D engineered heart tissues (EHTs) in combination with other cell types, to more closely replicate the structure of the heart *in vivo,* and also to study the effect of cellular interactions in physiology and disease (Breckwoldt *et al.*, 2017). Additionally, the generation of 3D EHTs has been shown to promote PSC-CM maturity, due to the structural support from the EHT mould providing the cardiomyocytes with mechanical strain (Tulloch *et al.*, 2011; Uzun *et al.*, 2016). EHTs may offer a more physiologically relevant disease model, as they promote coordinated electrophysiological and contractile responses due to the more physiological environment (Weinberger *et al.*, 2017). Previously, a study utilising hiPSC-CMs derived from DCM patients in a 3D culture system found that mutations affecting the titan protein contribute to disease pathogenesis by promoting sarcomere disarray, diminishing ability to respond to both mechanical and β-adrenergic stress and impairing contractility (Hinson *et al.*, 2015).

Furthermore, cardiomyocytes generated from patient-derived iPSCs have been used to investigate patient genotype-phenotype variability in terms of disease pathogenesis and severity, response to novel treatments and drug-induced cardiotoxicity (Liang *et al.*, 2013; Matsa *et al.*, 2016; Paik *et al.*, 2020). A recent study subjected EHTs consisting of iPSC-CMs derived from three donors to four different calcium channel blockers and carried out transcriptome analysis. iPSC-CMs were found to respond in both a line- and drug-specific manner, and results from transcriptome analysis indicated each drug induced specific transcriptomic effects in the individual lines, displaying little overlap, suggesting patient-dependent drug responsiveness (C. K. Lam *et al.*, 2019). Matsa *et al*. (2016) tested the cardiotoxicity of tacrolimus, a commonly used immunosuppressant, in five lines of iPSC-CMs. In one line only, tacrolimus was found to disrupt calcium homeostasis and promote sarcomere disarray, both characteristic of systolic dysfunction *in vivo*, suggesting a mechanism for patient-specific drug-induced cardiotoxicity (Matsa *et al.*, 2016). hiPSC-CM based drug screens for cardiotoxicity could potentially identify cardiotoxic drugs in the

preclinical stages of drug development, preventing progression to clinical trials – at which stage, currently almost 90% of drugs fail, associated with extremely high costs (DiMasi *et al.*, 2016). As such, a range of potential scoring systems for cardiotoxicity are being developed for safety testing. For example, Koplijar *et al.* (2018) have developed a scoring system for cardiac electrical risks by examining calcium transients. This study tested the effects of 587 new chemical entities in hiPSC-CMs, a subset of which were then validated in *ex vivo* and *in vivo* models to define a scoring system to rank test compounds, allowing identification of those most likely to present low cardiovascular risk (Kopljar *et al.*, 2018).

In the current project, the aim was to make use of hESC-CMs as a human relevant platform to model cellular signalling pathways and the consequences of both genetic and pharmacological manipulation of the apelin receptor on cardiomyocyte function. I elected to use H9 hESCs. This was because the Sinha group has expertise in the culturing of this cell type and has a pre-established and optimised protocol that reliably generates cardiomyocytes. hESCs have the advantage over iPSCs in that no reprogramming is necessary and the commercially available cell lines tend to be well characterised. The H9 line is the most frequently used hESC line, with 46.4% of all hESC papers published between 2008 and 2016 making use of this cell type (Guhr *et al.*, 2018). iPSCs can also display differing differentiation propensities, thought to be due to epigenetic memory, meaning they are more likely to differentiate back to their cell type of origin (Zhu and Huangfu, 2013). This is not seen with hESCs. It is important to note that the resulting hESC-CMs represent a mixed population, with the majority possessing an immature ventricular cardiomyocyte phenotype. In the adult heart, atrial, ventricular and nodal cardiomyocytes are all present, with each cell type displaying distinct electrophysiological and contractile properties (del Álamo *et al.*, 2016). The heterogeneity and immaturity of the resulting hESC-CMs are limitations of the project, as described further in Section 8, however efforts have been made to overcome these limitations.

1.4 The Apelin Receptor and its Endogenous Ligands

1.4.1 Discovery of the apelin receptor and its endogenous ligands

The apelin signalling system has emerged in recent years as a key pathway involved in cardiovascular development, health and disease. The apelin receptor is a class A GPCR, consisting of a single polypeptide with the characteristic seven hydrophobic transmembrane domain structure, extracellular N-terminus and intracellular C-terminus (Foord *et al.*, 2005). GPCRs are a large, diverse class of receptors present on the cell surface that can be activated by a range of molecules including peptides, lipids, ions, odorants and light (Lundstrom, 2009). GPCRs are important pharmacological targets, with approximately 35% of all approved drugs acting on GPCRs, due to their accessible druggable and allosteric modulatory sites, and because of their role in the regulation of a diverse range of physiological processes (Rask-Andersen *et al.*, 2014; Hauser *et al.*, 2017). Upon activation, GPCRs induce a cascade of signalling events, meaning even a low ligand concentration can cause a large downstream response (Hauser *et al.*, 2017). Class A GPCRs, also known as rhodopsin-like receptors, are the largest, most well-studied class of GPCRs and are also the class of receptors most commonly targeted by clinically approved drugs (Foord *et al.*, 2005; Lagerström and Schiöth, 2008).

The apelin receptor gene was originally discovered in 1993, cloned based on its high sequence similarity with the angiotensin II receptor type 1 (AT_1) (O'Dowd *et al.*, 1993). In humans, the gene encoding the apelin receptor (*APLNR,* originally known as *APJ*) is present on chromosome 11 and encodes a protein made up of 380 amino acids (O'Dowd *et al.*, 1993). The receptor is highly conserved across many species, with a sequence homology of 91% and 89% in mice and rats (both 377 amino acids), respectively (Pitkin *et al.*, 2010). The receptor also contains conserved sites for post-translational modification by palmitoylation, cAMP-dependent protein kinase phosphorylation and glycosylation, with each modification implicated to have roles in receptor expression and stability, ligand binding, internalisation and dimerisation (O'Dowd *et al.*, 1993; Wheatley and Hawtin, 1999; Huynh *et al.*, 2009). Only one receptor subtype exists in mammals, with Hill coefficients of close to one in saturation binding experiments (Katugampola *et al.*, 2001). Interestingly, however, in zebrafish two apelin receptor subtypes are expressed, *aplnra* and *aplnrb*, although the functional consequences of this are unclear (X. X. I. Zeng *et al.*, 2007; P. Yang *et al.*, 2015).

Despite a homology of 54% with the AT_1 receptor in the transmembrane regions (O'Dowd *et al.*, 1993), the apelin receptor does not bind angiotensin and remained an orphan for a number of years, having no known ligand.

In 1998, apelin was isolated from bovine stomach extracts and identified as the endogenous ligand for the apelin receptor using reverse pharmacology, by screening various tissue extracts against cells expressing the receptor of interest to identify interacting molecules (Tatemoto *et al.*, 1998). Using Chinese hamster ovary (CHO) cells artificially expressing the apelin receptor and a Cytosensor to measure extracellular acidification, apelin was found to specifically induce increases in acidification rate, which was not seen in control CHO cells (Tatemoto *et al.*, 1998). Apelin is present as a pre-pro-peptide consisting of 77 amino acid residues, which then undergoes proteolytic cleavage at the C-terminus to generate a number of active isoforms, including apelin-36, apelin-17 and apelin-13, which may also be subjected to post-translational modification (Habata *et al.*, 1999). The apelin peptide isoforms have been shown to possess different properties, displaying differing affinities and potencies for the apelin receptor, which may be important for biological function. Furthermore, it has also been shown that the potency of apelin peptides varies depending on the experimental system, for example apelin-13 and pyroglutamated apelin-13 ([Pyr^1]apelin-13) induce the most potent apelin receptor activation in cell lines (Pitkin *et al.*, 2010).

Apelin remained the sole ligand for the apelin receptor, until the discovery by two independent groups of a second peptide ligand known as Elabela/Toddler (ELA), shown to be important in embryological development in zebrafish (Chng *et al.*, 2013; Pauli *et al.*, 2014). The ELA peptide was identified from a conserved region of the genome previously identified as non-coding. In humans, the ELA encoding gene, *APELA*, encodes a 54 amino acid pre-pro-protein, predicted to undergo cleavage to form smaller active peptide isoforms such as ELA-11, ELA-21 and ELA-32, again displaying different apelin receptor binding properties (Chng *et al.*, 2013; Pauli *et al.*, 2014; Murza *et al.*, 2016). The ELA peptide is highly conserved, with the last 13 residues found to be almost invariant in all vertebrate species (Chng *et al.*, 2013), however, apelin and ELA display little sequence homology despite binding to similar regions of the apelin receptor (P. Yang *et al.*, 2015). Loss of function mutations in the ELA gene phenocopied apelin receptor KO mice, suggesting the apelin receptor is a

cognate binding partner for ELA (described further below). Additionally, ELA was shown to induce apelin receptor internalisation and injection of apelin mRNA rescued the ELA mutant phenotype (Pauli *et al.*, 2014), indicating that the apelin receptor is the shared target of both peptide ligands. It is relatively rare for a receptor to respond to two distinct peptide ligands, hence the function and evolutionary benefit behind the existence of the two apelin receptor ligands is of great interest.

1.4.2 Distribution of the apelin signalling system

The apelin receptor has been found to be widely distributed throughout the human body, both centrally and in the periphery. Apelin receptor mRNA has been detected in all regions of the brain, with northern blot used to report high levels in the amygdala, corpus callosum, hippocampus and spinal cord (Matsumoto *et al.*, 1996; Edinger *et al.*, 1998; Medhurst *et al.*, 2003). In human peripheral tissues, qRT-PCR, immunohistochemistry and autoradiography have shown that highest apelin receptor expression is seen in the spleen and placenta, with lower expression seen in a diverse range of tissues including the heart, lung and kidney (Medhurst *et al.*, 2003). Importantly, in the context of the current project, it has been shown that the apelin receptor is expressed in cardiomyocytes, vascular smooth muscle cells and endothelial cells (Kleinz *et al.*, 2005).

Corresponding to the localisation of the receptor, apelin peptide expression follows a similar distribution pattern in both the brain and the periphery. Again, highest expression has been reported in the placenta, with moderate levels seen in the heart, lung, mammary gland and kidney (Katugampola *et al.*, 2001; Medhurst *et al.*, 2003). Interestingly, variation in the level of expression of each isoform is reported in different tissues (Kawamata *et al.*, 2001), which may have biological relevance in terms of peptide and receptor function. For example, in the human heart the most abundantly expressed isoform is [Pyr^{1}]apelin-13 (Maguire *et al.*, 2009). In the heart, the endothelium is the main source of apelin production (Kleinz and Davenport, 2004). The expression of ELA peptide is less well studied, but it has been shown to be developmentally regulated. Ho *et al*. (2015) demonstrated that ELA is most highly expressed in the inner cell mass of the blastocyst, and is downregulated upon differentiation. Concurrently, ELA was also shown to be highly expressed in cultured

embryonic stem cells (Ho *et al.*, 2015). Additionally, however, ELA is expressed in adult tissues, although its expression is more restricted compared to apelin. *APELA* transcripts have been detected in adult human kidney and the endothelial cells of a range of blood vessels (Z. Wang *et al.*, 2015; P. Yang *et al.*, 2017b). Interestingly, human ELA plasma levels were shown to be significantly higher than apelin plasma levels but similarly to apelin peptide, no immunoreactivity for ELA was seen in cardiomyocytes and smooth muscle cells (P. Yang *et al.*, 2017b). The discrepancy between the expression of the receptor and its ligands and the fact that both are found in the plasma indicates that the ligands can have effects via an autocrine, paracrine or endocrine mechanism of action. Additionally, the spatial and temporal differences in expression of the two ligands and their distinct isoforms may be of biological relevance.

1.4.3 Signalling pathways activated by the apelin receptor

Activation of a GPCR induces a cascade of downstream signalling events (Figure 1.2). Upon ligand binding, the receptor undergoes a conformational change to catalyse the activation of an associated heterotrimeric G-protein, made up of an α, β and γ subunit. Upon activation, the G-protein exchanges the bound guanosine diphosphate (GDP) for guanosine triphosphate (GTP) and dissociates into active α-subunit and a βγ dimer, which in turn interact with and activate further cell signalling molecules. The GTP bound α-subunit has catalytic activity and will hydrolyse the GTP to GDP, promoting re-association with the βγ dimer and the GPCR (Rosenbaum *et al.*, 2009). Multiple families of G-proteins exist including $G_{\alpha s}$, $G_{\alpha i}$ and $G_{\alpha q}$, with the intracellular signalling pathway activated dependent on the family of G-protein that the receptor interacts with (Oldham and Hamm, 2008). Furthermore, GPCRs can also function through non G-protein dependent signalling pathways via β-arrestins. Upon activation, G-protein coupled receptor kinases (GRKs) are recruited to GPCRs and phosphorylate key residues within the intracellular domains. In turn, this promotes β-arrestin translocation and binding to receptor. The bound β-arrestin then recruits adaptor proteins to promote the formation of clathrin coated pits, and clathrin-mediated endocytosis occurs to form vesicles containing the phosphorylated GPCR and associated β-arrestin. The receptor can then be recycled back to the plasma

membrane, or it can interact with a range of other cellular effectors via β-arrestin to activate further signalling pathways (Goodman *et al.*, 1996; E. Kelly *et al.*, 2008).

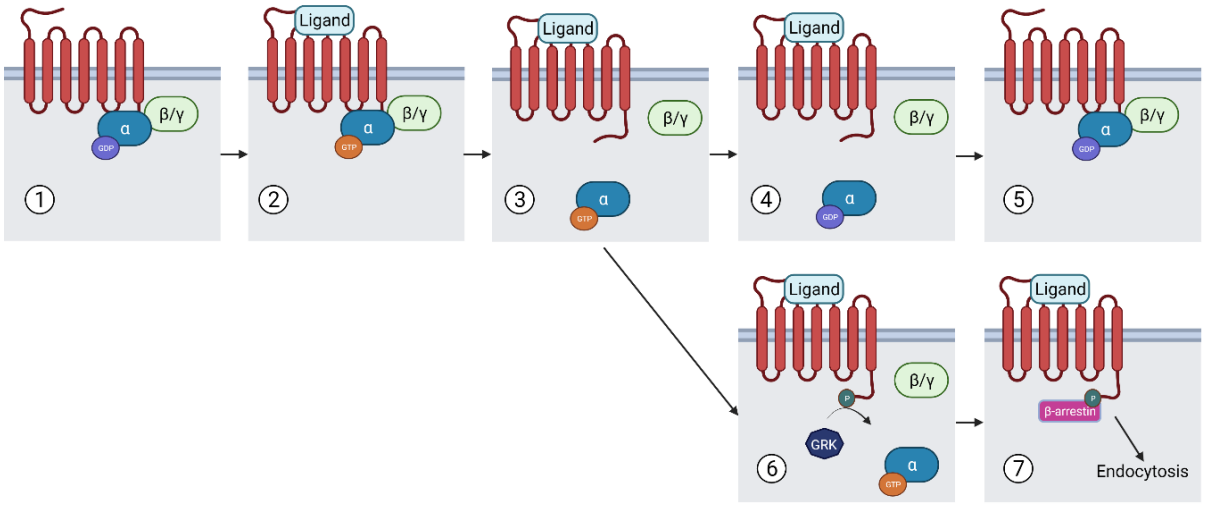

Figure 1.2: Generic GPCR signalling pathway. (1) GPCR present in membrane with trimer G-protein associated, with GDP (blue) bound. (2) Ligand binding promotes activation, G protein α-subunit exchanges GDP for GTP (orange), (3) leading to dissociation into α-subunit and βγ subunits, free to act on their respective downstream effectors. (4) GTP hydrolysis by α-subunit GTPase activity promotes (5) G-protein reassembly. Alternatively, (6) G-protein coupled receptor kinase (GRK) phosphorylates key residues within the activated GPCR, (7) leading to translocation and association of β-arrestin, resulting in clathrin-mediated endocytosis. GPCR is then either recycled to the plasma membrane or interacts with other cellular effectors via β-arrestin to induce distinct signalling cascades. Created using Biorender.com.

The apelin receptor is thought to function via both G-protein dependent and independent signalling pathways. Apelin was shown to inhibit forskolin-induced accumulation of cyclic AMP (cAMP) in CHO cells artificially expressing the apelin receptor (Habata *et al.*, 1999), indicating action through $G_{\alpha i}$ and subsequent inhibition of adenylyl cyclase. Further evidence for the apelin receptor's action through $G_{\alpha i}$ is that action of apelin peptides in CHO cells was shown to be sensitive to pertussis toxin (Hosoya *et al.*, 2000), which prevents $G_{\alpha i}$ G-protein from interacting with GPCR. The apelin receptor has also been shown to couple with $G_{\alpha q}$ proteins, promoting an increase in intracellular calcium via activation of phospholipase Cβ (PLCβ) to catalyse

the breakdown of phosphatidylinositol 4,5-bisphosphate (PIP_2) producing inositol trisphosphate (IP_3) and a diacylglycerol (DAG)-dependent activation of protein kinase C (PKC) (Szokodi *et al.*, 2002). The $G_{\alpha q}$ pathway is thought to be induced upon apelin receptor activation in cardiomyocytes, in turn promoting an increase in force of contraction (Japp and Newby, 2008) as detailed further below. Another study demonstrated that the apelin receptor acts to regulate myocyte enhancer factor 2 (MEF2) for correct cardiac development. However, overexpression of constitutively active $G_{\alpha q}$ or $G_{\alpha i}$ did not induce MEF2 luciferase reporter activity (Kang *et al.*, 2013). $G_{\alpha 13}$ had previously been reported to regulate MEF2 activity (G. Liu *et al.*, 2009), although had not been shown to interact with the apelin receptor. Upon overexpression of $G_{\alpha 13}$, MEF2 reporter activity was increased and overexpression of the apelin receptor or stimulation with apelin-13 was found to induce $G_{\alpha 13}$ activity (Kang *et al.*, 2013), indicating that the apelin receptor can signal through this third family of G-proteins and have biological effect.

The apelin receptor has also been shown to function through G-protein independent signalling mechanisms (Seo *et al.*, 2020). For example, in the heart the apelin receptor can respond to stretch, acting as a mechanosensor via β-arrestin recruitment and independent of ligand binding (Scimia *et al.*, 2012; Seo *et al.*, 2020). Finally, there is evidence to suggest that the apelin receptor can act via heterodimerisation to regulate other signalling pathways. For example, apelin was found to induce apelin receptor AT_1 receptor heterodimerisation, which in turn reduced angiotensin II binding and potency, suggesting the apelin receptor can cause negative allosteric modulation of its interacting receptor (Siddiquee *et al.*, 2013).

1.5 The Role of Apelin Receptor in Cardiovascular Development

As detailed above, the apelinergic signalling pathway is expressed throughout the cardiovascular system. As such, in recent years it has emerged as a key pathway in the regulation of cardiovascular development and physiology, and has also been implicated in cardiovascular disease pathogenesis.

1.5.1 The role of the apelin receptor in cardiac development

The apelin receptor is important for early cardiac development (Figure 1.3). A number of studies have determined that homozygous apelin receptor KO in mice results in significant embryonic lethality (Ishida *et al.*, 2004; Charo *et al.*, 2009; Kang *et al.*, 2013), with embryos displaying a range of cardiovascular defects including poor vascularisation of the yolk sac and abnormal heart formation. Interestingly, the majority of the embryonic lethality occurred between E10.5 to E12.5 (Kang *et al.*, 2013). The mice that survived to neonatal stage displayed ventricular defects, myocardium thinning and reduced capillary densities, as well as significantly decreased vascular smooth muscle cell recruitment. The same study found that the majority of the small number of mice that survive to adulthood displayed cardiac abnormalities such as ventricular septal defects and right atrial enlargement (Kang *et al.*, 2013). Other studies have found, however, that surviving apelin receptor KO mice are relatively normal (Charo *et al.*, 2009; Scimia *et al.*, 2012), although basal cardiac contractility was reduced and response to cardiovascular stress (such as exercise) was reported to be significantly impaired with receptor KO (Charo *et al.*, 2009). The role of apelin receptor signalling in development therefore appears complex, and it would be beneficial to determine if there is a cardiomyocyte-autonomous effect or if the observed developmental phenotypes are more dependent on vascular effects.

There is also disparity between apelin receptor and apelin peptide KO mice. Mice homozygous for loss of the apelin gene (*apln*$^{-/-}$) are born at the expected birth ratio, with no effect on cardiac development (Kidoya *et al.*, 2008; Charo *et al.*, 2009). It was found that *apln*$^{-/-}$ mice were generally healthy, however they possessed decreased exercise capacity and responded poorly to cardiovascular stress (Kuba *et al.*, 2007; Charo *et al.*, 2009), similar to that seen for surviving apelin receptor KO mice.

The discrepancy between the developmental phenotype of apelin receptor null and apelin peptide null mice was resolved with the discovery of ELA. In zebrafish, ELA KO strikingly recapitulated the phenotype seen in *aplnr*$^{-/-}$ mice (Chng *et al.*, 2013; Pauli *et al.*, 2014). Homozygous ELA KO in zebrafish led to a high proportion of embryonic lethality, with embryos displaying severe cardiac dysplasia and only rudimentary heart formation, along with defective vascular formation (Chng *et al.*, 2013), supporting a critical role of ELA in combination with the apelin receptor in cardiovascular developmental signalling. More recently, ELA KO mice have been generated. Again,

a high incidence of embryonic lethality was reported and defects in cardiovascular development recorded (Freyer *et al.*, 2017; Ho *et al.*, 2017). An aberrant upregulation of erythroid and myeloid markers has been suggested as the cause of the abnormalities. Importantly, apelin-ELA double KOs displayed the same phenotypic properties as ELA null mice, indicating that apelin does not compensate for loss of ELA in development (Freyer *et al.*, 2017).

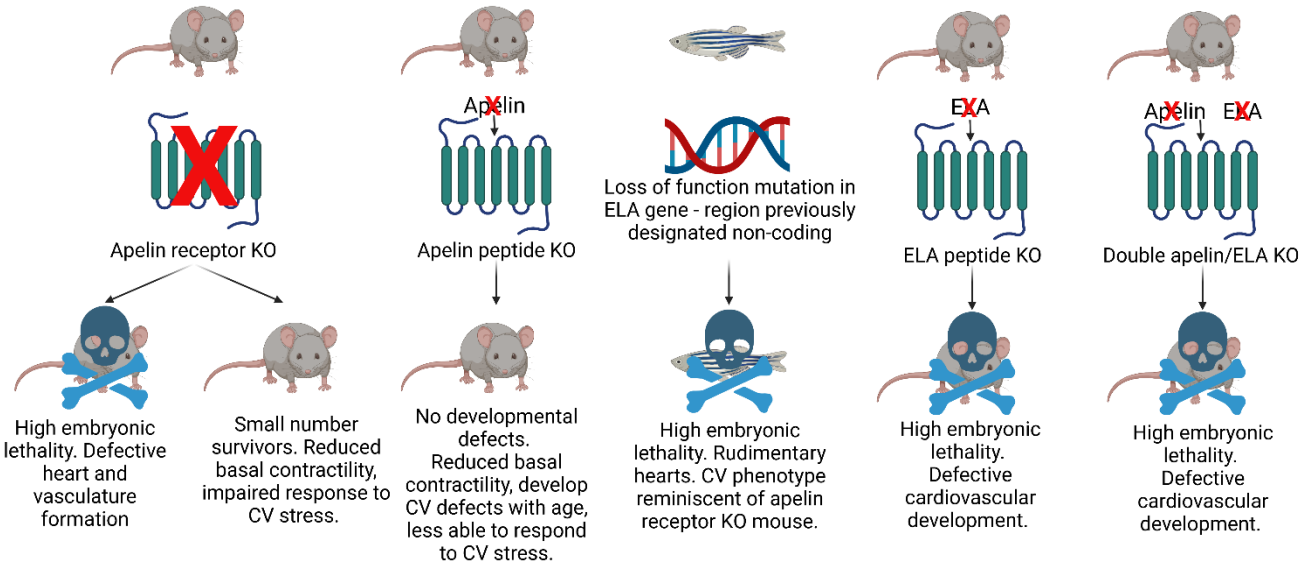

Figure 1.3: Summary of KO and genetic studies examining the effect of loss of apelin receptor and its ligands on cardiovascular development. Created using Biorender.com.

1.5.2 The role of the apelin receptor in embryonic stem cells

ELA has been shown to be highly expressed in both human and mouse ESCs, where it acts to promote self-renewal (Ho *et al.*, 2015; M. Li *et al.*, 2015). Upon knockdown of ELA, the stem cell characteristic ability to form teratomas was lost in hESCs (Ho *et al.*, 2015). However, these studies both report that ESCs do not express the apelin receptor. In two lines of hESCs (HES3 and SHEF4), expression of the apelin receptor was undetected at both the gene and protein level, with expression only upregulated upon differentiation to mesendoderm (Ho *et al.*, 2015). A further study utilising a fluorescently conjugated [Pyr^{1}]apelin-13 analogue showed a lack of binding in both HES3 and H9 hESCs (Yu *et al.*, 2012). Additionally, it has been suggested that *apela* RNA interacts with p53 in a negative feedback loop to regulate damage induced apoptosis in mouse ESCs (M. Li *et al.*, 2015).

These studies have led to the proposal and search for a second receptor for ELA which is expressed at least in early development. However, this has so far been unsuccessful, hence one aspect of the current project was to investigate expression of the apelin receptor in hESCs.

1.6 The Role of the Apelin Receptor in Adult Cardiovascular Physiology and Pathophysiology

As discussed above, the apelin receptor and its ligands are expressed in the adult cardiovascular system, where its activation has a number of physiological roles. Throughout Section 1.6, it is important to note that the concetrations of endogenous apelin and ELA are generally much lower than the pharmacological doses given. This difference in doses could cause different effects in terms of signalling, but importantly may cause changes to apelin receptor surface expression by inducing more internalisation due to the high ligand exposure, as discussed further below.

1.6.1 The apelin receptor in cardiovascular physiology

1.6.1.1 The role of the apelin receptor in vasodilatation

Firstly, activation of the apelin receptor has strong vasodilatory effects. In one of the first studies to examine the physiological effects of activation of the apelin receptor by its cognate apelin ligand, male Wistar rats were intravenously injected with a bolus of a synthetic apelin peptide (D. K. Lee *et al.*, 2001). A significant and immediate decrease in systolic and diastolic blood pressure was observed, which persisted for several minutes. The blood pressure effect was found to be dose dependent and interestingly, different isoforms of apelin were found to decrease blood pressure with differing potencies, with apelin-12 inducing the largest decrease in blood pressure compared to apelin-36 and apelin-13 (Tatemoto *et al.*, 2001). This hypotensive action occurs via the apelin receptor, and is abolished in apelin receptor KO mice (Ishida *et al.*, 2004). Furthermore, the decrease in blood pressure was found to be dependent on nitric oxide (NO), as the apelin-12 induced change in blood pressure was abolished in rats co-administered the NO synthase inhibitor, L-NAME (Tatemoto *et al.*, 2001). Further supporting the role of apelin via NO signalling, apelin promoted

vasoconstriction in denuded blood vessels, indicating an endothelium-dependent response (Tatemoto *et al.*, 2001; Maguire *et al.*, 2009). Concomitantly, in preconstricted mouse aortic rings, ELA peptide induced relaxation. In contrast to the observations for apelin, the ELA induced relaxation was not inhibited by endothelial denudation or L-NAME (Z. Wang *et al.*, 2015), indicating a different mechanism of action .

Similar vasodilatory effects have also been observed in human vessels. Administration of apelin induced relaxation of preconstricted mesenteric arteries *ex vivo* (Salcedo *et al.*, 2007), while intravenous apelin infusion resulted in an increase in forearm blood flow which was attenuated by co-administration of L-NAME (Japp *et al.*, 2008; Brame *et al.*, 2015).

1.6.1.2 The role of the apelin receptor in positive inotropy

As well as the vascular effects, activation of the apelin receptor induces positive cardiac inotropy, with apelin found to be one of the most potent inotropes identified to date in both rat and human hearts *ex vivo* (Szokodi *et al.*, 2002; Maguire *et al.*, 2009). This finding has been recapitulated *in vivo*, with apelin infusion in mice (Ashley *et al.*, 2005) and rats (Berry *et al.*, 2004) promoting significant increases in cardiac contractility. Similar findings have been reported for ELA, which induced increased cardiac contractility both *ex vivo* (Perjés *et al.*, 2016) and *in vivo* in rats (Murza *et al.*, 2016; P. Yang *et al.*, 2017b). In humans, infusion of [Pyr^{1}]apelin-13 also significantly increased cardiac output (Japp *et al.*, 2010). Importantly, apelin receptor-induced increase in contractility is not associated with hypertrophy, with no difference seen in heart weight for mice chronically infused with apelin (Ashley *et al.*, 2005). Additionally, further supporting the role of apelin receptor activation in cardiac contractility, both apelin and apelin receptor KO adult mice display reduced basal cardiac contractility with impaired sarcomeric shortening (Charo *et al.*, 2009). Similar results are seen for ELA, with a dose dependent increase in ejection fraction observed in rats treated with ELA-32 (P. Yang *et al.*, 2017b).

The combined effects of apelin receptor activation to promote vasodilatation and positive inotropy without hypertrophy has led to the proposition of the apelin receptor as a target for novel treatments for heart failure. This is discussed further in Section 1.6.3.

1.6.2 Signalling pathways induced in the inotropic effects of apelin receptor activation

The mechanisms underlying the positive inotropic effect of apelin receptor activation are controversial, with a simplified summary shown in Figure 1.4. In cardiomyocytes, evidence suggests the apelin receptor signals via $G_{\alpha q}$ signalling (Szokodi *et al.*, 2002), inducing activation of PLCβ to produce inositol triphosphate (IP_3) and PKCε activity (Perjés *et al.*, 2014). IP_3 can act on IP_3 receptors present on the sarcoplasmic reticulum to cause calcium (Ca^{2+}) release, in turn promoting calcium induced calcium release (CICR) via ryanodine receptors (RyR). Concurrently, PKCε is proposed to increase the activity of the sodium hydrogen exchanger (NHE) present on the sarcolemma, resulting in increased intracellular sodium (Na^{+}) concentration, and in turn allowing the sodium calcium exchanger (NCX) to increase intracellular Ca^{2+} (Szokodi *et al.*, 2002; Perjés *et al.*, 2014). However, it has also been shown that treatment of isolated rat ventricular cardiomyocytes with apelin induced an increase in contractility with no change in intracellular calcium concentration (Farkasfalvi *et al.*, 2007). Consistent with this, calcium transients were unchanged in cardiomyocytes from adult apelin receptor KO mice compared to control (Charo *et al.*, 2009). Additionally, the apelin receptor has been suggested to activate myosin light chain kinase (MLCK) via PKCε, which in turn promotes phosphorylation of the myosin II regulatory light chain (RLC), which increases the Ca^{2+} sensitivity of the contractile machinery (Perjés *et al.*, 2014). Interestingly, a recent study reported a decrease in the amplitude of Ca^{2+} transients following stimulation of isolated cardiomyocytes with apelin. Here, apelin treatment reduced protein kinase A (PKA) activation via $G_{\alpha i}$ coupled signalling, leading to decreased cardiac troponin I phosphorylation at two key serine residues ($Ser^{22}$and Ser^{23}) (Parikh *et al.*, 2018), which has previously been shown to increase myofilament Ca^{2+} sensitivity (Ramirez-Correa *et al.*, 2010). Conversely, two studies have reported an increase in intracellular Ca^{2+} following apelin treatment in isolated rat cardiomyocytes (C. Wang *et al.*, 2008) and cardiac muscle strips (Dai *et al.*, 2006). It has therefore been proposed that the positive inotropic effects of apelin receptor activation result from both Ca^{2+} dependent and Ca^{2+} independent effects (Seo *et al.*, 2020).

A potential link between the contractile effects of apelin receptor activation and voltage signalling has been proposed. Apelin receptor staining has been visualised at T-tubules and the intercalated disc area in isolated rat ventricular myocytes – key areas

for electrophysiological function. Furthermore, the significant increase in sarcomere shortening following apelin treatment in the isolated cardiomyocytes was accompanied by increased action potential conduction velocity (Farkasfalvi *et al.*, 2007). In this study, apelin was found to activate the NHE, resulting in increased pH, intracellular alkinization and increased calcium sensitivity (Farkasfalvi *et al.*, 2007).

Furthermore, inhibition of extracellular signal-regulated kinase 1/2 (ERK1/2) resulted in attenuation of the positive inotropic effect of apelin receptor activation, although the mechanism of action here is unclear (Perjés *et al.*, 2014).

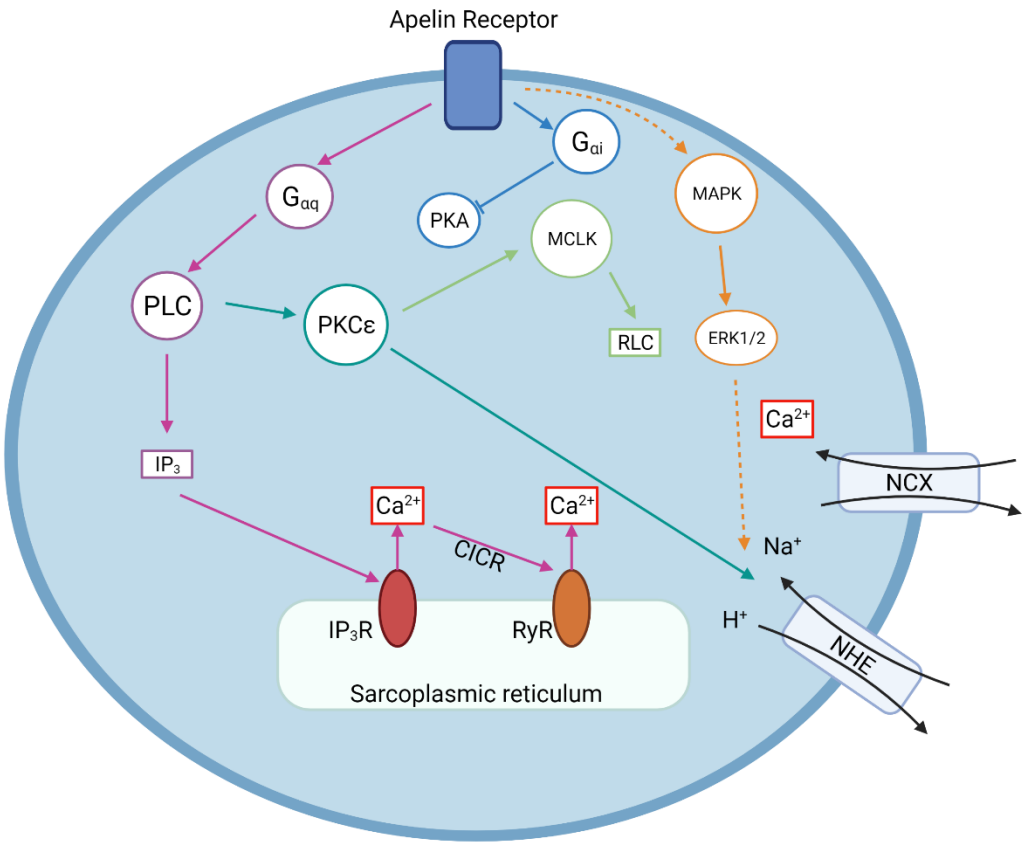

Figure 1.4: Summary of signalling pathways thought to be induced by apelin receptor ligand activation in cardiomyocytes. The positive inotropy induced by apelin receptor activation may have calcium dependent and calcium independent effects. The apelin receptor can also respond to stretch, signalling through β-arrestin, but this is not shown here. Dotted line = signalling pathway unknown. Created using Biorender.com.

1.6.3 The apelin receptor in heart failure

There has been significant interest in the role of apelin receptor signalling in heart failure (Kazemi-Bajestani *et al.*, 2012; Marsault *et al.*, 2019). A key study, compared paired samples of left ventricle obtained from patients with heart failure before and after placement of a left ventricular assist device, which significantly improves survival. The apelin receptor gene was found to be the most significantly increased of the ~12,000 genes measured following implantation. Additionally, they reported a rise in circulating apelin in early heart failure and a subsequent fall in severe disease, concluding the apelin receptor pathway was downregulated (M. M. Chen *et al.*, 2003). In agreement, a study of over 200 patients with chronic heart failure found significantly decreased apelin plasma concentrations regardless of aetiology when compared to age-matched controls, associated with decreased contractile performance and cardiac output (K. S. Chong *et al.*, 2006). This suggests a potentially important role of apelin receptor signalling in the pathogenesis of heart failure. Further supporting this, WT mice subjected to chronic pressure overload were found to upregulate apelin expression in the first two weeks following surgery, with subsequent downregulation in the following weeks, suggesting an initial compensatory mechanism followed by detrimental loss of expression in late stage disease. The same study found apelin KO mice developed more severe cardiac contractility impairments compared to WT when exposed to pressure-overload (Kuba *et al.*, 2007).

Changes to expression of apelin receptor in heart failure are less clear, with conflicting results published. In an isoproterenol-induced heart failure model, apelin receptor expression was decreased (Y.-X. Jia *et al.*, 2006). In another study, Dahl salt-sensitive hypertensive rats were found to increase apelin receptor expression initially, followed by subsequent decrease, with a similar pattern reported for the apelin ligand (Koguchi *et al.*, 2012). Others have reported no change in expression, for example in a dog model of induced heart failure, apelin expression was decreased with no change in receptor expression (M. Wang *et al.*, 2013). Although there may be differences between animal models and human subjects with heart failure, both are capable of responding to apelin receptor stimulation with exogenous agonist treatment as described below.

A number of animal studies have examined the potential of targeting the apelin receptor in heart failure. Firstly, [Pyr^{1}]apelin-13 infusion in Dahl salt-sensitive

hypertensive rats with end stage heart failure significantly improved cardiac contractile performance compared to vehicle treated control. This was associated with reduced expression of inflammatory factors including tumour necrosis factor-α (Koguchi *et al.*, 2012). Concurrently, disease state is improved with apelin treatment in a range of rat models of heart failure, including isoproterenol-induced (Y.-X. Jia *et al.*, 2006) and descending coronary artery ligation (Berry *et al.*, 2004; Atluri *et al.*, 2007). Comparably, in a canine model of heart failure, intravenous apelin infusion increased ejection fraction (M. Wang *et al.*, 2013). Similar results have also been observed in human patients with heart failure, with acute infusion of various apelin isoforms found to increase cardiac output (Japp *et al.*, 2010; Barnes *et al.*, 2013).

Recently, a selective, small molecular apelin receptor agonist with a subnamolar potency was developed, known as BMS-986224 (Gargalovic *et al.*, 2021). Acute administration of BMS-986224 increased cardiac output by up to 15% in anaesthetised rats without significant effects on blood pressure. In a heart failure model, prolonged drug administration increased stroke volume and cardiac output without inducing hypertrophy or fibrosis. This study suggested that the beneficial BMS-986224 effects arose from direct effects on cardiomyocytes as blood pressure remained unchanged (Gargalovic *et al.*, 2021). In another study, two small molecule apelin receptor agonists were designed to mimic the endogenous peptide ligand, displaying low nanomolar potency, and tested *in vitro* and *in vivo* (Ason *et al.*, 2020). The small molecule agonists were found to improve systolic function and cardiac output in three animal models of heart failure. This was due to a combination of a dose-dependent increase in cardiac contractility and a reduction systemic vascular resistance. This study also compared the effects of apelin receptor agonist compared to losartan (AT_1 receptor antagonist) and also tested the effects of co-administration. The apelin receptor agonist induced a similar improvement in cardiac output, without inducing the decrease in mean arterial pressure (MAP) seen with losartan treatment, indicating the apelin agonist can improve cardiac output without effects on blood pressure. There was no benefit of co-administration of the two compounds. It was therefore suggested that apelin agonists may be suited for heart failure patients in which antagonism of the angiotensin system is not suitable, for example those with low blood pressure (Ason *et al.*, 2020).

However, it has also been reported that apelin receptor KO mice are resistant to chronic pressure overload induced hypertrophy and associated heart failure (Scimia *et al.*, 2012), suggesting a ligand-independent function as described in Section 1.4.3. Isolated cardiomyocytes from *aplnr* KO mice displayed reduced stretch response, indicating the apelin receptor can act as a mechanosensor (Parikh *et al.*, 2018). Stretch activation of the apelin receptor resulted in cardiomyocyte hypertrophy, which was inhibited by knockdown of β-arrestin (Scimia *et al.*, 2012). This therefore suggests a dual function of the apelin receptor – the beneficial G-protein signalling, and the β-arrestin stretch signalling which is detrimental in heart failure (Seo *et al.*, 2020). Hence, it has been proposed that biased agonists which preferentially activate the G-protein over β-arrestin at the apelin receptor may be beneficial for the treatment of heart failure as discussed further below (Brame *et al.*, 2015; Read *et al.*, 2020).

1.6.4 The apelin receptor in cardiac fibrosis

The apelin receptor has a role in the regulation of both physiological and pathological organ fibrosis (S. Huang *et al.*, 2016). In heart failure, the heart undergoes detrimental remodelling, in part due to myocardial fibrosis which results in an increase in extracellular matrix deposition (particularly collagen), and in turn increased stiffness (T. Liu *et al.*, 2017). Associated with this, apelin receptor activation has been shown to have anti-fibrotic effects. In an angiotensin II (AngII)-induced mouse model of heart failure, co-administration of apelin resulted in decreased cardiovascular fibrosis, by inhibiting AngII-mediated expression of plasminogen activator inhibitor-1 (PAI-1) (Siddiquee *et al.*, 2011). In agreement, infusion of ELA has been shown to reduce AngII-induced heart failure and associated remodelling (Sato *et al.*, 2017). Furthermore, apelin treatment of cardiac fibroblasts isolated from pressure overload mouse hearts inhibited collagen production, via a reduction in sphingosine kinase 1 (SphK1) activity. Similarly, administration of apelin 14 days after surgically induced heart failure *in vivo* significantly improved ventricular remodelling and function, by attenuating established hypertrophy and fibrosis (Pchejetski *et al.*, 2012).

Taken together, these studies highlight the potential benefits of targeting the apelin receptor for the treatment of heart failure, promoting increased contractility and preventing detrimental cardiac fibrosis.

1.6.5 The apelin receptor in pulmonary arterial hypertension

Pulmonary arterial hypertension (PAH) is a complex disease characterised by the stiffening and remodelling of the pulmonary vasculature due to imbalances in vasoactive signalling, inflammation and inappropriate vascular smooth muscle cell proliferation, resulting in increased pulmonary pressure, right sided ventricular hypertrophy, and ultimately heart failure and death (Morrell *et al.*, 2009). In animal models of PAH, both ELA and apelin are downregulated (Chandra *et al.*, 2011; P. Yang *et al.*, 2017b), although some expression of apelin receptor is maintained. A similar phenotype is seen in PAH patients, with isolated cultured primary pulmonary artery endothelial cells found to produce less apelin than healthy donor controls (J. Kim *et al.*, 2013), and reduced plasma levels of apelin and ELA seen (P. Yang *et al.*, 2017b). Furthermore, apelin receptor KO mice develop more severe hypoxia induced PAH (Chandra *et al.*, 2011).

Concurrently, intravenous administration of [Pyr^{1}]apelin-13 in a rat model of monocrotaline (MCT)-induced PAH reduced detrimental vascular remodelling, right ventricular fibrosis and hypertrophy (Falcão-Pires *et al.*, 2009). In the same model, ELA-32 administration significantly attenuated right ventricular hypertrophy (P. Yang *et al.*, 2017b). Notably, an apelin receptor G-protein biased agonist MM07 (described further below) reduced right ventricular pressure and detrimental hypertrophy in a Sugen/hypoxic rat model of PAH (Davenport *et al.,* 2020). The Sugen/hypoxic model is considered to be one the best PAH models, as it generates severe disease and recapitulates the main pathologies seen in human patients in a short timeframe (Bogaard *et al.*, 2020). These studies therefore highlight the potential of targeting the apelin receptor for the treatment of PAH, which was recently validated in human patients. In an acute, double blind, randomised crossover clinical study, significant improvement in cardiac output and decrease in pulmonary vascular resistance was observed in PAH patients treated with intravenous [Pyr^{1}]apelin-13 (Brash *et al.*, 2018). Given that the half-life of [Pyr^{1}]apelin-13 *in vivo* is only a few minutes (Japp *et al.*, 2008), these results are particularly striking.

1.6.6 The apelin receptor in arrhythmia

Excitation-contraction coupling is a key concept in cardiac function, in which the cardiac action potential induces controlled opening and closing of voltage gated ion channels, promoting tightly regulated ion fluxes (Priest and McDermott, 2015). This results in an increase in intracellular calcium, which is free to interact with the contractile machinery, resulting in muscle contraction (Bers, 2002). In the heart, conduction of the cardiac action potential through the myocardium is essential for correct contraction, with electrical coupling mediated by gap junctions between neighbouring cardiomyocytes. The precise and coordinated response to electrical excitation is critical for cardiac contraction, and any disruption has the potential to lead to detrimental arrhythmias (Tse, 2016), which can have devastating consequences including sudden death (Koplan and Stevenson, 2007).

The role of the apelin receptor in arrhythmic disease has been poorly studied. However, plasma apelin levels are consistently reduced in atrial fibrillation patients (Ellinor *et al.*, 2006; Kallergis *et al.*, 2010). Interestingly, cardiac resynchronisation and electrical cardioversion therapy can restore plasma apelin levels (Francia *et al.*, 2007; Kallergis *et al.*, 2010), suggesting a link between cardiac voltage signalling, rhythm control and apelin receptor signalling.

1.7 Targeting the Apelin Receptor Therapeutically

The apelin receptor has emerged as a potential therapeutic target for the treatment of cardiovascular disease, particularly heart failure and PAH, due to its beneficial vasodilatory, inotropic and cardioprotective effects (Z. Wang *et al.*, 2015; Zhong *et al.*, 2017; Read *et al.*, 2019). As described above, studies have shown the ability of the endogenous apelin and ELA agonists to improve disease symptoms in a range of conditions. However, the application of the endogenous peptide is limited for two main reasons. Firstly, the peptides have a very limited plasma half-life (~5-8 minutes), resulting from degradation by circulating endogenous peptidases (Zhen *et al.*, 2013; Murza *et al.*, 2016). Several apelin isoforms have been shown to undergo cleavage by angiotensin converting enzyme 2 (ACE2) (W. Wang *et al.*, 2016; P. Yang *et al.*, 2017a). However, ACE2 mediated cleavage of [Pyr^{1}]apelin-13 produces [Pyr^{1}]apelin-13$_{(1\text{-}12)}$, which was found to bind apelin receptor and had significant biological effects

in both rats and humans *in vitro* and *in vivo*, promoting similar levels of vasodilatation as [Pyr^{1}]apelin-13 upon infusion into healthy volunteers (P. Yang *et al.*, 2017a). Despite the limited half-lives, the native ligands can still have pronounced effects *in vivo*, such as the significant decrease in pulmonary pressure and increase in cardiac output observed in PAH patients treated with intravenous [Pyr^{1}]apelin-13 (Brash *et al.*, 2018). Nevertheless, the plasma instability of the endogenous peptides mean their therapeutic application is limited, and modified versions with enhanced stability are needed.

Furthermore, peptide drug use is limited by their delivery. Oral delivery is the preferred mechanism for drug delivery, as this is non-invasive and promotes patient compliance due to ease and convenience (Alqahtani *et al.*, 2021). However, peptides tend to be unsuitable for oral delivery, due to limited gut absorption and degradation, and therefore tend to be delivered intravenously or subcutaneously (Bruno *et al.*, 2013). Hence, it would be beneficial to develop small molecule agonists, suitable for oral delivery.

As a result, a number of methods have been employed to develop novel peptide analogues or small molecule agonists with improved stability, efficacy and delivery methods compared to the natural receptor ligands. For example, PEGylation has been shown to promote apelin stability, resulting in the maintenance of the inotropic effects for 70 minutes longer than that seen for apelin-36 peptide infusion (Z. Q. Jia *et al.*, 2012). Furthermore, stability can be improved by introducing unnatural amino acids. For example, by introducing modifications to protect the C-terminal phenylalanine, ACE2 mediated cleavage of apelin was much decreased (W. Wang *et al.*, 2016). Additionally, three potent apelin peptide analogues with improved pharmacokinetic properties and reduced neprilysin degradation were produced by introducing modifications to the ‘RPRL’ region essential for neprilysin proteolysis (McKinnie *et al.*, 2017).

Despite the advances in plasma stability seen for peptide analogues, the development of oral apelin receptor small molecule agonists have a greater therapeutic potential. There have been a number of attempts to generate apelin receptor small molecule agonists, however success has been limited so far (Zhong *et al.*, 2017). Recently, screening of ~100 compounds identified a small molecule scaffold, designated

compound 1. By modifying side chain sites within the scaffold, 4 compounds were identified which displayed relatively low micromolar potencies (Narayanan *et al.*, 2016). This study provides proof of principle for small molecule apelin receptor agonists, but further work is need to improve available small molecule compounds. Recently, as described above, three small molecule apelin receptor agonists have been developed with subnanomolar potencies, which were shown to have beneficial effects *in vitro* and *in vivo*, including in disease states (Ason *et al.*, 2020; Gargalovic *et al.*, 2021).

1.7.1 Biased compounds at the apelin receptor

For the clinical application of targeting the apelin receptor, long term agonist administration may lead to receptor desensitisation, associated with β-arrestin mediated receptor internalisation, resulting in a loss of therapeutic efficacy (P. Yang *et al.*, 2015) (Figure 1.5).

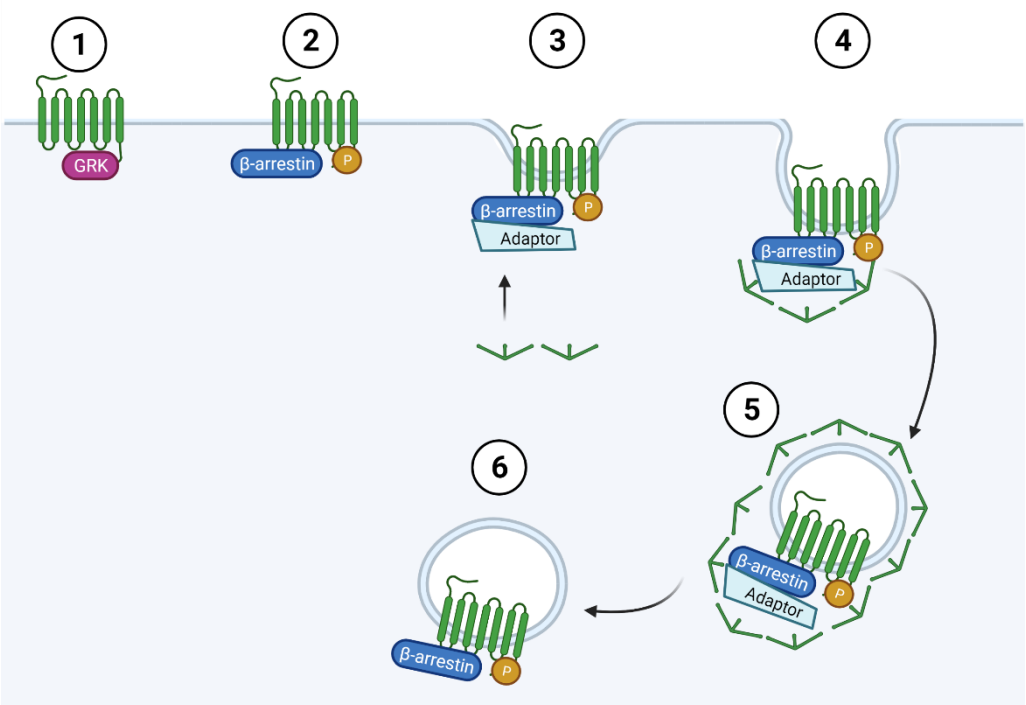

Figure 1.5: Simplified model of β-arrestin dependent GPCR internalisation. (1) GPCR kinase (GRK) binds to agonist-activated GPCR. (2) Phosphorylation (P) by GRK promotes β-arrestin translocation and binding to receptor. (3) β-arrestin acts to recruit adaptor proteins, (4) promoting assembly of clathrin coated pits. (5) Clathrin-mediated endocytosis occurs, and vesicles are formed containing the phosphorylated GPCR and associated β-arrestin. (6) Clathrin disassembles and the receptor can then either be recycled back to the plasma membrane or β-arrestin can interact with a range of other signalling molecules within the cell activating further signalling pathways. This figure was created using Biorender.com.

Several studies have therefore reported the generation of apelin receptor biased agonists, designed to activate the beneficial G-protein mediated effects, without inducing β-arrestin signalling. The Davenport group has developed the cyclic apelin peptide MM07, which preferentially activates G-protein signalling and is two-fold less potent in β-arrestin assays compared to native peptide. MM07 was found to induce an increase in human forearm blood flow, with a maximum dilation twice as high as that for [Pyr^{1}]apelin-13. Crucially, upon repeated dosing of MM07, the effects on blood flow were retained. Furthermore, in a rat model, MM07 infusion induced a significantly increased cardiac output compared to [Pyr^{1}]apelin-13 (Brame *et al.*, 2015). These results highlight the potential for preferentially stimulating the apelin receptor G-protein signalling pathway to improve clinical efficacy. However, MM07 is a peptide, and thus is limited by its oral bioavailability. The Davenport group has therefore also developed

a small molecule biased agonist known as CMF-019, which displayed improved half-life *in vivo* compared with native peptide (Read *et al.*, 2016). Again, CMF-019 was found to promote positive inotropy and dose-dependent vasodilatation *in vivo* without receptor desensitisation (Read *et al.*, 2020). This small molecule therefore could be used as starting point for the design of novel therapeutic compounds for conditions such as heart failure and PAH.

Furthermore, overexpression of the apelin receptor in mouse cardiomyocytes induced contractile dysfunction and cardiac hypertrophy (Murata *et al.*, 2016). As discussed above, the apelin receptor appears to function as a dual receptor, responding both to ligand interaction and stretch (Seo *et al.*, 2020). β-arrestin knockdown inhibits the stretch-mediated apelin receptor response, and prevents induction of hypertrophy (Scimia *et al.*, 2012). Therefore, biased agonists would have a further benefit in heart failure, inducing preferential activation of the beneficial G-protein signalling to promote inotropy and cardioprotective effects, without inducing β-arrestin signalling and associated hypertrophic response. Supporting this, MM07 was found to significantly reduce right ventricular remodelling and associated hypertrophy in a rat model of MCT induced PAH (P. Yang *et al.*, 2019).

1.8 Identifying Disease Modifying Variants in the Apelin Receptor

The apelin receptor has a key role in cardiovascular development and physiology. Hence, genetic variants in the apelin receptor gene have the potential to disrupt apelin receptor function, leading to pathophysiology. It would therefore be beneficial to identify and investigate disease associated genetic variants in the apelin receptor.

1.8.1 The 100,000 Genomes Project

In recent years, the dramatic fall in costs associated with whole genome sequencing (WGS) and the improvement in data analysis have resulted in a huge increase in the use of sequencing data for the identification and diagnosis of rare diseases (Boycott *et al.*, 2017; Splinter *et al.*, 2018). However, standard testing still fails to identify the molecular basis of disease for a large number of patients in the UK. Therefore, the 100,000 Genomes Project (Genomics England) was launched in 2013, to whole

genome sequence 100,000 genomes from NHS patients with rare diseases or cancer (Turnbull *et al.*, 2018; 100,000 Genomes Project Pilot Investigators, 2021). The project aims to provide clinical diagnosis, as well as wider scientific insights, in the hope that this will lead to development of new, more effective treatments and the implementation of genomic medicine within the NHS, resulting in patient benefit (Caulfield *et al.*, 2017).

1.8.2 The NIHR BioResource BRIDGE Project

A sub-study of the 100,000 Genomes Project known as the NIHR BioResource Rare Diseases BRIDGE consortium has combined the sequencing data of 13 Rare Disease projects in attempt to identify variants associated with unresolved inherited genetic disorders (Turro *et al.*, 2020). The project has analysed the sequencing data of patients presenting with varied diseases, including cardiovascular and bleeding disorders. Using case-control analysis of WGS in 7,423 subjects with rare diseases, ~50 variants in the apelin receptor have been identified (Gräf *et al.*, 2018). The Davenport group has selected 11 variants for further study (see Section 7 for details), and aims to determine the effects of the identified variants in cell based-models, in an attempt to understand any contribution to disease pathogenesis.

1.9 Project Hypothesis and Aims

The apelin receptor and its ligands appear to have an important role in cardiovascular development and disease, however the mechanism by which it exerts these effects and the cellular consequences are unclear.

Therefore, the hypothesis of this thesis was that (1) reduced apelin receptor signalling from the onset of differentiation is detrimental for the resulting hESC-CMs, and (2) knockdown of the apelin receptor in differentiated hESC-CMs has functional consequences on contractility.

The use of a human based model system for investigating the apelin receptor in cardiomyocyte function provides more clinically relevant results, which could lead to the development of therapeutic strategies targeting the apelin receptor. By utilising hESC-CMs, this provides a system that can generate large numbers of cardiomyocytes which can be maintained in culture, meaning functional screening and

characterisation can be performed. hESC-CMs also provide a platform to allow the investigation as to whether or not there is a cardiomyocyte-autonomous role for the apelin receptor during development, a question that is currently unanswered. Furthermore, hESCs are amenable to genetic editing, allowing manipulation of the apelin receptor and subsequent investigation into the effects of genetic changes on hESC-CM function.

The first aim of the study was to determine if hESCs and hESC-CMs express a functioning apelin signalling system. Following on, the second aim was to generate an apelin receptor inducible knockdown system in hESC-CMs, providing a platform to determine the effects of loss of apelin receptor signalling on cardiomyocyte development and function, by inducing knockdown at defined time points. Finally, the project also aimed to use single base editing technology to introduce an apelin receptor genetic variant identified from the NIHR BRIDGE project, and to characterise the effects of the genetic change on hESC-CM differentiation and function. Results generated in the hESC-CM model can be extrapolated to give an indication of apelin receptor function in human cardiomyocytes *in vivo*.

2. Materials and Methods

2.1 Materials

The reagents and materials used in the project are detailed in Table 2.1.

Reagent/Material/Equipment	Supplier	Cat. #
Cells		
H9 hESCs	WiCell	WA09
CHO-K1 cells	ECACC	CCL-61
HEK293T cells	ATCC	CRL-3216
HS-27A	ATCC	CRL-2496
Media/Cell Culture		
Dulbecco's Phosphate Buffered Saline (PBS), no calcium, no magnesium	ThermoFisher	14190-094
Water for embryo transfer	Sigma Aldrich	RNBJ2804
Gelatin from porcine skin	Sigma Aldrich	9000-70-8
Vitronectin XF	STEMCELL Technologies	7180
Matrigel	Corning	354234
Collagenase IV	ThermoFisher	17104019
ReLeSR	STEMCELL Technologies	5872
TryPLE Express	ThermoFisher	12604-021
DMEM F12	ThermoFisher	31330-038
Advanced DMEM F12	ThermoFisher	12634-028
IMDM	ThermoFisher	21980-065
Ham's F-12 Nutrient Mix	ThermoFisher	21765029
DMEM no glucose, no sodium pyruvate	ThermoFisher	11966025
DMEM F12 for CHO-K1 culture	ThermoFisher	11320033
RPMI	ThermoFisher	21875091
B27 plus insulin	ThermoFisher	17504044
Knockout serum replacer (KSR)	ThermoFisher	A3181502
Transferrin	R&D Systems	3188-AT-001G
Insulin	Sigma Aldrich	11376497001
Monothioglycerol	Sigma Aldrich	M6145
Chemically defined concentrated lipids	ThermoFisher	11905031
Bovine serum albumin	Europa Bio Products	EQBAH
Penicillin-Streptomycin	ThermoFisher	15140122
Foetal bovine serum (FBS)	ThermoFisher	10500064
Normocin Antimicrobial Reagent	InvivoGen	ant-nr-1
L-Glutamine	ThermoFisher	25030081

β-mercaptoethanol	Sigma Aldrich	M3148
Insulin-transferrin-selenium	ThermoFisher	41400045
Sodium bicarbonate	ThermoFisher	25080094
L-Ascorbic acid 2-phosphate	Sigma Aldrich	A8960
MEM non-essential amino acids	ThermoFisher	11140035
Sodium L-Lactate	Sigma Aldrich	L7022-10G
Trypan Blue Solution	ThermoFisher	T10282
DNase I (tissue culture)	New England BioLabs	M0303
Polydimethylsiloxane	Dow	1024001
Pluronic F-127	Sigma Aldrich	P2443
10X RPMI-1640	Sigma Aldrich	R1145
NaOH	Fisher Scientific	J/7620/15
Geltrex	Fisher Scientific	A1413202
Collagen I Rat Protein	ThermoFisher	A1048301
HEPES	Sigma Aldrich	H3375
Cytokines		
Fibroblast Growth Factor 2 (FGF2)	Qkine Ltd	Qk027
Activin-A	Qkine Ltd	Qk005
Transforming Growth Factor-β	Bio-Techne	100-B
Rho-associated protein kinase (ROCK) inhibitor (Y27632)	Insight Biotech	sc-281642A
Ly2904002	Stratech	A8250-APE
Bone Morphogenetic Protein 4 (BMP4)	R&D Systems	314-BP
Retinoic Acid	Sigma Aldrich	R2625
IWR1-endo	Tocris	3532/10
Molecular Biology		
GenElute Total RNA Purification Kit	Sigma Aldrich	RNB100
Nuclease Free Water	QIAGEN	129114
Reverse Transcription System	Promega	A3500
TaqMan Gene Expression Assay Master Mix	Applied Biosystems	4369016
Fast SYBR Green Master Mix	ThermoFisher	4385614
Isoprenaline	Sigma Aldrich	I-2760
Acetylcholine	Sigma Aldrich	A-6625
[Pyr^{1}]apelin-13	Severn Biotech	Custom order
ELA	Severn Biotech	Custom order
Apelin-12 (Human, Rat, Mouse, Bovine) EIA kit	Phoenix Pharmaceuticals	EK-057-23
[pGlu^{1}]-ELA-32 (Human) EIA Kit	Phoenix Pharmaceuticals	EK-007-19
DharmaFECT 1 Transfection Reagent	Horizon	T-2001
Opti-MEM I Reduced Serum Media	ThermoFisher	31985062

pAAV-Puro_siKD	Addgene plasmid #86695; http://n2t.net/addgene:86695; RRID:Addgene_86695	-
BglII FastDigest Restriction Enzyme	ThermoFisher	FD0083
SalI FastDigest Restriction Enzyme	ThermoFisher	FD0644
FastDigest Green Buffer	ThermoFisher	B72
UltraPure Agarose	ThermoFisher	16500100
QIAEX II Gel Extraction Kit	QIAGEN	20021
3 M Sodium Acetate pH 5.5	ThermoFisher	AM9740
Tris-HCl	ThermoFisher	15567-027
UltraPure 0.5M EDTA, pH 8.0	ThermoFisher	15575020
NaCl	Fisher Scientific	7647-14-5
T4 DNA Ligase	New England BioLabs	M0202
T4 Ligase Buffer	New England BioLabs	B0202S
α-Select Gold Efficiency Chemically Competent Cells	Bioline	BIO-85027
SOC medium	Fisher Scientific	15544034
Lysogeny Broth (LB)	Sigma Aldrich	L3022
Agar	Fluka	05040
Ampicillin	Sigma Aldrich	A9393
GenElute Plasmid Miniprep Kit	Sigma Aldrich	PLN70-1KT
LongAmp Taq DNA Polymerase kit	New England BioLabs	E5200S
Plasmid Plus Midi Kit	QIAGEN	12941
Lipofectamine 2000	ThermoFisher	11668019
Puromycin	Sigma Aldrich	P8833
GenElute Mammalian Genomic DNA Miniprep Kit	Sigma Aldrich	G1N70
Tetracycline Hydrochloride	Sigma Aldrich	T8032
TRIzol	ThermoFisher	15596026
Chloroform	Macron Fine Chemicals	4444-25
Isopropanol (Molecular Grade)	Sigma Aldrich	I9516
TapeStation RNA ScreenTape Assay	Agilent	5067-5576
NEBNext rRNA Depletion Kit (Human/Mouse/Rat)	New England BioLabs	E6310
CORALL Total RNA-Seq Library Prep Kit	Lexogen	095.24
AMPure XP PCR Purification Beads	Beckman Coulter	A63880
ACRTURUS PicoPure RNA Isolation Kit	ThermoFisher	KIT0204
Lysing Matrix D Beads	MP Biomedicals	116913100
RNase-Free DNase Set	QIAGEN	79254

pGL3-U6-sgRNA-PGK-puromycin	Addgene plasmid # 51133; http://n2t.net/addgene:51133; RRID:Addgene_51133)	-
pCMV_BE4max	Addgene plasmid # 112093 ; http://n2t.net/addgene:112093 ; RRID:Addgene_112093	-
T4 Polynucleotide Kinase	New England BioLabs	M0201
Tango Buffer	ThermoFisher	BY5
DTT (0.1 mM)	ThermoFisher	Y00122
ATP (10 mM)	New England BioLabs	9804
BsaI FastDigest Restriction Enzyme	ThermoFisher	FD0293
10X PlasmidSafe Buffer	CamBio	E3101K
PlasmidSafe ATP-dependent DNase	CamBio	E3101K
Q5 High Fidelity DNA Polymerase PCR Kit	New England BioLabs	E0555
TransIT-LT1	Mirus Bio	MIR 2300
QIAquick PCR Purification Kit	QIAGEN	28104
NEBuffer 2	New England BioLabs	B7002S
T7 Endonuclease I	New England BioLabs	M0302
P3 Primary Cell 4D-Nucleofector X Kit	Lonza	V4XP-3024
CloneR	STEMCELL Technologies	05888
SYBR Safe DNA Gel Stain	ThermoFisher	S33102
DNA Gel Loading Dye (6X)	Fisher Scientific	R0611
Ethanol (Molecular Grade)	Sigma Aldrich	51976
Staining, Immunocytochemistry and Flow Cytometry		
4% Paraformaldehyde	ThermoFisher	J61899
Goat Serum	Sigma Aldrich	G9023
Triton X-100	Sigma Aldrich	X100
Tween 20	Fisher Scientific	BP337
DAPI nuclear dye	ThermoFisher	62248
Hoescht 3342 Nuclear Stain	ThermoFisher	H3570
BD Cytofix/Cytoperm Fixation/Permeabilization Kit	BD Biosciences	554714
CD90 (Thy-1) Monoclonal Antibody (eBio5E10 (5E10)), PE, eBioscience™	ThermoFisher	12-0909-42
Anti-Cardiac Troponin T-APC	Miltenyi BioTech	130-120-54300
Ethidium Homodimer-1 (EthD-1)	ThermoFisher	E1169
NucBlue Live ReadyProbes Reagent	ThermoFisher	R37605

CellCarrier-96 Black, Optically Clear Bottom plates	Perkin Elmer	6055302
Hanks Balanced Salt Solution	Sigma Aldrich	55037C
Fluorescently tagged apelin647	Cambridge Research Biochemicals	Custom Order
Phalloidin-iFluor 488	Abcam	23115-AAT
FluoVolt Membrane Potential Kit	ThermoFisher	F10488
LabCam for iPhone 7/8/SE2 Adaptor	iDu Optics LabCam	-
Fluo-4, AM	ThermoFisher	F14201
Sucrose	Fisher Scientific	57-50-1
Tissue Tek OCT	Sakura Fintek	4583
$CaCl_2$ for Tyrode's Solution	Sigma	C3306
$MgCl_2$ for Tyrode's Solution	Fisher	BP214
KCl for Tyrode's Solution	Fisher	P/4240/53
NaCl for Tyrode's Solution	VWR Chemicals	7647
NaH_2PO_4 for Tyrode's Solution	Sigma	71505
HEPES for Tyrode's Solution	Sigma	H4034
Glucose for Tyrode's Solution	Sigma Aldrich	G7528
Radioligand Binding		
NaOH	Fisher Scientific	J/7620/15
Sodium Dodecyl Sulphate (SDS)	Sigma Aldrich	151-21-3
DC Protein Assay	Bio-Rad	5000111
Sigmacote	Sigma Aldrich	SL2
TRIZMA Base for Binding Buffer	Sigma Aldrich	T6066
$MgCl_2$ for Binding Buffer	Sigma Aldrich	104-20
[^{125}I]apelin-13	Perkin Elmer	Custom order
[Pyr^{1}]apelin-13	Severn Biotech	Custom order
Equipment		
Countess Automated Cell Counter	Invitrogen	-
Nanodrop 1000	ThermoFisher	-
ABI 7500 Real-Time PCR System	Applied Biosystems	-
LSM 700 Confocal Microscope	Zeiss	-
EVOS FL Cell Imaging System	Invitrogen	-
LSRFortessa Cell Analyzer	BD Biosciences	-
FLUOstar Omega Microplate Reader	BMG Labtech	-
COBRA 5003 Gamma Counter	Packard	-
Opera Phenix High-Content Screening System	Perkin Elmer	-
2100 BioAnalyzer	Agilent	-
HiSeq2500 Next Generation Sequencing System	Illumnia	-

C-Pace EM	IonOptix	-
Axio Observer A1 Inverted Phase Contrast Fluorescence Microscope	Zeiss	-
Cryostat	Bright Instruments	-
LSM880 Multiphoton Microscope	Zeiss	-
FastPrep-24 5G Instrument	MP Biomedicals	-
Amaxa 4D Nucleofector	Lonza	-
CKX41 Brightfield Microscope	Olympus	-

Table 2.1: Details of the materials used in the project, with supplier and catalogue number.

2.2 Cell Culture

All cells were maintained in a humidified atmosphere containing 5% CO_2 at 37°C.

2.2.1 H9 hESCs on gelatin/MEF media plates

Pluripotent, undifferentiated H9 hESCs were maintained as colonies in culture on gelatin/MEF media (Table 2.2) coated 6-well plates in chemically defined medium (CDM-BSA, Table 2.2), supplemented with Fibroblast Growth Factor 2 (FGF2, 12 ng/ml) and Activin-A (10 ng/ml) (maintenance media) with daily media change. Confluent H9s were washed with PBS, and collagenase (Table 2.2) was added for 3 minutes to detach cells. Collagenase was then aspirated and maintenance media added, before cells were scraped, triturated and collected. Cells were allowed to settle to the bottom of the collection tubes then media was aspirated and cells resuspended as small colonies. H9 colonies were plated in pre-prepared gelatin/MEF media coated 6-well plates in 2 ml of maintenance media. To produce gelatin/MEF plates, 1.5 ml of 0.1% gelatin in PBS was added per well for 20 minutes at room temperature (RT). Gelatin was aspirated and 2 ml/well of MEF media added and incubated at 37°C for at least 24 hours.

2.2.2 H9 hESCs on vitronectin coated plates

For some experiments, pluripotent, undifferentiated H9 hESCs were maintained as colonies in culture on Vitronectin XF coated 6-well plates in Essential 8 (E8) media

(Table 2.2), supplemented with FGF2 (24 ng/ml) and Transforming Growth Factor-β (TGF-β, 1.74 ng/ml) (E8 complete) with daily media change. Confluent H9s were washed with PBS, ReLeSR added for 30 seconds then aspirated and cells left for 3 minutes until a film formed. E8 media was added and cells were sprayed, triturated and collected. Cells were allowed to settle to the bottom of the collection tubes then media was aspirated and cells resuspended as small colonies. H9 colonies were then plated in pre-prepared Vitronectin XF coated 6-well plates in 1.5 ml of E8 media. To produce Vitronectin XF plates, 1 ml of 10 µg/ml Vitronectin XF diluted in PBS was added per well and incubated for 1 hour at RT.

2.2.3 HEK293T cells

HEK293T cells were cultured in gelatin coated T75 flasks in MEF media (Table 2.2), with media refreshed every other day. Once confluent, cells were washed with PBS and TryPLE Express added and incubated at 37°C for 3 minutes. MEF media was added for neutralisation and cells triturated to a single cell suspension and collected. Cells were pelleted by centrifugation at 300 xg for 3 minutes, resuspended in an appropriate volume of MEF media and replated in a new pre-prepared gelatin coated T75 flask. T75 flasks were prepared by adding 5 ml of 0.1% gelatin in PBS and incubating for 20 minutes at RT.

2.2.4 CHO-K1 cells

CHO-K1 cells were cultured in T175 flasks in DMEM F12 containing L-glutamine, and supplemented with 10% FBS and 0.1 mg/ml Normocin antimicrobial reagent. Media was refreshed every other day and cells were passaged using trypsin when confluence was reached.

2.2.5 HS-27A cells

HS-27A cells were maintained on gelatin coated 6-well plates in MEF media, with media refresh every other day. Upon reaching confluence, cells were washed with PBS and trypsinised. Following neutralisation, cells were triturated to single cells and collected before pelleting by centrifugation (300 xg for 3 minutes). Cells were

resuspended in fresh MEF media and plated in pre-prepared gelatin coated 6-well plates. Gelatin coated 6-well plates were prepared by adding 1.5 ml/well 0.1% gelatin in PBS and incubating for 20 minutes at RT.

Medium	**Components**	**Concentration**
CDM-BSA	IMDM:F12 (1:1)	-
	Transferrin	15 µg/ml
	Insulin	7 µg/ml
	Monothioglycerol	450 mM
	Chemically defined concentrated lipids	1%
	Bovine Serum Albumin	5 mg/ml
	Penicillin-Streptomycin	100 U/ml
MEF Medium	Advanced DMEM F12	-
	Foetal Bovine Serum (FBS)	10%
	L-Glutamine	1%
	β-mercaptoethanol	100 µM
	Penicillin-Streptomycin	100 U/ml
Essential 8 Medium	DMEM F12	-
	Insulin-transferrin-selenium	20 mg/ml – 11 mg/ml – 13.4 ng/ml
	Sodium bicarbonate	0.05 %
	L-Ascorbic acid 2-phosphate	7 µM
	Penicillin-Streptomycin	100 U/ml
Lactate Select Medium	DMEM no glucose, no sodium pyruvate	-
	MEM Non-Essential Amino Acids	1X
	Sodium L-lactate dissolved in HEPES	4 mM
Gelatin	Embryo transfer water	-
	Gelatin from porcine skin	0.1%
Collagenase	Advanced DMEM/F12	-
	Knockout serum replacer (KSR)	20%
	L-Glutamine	1%
	Collagenase IV	1 mg/ml

Table 2.2: Composition of media used for cell culture.

2.3 Cardiomyocyte Differentiation and Maintenance

H9 hESCs were induced to differentiate to cardiomyocytes following a previously optimised protocol (adapted from Mendjan *et al*., 2014) as detailed below.

2.3.1 Plating for differentiation

Confluent H9 hESCs in 6-well plates were washed with PBS, and cells were dissociated with 750 µl of TrypLE Express per well, incubated for 3 minutes at 37°C. TrypLE Express was neutralised with CDM-BSA, and cells collected as a single cell suspension. A small volume of cells was then mixed with 0.4% Trypan Blue Solution (1:1) and cells counted using a Countess Automated Cell Counter (Invitrogen). Cells were then centrifuged for 3 minutes at 300 xg, resuspended to the desired concentration (8×10^5/well) in CDM-BSA supplemented with FGF2 (12 ng/ml), Activin-A (30 ng/ml) and Rho-associated protein kinase inhibitor (ROCKi, 10 µM) and plated on Matrigel-coated 6-well plates. To produce Matrigel-coated plates, Matrigel was diluted in Advanced DMEM F12 according to manufacturer's recommendation, 2 ml added per well and incubated for one hour at RT.

2.3.2 Mesoderm induction

After around 4 hours of incubation at 37°C to allow for cell attachment, mesoderm induction was initiated. Media was aspirated and cells treated with 2 ml per well of CDM-BSA supplemented with FGF2 (20 ng/ml), Ly294002 (phosphoinositide 3-kinase inhibitor, 10 µM), Activin-A (50 ng/ml) and Bone Morphogenetic Protein 4 (BMP4, 10 ng/ml). This mesodermal induction media is referred to as FLyAB media subsequently.

2.3.3 Differentiation to cardiac progenitors

After 42 hours incubation at 37°C, FLyAB media was removed, and cells washed with PBS. Media was replaced with 2 ml per well of CDM-BSA supplemented with FGF2 (8 ng/ml), BMP4 (10 ng/ml), retinoic acid (1 µM) and the WNT signalling pathway inhibitor IWR1-endo (1 ng/ml) (FBRI media). After 48 hours FBRI media was refreshed. After a further 48 hours, cells were washed with PBS and media was

changed to 2 ml per well of CDM-BSA supplemented with FGF2 (8 ng/ml) and BMP4 (10 ng/ml) subsequently referred to as FB media.

2.4.4. Initiation of spontaneous contraction

After 2 days, FB media was removed, and cells washed with PBS. 2 ml per well of CDM-BSA was added. hESC-derived cardiomyocytes were maintained in CDM-BSA media, with media changes every other day until the commencement of beating.

2.4.5 Metabolic selection

At least 14 days after differentiation initiation, and once strong beating was established, media was aspirated and cardiomyocytes washed with PBS. 750 µl of TryPLE per well was added and incubated for 10 minutes at 37°C. TrypLE was neutralised with 1 ml of CDM-BSA supplemented with DNase I (5 µg/ml) to prevent hESC-CMs from clumping. Cardiomyocytes were collected and centrifuged at 300 xg for 3 minutes. Following centrifugation, media was aspirated and cells resuspended in CDM-BSA. Cells were then replated 1:1 in Matrigel-coated 6-well plates in CDM-BSA supplemented with ROCKi (10 µM) to promote survival. Cells were incubated overnight to allow adherence and recovery before transferring to lactate selection media (Table 2.2) for 3 days with one media refresh, in order to generate a pure population of cardiomyocytes. After 72 hours, media was changed to CDM-BSA and refreshed every second day.

2.4 Analysis of Gene Expression by qRT-PCR

2.4.1 RNA isolation

RNA extraction was performed using the GenElute Total RNA Purification Kit. Briefly, cells were lysed in 350 µl of RNA lysis buffer and RNA was precipitated with an equal volume of 70% ethanol. Samples were transferred to GenElute Columns for RNA binding, washing, and elution. Samples were eluted in 30 µl Nuclease Free Water, with RNA concentration determined using a NanoDrop 1000 (ThermoFisher).

2.4.2 Reverse transcription

cDNA was produced from 1 µg of RNA using the Promega Reverse Transcription System in a 20 µl reaction following manufacturer's recommendation. To 1 µg RNA, 1 µl of each of Random Primers and Oligo(dT)15 primers were added, made up to 11.9 µl with nuclease free water and incubated at 70°C for 10 minutes. A mastermix containing 4 µl $MgCl_2$ (25 mM), 2 µl Reverse Transcription 10X Buffer, 2 µl dNTPs (10mM), 0.5 µl Recombinant RNasin Ribonuclease Inhibitor and 0.6 µl AMV Reverse Transcriptase per sample was made and 9.1 µl added to each. Samples were then run on a thermocycler (Table 2.3).

Temperature	**Time**
22°C	5 min
40°C	60 min
95°C	5 min
4°C	5 min
4°C	Forever

Table 2.3: Thermocycler programme for reverse transcription reaction.

2.4.3 qRT-PCR

Quantitative real-time polymerase chain reaction (qRT-PCR) was performed for 45 cycles using the ABI 7500 Real-Time PCR System (Applied Biosystems) to analyse mRNA expression using 96-Well TaqMan Gene Expression Assays or SYBR Green Based Assays with primer sequences shown in Table 2.4. Human *18S* rRNA or *GAPDH* were used as house-keeping genes, owing to their stable expression level across cells used. Relative expression was normalised to housekeeping gene expression using the $2^{(-\Delta CT)}$ or the $2^{(-\Delta\Delta CT)}$ method (Schmittgen and Livak, 2008). CT values over 36 were excluded as non-specific amplicon.

Target	Assay Type	Primer Sequence or ID	Acquired From
GAPDH	SYBR Green	FOR: AACAGCCTCAAGATCATCAGC REV: GGATGATGTTCTGGAGAGCC	Sigma Aldrich
SOX2	SYBR Green	FOR: ATGCACCGCTACGACGTGA REV: CTTTTGCACCCCTCCCATTT	Sigma Aldrich
POU5F1	SYBR Green	FOR: AGGGCAAGCGATCAAGCA REV: GGAAAGGGACCGCGGAGTA	Sigma Aldrich
TNNT2	SYBR Green	FOR: CCCAATGGAGGAGTCCAAAC REV: CCCGACGTCTCTCGATCC	Sigma Aldrich
ATP2A2	SYBR Green	FOR: TACCTGGAACCTGCAATACTGG REV: TGCACAGGGTTGGTAGATGTG	Sigma Aldrich
RYR2	SYBR Green	FOR: ACAACAGAAGCTATGCTTGGC REV: GAGGAGTGTTCGATGACCACC	Sigma Aldrich
MYH6	SYBR Green	FOR: GCCCTTTGACATTCGCACTG REV: GGTTTCAGCAATGACCTTGCC	Sigma Aldrich
ACTN1	SYBR Green	FOR: TCAACCACTTTGACCGGGAT REV: GCAAATTCTGCTTCTCCCTGG	Sigma Aldrich
MYL7	SYBR Green	FOR: CCGTCTTCCTCACGCTCTT REV:TGAACTCATCCTTGTTCACCAC	Sigma Aldrich
18S	TaqMan	Hs99999901_s1	ThermoFisher
APLNR	TaqMan	Hs00270873_s1	ThermoFisher
APLN	TaqMan	Hs00175572_m1	ThermoFisher
APELA	TaqMan	Sense: GAAGAAGAAGAGGAGTGAAGGA Antisense: CCATTCCAGGTGCTTTCAAAT	Primer Design
MESP1	SYBR Green	FOR: GAAGTGGTTCCTTGGCAGAC REV: TCCTGCTTGCCTCAAAGTGT	Sigma Aldrich
NKX2-5	SYBR Green	FOR: AGCCGAAAAGAAAGAGCTGTGCG REV: GACCTGCGCCTGCGAGAAGAG	Sigma Aldrich
TBXT	SYBR Green	FOR: TGCTTCCCTGAGACCCAGTT REV: GATCACTTCTTTCCTTTGCATCAAG	Sigma Aldrich
THY1	SYBR Green	FOR: TCCCGAACCAACTTCACCAG REV: ACCAGTTTGTCTCTGAGCACT	Sigma Aldrich

Table 2.4: Primer sequences or IDs used for qRT-PCR.

2.5 Immunocytochemistry

For immunocytochemistry, cells were washed with PBS, fixed with 4% paraformaldehyde for 20 minutes at RT, and then washed twice with PBS. Cells were then blocked for 1 hour at RT in either 5% serum of the same species that the secondary antibody was raised in, or 3% BSA in PBS. Depending on protein of interest, cells were permeabilised during this 1 hour incubation by the addition of 0.5% Triton-X. Primary antibody was diluted to the desired concentration (Table 2.5) in either 3% serum in PBS/Tween (PBS/T) or 3% BSA plus 0.5% Triton-X in PBS, and incubated overnight at 4°C. The following day, cells were subjected to three 5 minute washes with PBS, at RT. Secondary antibody was diluted to the desired concentration (Table 2.5) in either 3% serum in PBS/T or 3% BSA plus 0.5% Triton-X in PBS, and incubated for 1 hour at RT in the dark. DAPI nuclear dye was included at a concentration of 1:10,000 alongside the secondary antibody. Following secondary antibody incubation, cells were then washed a further three times for 5 minutes with PBS, at RT, then stored in PBS prior to imaging using either the Zeiss LSM 700 confocal microscope or the EVOS FL Cell Imaging System. Negative controls included cells incubated with secondary antibody alone and cells incubated with isotype control antibodies. Furthermore, the apelin receptor antibody was validated by staining tissue from apelin receptor KO mice, where no antibody staining was seen. The apelin receptor antibody has also been validated in cross-sections from WT mouse cerebellum, which is known to have high apelin receptor expression. Correspondingly, a high level of antibody staining was seen (Medhurst *et al.*, 2003). Secondary antibodies with narrow excitation windows were selected in order to minimise crosstalk in co-staining experiments. Antibody concentrations were determined empirically based on manufacturer's recommendations and optimised to give the best signal to background ratio.

Protein	Species	Manufacturer (Cat#)	Concentration
Primary Antibodies			
Apelin Receptor	Rabbit	Sigma Aldrich (SAB2700205)	1:50 in hESC-derived cardiomyocytes, 1:100 in CHO cells
Troponin T	Goat	Abcam (ab64623)	1:200
α-Actinin	Mouse	Abcam (ab9465)	1:200
Oct 3/4	Mouse	Santa Cruz (sc-5279)	1:200
Nanog	Goat	R&D Systems (AF1997)	1:200
Sox2	Goat	R&D Systems (AF2018)	1:200
Secondary Antibodies			
anti-rabbit Alexa Fluor 488	Goat	ThermoFisher (A11034)	1:200
anti-goat Alexa Fluor 488	Donkey	ThermoFisher (A11054)	1:400
anti-mouse Alexa Fluor 488	Goat	ThermoFisher (A21121)	1:400
anti-mouse Alexa Fluor 568	Rabbit	ThermoFisher (A11061)	1:400
anti-goat Alexa Fluor 488	Chicken	ThermoFisher (A21467)	1:400

Table 2.5: Antibodies used for immunocytochemistry.

2.6 Flow Cytometry for Cell Markers

Flow cytometry was performed to determine cardiomyocyte differentiation efficiency. hESC-CMs were washed with PBS, detached using TryPLE Express (incubated for 10 minutes at 37°C), collected and pelleted by centrifugation at 300 xg for 3 minutes. Pellets were resuspended in PBS supplemented with 0.1% BSA and 2 mM EDTA (PBE), with CD90 (Thy-1) Monoclonal Antibody directly conjugated to PE diluted at 1:50, for 1 hour at 4°C. Cells were then washed with PBE and resuspended in Fixation/Solubilization solution (BD Cytofix/Cytoperm Fixation/Permeabilization Kit, Biosciences) for 20 minutes at 4°C. Following incubation, cells were washed using 1X BD Perm/Wash Buffer (Biosciences) and then resuspended in 1X BD Perm/Wash Buffer containing directly conjugated Anti-Cardiac Troponin T-APC antibody diluted at 1:50 and incubated for 2 hours at 4°C. Cells were then washed in 1X BD Perm/Wash Buffer, resuspended in PBE and transferred to flow tubes. Samples were run on the

LSRFortessa Cell Analyzer (BD Biosciences) and analysis performed using FlowJo v10.8.1 software.

2.7 Determination of Protein Content and Radioligand Binding

2.7.1 Protein assay

hESCs or hESC-CMs were scraped, collected and centrifuged at 300 xg for 3 minutes. Pelleted cells were resuspended in 1 ml ice-cold Tris-HCl (50 mM, 5 mM $MgCl_2$, pH 7.4) and triturated to induce hypotonic lysis. Samples were centrifuged (20,000 xg, 20 minutes at 4°C) and resuspended in ice-cold Tris-HCl buffer. 20 µl of cell lysate was combined with 20 µl solubilisation buffer (0.5 M NaOH, 1% SDS) and incubated at 80°C for 30 minutes, with remaining lysate frozen at -80°C. Samples were centrifuged (14,000 xg, 5 minutes at RT) and supernatant collected. Protein content was assessed using the DC Protein Assay following the manufacturer's protocol, using assay kit standards as a reference and solubilisation buffer alone as a blank. Absorbance was measured at 450 nm using a FLUOstar Omega Microplate Reader, a standard curve plotted and sample protein concentration extrapolated.

2.7.2 Radioligand binding

Saturation and fixed concentration radioligand binding experiments were carried out in hESCs and hESC-CMs as described previously (Katugampola *et al.*, 2001; Maguire *et al.*, 2012; P. Yang *et al.*, 2017b) using [Glp^{65},Nle^{75},Tyr^{77}][^{125}I]apelin-13 (referred to as [^{125}I]apelin-13 subsequently). The peptide modifications and this protocol have been optimised previously to prevent oxidation, metabolism and degradation of the [^{125}I]apelin-13 radioligand. All plasticware used was coated with Sigmacote siliconizing reagent to reduce radioligand non-specific binding.

For fixed concentration binding (FCB), 50 µl of cell protein lysate was incubated with 50 µl of [^{125}I]apelin-13 at a concentration of 0.15 nM in binding buffer containing 50 mM Tris-HCl and 5 mM $MgCl_2$, pH 7.4, for 90 minutes at RT. 50 µl of binding buffer containing 0.15 nM [^{125}I]apelin-13 and 10 µM [Pyr^1]apelin-13 (Severn Biotech) was used to define non-specific binding (NSB).

For saturation binding, 50 µl of cell protein lysate was incubated with 50 µl of 10 increasing concentrations (2 pM – 1 nM) of [^{125}I]apelin-13 in binding buffer for 90 minutes at RT. Again, 50 µl of binding buffer containing [^{125}I]apelin-13 plus 5 µM [Pyr^{1}]apelin-13 was used to define NSB.

This protocol has previously been optimised to minimise ligand depletion (Hulme and Trevethick, 2010). Only very small amounts of protein were present in each reaction hence, as a high volume of radioligand was used, ligand depletion was negligible.

Following incubation, centrifugation (20,000 xg, 10 minutes at 4°C) was used to break equilibrium and pellets washed with Tris-HCl, pH 7.4 at 4°C. Bound radioactivity in cell pellets was counted in a COBRA 5003 Gamma counter (Packard) and data analysed using iterative curve fitting programs EBDA and LIGAND (KELL Package, Biosoft). EBDA software performs Scatchard analysis and generates initial estimates of K_D and B_{Max}, which are then inputted to LIGAND. LIGAND software uses weighted, non-linear curve fitting to generate reliable K_D and B_{Max} values, and also performs a runs test to determine if the points are randomly distributed around the fitted line (McPherson, 1985). The program also takes into account receptor occupancy and ligand depletion as total binding, non-specific binding, specific activity of the total radioactivity added, and dissociation constant are inputted. Values generated were used to calculate receptor density in mole per mg of protein by dividing B_{Max} by starting protein concentration.

2.8 Determination of Peptide Production by ELISA

Conditioned supernatant was collected from hESCs and hESC-CMs. Supernatant from hESC-derived endothelial cells (hESC-ECs) was from M.T. Colzani (University of Cambridge). Apelin or ELA peptide production was determined by sandwich ELISA using either Apelin-12 (Human, Rat, Mouse, Bovine) EIA kit or the [pGlu^{1}]-ELA-32 (Human) EIA Kit according to manufacturer's protocol. Briefly, samples were added to the secondary antibody coated wells. Primary antibody directed against apelin or ELA was added, along with biotinylated apelin or ELA peptide and incubated for 2 hours at RT with orbital shaking (300 rpm). Wells were washed and blot dried then streptavidin-conjugated horseradish peroxidase (SA-HRP) was added and incubated

for 1 hour at RT with orbital shaking. Wells were then washed and dried and substrate added for 1 hour at RT with orbital shaking. The reaction was stopped by the addition of 2N HCl and absorbance measured at 450 nm using the FLUOstar Omega Microplate Reader. Absorbance is inversely proportional to the concentration of peptide in the sample. Concentrations were determined by extrapolation to a standard curve of known concentrations. The manufacturer has determined an intra-assay and inter-assay variation coefficient of <15% for both peptides. Furthermore, both assays have demonstrated no cross reactivity with other related peptides, including the opposing peptide.

2.9 siRNA-mediated *APLNR* Knockdown Strategy

Two different Silencer Select Pre-designed siRNAs targeting the apelin receptor were obtained, and arbitrarily named siAPLNR 1 and siAPLNR 2, with sequences shown in Table 2.6. For transfection of hESC-CMs in 6-well plates, DharmaFECT 1 Transfection Reagent and Opti-MEM Reduced Serum Media were utilised following the DharmaFECT 1 recommended protocol. Cardiomyocytes used were at day 20-25. Briefly, 2.5 µl/well DharmaFECT 1 was added to 97.5 µl/well of Opti-MEM (mix A) and incubated for 5 minutes at RT. Concomitantly, siAPLNR 1, siAPLNR 2 or siScramble were mixed with Opti-MEM (mix B) to give a final concentration of 20 nM or 40 nM in a total volume of 100 µl/well and also incubated for 5 minutes at RT. 100 µl/well of each of mix A and mix B were then combined and incubated for a further 20 minutes at RT to allow complexes to form. During this time, media was aspirated from hESC-CMs and cells washed with PBS. 800 µl of CDM-BSA per 200 µl of transfection mix was then added to the A and B mixture and 1 ml of this mix dispensed per well. hESC-CMs were incubated with transfection mix overnight, then washed with CDM-BSA and allowed to recover for 1-2 days, with media refreshed every day. Cells were then collected for RNA extraction and qRT-PCR as described in Section 2.4.

Name	Manufacturer (Cat#)	Sequence (5'→3')	Stock Concentration
siAPLNR 1	ThermoFisher (s1186)	UGUGGGCUACCUACACGUAtt	100 µM
siAPLNR 2	ThermoFisher (s1187)	ACACGUACCGGGACUACUGAtt	100 µM
siScramble	QIAGEN (SI03650318)	-	40 µM

Table 2.6: Sequences of siRNA used for targeting the apelin receptor for knockdown.

2.10 Generation of shRNA Clones Targeting the Apelin Receptor for Knockdown (*APLNR* KD)

An apelin receptor tetracycline (Tet) inducible short hairpin RNA (shRNA) knockdown system was generated by utilising the single-step optimised inducible knockdown system (sOPTiKD) developed by Bertero *et al.* (2016). The pAAV-Puro_siKD targeting vector (Bertero *et al.*, 2016) targets the *AAVS1* locus for transgene expression and is designed to carry both the shRNA and tetracycline response (tetR) expression cassette. pAAV-Puro_siKD was a gift from Ludovic Vallier (Addgene plasmid #86695; http://n2t.net/addgene:86695; RRID:Addgene_86695). This system has previously been validated, with expression of the transgene shown to be stably driven from the *AAVS1* locus in hESCs and upon differentiation to the three primary germ layers and in hESC-CMs (Bertero *et al.*, 2016).

2.10.1 Vector digestion

Firstly, pAAV-Puro_siKD was digested with BglII and SalI FastDigest restriction enzymes. 5 µg of plasmid was added to 5 µl of each enzyme plus 10 µl of FastDigest Green buffer (10X) and made up to 100 µl with nuclease free water. The reaction was incubated at 37°C for 30 minutes and digested product was separated on a 1% UltraPure Agarose gel containing SYBR safe DNA gel stain, then extracted and purified using the QIAEX II Gel Extraction Kit. Briefly, the DNA band was excised from the gel using a scalpel and UV transluminator. The excised band was weighed and 3

volumes Buffer QX1 added plus 2 volumes of water (band size ≥4kb), followed by 30 µl QIAEX II which was incubated at 50°C for 10 minutes, with vortexing every 2 minutes to promote solubilisation. 10 µl of 3 M sodium acetate, pH 5, was then added and incubated for a further 5 minutes. The sample was centrifuged for 1 minute at 17,900 xg and supernatant discarded. The pellet was then washed with 500 µl Buffer QX1 followed by two washes with 500 µl Buffer PE. The pellet was then left to air-dry for 30 minutes at RT before eluting DNA by adding 20 µl nuclease free water, incubating for 5 minutes, centrifuging for 1 minute at 17,900 xg and collecting the supernatant. DNA concentration was determined using a NanoDrop 1000.

2.10.2 shRNA oligonucleotide design, annealing and ligation

Known short hairpin RNAs (shRNAs) targeting *APLNR* were identified from the MISSION shRNA TRC database (Sigma Aldrich). This a freely available resource developed by the RNAi Consortium to generate short hairpin RNAs composed of 21 base stems and 6 base loops, with a number of constructs for each gene, designed to target different regions of the mRNA to induce variable levels of knockdown. Five shRNAs targeting different *APLNR* mRNA regions were selected for cloning and arbitrarily named shAPLNR 1-5 (Table 2.7). Single stranded oligonucleotides were designed by modifying sequences to include BglII and SalI overhangs for cloning into the pAAV-Puro_siKD vector, along with a starting guanine (G) for the U6 promoter if it was not already present on the shRNA (Table 2.8).

shRNA	TRC Number	Sequence
APLNR1	TRCN0000356634	CCGGTTAGATCTGCAATCGTCTTTCCTCGAGGAAA GACGATTGCAGATCTAATTTTTG
APLNR2	TRCN0000356635	CCGGGAGAACAGATGCACGAGAAATCTCGAGATTTC TCGTGCATCTGTTCTCTTTTTG
APLNR3	TRCN0000356636	CCGGCCTGAGTCTGGACGCAGTAAACTCGAGTTTAC TGCGTCCAGACTCAGGTTTTTG
APLNR4	TRCN0000008098	CCGGGCTGACCTGTTACTTCTTCATCTCGAGATGAA GAAGTAACAGGTCAGCTTTTT
APLNR5	TRCN0000008099	CCGGCGCTCAGCTGATATCTTCATTCTCGAGAATGA AGATATCAGCTGAGCGTTTTT

Table 2.7: TRC numbers and sequences of shRNAs targeting the apelin receptor gene (Sigma Aldrich MISSION shRNA TRC Database).

Oligo Name	Top Oligo (5' to 3')	Bottom Oligo (5' to 3')
APLNR1	GATCCC**G**TTAGATCTGCAATCGTCTTTCCTCGAGGAAAGACGATTGCAGATCTAATTTTTG	TCGACAAAAATTAGATCTGCAATCGTCTTTCCTCGAGGAAAGACGATTGCAGATCTAACGG
APLNR2	GATCCCGAGAACAGATGCACGAGAAATCTCGAGATTTCTCGTGCATCTGTTCTCTTTTTG	TCGACAAAAAGAGAACAGATGCACGAGAAATCTCGAGATTTCTCGTGCATCTGTTCTCGG
APLNR3	GATCCC**G**CCTGAGTCTGGACGCAGTAAACTCGAGTTTACTGCGTCCAGACTCAGGTTTTTG	TCGACAAAAACCTGAGTCTGGACGCAGTAAACTCGAGTTTACTGCGTCCAGACTCAGG**C**GG
APLNR4	GATCCCGCTGACCTGTTACTTCTTCATCTCGAGATGAAGAAGTAACAGGTCAGCTTTTTG	TCGACAAAAAGCTGACCTGTTACTTCTTCATCTCGAGATGAAGAAGTAACAGGTCAGCGG
APLNR5	GATCCC**G**CGCTCAGCTGATATCTTCATTCTCGAGAATGAAGATATCAGCTGAGCGTTTTTG	TCGACAAAAACGCTCAGCTGATATCTTCATTCTCGAGAATGAAGATATCAGCTGAGCG**C**GG
B2M	GATCCCGGACTGGTCTTTCTATCTCTTCAAGAGAGAGATAGAAAGACCAGTCCTTTTTTG	TCGACAAAAAAGGACTGGTCTTTCTATCTCTCTCTTGAAGAGATAGAAAGACCAGTCCGG

Table 2.8: Sequences of oligonucleotides used for shRNA cloning. Underlined = sense and antisense shRNA strands, red = overhangs necessary for cloning into BglII and SalI cut sites of pAAV-Puro_siKD, green = hairpin loop, blue = RNA polymerase III terminator.

Single stranded shRNA oligonucleotides (200 µM stocks) were annealed in a 10 µl volume containing 1 µl of top oligo, 1 µl bottom oligo, 1 µl annealing buffer (10X, containing 100 mM Tris-Cl (pH 8), 10 mM EDTA and 1 M NaCl) and 7µl nuclease free water. Annealing thermocycling is detailed in Table 2.9.

Temperature	Time
94°C	5 min
93°C	20 secs
Reduce by 1°C/cycle for 12 cycles	
80°C	4 min
79°C	20 secs
Reduce by 1°C/cycle for 3 cycles	
75°C	4 min
74°C	20 secs
Reduce by 1°C/cycle for 3 cycles	
70°C	4 min
69°C	20 secs
Reduce by 1°C/cycle for 60 cycles	
10°C	Forever

Table 2.9: Thermocycler programme for annealing of oligonucleotides.

Annealed oligonucleotides were diluted 1:10 with nuclease free water, then 1:50 with 1X annealing buffer to give a final dilution of 1:500. 4 µl of annealed shRNA (1:500) was ligated into 50 ng cut pAAV-Puro_siKD in a reaction containing 1 µl T4 ligase, 1 µl T4 ligase buffer and made up to 10 µl with nuclease free water, and incubated at RT for 2 hours. Ligated products were transformed into α-Select Gold Efficiency Chemically Competent Cells. Bacterial cells were thawed on wet ice and 1 µl of ligated plasmid was added to 25 µl bacterial cells and incubated on ice for 30 minutes. Heat shock transformation was then performed by incubating samples at 42°C for 30 seconds before returning to ice for 2 minutes. SOC medium (500 µl) was added and incubated at 37°C, shaking at 250 rpm for 1 hour. Bacterial cells were then streaked on pre-prepared ampicillin (100 µg/ml) Lysogeny broth (LB)-agar plates and cultured overnight at 37°C. Following initial culture, individual colonies were selected for liquid culture overnight (37°C, 250 rpm) in 5 ml LB + ampicillin (100 µg/ml).

2.10.3 Plasmid preparation and screening

The following day, 4.5 ml of bacterial culture was pelleted by centrifugation and plasmid DNA was extracted using the GenElute Plasmid Miniprep Kit as described previously (Bertero *et al.*, 2016). Briefly, pelleted cells were resuspended thoroughly and lysed for 4.5 minutes before the reaction was neutralised. Samples were then centrifuged at 12,000 xg for 10 minutes, to remove cell debris and chromosomal DNA, and supernatant collected. Cleared lysate was added to pre-prepared GenElute Miniprep Binding Columns and centrifuged at 12,000 xg for 1 minute. Columns were washed and plasmid DNA eluted in 50 µl nuclease free water with concentration determined by nanodrop.

Successful insertion of shRNA oligonucleotides into the pAAV-Puro_siKD was assessed by PCR using LongAmp *Taq* DNA Polymerase protocol. 1 ng of purified plasmid DNA was amplified with AAVSeqF (CGAACGCTGACGTCATCAACC) AAVSeqR (GGGCTATGAACTAATGACCCCG) as described previously (Bertero *et al.*, 2016), with an annealing temperature of 60°C. PCR products were run on a 1.5% agarose gel, alongside uncut plasmid as a control. pAAV-Puro_siKD plasmid containing the shRNA insert will give a PCR product of ~390bp, whereas the empty pAAV-Puro_siKD will produce an identifiable smaller fragment (~295bp). Amplified products from positive clones were analysed by Sanger Sequencing (Source Biosciences) to confirm insertion of the correct oligonucleotide. Following sequencing, positive clones carrying the correct oligonucleotide were regrown in 50 ml liquid culture (LB broth + 100 µg/ml ampicillin) overnight at 37°C, shaking at 250 rpm. The following day, the Plasmid Plus Midi Kit (high yield protocol) was used to purify plasmids. Bacterial culture was centrifuged at 4,000 xg for 15 minutes at 4°C. Pellets were resuspended, lysed and neutralised then added to a pre-prepared QIAfilter cartridge and incubated for 10 minutes at RT. Lysate was then filtered, binding buffer added and transferred to QIAGEN Plasmid Plus spin columns on a QIAvac 24 Plus. Vacuum pressure was applied to draw liquid through, columns were washed and then spun at 10,000 xg for 1 minute to remove residual wash buffer. Plasmid DNA was eluted by centrifugation at 10,000 xg for 1 minute in 100 µl nuclease free water and nanodropped.

2.10.4 Transfection of H9 hESCs

H9 hESCs on gelatin/MEF media coated 6-well plates were prepared for transfection by aspirating media, washing once with PBS and incubating in 1 ml of Opti-MEM. During this time, Lipofectamine 2000 based transfection mixtures were prepared. Briefly, per well 10 µl of Lipofectamine 2000 was added to 240 µl of Opti-MEM (mixture A), and incubated for 5 minutes at RT. Concomitantly, for each well, 250 µl of Opti-MEM was mixed with 4 µg DNA, divided equally between the targeting shRNA vector and two *AAVS1* zinc finger nuclease plasmids, designed to ensure specific targeting (Bertero *et al.*, 2016) (mixture B). For each well, 250 µl of mixture A was added to 250 µl mixture B and incubated for a further 20 minutes at RT. Following incubation, 500 µl of transfection mixture was added to each well in a dropwise manner and cells were incubated at 37°C overnight. The following day, transfection mix was aspirated, cells washed with H9 maintenance media and allowed to grow to 80% confluence, with media refreshed every day. At this stage, cells were maintained in the presence of 1 µg/ml puromycin with media refreshed every day. Surviving, resistant colonies were mechanically selected and allowed to grow clonally. Clones were expanded and maintained as detailed in Section 2.2, in the presence of puromycin.

2.10.5 Genotyping of shAPLNR clones

Genotyping was performed to determine site specific insertion of the transgene. Upon reaching ~80% confluence, clonal cells were collected and pelleted by centrifugation. Genomic DNA extraction was performed on pelleted cells using the GenElute Mammalian Genomic DNA Miniprep Kit following the manufacturer's protocol for cultured cell preparations. DNA concentration was determined by nanodrop and 100 ng of genomic DNA was used for each genotyping reaction. Three reactions were performed using the LongAmp Taq DNA Polymerase PCR protocol with different combinations of primers to determine site-specific targeting of the vector, as well as whether the allele is heterozygously or homozygously targeted. Details of each reaction are shown in Table 2.10. PCR products were then run on 1% agarose gels, with clones with successful targeting determined according to band pattern (Bertero *et al.*, 2016).

2.10.6 Tet induction and determination of knockdown efficiency

Targeted hESC clones were cultured in maintenance media plus 1 μg/ml tetracycline hydrochloride to induce apelin receptor knockdown for 4 days. Cells were then harvested and analysed by qRT-PCR as described above.

PCR Type	Primer Location	Primer Sequence	Amplicon wild-type (bp)	Amplicon for transgene insertion	Annealing temp. (°C)	Extension time	Result?
LOCUS	Genomic; 5' to 5'-HAR	CTGTTTCCCCTTCCCAGGCAGGTCC	1692	No band for homozygous targeting, faint band for heterozygous	65	> 3 min	Has vector inserted in genomic locus?
	Genomic; 3' to 3'-HAR	TGCAGGGGAACGGGGCTCAGTCTGA					
5'-INT	Genomic; 5' to 5'-HAR	CTGTTTCCCCTTCCCAGGCAGGTCC	No band	1103	65	1 min 30	Has the correct vector integrated?
	Puromycin	TCGTCGCGGGTGGCGAGGCGCACCG					
3'-INT	OPTtetR	CCACCGAGAAGCAGTACGAG	No band	1447	60	1 min 30	Has the correct vector integrated?
	Genomic; 3' to 3'-HAR	TGCAGGGGAACGGGGCTCAGTCTGA					

Table 2.10: Primer locations and sequences and PCR conditions used for genotyping of targeted hESCs.

2.11 Ethidium Homodimer Staining

hESCs were plated for differentiation as normal in 6-well plates (see Section 2.3). Before each media change time point, cells were stained with Ethidium Homodimer-1 (EthD-1) cell impermeant dye (40 µg/ml) diluted in CDM-BSA (1 ml/well) plus two drops of NucBlue Live ReadyProbes Reagent and incubated for 30 minutes at 37°C. Staining solution was then aspirated and replaced with 1 ml/well CDM-BSA and plates imaged using the EVOS FL Imaging System. Number of red cells (EthD-1 positive, dead cells) and number of cells (blue, nuclei stain) were counted using Fiji Image J analysis software and expressed as a ratio (number of dead cells/number of nuclei).

2.12 Binding of Apelin Fluorescent Ligand

Beating control and *APLNR* KD hESC-CMs were washed with PBS, TrypLE Express added and incubated at 37°C for 8-10 minutes. Trypsin was neutralised by the addition of CDM-BSA containing DNase (5 µg/ml) to prevent clumping and cells counted using the Countess Automated Cell Counter, with cells diluted 1:1 in 0.4% Trypan Blue to determine cell viability. Cells were aliquoted into clean 15 ml falcon tubes to provide 1 x 10^5 cells/well and centrifuged at 300 xg for 3 minutes. Media was aspirated and hESC-CMs resuspended in CDM-BSA + ROCKi (10 µM). Cells were then plated into pre-prepared matrigel coated CellCarrier-96 Black, Optically Clear Bottom plates (10 µg/ml, incubated for 1 hour at room temperature) in 100 µl media. Plates were shaken to ensure uniform cell dispersal and transferred to the incubator. Cells were allowed to attach and recover for 4 days, with two CDM-BSA media refreshes and tetracycline treatment maintained throughout.

Following recovery and once robust beating was re-established, media was aspirated and hESC-CMs washed three times with Hanks Balanced Salt Solution (HBSS). Fluorescently tagged apelin647 (previously designed and validated by the Davenport group. Custom order, Cambridge Research Biochemicals) was then added to each well at a concentration of 300 nM, diluted in HBSS and incubated for 90 minutes at RT in the dark. To determine non-specific binding, a saturating concentration of [Pyr^1]apelin-13 (10 µM) was also added. hESC-CMs were then washed three times with HBSS and fixed with 4% PFA for 5 minutes at RT. A further three washes were performed, and then cells were stained with Hoechst 3342 nuclear dye at a

concentration of 10 µg/ml in HBSS for 15 minutes at RT, shielded from light. Three final washes with HBSS were performed, then cells were covered with HBSS and stored at 4°C until imaging.

Plates were imaged on the Opera Phenix High-Content Screening System (Perkin Elmer) with assistance from T.L. Williams (University of Cambridge). The Opera Phenix imaging platform scans and images the full plate with low intensity and low dwell time, meaning photobleaching is minimised, enabling unbiased imaging and reliable quantification.

2.13 RNA Sequencing

Unless otherwise stated, methods described in this section were carried out by E.L. Robinson (University of Colorado), with assistance from the author.

2.13.1 RNA extraction

hESC-CMs at day 15 of differentiation, cultured in the absence or presence of tetracycline to induce *APLNR* KD were washed with PBS and cells scraped and collected. Samples were spun at 3,000 xg for 3 minutes, media aspirated, washed with PBS, spun again and PBS aspirated. RNA extraction was performed using TRIzol reagent. To promote nucleoprotein dissociation, cell pellets were resuspended in 400 µl of TRIzol and incubated for 5 minutes at RT. Chloroform (80 µl/sample) was then added for 3 minutes after thorough mixing, and phase separation induced by centrifugation at 12,000 xg for 15 minutes at 4°C. The RNA is contained within the upper aqueous phase, hence this was collected into a clean tube, and 200 µl of isopropanol added and incubated for 10 minutes for RNA precipitation. RNA precipitate was then pelleted by centrifugation at 12,000 xg for 10 minutes at 4°C and RNA washed by resuspending the pellet in 75% ethanol, followed by centrifugation at 7,500 xg for 5 minutes at 4°C. Following removal of the supernatant, pellets were air dried at RT for 10 minutes before being resuspended in 20 µl RNase-free water and incubated at 55°C for 15 minutes, with RNA concentration determined by NanoDrop 1000.

2.13.2 Quality control

Quality control was performed at the Cambridge Genomics Services (Department of Pathology, University of Cambridge). To determine RNA quality, an RNA Integrity Number (RIN^e) was generated by subjecting samples to electrophoretic separation of total RNA using the TapeStation RNA ScreenTape assay. RIN^e values range from 1-10 and a higher RIN^e value indicates highly intact RNA (Schroeder *et al.*, 2006). RIN^e values for all hESC-CM samples were 7.4-8.2 (mean = 7.74±0.25).

2.13.3 Removal of ribosomal RNA

Due to the high abundancy of ribosomal RNA (rRNA) (80-90% of total cellular RNA) (Lodish *et al.*, 2000), it must be removed to ensure cost effective RNA sequencing and to stop the read coverage being overwhelmed. Therefore, prior to library preparation, 6 µl total RNA was used in the NEBNext rRNA Depletion Kit (Human/Mouse/Rat) following manufacturer's protocol.

2.13.4 Total stranded RNA sequencing library preparation

The CORALL Total RNA-Seq Library Prep Kit was used following recommended protocol to generate Unique Molecular Identifier (UMI) labelled total stranded libraries for whole RNA sequencing. For the final amplification step, 15 PCR cycles were used. The protocol was amended in that, for the purification steps, AMPure XP PCR Purification Beads in combination with 80% nuclease-free ethanol made freshly were used at a volume of 1.8X, apart from for the final amplification step where a volume of 1X was used.

Further quality control was performed by the Babraham Institute Next Generation Sequencing Facility. To assess fragment size and range and presence of primer and adaptor dimers, libraries were sent for analysis by a 2100 BioAnalyzer (Agilent). The majority of the library should have a fragment size range 200-600 bp.

Next generation sequencing was carried out on prepared libraries at the Babraham Institute Next Generation Sequencing Facility using the HiSeq2500 System (Illumina) with 15 RNA-seq libraries sequenced per lane as 100bp Single-End sequencing runs.

2.13.5 Processing and analysis of next generation sequencing data

Work in this section was carried out by Simon Andrews and Felix Krueger at The Babraham Institute Bioinformatics Group. First, outputted fastq next generation sequencing files were subjected to basic quality checks using FastQC analysis (https://www.bioinformatics.babraham.ac.uk/projects/fastqc/). Next, Trim Galore! was used to trim reads and remove adaptor sequences, using a Phred score of 20 as a threshold, equivalent to an error of less than 1 in 100 bases and a trimming rate of less than 0.1 (https://www.bioinformatics.babraham.ac.uk/projects/trim_galore/). The data were then aligned to the reference genome Homo sapiens GRCh38/hg38 using the HiSAT2 program (http://daehwankimlab.github.io/hisat2/).

2.13.6 Differential gene expression

For visualisation and analysis, the processed files were then imported into SeqMonk (v1.42.0, https://www.bioinformatics.babraham.ac.uk/projects/seqmonk/) as BAM files. Read count quantitation was performed and total read count per replicate used for global normalisation. Sequencing reads were expressed as reads per million (RPM) and global normalisation performed to total library size by inputting data into DESeq2 R-based software (Love *et al.*, 2014) as raw (non-log transformed) counts. RPM ≥ 1.0 was used as a threshold for above noise, and a false discovery rate (FDR) of 5% defined as acceptable following Benjamini-Hochberg multiple testing correction.

2.13.7 XGR pathway analysis

With assistance from E.E. Davenport (Wellcome Sanger Institute), eXploring Genomic Relations (XGR) pathway analysis was performed, which is an open source tool designed to produce genetic summary data allowing enhanced interpretation of genomic datasets. This software incorporates established biological relationships, annotation and ontology, providing more informative and interpretable results than other commonly used analysis strategies (Fang *et al.*, 2016).

2.14 Adhesion Assay

To assess the role of the apelin receptor in adhesion, hESC-CMs at day 16-20 were washed with PBS, 750 µl TrypLE Express added and incubated at 37°C for 8-10 minutes. Trypsin was neutralised by the addition of 1.5 ml of CDM-BSA containing DNase (5 µg/ml) to prevent clumping and cells counted. Cells were aliquoted into clean 15 ml falcon tubes to provide 7 x 10^4 cells/well and centrifuged at 300 xg for 3 minutes. hESC-CMs were resuspended in CDM-BSA + ROCK inhibitor (10 µM). And plated into pre-prepared matrigel coated CellCarrier-96 Black, Optically Clear Bottom plates. Plates were shaken to ensure uniform cell dispersal and transferred to the incubator.

At pre-defined time points (3 hours, 12 hours and 24 hours), media was aspirated, hESC-CMs washed once with PBS and then fixed with 100 µl/well 4% paraformaldehyde for 20 minutes at RT. Following incubation, cells were washed with PBS, PBS replaced and plates stored at 4°C until staining performed.

Cells were permeabilised using PBS containing 0.5%Triton-X and 5% BSA for 15 minutes at RT, before blocking in 3% BSA PBS for 1 hour at RT. Phalloidin-iFluor 488 was diluted 1:500 in 0.5% BSA PBS, 100 µl/well added and incubated at RT for 2 hours in the dark. hESC-CMs were then washed 3 times with PBS before incubating with DAPI diluted 1:10,000 in 0.5% BSA PBS for 20 minutes at RT in the dark. Cells were then washed with PBS once more and covered with fresh PBS. Plates were stored at 4°C shielded from light until imaging.

Plates were imaged on the Opera Phenix High-Content Screening System and quantification performed using Harmony image analysis software (Perkin Elmer). Imaging and Harmony analysis was performed with assistance from T.L. Williams (University of Cambridge). Data were acquired for cell count, cell area and width/length ratio.

2.15 Measurement of Voltage Signalling

To assess voltage signaling, hESC-CMs were loaded with FluoVolt Membrane Potential voltage sensitive dye according to manufacturer's instructions. FluoVolt was diluted 1:1000 in 1X Tyrode's solution supplemented with glucose (10X Tyrode's

Solution diluted with mH20, 5 mM glucose, pH 7.4, Table 2.11), along with PowerLoad solution diluted 1:100. For hESC-CMs in 6-well plates, media was aspirated and replaced with 2 ml/well diluted FluoVolt solution and incubated for 30 minutes at 37°C. FluoVolt was then aspirated and replaced with 3 ml/well Tyrode's solution. Cells were imaged using an Axio Observer A1 Inverted Phase Contrast Fluorescence Microscope with LabCam adaptor mounted, and videos recorded in slow motion using an iPhone 7. Cells were paced at 1 Hz, 1.5 Hz and 2 Hz using the C-Pace EM fitted with 6-well plate adaptor (IonOptix). Generated videos were loaded into a custom MATLAB (R2021a) code written by S. Bayraktar (University of Cambridge) designed to extract values for time to peak and decay time. For analysis, regions of interest were selected to isolate effects in hESC-CMs, with data analysed across the region of interest.

	For 10X	**1X concentration**
$CaCl_2$	2.65 g	1.8 mM
$MgCl_2$	2.033 g	1 mM
KCl	4 g	5.4 mM
NaCl	81 g	140 mM
NaH_2PO_4	509 mg	0.33 mM
HEPES	24 g	10 mM

Table 2.11: Composition of 1 litre of 10X Tyrode's solution, made up with milliQ water.

Voltage sensitive dyes be cardiotoxic, which can induce disrupted beating patterns and arrhythmia (van Meer *et al.*, 2016). FluoVolt has previously been tested for cardiomyocyte cellular toxicity, and found to be only moderately toxic over a period of more than 3 hours (Bedut *et al.*, 2016). To minimise any toxicity effects, hESC-CMs were subjected to a maximum incubation time of 30 minutes. Furthermore, all conditions were incubated with the dye for equal time periods, meaning that when comparing control and genetically manipulated hESC-CMs, any dye toxicity would be observed in both conditions. Therefore, effects of the genetic manipulation can be observed compared to the control.

2.16 Measurement of Calcium Signaling

hESC-CMs in 6-well plates were loaded with 2ml/well Fluo-4, AM diluted 1:1000 in CDM-BSA for 30 minutes at 37°C. Following incubation, dye was aspirated and 3ml/well Tyrode's solution added. Cells were imaged as described above for voltage signaling (Section 2.15), including pacing at 1 Hz, 1.5 Hz and 2 Hz. Again, videos were analysed using a custom MATLAB code with values for time to peak and time to 90% decay extracted. For analysis, regions of interest were selected to isolate effects in hESC-CMs, with data analysed across the region of interest.

2.17 Effect of Apelin Receptor Ligands on hESC-CM Differentiation

hESCs cultured with or without tetracycline for 4 days were plated for differentiation as described in Section 2.3. Throughout differentiation, various apelin receptor targeting ligands were included (Table 2.12). Compounds were refreshed every 2 days with each media change. At day 14 of differentiation, hESC-CMs were collected using TrypLE Express and stained for TnT and Thy-1 as described in Section 2.6.

Ligand	Concentration	Mechanism	Supplier
[Pyr^{1}]apelin-13	10 nM or 1 µM	Unbiased	Severn Biotech
MM07	1 µM	G-protein biased	Severn Biotech
26525	300 nM	G-protein biased	Gifted by Sosei Heptares
31515	300 nM	Unbiased	Gifted by Sosei Heptares

Table 2.12: Apelin receptor ligands included in hESC-CM cultures throughout differentiation including concentrations used and ligand mechanism of action.

2.18 Generation of 3D Engineered Heart Tissues

A previously published protocol was used to generate 3D tissue constructs known as engineered heart tissues (EHTs) (Tulloch *et al.*, 2011; Ruan *et al.*, 2015). hESC-CMs were generated as described in Section 2.3, replated and subjected to metabolic selection for 3 days. Cells were allowed to recover in CDM-BSA for 2 days.

For casting hESC-CM constructs, previously prepared polydimethylsiloxane (PDMS) moulds were used (production of moulds described in Bargehr *et al.,* 2019). Prior to

casting, PDMS moulds containing two upright posts were sterilised by submerging in 70% ethanol and then treated with 5% pluronic acid F127 for 1 hour at RT.

Metabolically selected hESC-CMs in 6-well plates were detached by incubation with trypsin at 37°C for 8-10 minutes. Trypsin was neutralised by the addition of CDM-BSA containing DNase (5 µg/ml) to prevent clumping. hESC-CMs were centrifuged at 300 xg for 3 minutes, media aspirated and resuspended in 5-10 ml of CDM-BSA depending on pellet size. Cells were diluted 1:1 with 0.4% Trypan Blue and counted using an automated cell counter as described above.

To support the hESC-CMs in the EHT, cardiomyocytes were cast alongside HS-27A fibroblast immortalised cell line. HS-27A cells were maintained as described in Section 2.2. When ready for construct casting, HS-27A cells were trypsinised for 3 minutes, collected and counted as described for hESC-CMs.

hESC-CMs and HS-27A cells were aliquoted to provide either 5 x 10^5 hESC-CMs alone or 5 x 10^5 hESC-CMs plus 5 x 10^4 HS-27A cells per construct and kept on ice. An excess of collagen gel was prepared, with composition and order of reagent addition described in Table 2.13, and placed on ice.

Component	**Volume/ml (µl)**
10x RPMI-1640 medium	85.75
1M NaOH	12.60
Geltrex	142.91
Collagen I Rat Protein	541.77
Sterile mH_20	150.00
HEPES buffer	20
Additional NaOH	N (dependent on visualised colour change)
Additional sterile mH_20	46.97 – N

Table 2.13: Components of collagen gel used for casting 3D EHTs, with volume used per ml of mixture and reagents listed in the order in which they were added.

Cell mixtures were centrifuged at 300 xg for 3 minutes, media aspirated and resuspended thoroughly in collagen gel to give a total volume of 30 µl/construct.

Pluronic acid was aspirated from the PDMS moulds and 30 µl of cell/gel mixture added per mould well, ensuring gel surrounded the two upright posts and filled the entire well. Cast EHTs were then incubated at 37°C for 30 minutes to allow solidification. RPMI media supplemented with B27 plus insulin was added (6 ml/well), and refreshed every other day. EHTs were allowed to mature for 14 days, with spontaneous contraction observed within 2-5 days. Tetracycline was included throughout this 14 day period at a concentration of 1 µg/ml to induce *APLNR* KD.

2.19 Measuring Voltage and Calcium Signalling in EHTs

At day 14, voltage and calcium signalling were measured in EHTs as described in Sections 2.15 and 2.16, using FluoVolt and Fluo-4, AM, respectively. The same concentrations of dyes were used, but 3 ml/well was added. For performing measurements, EHTs were kept on the PDMS moulds to ensure EHTs did not move excessively.

2.20 Force Measurements of EHTs

After 14 days in culture, EHTs were subjected to force measurements as described in Bargehr *et al.,* 2019. EHTs were removed from their moulds and attached between a force transducer (model 400A, Aurora Scientific) and length controller (model 312B, Aurora Scientific), bathed in Tyrode's solution at 37°C (Figure 2.1). 3D constructs were then subjected to additive strain, with the length controller stretching the EHTs from their resting length to 24% strain in 4% intervals. Spontaneous contraction was recorded, followed by force generation with pacing at 1 Hz, 1.5 Hz and 2 Hz (5 V and 50 ms pulse duration). Generated force was recorded using LabView software, and output analysed using a custom MATLAB code (written by S. Bayraktar, University of Cambridge).

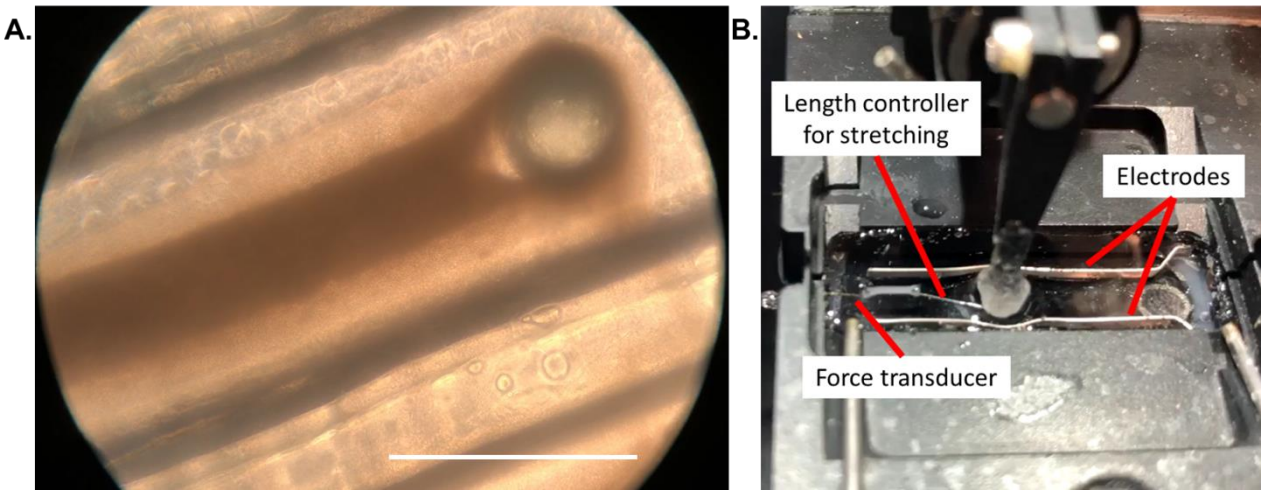

Figure 2.1: (A) Representative image of EHT on PDMS mould at day 14. Scale bar = 1 mm. (B) Myograph set-up used to subject EHTs to stretch and electrical stimulation, with force transducer measuring resulting force generation.

2.21 Second-Harmonic Imaging Microscopy of EHTs

EHTs were detached from their moulds and fixed in 4% PFA for 1 hour at RT. EHTs were then transferred to 30% sucrose solution, incubated overnight and then snap frozen on dry ice in Tissue Tek OCT. Tissues were sectioned (10 µm) using a cryostat (Bright Instruments) onto slides and glass coverslips mounted using Permanent Aqueous Mounting Media. Second-harmonic imaging microscopy (SHIM) was performed to visualise collagen without exogenous staining (X. Chen *et al.*, 2012). Slides were imaged by the Jeffrey Cheah Biomedical Centre Imaging Hub, using a Zeiss LSM880 multiphoton system, with a Newport Spectraphysics Insight DS+ laser. SHIM images were acquired using a 10x 0.5NA water dipping objective, excitation at 920 nm and detection at 437-463 nm.

2.22 RNA Extraction from EHTs

Upon completion of measurements, EHTs were snap frozen on dry ice and stored at -70°C until ready for use. EHTs were thawed on ice and total RNA extracted using the ACRTURUS PicoPure RNA Isolation Kit. EHTs were transferred to Lysing Matrix D beads in 250 µl Extraction Buffer and subjected to homogenisation in a FastPrep-24 5G Instrument (MP Biomedicals). Samples were then centrifuged at 4°C at 16,000

xg for 10 minutes. Tube contents were transferred to a clean tube and incubated at 42°C for 30 minutes, before spinning at 3,000 xg for 2 minutes to remove debris. Samples were then transferred to a clean tube and RNA extraction kit used according to manufacturer's protocol.

First, 250 µl of Conditioning Buffer was added to the column and incubated for 5 minutes before centrifuging at 16,000 xg for 1 minute. Equal volumes of 70% ethanol was then added to prepared lysates, mixed and transferred to the pre-conditioned columns. Samples were centrifuged for 2 minutes at 100 xg, immediately followed by 16,000 xg for 30 seconds. Wash Buffer 1 was added to the column before spinning at 8,000 xg for 1 minute. DNase solution was then prepared by adding 10 µl DNase 1 to 30 µl Buffer RDD per sample, with 40 µl of mixed solution added per column and incubated for 15 minutes at RT. A further 40 µl of Wash Buffer 1 was added and samples centrifuged at 8,000 xg for 30 seconds, followed by two washes with Wash Buffer 2. Purification columns were then transferred to clean 0.5 ml tubes and 12 µl Elution Buffer added directly to column membrane. After incubating for 1 minute at RT, columns were centrifuged for 1 minute at 100 xg followed immediately by 1 minute at 16,000 xg to elute. Samples were nanodropped to determine RNA concentration and gene expression analysis performed as described in Section 2.4.

2.23 Genome Editing using Base Editor Technology to generate R168H Apelin Receptor Variant hESCs

Base editing is a form of CRISPR/Cas technology which induces precise genetic changes without causing double stranded breaks (DSBs), requiring donor templates or relying on homology directed repair (HDR), in contrast to classic CRISPR/Cas technology. Base editing was used as described previously (Komor *et al.*, 2016; Koblan *et al.*, 2018) to generate hESCs carrying *APLNR* genetic variants identified from the NIHR BioResource BRIDGE study (Gräf *et al.*, 2018). Here, a cytosine base editor was used in combination with custom guide RNAs (gRNAs) to induce a change in sequence from G-C to A-T, resulting in a substitution mutation of an arginine to a histidine at apelin receptor amino acid position 168 (referred to as R168H subsequently).

2.23.1 Guide RNA design

To design gRNA, Benchling online CRISPR design tool was used (https://www.benchling.com/). A 1 kb genomic sequence was inputted as target sequence and the software generated a ranked list of potential 20 bp gRNAs, based on computationally predicted on and off target effects. All gRNAs identified directly preceded the PAM motif 5'-NGG, where N represents any base. This PAM sequence is specific for the SpCas9 ortholog and the PAM sequence can occur in the positive or negative strand.

For cloning gRNA into the expression plasmid (pGL3-U6-sgRNA-PGK-puromycin plasmid), the vector must be cut with BsaI type II restriction enzyme, creating non-compatible sticky ends for the ligation of gRNA. Hence, gRNA sequence must be designed to produce two complementary oligonucleotides with the addition of bases to produce compatible ends for insertion into the enzyme digest. As above, the U6 promoter requires a starting guanine (G), therefore this must also be added if not present. The designed gRNA sequences are shown in Table 2.14.

gRNA Name	**Top Oligo (5' to 3')**	**Bottom Oligo (5' to 3')**
R186H	CCGGGTGGTGCGTAACACCATG AC	AAACGTCATGGTGTTACGCACC AC

Table 2.14: Sequences of oligonucleotides used for base editing gRNA. Black = gRNA sequence, red = starting guanine for U6 promoter, blue = overhangs necessary for cloning into expression vector.

2.23.2 Plasmid preparation

gRNA expression plasmid and base editor plasmid were purchased from Addgene as bacterial stabs (Table 2.15). Each vector was expanded by plating on LB Agar plates containing ampicillin (100 µg/ml), followed by liquid culture in LB broth containing ampicillin (100 µg/ml). Plasmids were isolated using the Plasmid Plus Midi Kit as described in Section 2.10 and nanodropped to determine DNA concentration.

Plasmid name	Function	Addgene reference	Restriction enzyme	Reference
pGL3-U6-sgRNA-PGK-puromycin	Expresses gRNA from the U6 promoter. Puromycin resistance	Gift from Xingxu Huang (Addgene plasmid # 51133; http://n2t.net/addgene:51133 ; RRID:Addgene_51133)	BsaI	(Shen *et al.*, 2014)
pCMV_BE4max	C:G-to-T:A base editing	Gift from David Liu (Addgene plasmid # 112093 ; http://n2t.net/addgene:112093 ; RRID:Addgene_112093)	Not applicable	(Koblan *et al.*, 2018)

Table 2.15: Details of plasmids used for R168H base editing.

2.23.3 Annealing and ligation of gRNA oligonucleotides

Firstly, gRNA oligonucleotides were phosphorylated and annealed to form double stranded fragments. Reaction mixture containing 1µl of each of top and bottom oligonucleotide (100 µM), 1 µl of T4 Ligase 10X Buffer, 1 µl T4 Polynucleotide Kinase and 6 µl nuclease free water were incubated at 37°C for 30 minutes followed by 95°C for 5 minutes, and then temperature ramped down to 25°C at 5°C per minute.

Annealed R168H oligonucleotides were then diluted 1:200 in nuclease free water and reactions set up for ligation of oligonucleotide into the gRNA expression vector (pGL3-U6-sgRNA-PGK-puromycin). Reaction mix consisted of 2 µl diluted annealed oligonucleotides, 100 ng vector, 2 µl Tango Buffer (10X), 1 µl 10 mM DTT, 1 µl 10 mM ATP, 1 µl BsaI FastDigest restriction enzyme, 1 µl T4 Ligase and made up to 20 µl with nuclease free water. Samples were incubated for 6 cycles of 37°C for 5 minutes followed by 21°C for 5 minutes.

To remove residual linearised DNA fragments, 11 µl of ligation reaction was mixed with 1.5 µl 10X PlasmidSafe Buffer, 1.5 µl 10 mM ATP and 1 µl PlasmidSafe ATP-dependent DNase, and incubated at 37°C for 30 minutes followed by 70°C for a further 30 minutes.

Next, 2 µl of the treated ligation reaction was transformed into 25 µl of α-Select Gold Efficiency Chemically Competent Cells as described above and plated on LB Agar +

ampicillin (100 µg/ml) plates. Single colonies were selected for liquid starter culture and plasmid DNA isolated using the GenElute Plasmid Miniprep Kit and analysed by Sanger Sequencing (Source Bioscience) using the U6-FOR primer (GACTATCATATGCTTACCGT) to verify presence of gRNA. Positive clones were then regrown in 50 ml liquid culture overnight and plasmid isolated using the Plasmid Plus Midi Kit with an elution volume of 100 µl nuclease free water and concentration determined by nanodrop.

2.23.4 T7 endonuclease assay

To validate the ability of the generated vector containing gRNA targeting the apelin receptor gene to cut DNA at the specified genomic region, T7 endonuclease assays were performed using transfected HEK293T cells. Firstly, endonuclease primers were designed to span the region where the gRNA directs the base editor, allowing subsequent base change to modify DNA sequence. Sequences ~1 kb up and down stream of the predicted mutation site were inputted to Primer BLAST (https://www.ncbi.nlm.nih.gov/tools/primer-blast/) online tool and primer pairs generating products with length of 2 kb and minimal off target effects selected (sequences shown in Table 2.16). Annealing temperatures were determined for each primer pair based on predictions by the New England BioLabs Tm Calculator (https://tmcalculator.neb.com/) followed by performing gradient PCR using the Q5 High Fidelity DNA Polymerase PCR kit and running products on 1% agarose gel.

Primer Name	**Sequence (5'→3')**	**Tm (°C)**
APLNR_ENDO_FOR	TCTGGACCGTGTTTCGGAG	68
APLNR_ENDO_REV	GGAAACCCTTCAGCTCACAGT	

Table 2.16: Sequences and annealing temperatures for primers used in endonuclease assay.

HEK293Ts were maintained in culture until 80% confluent. Transfection mixtures were prepared by adding 7.5 µl TransIT-LT1 (Mirus Bio) to 250 µl Opti-MEM media, plus gRNA vector and base editing vector at a ratio of 1:3, with a total DNA content of 4 µg (i.e. 1 µg gRNA vector and 3 µg of base editor vector). Control reactions were also

set up, with either empty plasmid, no plasmid (untransfected, media + TransIT-LT1) or no transfection (media only). Mixes were incubated at RT for 20 minutes. Concomitantly, HEK293Ts were washed with PBS and dissociated by incubation with TrypLE Express for 3 minutes at 37°C. Following neutralisation, cells were collected and centrifuged at 300 xg for 3 minutes, resuspended in fresh media and counted. For each transfection, 2 x 10^5 cells were aliquoted to a fresh tube and again centrifuged at 300 xg for 3 minutes. Cells were resuspended in 1.5 ml of pre-prepared transfection mix, plated in one well of a 6-well plate and incubated overnight. The following day, media was changed to MEF media containing puromycin (1 µg/ml) to select for cells that had taken up the gRNA plasmid. After 48 hours, media was changed for normal MEF and cells maintained for a further 48 hours, and then collected for genomic DNA extraction using the GenElute Mammalian Genomic DNA Miniprep Kit as described in Section 2.10.

The Q5 Hot Start High Fidelity DNA Polymerase kit was used in combination with designed endonuclease assay primers on DNA from both transfected and untransfected HEK293Ts. Thermocycling conditions are detailed in Table 2.17. The QIAquick PCR Purification Kit was then used following manufacturer's protocol.

Temperature	**Time**
98°C	30 secs
98°C	10 secs
68°C	30 secs
72°C	2 min
Loop to step 2 for 35 cycles	
72°C	2 min

Table 2.17: Thermocycling conditions for PCR amplification of base editor transfected HEK293T DNA.

Heteroduplex annealing reactions were set up as detailed in Table 2.18, consisting of either PCR products from untransfected cells alone (1200 ng) or a combination of untransfected and transfected cells (600 ng of each), with thermocycling conditions shown in Table 2.19.

Control Reaction		Experimental Reaction	
Component	**Volume**	**Component**	**Volume**
NEBuffer 2	2 µl	NEBuffer 2	2 µl
DNA (untransfected)	1200 ng	DNA (untransfected)	600 ng
H20	To 20 µl	DNA (transfected)	600 ng
		H20	To 20 µl

Table 2.18: Reaction composition for heteroduplex formation for T7 endonuclease assay.

Temperature	**Time**
95°C	10 min
95°C to 85°C	-2.0°C/sec
85°C	1 min
85°C to 75°C	-0.3°C/sec
75°C	1 min
75°C to 65°C	-0.3°C/sec
65°C	1 min
65°C to 55°C	-0.3°C/sec
55°C	1 min
55°C to 45°C	-0.3°C/sec
45°C	1 min
45°C to 35°C	-0.3°C/sec
35°C	1 min
35°C to 25°C	-0.3°C/sec
25°C	1 min
4°C	∞

Table 2.19: Thermocycling conditions for heteroduplex formation for T7 endonuclease assay.

Annealed heteroduplexes were then treated with 1 µl T7 endonuclease and incubated at 37 °C overnight. Samples were run on a 1.5% gel and base editor cutting efficiency determined from band pattern.

2.23.5 hESC nucleofection

Next, H9 hESCs were nucleofected with BE4max base editor vector plus gRNA vector, using the Amaxa 4D Nucleofector (Lonza) and P3 Primary Cell 4D-Nucleofector X Kit according to manufacturer's instructions. First, for each reaction 18 µl of Supplement was added to 82 µl Nucleofector solution and mixed by vortexing, to give 100 µl total/reaction.

Concomitantly, H9 hESCs were prepared for nucleofection. For 1 hour prior to collection, hESCs were incubated in E8 complete media containing ROCKi (10 µM). For each reaction, two 10 cm dishes were prepared by coating with Vitronectin XF and incubating for 1 hour at RT. Media was aspirated, cells washed with PBS and dissociated using TryPLE by incubating at 37°C for 3 minutes. TryPLE was neutralised, hESCs collected into falcon tubes, centrifuged at 300 xg for 3 minutes, resuspended in fresh media and counted. For each nucleofection reaction, 1 x 10^6 cells/reaction were added to 100 µl Nucleofector solution.

For the base editor reaction, the two vectors were added to Nucleofector solution at a ratio of 1:3 gRNA:base editor, with a total DNA content of 8 µg (2 µg gRNA vector, 6 µg base editor). A control reaction was also set up, with 2 µg of pmaxGFP vector added to Nucleofector solution, in order to visualise successful nucleofection. Each reaction was then transferred to a nucleofector cuvette and placed into the Amaxa 4D Nucleofector, and pulse program CA137 used. Cells were then allowed to recover for 5 minutes, before adding 500 µl E8 complete media supplemented with CloneR (diluted 1:10, Stem Cell Technologies) and leaving for a further 5 minutes. Using the provided plastic transfer pipette, the entire cuvette contents were added to 12 ml of E8 complete + CloneR and plated onto the two previously prepared vitronectin coated 10 cm dishes. Plates were transferred to 37°C and incubated overnight to allow attachment.

After 24 hours, media was changed to E8 complete + puromycin (1 µg/ml), which was maintained for 48 hours with daily refresh, before transferring to normal E8 complete. Cells were cultured until visible colonies were present. Resistant colonies were selected manually for expansion and allowed to grow clonally.

2.23.6 Apelin receptor genotyping

Genotyping primers were designed for the *APLNR* nucleotide targeted for genetic manipulation. Sequences ~1 kb up and down stream of the residue of interest were inputted to Primer BLAST online tool and primer pairs generating products with length ~1.5 kb with minimal off target binding and amplification selected. Annealing temperature was determined for the selected primer pair using the New England BioLabs Tm Calculator and performing gradient PCR, with sequences and extension time of the selected genotyping primers shown in Table 2.20.

Primer Name	**Sequence (5'→3')**	**Tm (°C)**	**Ext. time**
APLNR_R168H__FOR	TCTGGACCGTGTTTCGGAG	68	90 secs
APLNR_R168H_REV	ACAGGGTCAGTCTCTGCAAGCT		
APLNR_R168H_Seq	GAAGCGGGGGTCGAAAAAGGCA	NA	NA

Table 2.20: Sequences, annealing temperatures (Tm) and extension time (Ext. time) for primers used for *APLNR* genotyping.

Clonal cells were collected and pelleted by centrifugation. Genomic DNA extraction was performed on pelleted cells using the GenElute Mammalian Genomic DNA Miniprep Kit as described in Section 2.10. DNA concentration was determined by nanodrop and 100 ng of genomic DNA used for each genotyping reaction. The Q5 Hot Start High Fidelity DNA Polymerase kit was used in combination with designed sequencing primers with thermocycling conditions as described in Table 2.17 but with an extension time of 90 seconds.

For each reaction, 5 µl was taken for gel electrophoresis to check for appearance of a band at the appropriate size. The remaining 20µl of reactions producing bands at the predicted size were then PCR purified, nanodropped and sent for Sanger Sequencing (Source Bioscience) using the APLNR_R168H_Seq primer shown in Table 2.20. Positive clones were then expanded in culture and differentiated to hESC-CMs for use in further assays.

2.24 Data Analysis and Statistics

All data are represented as mean±sem. The n values are stated in the figure legends. For statistical analysis, unpaired, two-tailed Student's t-tests or one-way ANOVA tests with Tukey's correction for multiple comparisons were performed as appropriate. A p value <0.05 was deemed significant. Graphical presentation and statistical analyses were performed using GraphPad Prism v7.05 unless otherwise stated. Independent replicates for hESCs are defined as cells from distinct passages and for cardiomyocytes are defined as cells generated from distinct differentiations.

3. Study of the Apelin Receptor in hESC-Derived Cardiomyocytes

3.1 Introduction

Pluripotent stem cells will self-renew indefinitely in culture and can be induced to differentiate to any cell type of the body as described in detail in Section 1. hESCs isolated from the inner cell mass of the blastocyst have been used extensively for a range of developmental and disease modelling purposes, by differentiating to varied cell types of interest.

The Sinha group has previously optimised a protocol to differentiate hESCs to cardiomyocytes (adapted from Mendjan *et al*., 2014). The first aim of this project was to establish if the resulting cardiomyocytes possess standard cardiomyocyte characteristics, similar to that seen in human cardiomyocytes *in vivo*.

The apelin receptor is a G-protein coupled receptor with demonstrated cardiovascular roles in development and adult physiology, where activation promotes vasodilatation and positive inotropy (Read *et al.*, 2019). To date, the apelin signalling pathway has been poorly characterised in PSCs and hESC-CMs. Therefore the next aim was to determine if the resulting hESC-CMs express the apelin receptor and its two peptide ligands, apelin and ELA, at similar levels as found in human adult cardiomyocytes. As detailed in Section 1, hESCs are known to express ELA but there is controversy as to whether they express the apelin receptor (Ho *et al.*, 2015; M. Li *et al.*, 2015), hence a further aim was to determine if the H9 hESCs used in this project possess a functioning apelin receptor.

This chapter details the differentiation and characterisation of the resulting hESC-CMs and data confirms that hESC-CMs express standard cardiac markers and functionality, validating this system as a suitable model for the human heart. Additionally, apelin receptor expression was found to be similar to adult human heart, providing a platform for the investigation of the role of the apelin receptor in cardiomyocyte development and function.

3.2 Methods

The methods relevant to this section are listed in Table 3.1 and described in Section 2, with further detail for selected methods below.

Method	Section
Cell culture and hESC-CM differentiation	2.2 and 2.3
Analysis of gene expression by qRT-PCR	2.4
Immunocytochemistry	2.5
Anti-troponin T flow cytometry staining	2.6
Saturation radioligand binding	2.7
Peptide production determined by ELISA	2.8
Data analysis and statistics	2.24

Table 3.1: Descriptions of the methods used in this section found can be found in the listed corresponding section.

3.2.1 Cell culture and hESC-CM differentiation

Undifferentiated H9 hESCs were maintained in culture as described in Section 2.2. For differentiation to cardiomyocytes, hESCs were plated at 8 x 10^5 cells/well on Matrigel coated 6-well plates and standard differentiation protocol performed (Figure 3.1) as detailed in Section 2.3. Images and videos of hESCs and hESC-CMs were captured using an iPhone 7 mounted on a standard brightfield microscope with LabCam iPhone Adaptor fitted.

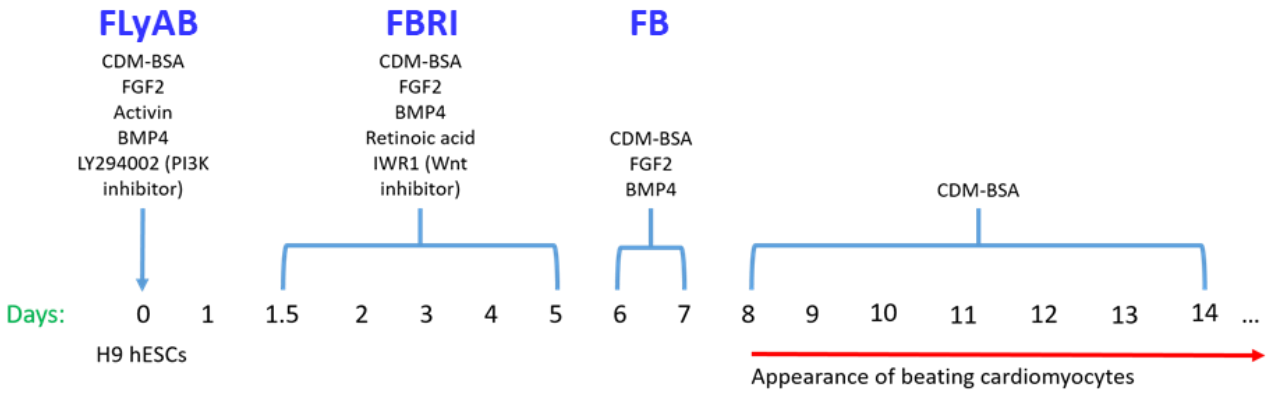

Figure 3.1: Schematic representation of the protocol and main media components used at each stage to direct differentiation of hESCs to cardiomyocytes.

3.2.2 qRT-PCR

qRT-PCR was performed using SYBR Green as detailed in Section 2.4 for standard pluripotency and cardiac markers, using RNA isolated from hESCs and hESC-CMs, with human *GAPDH* used as a housekeeping gene. For pluripotency versus cardiac marker genes, relative expression was calculated compared to H9 hESC expression using the $2^{(-\Delta\Delta CT)}$ method (Schmittgen and Livak, 2008). For apelin signalling system components, RNA from hESCs, hESC-CMs and adult cardiomyocytes was used in TaqMan Gene Expression assays, with human *18S* rRNA used as a housekeeping gene. Primer sequences are detailed in Table 2.4. Relative expression was normalised to housekeeping gene expression using the $2^{(-\Delta CT)}$ method (Schmittgen and Livak, 2008).

3.2.3 Stimulation of hESC-CMs with pharmacological stimuli

Baseline spontaneous contraction rate was counted for 60 seconds using a brightfield microscope. hESC-CMs were exposed to isoprenaline alone (100 nM), acetylcholine alone (ACh, 1 µM) or isoprenaline followed by ACh and resulting change in beating rate in response counted.

3.3 Results

3.3.1 Characterisation of cardiomyocytes generated from hESCs

3.3.1.1 hESC-CMs possess distinct morphology compared to hESCs

The starting H9 hESC cell population displayed characteristic morphology of hESCs, forming distinct compact colonies of pluripotent cells (Figure 3.2A). Upon completion of the differentiation protocol, cell morphology transformed into that characteristic of cardiomyocytes, including the initiation of spontaneous contraction (Figure 3.2B and Video 3.1).

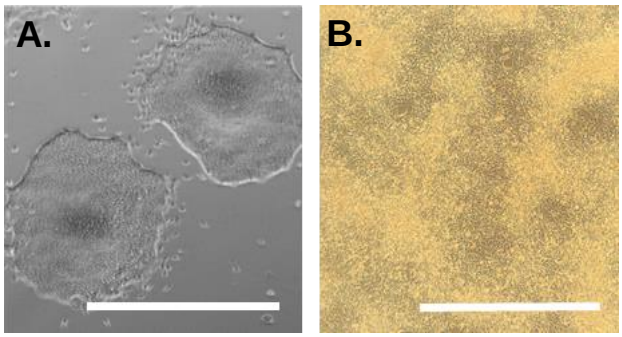

Figure 3.2: (A) Representative brightfield image of undifferentiated H9 hESC colonies (scale bar = 1 mm). (B) Representative brightfield image of hESC-derived cardiomyocytes (hESC-CM) at day 14 (scale bar 200 µm).

3.3.1.2 Expression of standard pluripotency and cardiomyocyte markers in hESCs and hESC-CMs

qRT-PCR analysis revealed expression of standard pluripotency markers *POU5F1* (OCT3/4) and *SOX2* in undifferentiated hESCs, which was lost upon differentiation. Conversely, the expression of standard cardiac markers (Burridge *et al.*, 2014), cardiac troponin T (*TNNT2*), SERCA2A (*ATP2A2*), ryanodine receptor 2 (*RYR2*), myosin heavy chain 6 (*MYH6*), alpha-actinin (*ACTN1*) and myosin light chain 7 (*MYL7*) were upregulated upon differentiation to cardiomyocytes (Figure 3.3A).

Additionally, hESCs were found to express the pluripotency markers Nanog and OCT 3/4 protein (Figure 3.3B), while hESC-derived cardiomyocytes expressed the cardiac markers troponin T and α-actinin at the protein level by immunocytochemistry (Figure 3.3C).

Furthermore, hESC-CM differentiation efficiency was found to be 78±3.5% as determined by positive cardiac troponin T (TnT) staining measured by flow cytometry (Figure 3.3C).

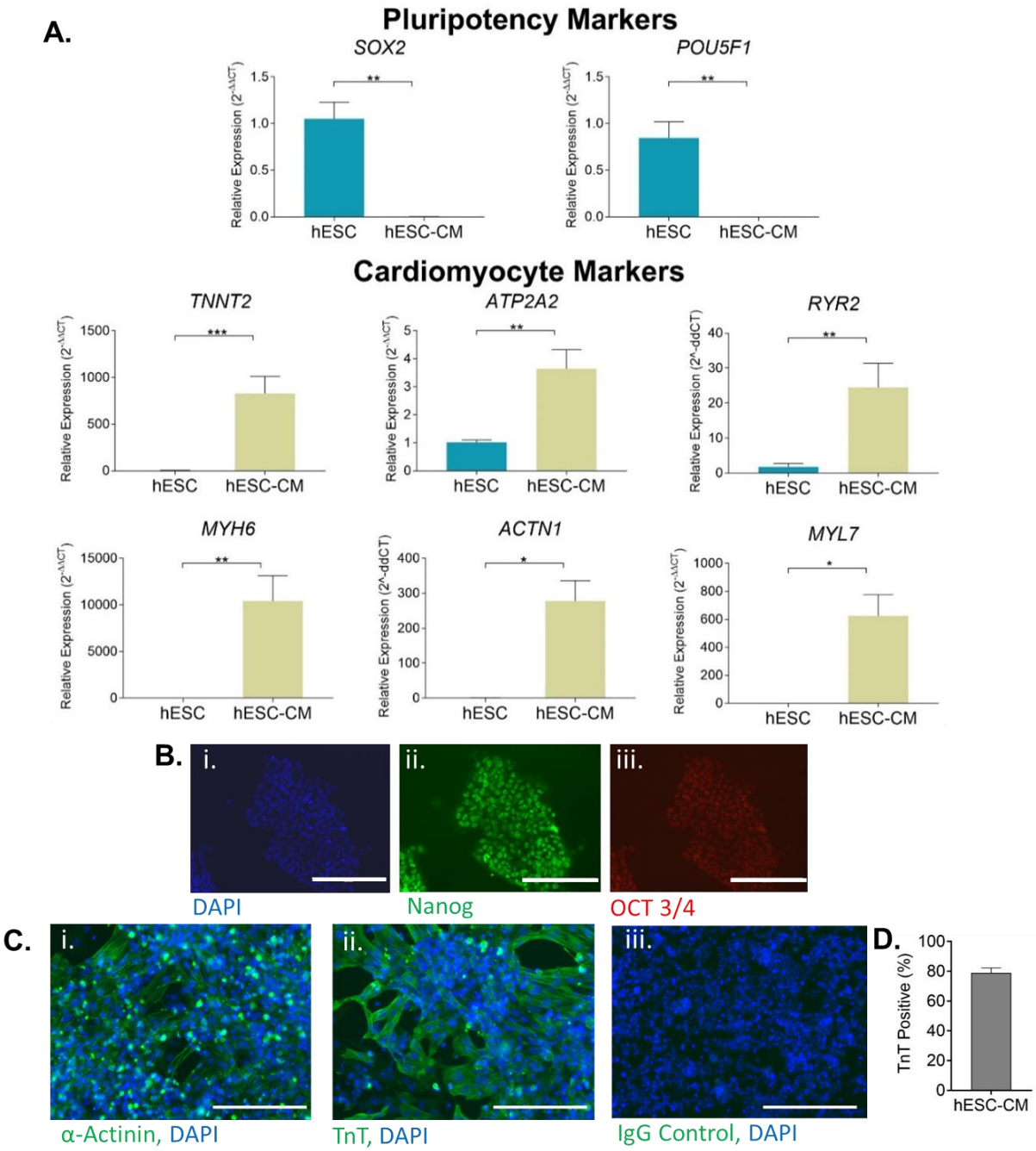

Figure 3.3: (A) Comparison of relative expression of standard pluripotency and cardiac markers in hESCs and hESC-CMs at the gene level by qRT-PCR. Expression displayed relative to mean expression in hESCs. n = 5 hESCs, n = 4 hESC-CMs, expression levels compared by unpaired, two-tailed Student's t-test, *p<0.05, **p<0.01, ***p<0.001. (B) Representative images of hESCs stained for (i) DAPI nuclear stain and with antibody directed against (ii) Nanog (green) and (iii) OCT 3/4 (red), scale bar = 200 μm. (C) Representative images of hESC-CMs stained with antibody directed against (i) α-actinin (green), (ii) cardiac troponin T (TnT) (green) or (iii) isotype negative control. Blue = DAPI nuclear stain, scale bar = 200 μm. (D) TnT positive percentage of hESC-CMs by flow cytometry, n = 5. Data represent mean±sem.

3.3.1.3 hESC-CMs respond to known pharmacological chronotropic agents

hESC-CMs were assessed for their ability to respond to pharmacological agents known to have chronotropic effects in the human heart, following the protocol displayed in Figure 3.4A. Exposure to the β-adrenoceptor agonist isoprenaline (100 nM) induced an increase in beating rate (baseline = 47±5.2 bpm, + isoprenaline = 86±9 bpm), which significantly decreased to around baseline level following washout (52±7 bpm). Additionally, subsequent additive application of acetylcholine (ACh, 1 μM) reduced the rate of contraction towards baseline (+ isoprenaline = 110±25, + ACh 77±23 bpm). Interestingly, application of acetylcholine alone had little effect on beating rate (Figure 3.4B).

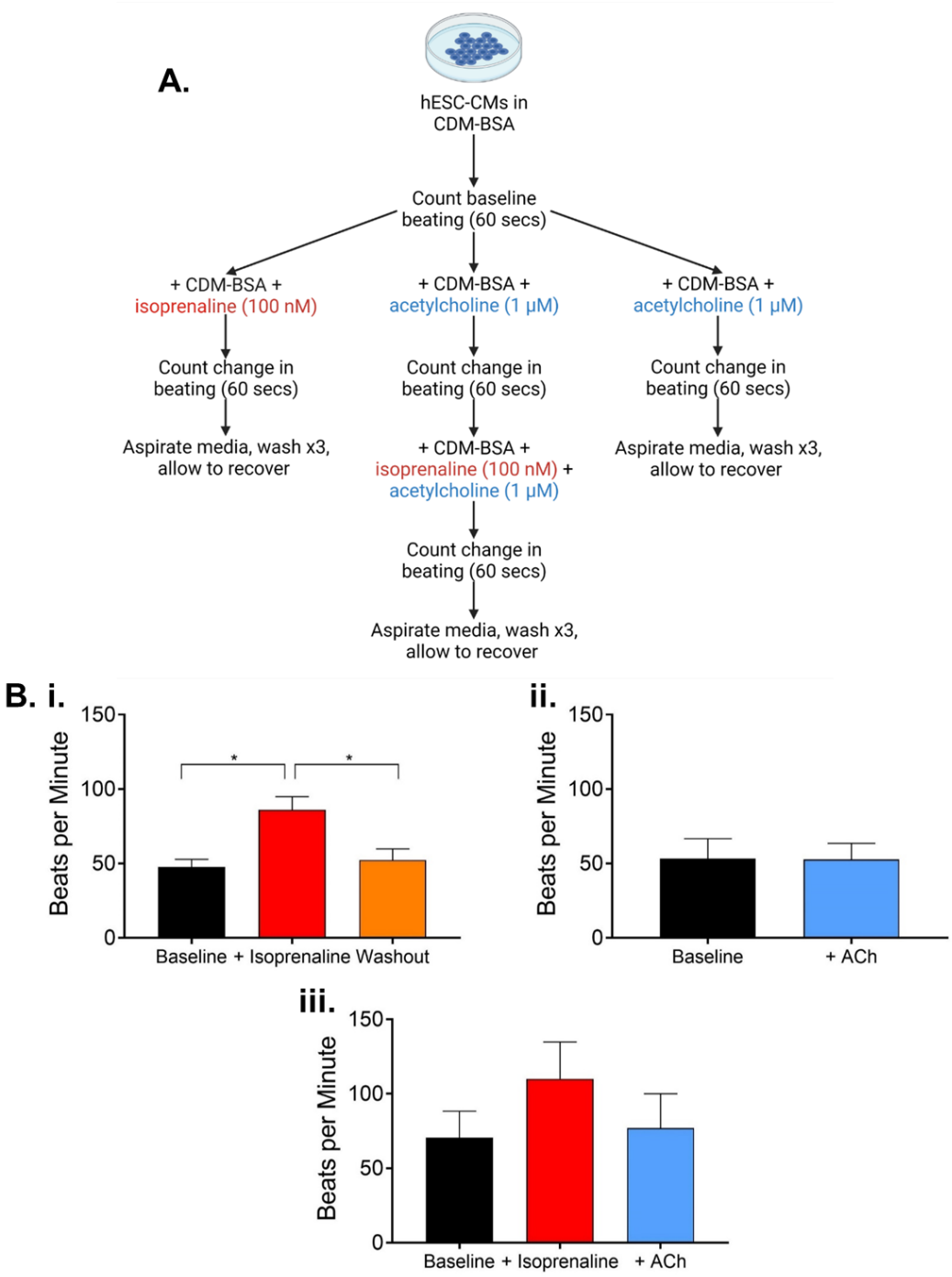

Figure 3.4: Stimulation of hESC-derived cardiomyocytes with characterised cardiac pharmacological stimuli. (A) Schematic representation of experimental protocol used for cardiomyocyte stimulation. Created with BioRender.com. (B) Mean beats per minute for hESC-CMs following exposure to (i) isoprenaline alone (100 nM), (ii) acetylcholine alone (1 µM) or (iii) isoprenaline (100 nM) followed by acetylcholine (1 µM). Washout counts were made following 10 minute incubation at 37°C after aspiration of compound containing media. n = 3 for all conditions, compared by paired, two-tailed Student's t-test (ii), or one-way ANOVA with Tukey's multiple comparisons test (i and iii), *$p<0.05$. Data represent mean±sem.

3.3.2 hESC-derived cardiomyocytes express the apelin signalling system

3.3.2.1 Expression of genes encoding the apelin signalling system in hESCs and hESC-CMs

Expression of the genes encoding the apelin receptor (*APLNR*) and its two endogenous ligands, apelin (*APLN*) and ELA (*APELA*), in hESCs and hESC-CMs was quantified by qRT-PCR, and compared to their expression in human adult cardiomyocytes (Davenport group stock, isolated by G. O'Reilly (University of Cambridge) as described in Molenaar *et al.,* 1993) (Figure 3.5). Both hESCs and hESC-CMs were found to express *APLNR* at similar levels to adult CMs, whilst little *APLN* expression was observed in hESCs and hESC-CMs, with no *APLN* expression detected in adult cardiomyocytes. Conversely, relative expression of *APELA* appeared higher in hESC-derived cardiomyocytes compared to adult cells, with hESCs expressing a significantly higher level of *APELA* gene compared to hESC-CMs.

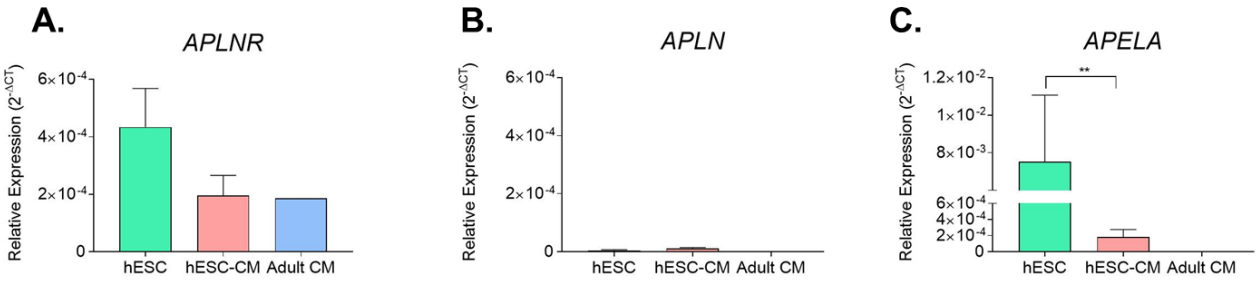

Figure 3.5: Comparison of relative expression of (A) *APLNR*, (B) *APLN* and (C) *APELA* in hESCs, hESC-derived and adult cardiomyocytes determined by qRT-PCR. hESC n = 4, hESC-CMs n = 8, adult CMs n = 1. hESCs and hESC-CMs were compared by unpaired, two-tailed Student's t-test, **p<0.01. Adult cardiomyocytes were not included in statistics as only n = 1 available. Data represent mean±sem.

3.3.2.2 Expression of apelin receptor protein in hESCs and hESC-CMs

Expression of the *APLNR* gene does not guarantee expression of functional apelin receptor protein, therefore immunocytochemistry using anti-apelin receptor antibody was performed. Non-permeabilised hESC-CMs were found to stain positively for apelin receptor protein (Figure 3.6), indicating cell surface expression as seen in native adult cardiomyocytes where the receptor is active. Chinese hamster ovary (CHO) cells artificially expressing the apelin receptor (CHO-APLNR, from J. Brown, Sosei Heptares) were used as a positive control. Overexpressing CHO lines demonstrated

positive staining for the apelin receptor, however this expression profile was greatly increased following 60 minute incubation with endogenous peptide ligand, [Pyr^{1}]apelin-13 (1 μM). Wild-type CHO cells without apelin receptor expression were used to test antibody specificity, with no positive staining observed in these cells.

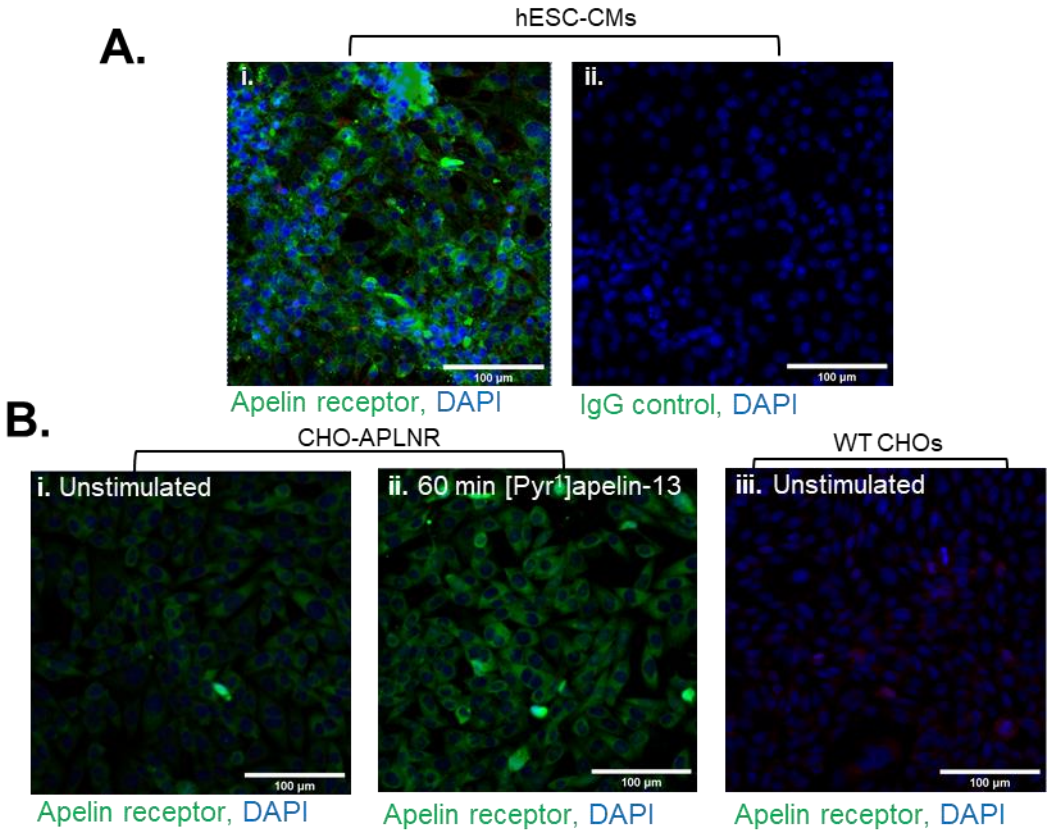

Figure 3.6: (A) Representative images of surface expression of (i) apelin receptor and (ii) IgG negative control in hESC-CMs. (B) CHO cells with artificial apelin receptor expression (CHO-APLNR) were used as a positive control. Representative images of surface expression of apelin receptor in (i) unstimulated CHO-APLNR cells and (ii) CHO-APLNR cells stimulated with 1 μM [Pyr^{1}]apelin-13 for 60 minutes and (iii) WT CHO cells with no artificial apelin receptor expression to demonstrate antibody specificity. Scale bar = 100 μm.

Additionally, saturation radioligand binding studies using [^{125}I]apelin-13 were performed on both hESCs and hESC-CMs. This technique is powerful as it uses a radiolabelled version of the native ligand, therefore demonstrating that receptor protein is expressed in a form capable of binding its ligand.

Firstly, total protein content was determined in order to express relative apelin receptor density. Saturation curves for specific binding were plotted by incubating with a high concentration of unlabelled ligand to define non-specific binding, which was then subtracted from total binding. Over the concentration range tested, [^{125}I]apelin-13 bound with a subnanomolar affinity (K_D) of 3.1 x10^{-10} M in hESCs and 2.2 x 10^{-10} M in hESC-CMs as expected for this ligand, and binding was saturable in both cell types (Figure 3.7 and Table 3.2), indicating expression of functional apelin receptor. Receptor density (B_{Max}) was calculated to be 43.3±7.0 fmol/mg for hESCs. In hESC-CMs, receptor density was found to be 15.8±3.7 fmol/mg comparable to that found in human adult left ventricle (B_{Max} = 13.8±1.8 fmol/mg). Hill slope was calculated to be 0.93±0.05 and 0.98±0.03 for hESCs and hESC-CMs respectively, consistent with a one site fit model.

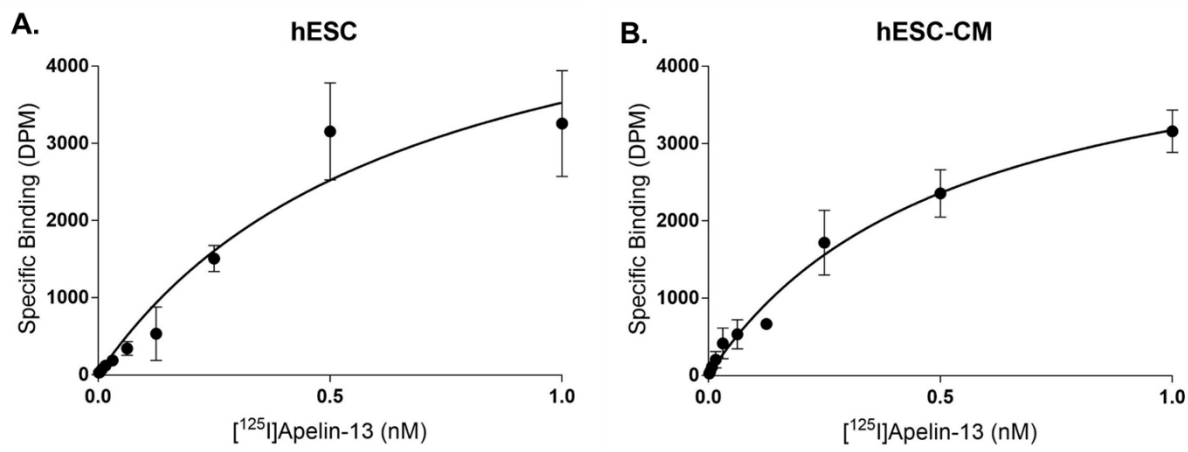

Figure 3.7: Specific binding of [^{125}I]apelin-13 in (A) hESCs and (B) hESC-derived cardiomyocytes. hESCs n = 4, hESC-CMs n = 4 with assay performed in triplicate for each replicate. Data represent mean±sem.

	Affinity (K_D)	**Receptor density (B_{Max})**	**Hill slope**
hESC	0.31 nM	43.3±7.0 fmol/mg	0.93±0.05
hESC-CM	0.22 nM	15.8±3.7 fmol/mg	0.98±0.03
Adult heart	0.08 nM	13.8±1.8 fmol/mg	0.95±0.11

Table 3.2: Summary of affinity, receptor density and hill slope in hESCs, hESC-CMs and adult heart. Data for adult heart from R.E. Kuc (University of Cambridge).

3.3.2.3 Expression of apelin receptor peptide ligands in hESCs and hESC-CMs

The next aim was to determine the level of apelin receptor ligand production by hESCs and hESC-CMs, given that apelin receptor protein expression was found in both cell types. ELISA assays specific for apelin and ELA peptides were used, with conditioned supernatant collected from hESCs and hESC-CMs. Conditioned supernatant from hESC-derived endothelial cells (hESC-ECs) (from M.T. Colzani, University of Cambridge) was used as a control, as endothelial cells are the main source of both peptides in human adults.

hESCs and hESC-CMs were found to express both ELA and apelin peptide ligands (Figure 3.8). However this was at a lower level than that seen for hESC-ECs (0.26±0.02 ng/ml ELA and 0.10±0.04 ng/ml apelin in hESCs and 0.24±0.07 ng/ml ELA and 0.10±0.02 ng/ml apelin in hESC-CMs vs 0.66±0.17 ng/ml ELA and 0.26±0.04 ng/ml apelin in hESC-ECs). This is in agreement with previous reports demonstrating apelin and ELA expression in adult endothelial cells, with ELA expression in the adult heart found principally in the non-cardiomyocyte fraction (Perjés *et al.*, 2016). Although the concentration seen in hESC-CMs is low, as the apelin receptor is a GPCR, activation of the receptor induces activation of multiple G proteins, promoting amplification of the signalling pathway (Ross, 2014), meaning this concentration is likely sufficient to produce a response in a paracrine/autocrine manner.

Interestingly, ELA expression was significantly higher in hESCs compared to apelin expression (compared by paired, two-tailed Student's t-test, $p<0.05$). In contrast, whilst a trend for increased ELA production compared to apelin was seen in hESC-CMs, this did not reach significance. Furthermore, although low apelin gene expression was seen in both cell types, hESCs and hESC-CMs were found to express apelin peptide, albeit at a low level (~0.1 ng/ml). Importantly, apelin and ELA were undetected in fresh culture media.

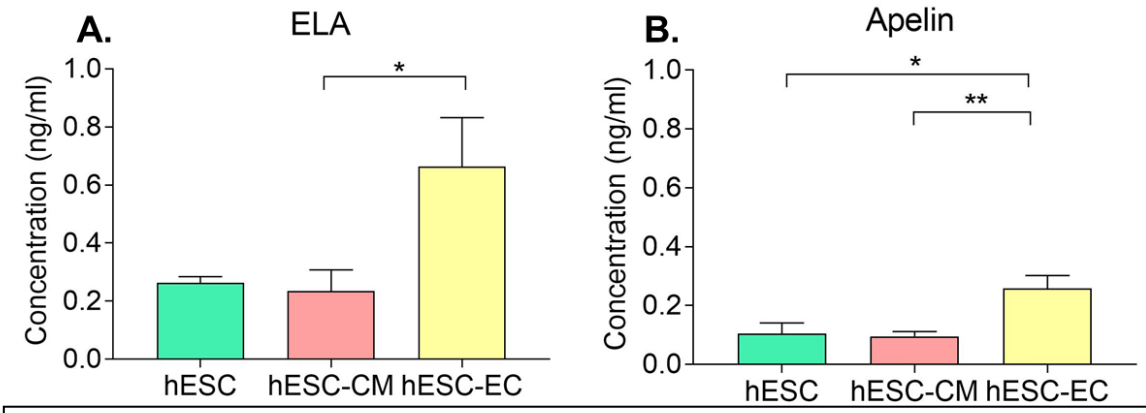

Figure 3.8: Comparison of concentration of (A) ELA and (B) apelin in conditioned supernatant from hESCs (n = 3 for ELA, n = 5 for apelin), hESC-CMs (n = 8 for ELA, n = 6 for apelin) and hESC-ECs (n = 4 for both). Means compared by one way ANOVA with Tukey's post hoc test, *p<0.05, **p<0.01. Data represent mean±sem.

3.4 Discussion

3.4.1 hESC-CMs express standard cardiac markers and respond to known pharmacological stimuli

By using an established protocol, hESC-CMs were generated which downregulated expression of pluripotency markers and upregulated expression of standard cardiac markers throughout differentiation. The resulting hESC-CMs also stained positively for α-actinin by immunocytochemistry and cardiac troponin T by immunocytochemistry and flow cytometry, which are both known cardiac markers. Most importantly, the hESC-CMs display spontaneous contraction which, in general, becomes more robust with increased time in culture.

One of the overarching aims of this project is to utilise a more clinically relevant model which could ultimately be used as a platform for human based drug screening. It is therefore essential to determine how the system responds to pharmacological agents with well-established effects in the human body. Isoprenaline is a potent chronotropic and inotropic agent (Silverman *et al.*, 1973), inducing marked increases in beating rate and force of contraction in human subjects through action on β1 adrenoceptors . Here, addition of isoprenaline to culture medium significantly increased rate of spontaneous contraction of hESC-CMs. Importantly, this increase in beating rate was reversible with washout of ligand.

In contrast to isoprenaline, ACh slows heart rate via activation of the M2 muscarinic receptor (Roy *et al.*, 2013). Addition of ACh alone had no effect on hESC-CM beating rate over the time period studied. There are a number of limitations of this experiment which could explain why the ACh response was not as robust as the observed isoprenaline response. Firstly, the concentration of ACh selected (1 µM) may not be optimal. ACh was added to culture plate well diluted in 500 µl pre-warmed media – this method was selected in attempt to cause least disruption to cellular physiology whilst allowing widespread dispersal of drug, but it may not allow ACh to access and act on a sufficient number of receptors to induce a significant response. Furthermore, the time period over which the cells were observed may not be long enough to allow an effect to occur. The protocol was designed to minimise the time hESC-CMs spent outside of the incubator, as a drop in temperature can adversely affect beating rate.

Despite these limitations, immediate subsequent addition of ACh following addition of isoprenaline induced a trend towards return to baseline beating rate. It could therefore be hypothesised that the hESC-CMs have a minimum spontaneous contraction rate that cannot be reduced further, meaning ACh can only induce an effect if beating rate has previously been increased.

Overall, these results demonstrate that it is possible to generate hESC-derived cardiomyocytes, which display spontaneous contraction, express standard cardiac markers and can respond to known pharmacological stimuli, confirming that this platform can be used for further investigation into the physiology and pharmacological responses of cardiomyocytes *in vitro.*

3.4.2 H9 hESCs express the apelin receptor

Given the existing controversy regarding apelin receptor expression in hESCs, the expression profile was investigated in the H9 hESCs, at both the gene and protein level.

It has previously been reported that two lines of hESCs, HES-3 and SHEF4, do not express the apelin receptor at either the gene or protein level by qRT-PCR and flow cytometry, respectively, and that expression was only upregulated upon differentiation

to mesendoderm (Ho *et al.*, 2015). Additionally, in HES3 and H9 hESCs, binding of fluorescein-conjugated [Pyr^{1}]apelin-13 was absent (Yu *et al*., 2012).

Contrastingly, H9 hESCs expressed *APLNR* transcripts at a similar level to that seen in both hESC-derived and adult cardiomyocytes. Notably, radiolabelled [^{125}I]apelin-13 bound with a subnanomolar affinity in H9 hESCs, with receptor density calculated to be 43.3±7.0 fmol/mg – higher than that seen in the adult heart. Based on literature searches, this is the first time saturation radioligand binding has been used to assess the expression of apelin receptor in hESCs.

Further, an advantage of the saturation radioligand binding technique over other protein detection methods, such as flow cytometry or western blotting, is that it gives an indication of receptor functionality, as it demonstrates that the receptor is capable of binding the endogenous ligand in radiolabelled form (Maguire *et al.*, 2012). Additionally, radioligand binding studies generate quantitative measurements of ligand affinities (K_D) and receptor density (B_{Max}), which may be altered, for example by post-translational modification, in uncharacterised cell types or under pathophysiological conditions (Maguire *et al.*, 2012).

A reason for the disparities between this study's results and previously published results of other groups may arise from the fact that all lines of hESCs are derived from individual donors, and therefore have distinct genetic backgrounds. This may mean that apelin receptor expression is different in different hESC lines and therefore further studies investigating apelin receptor expression in a variety of lines would be beneficial. To start to address this, expression of the *APLNR* gene was quantified in RUES2 embryonic stem cells (RNA from L.P. Ong, University of Cambridge), with increased expression found at the gene level compared to H9 hESCs (Figure 3.9). This was however only in a single replicate and therefore must be repeated before any conclusions can be drawn.

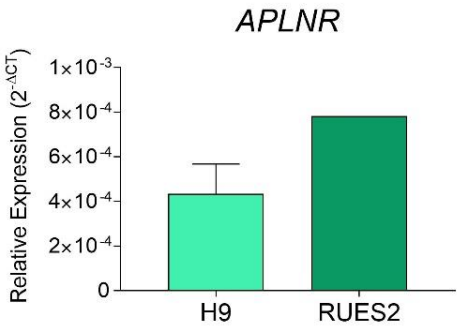

Figure 3.9: Comparison of relative expression of *APLNR* in H9 (n = 4) and RUES2 (n = 1) hESCs by qRT-PCR.

It has, however, been reported that H9 hESCs are the most frequently used hESC line, constituting 46.4% of all hESC papers published between 2008 and 2016, compared to only 6% of papers making use of HES-3 cells (Guhr *et al.*, 2018). Therefore, demonstrating expression of apelin receptor in H9 hESCs is likely more widely applicable to the hESC research field.

3.4.3 hESC-CMs express the apelin receptor

Based on literature searches, expression of the apelin receptor in hESC-CMs has previously not been studied. Hence, I have investigated the expression of the apelin receptor at both the gene and protein level.

By qRT-PCR, hESC-CMs were found to express the *APLNR* gene at a similar level to that seen for RNA isolated from adult cardiomyocytes. The adult cardiomyocyte RNA was isolated by G. O'Reilly (University of Cambridge), using a previously published method (Molenaar *et al.*, 1993). However, it is difficult to access healthy human heart tissue as healthy organ donations are most often used for transplant surgery, therefore only one replicate from a single donor was available for gene expression analysis studies. However, as described in detail in Section 5, RNA sequencing of hESC-CMs was performed, and reads per million (RPM) for *APLNR* gene determined. Comparing this to RNA sequencing data from control human left ventricle (data generated by E.L. Robinson, University of Colorado), no significant difference was found between the two sample groups (Figure 3.10). The left ventricle samples will not be a pure

cardiomyocyte only population, however the result suggests that hESC-CMs express the apelin receptor transcript at a similar level to that seen in adult heart. For further detail on RNA sequencing experiments performed, see Section 5.

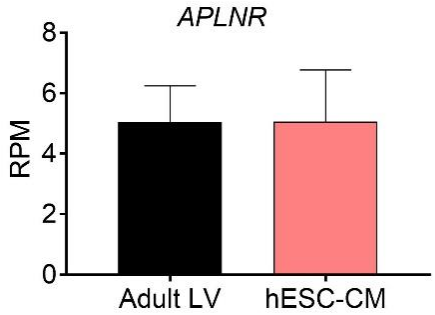

Figure 3.10: Comparison of reads per million (RPM) for *APLNR* gene in adult human left ventricle (LV, n = 7) and hESC-CMs (n = 3) by RNA sequencing. Adult LV data generated by E.L. Robinson. Data represent mean±sem.

hESC-CMs were also found to express the apelin receptor at the protein level by immunocytochemistry. Here, stained cells were not permeabilised, indicating surface expression of the apelin receptor. Previously, in sections of atrial and ventricular human myocardium, cardiomyocytes were shown to stain positively for apelin receptor with distribution primarily seen at the cell surface membrane (Kleinz *et al.*, 2005).

In agreement with this, in hESC-CMs binding of radiolabelled [^{125}I]apelin-13 was saturable, with a K_D and B_{Max} of 2.2 x 10^{-10} M and 15.8±3.7 fmol/mg calculated, respectively. As discussed above, this indicates that apelin receptor is expressed in a functional form capable of binding ligand. Crucially, apelin receptor density was comparable to that seen in human adult heart.

Together, these data confirm the suitability of hESC-CMs as a model for investigation of apelin receptor function in human cardiomyocyte development and physiology.

3.4.4 hESCs and hESC-CMs produce apelin and ELA peptides

Both hESCs and hESC-CMs were show to express apelin receptor capable of binding its cognate ligand. It was therefore important to determine whether these cell types produce either of the endogenous peptide ligands, apelin or ELA.

qRT-PCR and ELISA revealed that hESCs produce both apelin and ELA. Interestingly, although only very little apelin expression was detected at the gene level compared to the *APELA* gene, apelin peptide was detected, supporting the need to quantify at both the gene and protein level. Expression of ELA was significantly higher in hESCs than apelin expression, in agreement with previously published studies which have reported high ELA expression in the blastocyst, and a critical role of ELA in the key stem cell characteristic of self-renewal (Ho *et al.*, 2015; M. Li *et al.*, 2015). Furthermore, it has also been shown that apelin peptide is not expressed in early development and is only upregulated as development progresses, with ELA peptide displaying an opposite trend being highly expressed in early development with a subsequent downregulation to a lower level in adult tissues (Chng *et al.*, 2013; Ho *et al.*, 2015).

In supernatant from hESC-CMs, both peptides were detected at a level not significantly different from that seen in hESCs. A limitation of hESC-CMs is that they possess a more foetal-like than adult cardiomyocyte phenotype (Sterneckert *et al.*, 2014), hence the hESC-CMs seem to express a more developmental than adult profile for apelin receptor ligand production. In adult humans, endothelial cells act as the primary source of both peptides (Kleinz and Davenport, 2004; Perjés *et al.*, 2016; P. Yang *et al.*, 2017b). In agreement with this, hESC-ECs were found to produce a significantly higher level of both peptides than hESC-CMs and of apelin than hESCs.

It is essential to determine peptide expression in the hESC-CM system for two reasons. Firstly, the apelin receptor has been suggested to act in a ligand-independent manner, acting as a stretch receptor in cardiomyocytes. Scimia and colleagues demonstrated that cardiomyocytes isolated from apelin receptor null mice displayed a reduced response to stretch, with the stretch signals mediated through β-arrestin signalling (Scimia *et al.*, 2012). As ligand expression was observed, it is likely that there is some autocrine/paracrine ligand-dependent signalling occurring in the hESC-CM model system used here. However I have not investigated whether there is ligand-independent signalling occurring, and if so, how the dual function of the receptor is divided.

Secondly, expression of endogenous ligand will affect apelin receptor surface expression, as upon stimulation of a GPCR, a GPCR kinase signalling cascade is

induced, promoting beta-arrestin recruitment and ultimately, clathrin-mediated endocytosis (Figure 1.5). This ligand-induced receptor internalisation can promote cellular desensitisation if a high concentration of ligand is present (E. Kelly *et al.*, 2008), which may affect results.

3.5 Conclusions

Cardiomyocytes derived from hESCs display spontaneous contraction and express standard cardiac markers. hESC-CMs also express apelin receptor protein at a level similar to that seen in the adult heart. Together, these results confirm this as a suitable model to investigate human cardiomyocyte physiology and the role of apelin receptor signalling in hESC-CM differentiation and function, indicative of its role in the human heart.

4. Generation of an shRNA Inducible Apelin Receptor Knockdown System

4.1 Introduction

A key advantage of using PSCs is their amenability to genetic editing, with a wide range of techniques used to manipulate the expression of proteins of interest as detailed in Section 1. Of particular use in hESCs are inducible systems, allowing temporal control of gene expression, meaning the role of a particular protein can be interrogated at distinct stages of differentiation.

One of the aims of this project was to investigate the role of the apelin receptor both throughout the differentiation process to hESC-CMs and in differentiated hESC-CM function. To do this, a previously developed and optimised protocol (Bertero *et al.*, 2016) was used to generate, for the first time, a novel apelin receptor inducible knockdown system.

This system consists of a stably expressed transgene integrated at the *AAVS1* locus, using the artificial CAG promoter to drive transgene expression (Bertero *et al.*, 2016) (Figure 4.1). The *AAVS1* locus is a genomic safe harbour, meaning it is capable of integrating new genetic material, facilitating predictable expression without introducing damaging alterations to the host genome (Papapetrou and Schambach, 2016). Integration of a transgene at the *AAVS1* locus using the CAG promoter has also been shown to drive stable transgene expression in hESCs and upon differentiation to the three primary germ layers, validating this locus for expression of the transgene in differentiated downstream cell types, including cardiomyocytes (DeKelver *et al.*, 2010; Bertero *et al.*, 2016).

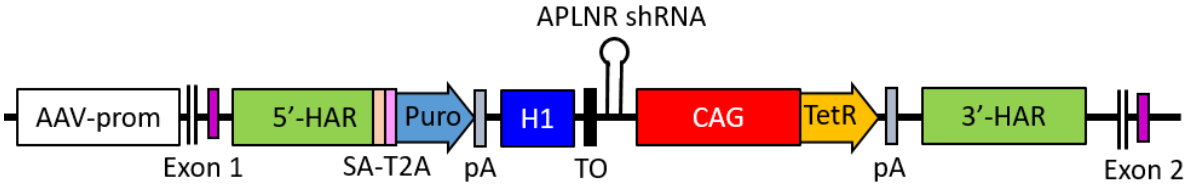

Figure 4.1: Transgene generated containing apelin receptor shRNA targeted to the *AAVS1* locus. 5′-HAR/3′-HAR = upstream/downstream homology arm, SA = splice acceptor, T2A = self-cleaving T2A peptide, Puro = puromycin resistance, pA = polyadenylation signal, H1 = H1 promoter, CAG = CAG promoter, TO = Tet operon, tetR = tetracycline-controlled repressor. Adapted from Bertero *et al.*, 2016.

The approach used is known as single step optimized inducible knockdown (sOPTiKD). The transgene consists of a short hairpin RNA (shRNA) targeting the gene of interest – in this case, *APLNR* – under the control of a tetracycline response element. The sOPTiKD system has been shown to induce reversible and rapid knockdown, displaying tetracycline dose responsiveness. Furthermore, this system has been used to induce substantial knockdown in a range of differentiated cell types, including cardiomyocytes. Bertero *et al*. demonstrated that 5 days of tetracycline treatment resulted in over 90% knockdown of an eGFP reporter transgene in hESCs. This study also induced knockdown of various genes known to be involved in development, resulting in severe differentiation deficiencies, providing evidence of the applicability of this system to study human development *in vitro* (Bertero *et al.*, 2016). Together, these results suggest that this system provides a method for modulating apelin receptor expression both during differentiation of and in differentiated hESC-CMs.

This section describes the generation and validation of the apelin receptor inducible knockdown system in hESC-CMs. Based on literature searches, this is the first application of the sOPTiKD system to knockdown not only the apelin receptor, but any GPCR.

4.2 Methods

The methods relevant to this section are listed in Table 4.1 and described in Section 2, with further detail for selected methods below.

Method	**Section**
Cell culture and hESC-CM differentiation	2.2 and 2.4
siRNA mediated *APLNR* knockdown	2.9
Generation of shRNA clones targeting the apelin receptor for knockdown	2.10
Analysis of *APLNR* gene expression by qRT-PCR	2.4
Saturation radioligand binding	2.7
Data analysis and statistics	2.24

Table 4.1: Descriptions of the methods used in this section found can be found in the listed corresponding section.

4.2.1 siRNA mediated apelin receptor knockdown

Wild-type hESC-CMs at day 20-30 of differentiation were transfected with one of two short interfering RNAs (siRNAs) targeting *APLNR* or a control siScramble as described in Section 2.9, using DharmaFECT 1 and Opti-MEM media. Cells were incubated with transfection mixture overnight and then washed with CDM-BSA and fresh media added. After 1-2 days of recovery, cells were collected for RNA extraction and qRT-PCR as described below.

4.2.2 Generation of hESC cell lines carrying shRNA targeting the apelin receptor

An apelin receptor tetracycline (Tet) inducible shRNA knockdown system was generated by utilising the single-step optimised inducible knockdown system (sOPTiKD) developed by Bertero *et al*. (2016) as described in Section 2.10. The pAAV-Puro_siKD plasmid was digested and one of five annealed and modified shRNAs targeting the *APLNR* gene ligated into the plasmid. Successful shRNA insertion was confirmed by Sanger Sequencing.

H9 hESCs were transfected with targeting shRNA vector (Figure 4.1), along with two *AAVS1* zinc finger nuclease plasmids designed to ensure specific targeting using Lipofectamine 2000 and Opti-MEM. Cells were allowed to grow to 80% confluence before performing selection based on puromycin resistance (Figure 4.2).

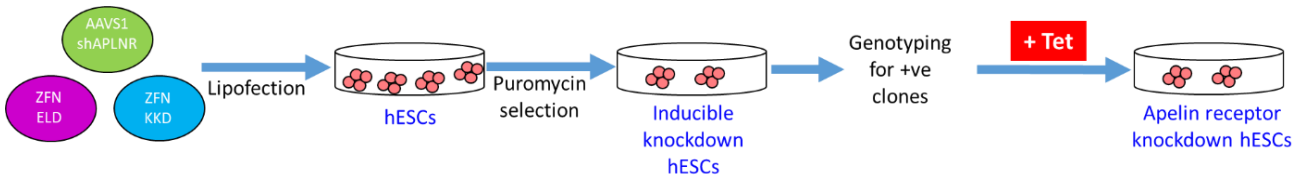

Figure 4.2: Simplified schematic of the strategy used for generation of apelin receptor iKD hESCs. ELD and KKD ZFNs = zinc finger nuclease variants.

Cells surviving antibiotic selection were manually selected, grown clonally and genotyped by PCR using different combinations of primers to determine if integration of the transgene was successful (Figure 4.3). See Section 2.10 for primer sequences and further details.

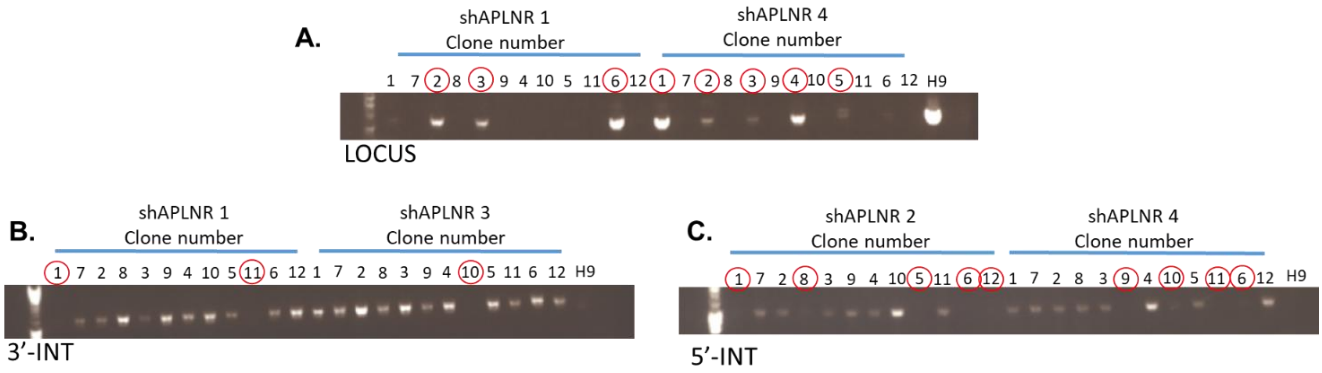

Figure 4.3: Representative agarose gels of PCR products from genotyping. H9 = untransfected control. Red circle = negative result. (A) LOCUS PCR: No band = transgene integrated, (B) 3'-INT: Band around 1.1 kb = correct transgene integrated (3' end), (C) 5'-INT: Band around 1.4 kb = correct transgene integrated (5' end).

hESCs with positive genotyping results were then cultured with tetracycline hydrochloride (+ Tet) included in the culture medium at a concentration of 1 µg/ml for three days, with daily refresh, in attempt to induce knockdown of the apelin receptor. Tetracycline titration has previously been performed and identified this concentration as optimal to induce substantial gene knockdown (Bertero *et al.*, 2016). qRT-PCR and saturation radioligand binding were performed as described below to determine knockdown efficiency at the gene and protein level, respectively.

For hESC-CMs, H9 hESCs cultured in the presence of tetracycline for 4 days were plated for differentiation as described in Section 2.3. Throughout differentiation, tetracycline was included in the culture medium, with refresh at each media change stage (every 2 days). At day 14 of differentiation, hESC-CMs were collected for determination of knockdown efficiency by qRT-PCR and saturation radioligand binding.

As a control, an additional line was generated, carrying a transgene with shRNA targeting the β2 microglobulin gene (*B2M)*. β2 microglobulin is a component of MHC molecules, expressed in almost every cell of the body and has only a single genetic variant in humans (L. Li *et al.*, 2016). Because of this universal and conserved expression, the *B2M* gene is frequently used as a housekeeping gene for qRT-PCR (Vandesompele *et al.*, 2002; Kodama *et al.*, 2019), and as an endogenous control in knockdown experiments (Bertero *et al.*, 2016; Ervin *et al.*, 2019). *B2M* knockdown

has previously been shown to reduce immunogenicity, however it does not affect stem cell self-renewal or pluripotency (Matin *et al.*, 2004; D. Wang *et al.*, 2015). Additionally, knockdown of *B2M* in mouse ESC-CMs had no effect on expression of cardiac markers or spontaneous contraction (Karabekian *et al.*, 2015).

4.2.3 qRT-PCR for determination of knockdown efficiency

qRT-PCR was performed using TaqMan Gene Expression Assays, as detailed in Section 2.4, for *APLNR* gene expression using RNA isolated from hESCs and hESC-CMs cultured with and without tetracycline. Human *18S* rRNA was used as a housekeeping gene. Primer sequences are detailed in Table 2.4. *APLNR* expression was normalised to housekeeping gene expression and relative expression compared to the corresponding cell line cultured without tetracycline calculated using the $2^{(-\Delta\Delta CT)}$ method (Schmittgen and Livak, 2008).

4.2.4 Saturation radioligand binding for determination of knockdown efficiency

hESCs and hESC-CMs cultured with and without tetracycline were collected and lysed and protein content determined as described in Section 2.7. For apelin receptor KD lines, saturation binding was performed using increasing concentrations of [^{125}I]apelin-13 as described in Section 2.7. For control line cells carrying the shB2M transgene, binding assays using a fixed concentration (FCB) of [^{125}I]apelin-13 were performed as described in Section 2.7.

4.3 Results

4.3.1 Using siRNA to knockdown *APLNR* expression in hESC-CMs

Initially, to investigate apelin receptor function in hESC-CMs, siRNA targeting *APLNR* was used in attempt to induce knockdown. Here, two distinct siRNAs (siAPLNR1 and siAPLNR2) were used at two concentrations (20 nM and 40 nM), and hESC-CM transfection protocol was optimised to maximise siRNA uptake without inducing toxicity or cardiomyocyte death. *APLNR* expression was determined by qRT-PCR 72

hours after transfection and compared to expression level measured for the corresponding siScramble transfected cells (Figure 4.4).

In one experiment, siAPLNR1 transfected hESC-CMs were found to express a similar level of *APLNR* gene compared to siScramble cells at both concentrations, indicating unsuccessful knockdown. In contrast, at 20 nM concentration, siAPLNR2 reduced *APLNR* expression by over 90% (relative expression of 0.07). Intriguingly, when 40 nM siAPLNR2 was used, relative expression was only reduced to 0.7. However, in two further replicates this successful knockdown was not reproducible, and *APLNR* expression was in fact increased in some samples compared to siScramble (data not shown). Hence using siRNA to target apelin receptor expression in hESC-CMs was abandoned.

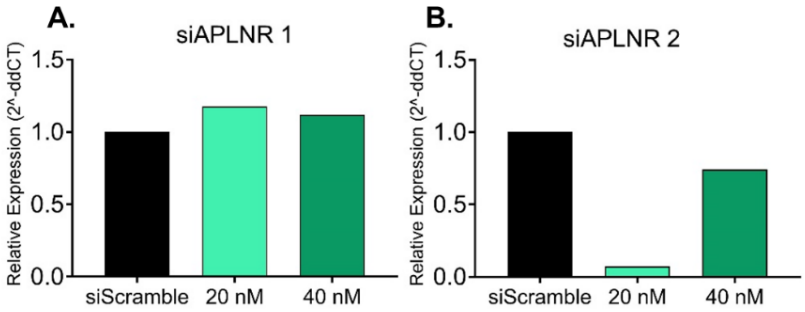

Figure 4.4: Comparison of relative expression of the apelin receptor gene (*APLNR*) in siRNA transfected hESC-CMs using two different siRNAs (A and B). n = 1 for all conditions. In subsequent experiments, results were not reproducible and knockdown was unsuccessful (data not shown).

4.3.2 Generation of shRNA based apelin receptor inducible knockdown hESCs

Owing to the limited efficiency of siRNA-mediated knockdown, a previously described and optimised method was used to generate hESC-lines stably expressing an inducible knockdown shRNA based system, known as sOPTiKD (Bertero *et al.*, 2016). Lines were generated as described in Section 4.2.2, and cell clones with positive genotyping results cultured in the presence of tetracycline for 3 days in attempt to induce apelin receptor knockdown. At the gene level, a number of lines were shown to have successful *APLNR* knockdown (iKD) (Figure 4.5). Most efficient knockdown was seen for homozygously targeted shAPLNR 2 clone 2 with relative expression of 0.11±0.02 + Tet compared to 1.01±0.16 in Control cells (expression normalised to –

Tet). In heterozygously targeted clones, a smaller reduction in *APLNR* gene expression was seen, as expected for lines carrying only one allelic copy of the transgene. Crucially, in control hESCs carrying a transgene with shRNA targeting the *B2M* gene no difference in *APLNR* gene expression was seen independent of tetracycline inclusion.

Two homozygously targeted clones were expanded for further culture and use in all subsequent apelin receptor iKD experiments – shAPLNR 2 clone 2 which displayed ~90% reduction in expression and shAPLNR 5 clone 3 which displayed a slightly lower level of reduction in expression (~80%). These two clones were selected as both showed substantial *APLNR* knockdown, but shAPLNR 2 clone 2 had slightly higher knockdown than shAPLNR 5 clone 3. shB2M clone 8 was also expanded for use as a control throughout the project. Subsequently, shAPLNR 2 clone 2 and shAPLNR 5 clone 3 are referred to as 2.2 and 5.3, respectively, and shB2M clone 8 is simply referred to as B2M.

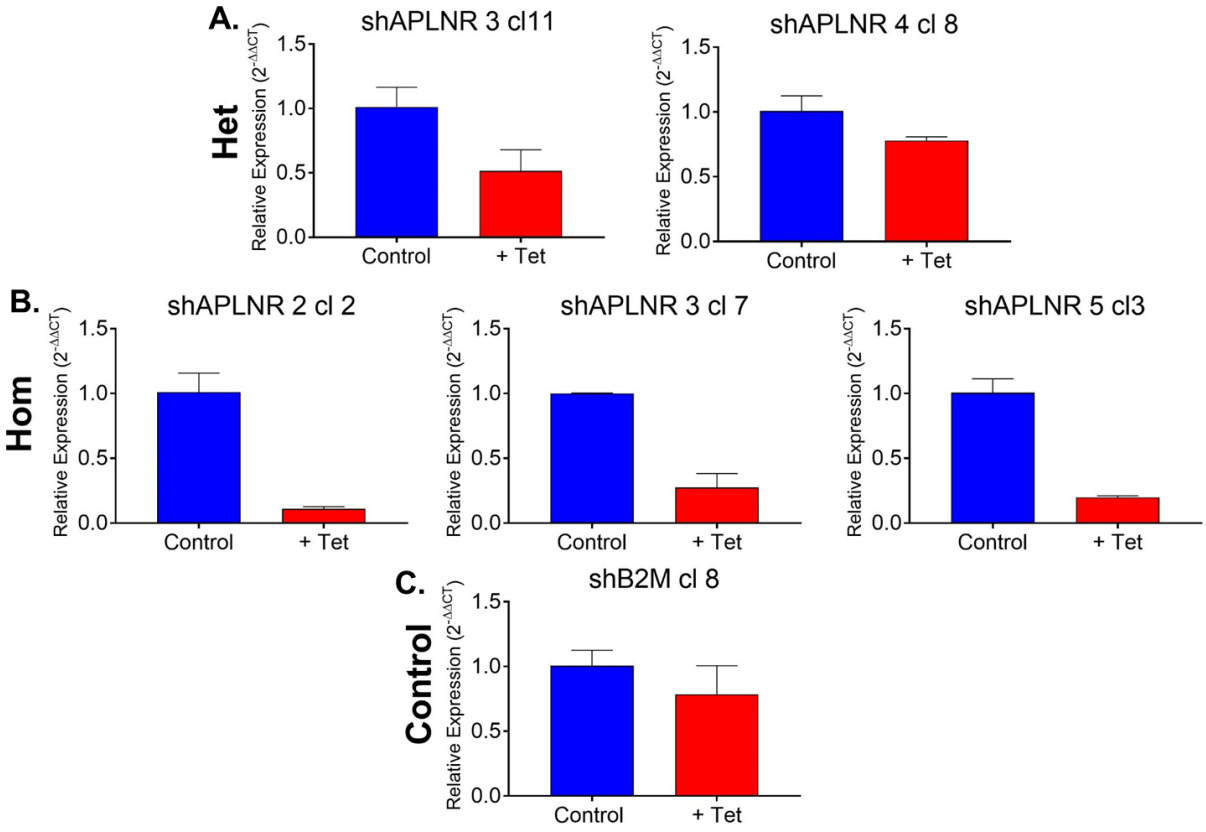

Figure 4.5: Comparison of relative expression of the apelin receptor gene (*APLNR*) in iKD transgene targeted hESCs cultured in the presence of tetracycline. Expression normalised to Control – Tet mean expression. (A) Mid-level knockdown in heterozygously targeted clones, (B) substantial knockdown in homozygously targeted clones and (C) no change in expression in positive control cells carrying shRNA targeting β2 microglobulin. n = 2 technical replicates for all conditions, hence statistical significance could not be determined. Data represent mean±sem.

4.3.3 Determination of apelin receptor knockdown efficiency in hESCs

4.3.3.1 Apelin receptor knockdown efficiency at the gene level in hESCs

The two iKD lines, 2.2 and 5.3, were expanded in culture and tetracycline included in the culture medium for 4 days in attempt to induce knockdown. Tetracycline treatment significantly reduced expression of *APLNR* gene in both lines (Figure 4.6A). There was no significant difference in level of knockdown between the 2.2 and 5.3 hESCs lines, as well as no difference in expression of *APLNR* in control cells cultured without tetracycline, therefore the results for the two lines were pooled (Figure 4.6B). Pooled results displayed an 87% decrease in expression of the *APLNR* gene in KD compared to control. Crucially, no differences in expression of *APLNR* were seen in B2M control cells (Figure 4.6C).

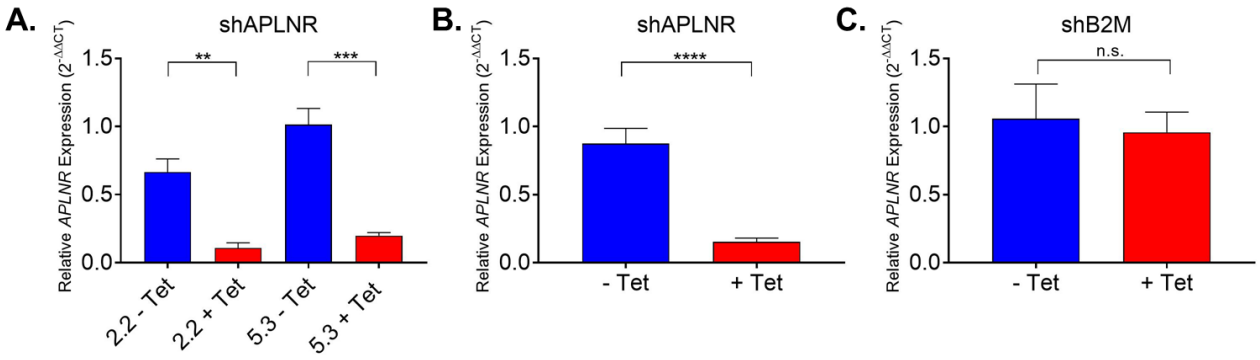

Figure 4.6: Comparison of relative expression of the *APLNR* gene in iKD hESCs. (A) Expression in two lines of apelin receptor iKD hESCs, 2.2 and 5.3 (n = 3 for both) was similar in both control (- Tet) and apelin receptor KD (+ Tet, 4 days). Therefore, results for the two lines were pooled (B), to give n = 6. (C) Expression of *APLNR* in B2M control line cultured with or without tetracycline for 4 days. n = 3. Relative expression compared to line – Tet mean expression. Expression compared by one-way ANOVA with Tukey's multiple comparisons test (A) or unpaired, two-tailed Student's t-test (B and C), **p<0.01, ***p<0.001, ****p<0.0001. Data represent mean±sem.

4.3.3.2 Apelin receptor knockdown at the protein level in hESCs

The next aim was to determine the level of apelin receptor knockdown at the protein level in apelin receptor iKD hESCs cultured in the presence of tetracycline for 4 days. After determining total protein content, saturation radioligand binding using [^{125}I]apelin-13 was performed (Figure 4.7A). As described above, no difference was seen in the level of knockdown for 2.2 and 5.3 at the gene level, therefore results from the two

lines have been pooled here. As described previously, specific binding was plotted and for control cells cultured in the absence of tetracycline, binding was found to be saturable over the concentration range tested, with affinity for [^{125}I]apelin-13 calculated to be 3.6 x 10^{-10} M. In *APLNR* KD hESCs, binding of [^{125}I]apelin-13 was almost completely abolished, with specific binding appearing as a straight line rather than a saturating curve. Measured specific binding was very low, almost comparable to that seen for non-specific, indicating little to no expression of apelin receptor protein. Note that due to the low specific binding seen in *APLNR* KD hESCs, and the fact that a curve was not generated, LIGAND software was not able to calculate accurate values for affinity and receptor density in *APLNR* KD hESCs.

In contrast, binding of a fixed concentration of [^{125}I]apelin-13 was unaffected by tetracycline treatment in shB2M transgene carrying hESCs (Figure 4.7B), indicating no change in expression of the apelin receptor at the protein level.

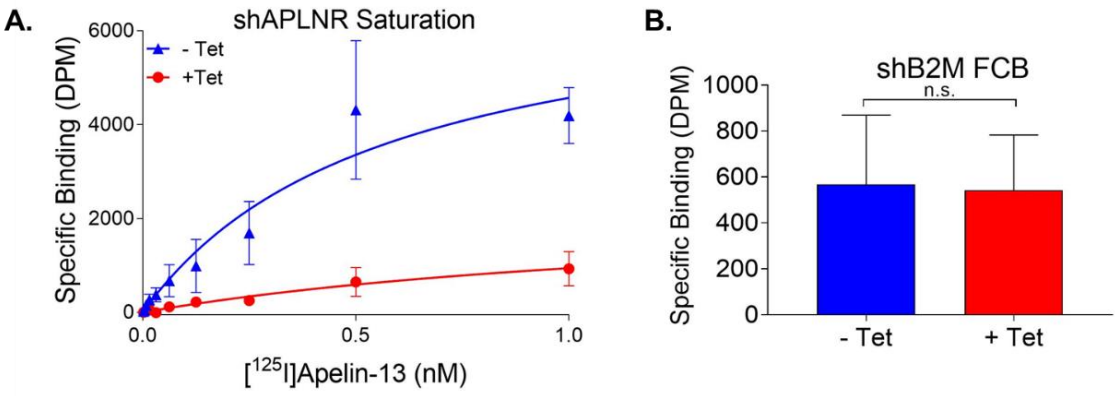

Figure 4.7: (A) Saturation specific [^{125}I]apelin-13 binding in hESCs expressing the shAPLNR transgene cultured with or without tetracycline for 4 days. (B) Specific binding of a fixed concentration of [^{125}I]apelin-13 in hESCs expressing shB2M transgene cultured with or without tetracycline for 4 days. Specific binding levels compared by unpaired, two-tailed Student's t-test. n = 3 for all. Data represent mean±sem.

4.3.4 Determination of apelin receptor knockdown efficiency in hESC-CMs

4.3.4.1 Apelin receptor knockdown efficiency at the gene level in hESC-CMs

Following successful *APLNR* KD in hESCs, the next aim was to determine whether it was possible to knockdown apelin receptor in hESC-CMs. Here, hESCs were cultured in the presence of tetracycline for 4 days before inducing differentiation to cardiomyocyte, with tetracycline treatment maintained throughout differentiation

(referred to subsequently as early KD) and until collection on day 14-17. *APLNR* KD was successful in both lines, however in contrast to what was observed in hESCs, interestingly here the 2.2 and 5.3 lines displayed differing levels of knockdown. In 2.2 hESC-CMs treated with tetracycline, *APLNR* expression was reduced by 91% compared to control (Figure 4.8A). In 5.3 hESC-CMs, a smaller reduction in expression of ~60% was seen following tetracycline treatment (Figure 4.8B). Although both lines displayed a significant decrease in *APLNR* expression, because of this difference in knockdown level, for all subsequent experiments the 2.2 and 5.3 lines were treated separately to investigate the effect of level of *APLNR* KD on hESC-CMs.

Again, as seen in hESCs, expression of *APLNR* in shB2M control hESC-CMs was unaffected by tetracycline treatment (Figure 4.8C).

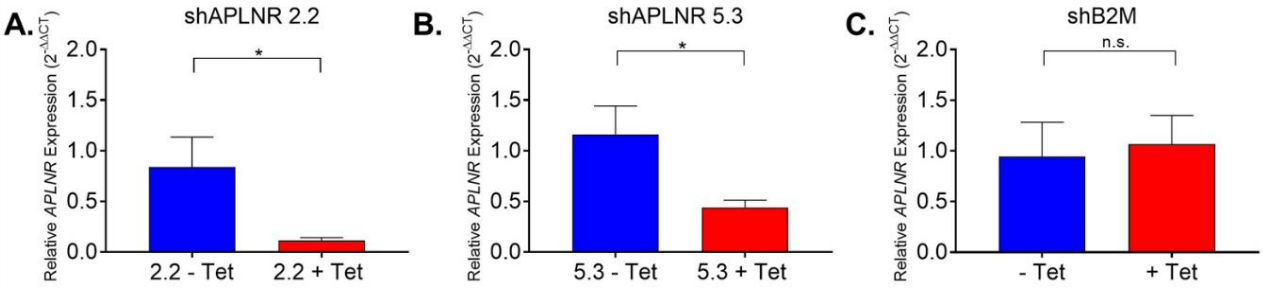

Figure 4.8: Comparison of relative expression of the *APLNR* gene in iKD hESC-CMs, with or without tetracycline treatment in hESCs for 4 days prior to initiating differentiation and then maintained throughout cardiomyocyte differentiation (early KD). Expression of *APLNR* in two lines of apelin receptor iKD hESC-CMs, (A) 2.2 and (B) 5.3. (C) Expression of *APLNR* in B2M control line hESC-CMs cultured with or without tetracycline. n = 4 for all. Relative expression compared to line – Tet mean expression. Expression compared by unpaired, two-tailed Student's t-test, *p<0.05. Data represent mean±sem.

4.3.4.2 Apelin receptor knockdown at the protein level in hESC-CMs

In hESC-CMs with early KD, saturation radioligand binding was also performed. As seen for WT cardiomyocytes, for both 2.2 and 5.3 control lines cultured without tetracycline, [^{125}I]apelin-13 bound with a subnamolar affinity of 3.8 x 10^{-10} M and 1.3 x 10^{-10} M, respectively, and binding was saturable over the concentration range tested (Figure 4.9A and B). In contrast, in 2.2 hESC-CMs treated with tetracycline, [^{125}I]apelin-13 binding was greatly reduced, again indicating little expression of apelin

receptor protein. In the 5.3 line, hESC-CMs were found to bind more [^{125}I]apelin-13 than 2.2, although this was still reduced compared to control hESC-CMs. These results are in agreement with what was seen at the gene level in terms of *APLNR* expression.

Consistent with previous experiments, binding of a fixed concentration of [^{125}I]apelin-13 in shB2M hESC-CMs was unchanged with tetracycline treatment (Figure 4.9C).

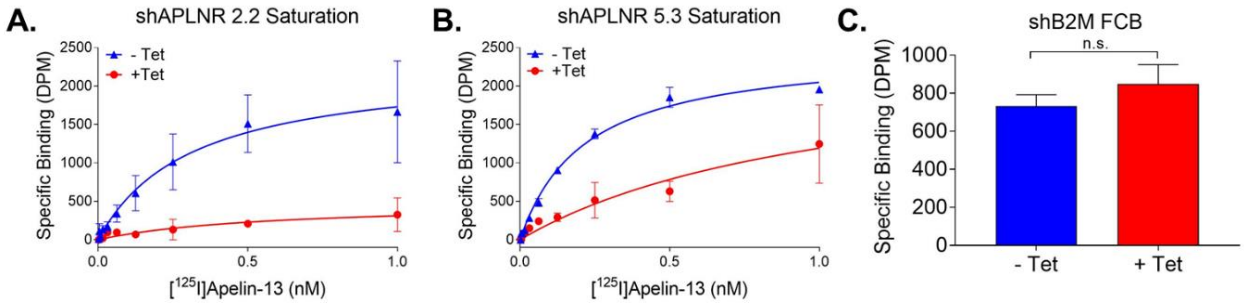

Figure 4.9: (A) Saturation specific [^{125}I]apelin-13 binding in shAPLNR 2.2 hESC-CMs cultured with or without tetracycline throughout differentiation (early KD). n = 4. (B) Saturation specific [^{125}I]apelin-13 binding in shAPLNR 5.3 hESC-CMs cultured with or without tetracycline throughout differentiation (early KD). n = 3. (C) Specific binding of a fixed concentration of [^{125}I]apelin-13 in hESC-CMs expressing shB2M transgene cultured with or without tetracycline throughout differentiation. Specific binding levels compared by unpaired, two-tailed Student's t-test. n = 3. Data represent mean±sem.

4.4 Discussion

Here the aim was to knockdown the expression of the apelin receptor in hESC-CMs to generate a model that can be used to gain insights into the receptor's role in cardiomyocyte function. Two approaches were utilised – transfection of siRNA targeting *APLNR* into hESC-CMs, and generation of a hESC line stably expressing a transgene producing a shRNA directed against the apelin receptor and expressed under the control of a tetracycline inducible element.

4.4.1 Unsuccessful siRNA mediated knockdown of the apelin receptor in hESC-CMs

Initially, I attempted to induce *APLNR* knockdown in hESC-CMs directly, by transfecting apelin receptor specific siRNAs. This method produced highly variable

results, and although successful knockdown was seen with one siRNA, this was not reproducible using the same transfection concentrations and conditions.

There are a number of reasons why siRNA mediated knockdown may have been unsuccessful. Firstly, hESCs-CMs are particularly difficult to transfect (Tan *et al.*, 2019; Bodbin *et al.*, 2020). Optimisation of hESC-CM transfection has been poorly studied, with few papers published addressing the matter. There are multiple methods of transfection available, such as lipofection, viral-transduction and nucleofection, however the efficiency of these methods in PSC-CMs remains low, often with high toxicity (Bodbin *et al.*, 2020). For example, transfection using magnetic nanoparticles to transfect hiPSC-CMs achieved a transfection efficiency of only 18% (Yamoah *et al.*, 2018). In this thesis, DharmaFECT transfection reagent was selected, which has been optimised for siRNA delivery via lipofection. However, the maximum transfection efficiency that has been reported for lipofection transfection is only 56% (Tan *et al.*, 2019), which may not be sufficient to produce substantial knockdown.

Inducing knockdown of the apelin receptor is further complicated by the fact that GPCRs are typically expressed at very low levels (Chakraborty *et al.*, 2015; Insel *et al.*, 2015). As reported in Section 3, wild-type hESC-CMs express the apelin receptor at a density of ~16 fmol/mg, which is particularly low even for a GPCR. In comparison, regions of the rat brain have a reported density of 220 fmol/mg for the GPCR α2-adrencoeptor (Phan *et al.*, 2017), while in the human lower urinary tract muscarinic receptor density was found to be around 700 fmol/mg (Anisuzzaman *et al.*, 2008). It has previously been demonstrated that level of target gene expression is a critical determinant of siRNA mediated knockdown efficiency, with superior gene silencing seen for highly expressed transcripts (Hong *et al.*, 2014). Hence this low level apelin receptor expression is not optimal. The combination of low initial receptor expression with a poor transfection efficiency is likely why the siRNA method of gene silencing was unsuccessful.

4.4.2 Generation of a novel apelin receptor inducible knockdown system

Following on from the failed attempts to induce knockdown with siRNA, I opted to generate an apelin receptor inducible knockdown system in hESCs, using the previously described sOPTiKD system (Bertero *et al.*, 2016). Using this tetracycline

inducible system, robust apelin receptor KD at the gene and protein level has been demonstrated in both hESCs and hESC-CMs generated from apelin receptor KD hESCs.

A small number of studies have previously knocked down GPCRs in a variety of stem cell types (Q. Wang *et al.*, 2020; C. S. Lee *et al.*, 2021; Eichberg *et al.*, 2021). However, based on literature searches this is the first use of an inducible knockdown system to target a GPCR in stem cells.

4.4.2.1 The power of the sOPTiKD inducible knockdown system

There are a number of advantages of using the sOPTiKD system. Firstly, the shRNA transgene is designed to integrate into the host cell genome (Bertero *et al.*, 2016), ensuring stable long-term expression, in contrast to the transient transfection seen for the siRNA approach described above. This means that one round of hESC transfection can be performed and the transgene expression will remain at a stable level in proliferating descendants of the transfected cell. This is an advantage, as in proliferating cells such as hESCs, transiently transfected genetic material is diluted over time as the cells divide (T. K. Kim and Eberwine, 2010).

Furthermore, transfection efficiency is often higher for shRNA compared to siRNA, and potency is often increased as shRNA makes use of endogenous processing machinery, meaning lower copy numbers and concentrations of transfection materials can be used (Rao *et al.*, 2009). The apelin receptor targeting shRNA is expressed under the control of a H1 promoter (Bertero *et al.*, 2016), producing a double stranded transcript that mimics the structure of a pre-miRNA, meaning the hairpin is processed as an endogenous miRNA, which function to promote mRNA decay and repress gene expression (Sheng *et al.*, 2020). The shRNA is then transported to the cytoplasm by Exportin5, where it is processed by Dicer to form a siRNA duplex (normally ~22 nucleotides long). The double stranded RNA is then loaded on to the RNA-induced silencing complex (RISC), where one strand (the 'passenger strand') is cleaved by AGO2. This leaves the guide strand complexed with RISC, which goes onto bind to its complementary mRNA target, promoting mRNA cleavage (J. K. W. Lam *et al.*, 2015) (Figure 4.10).

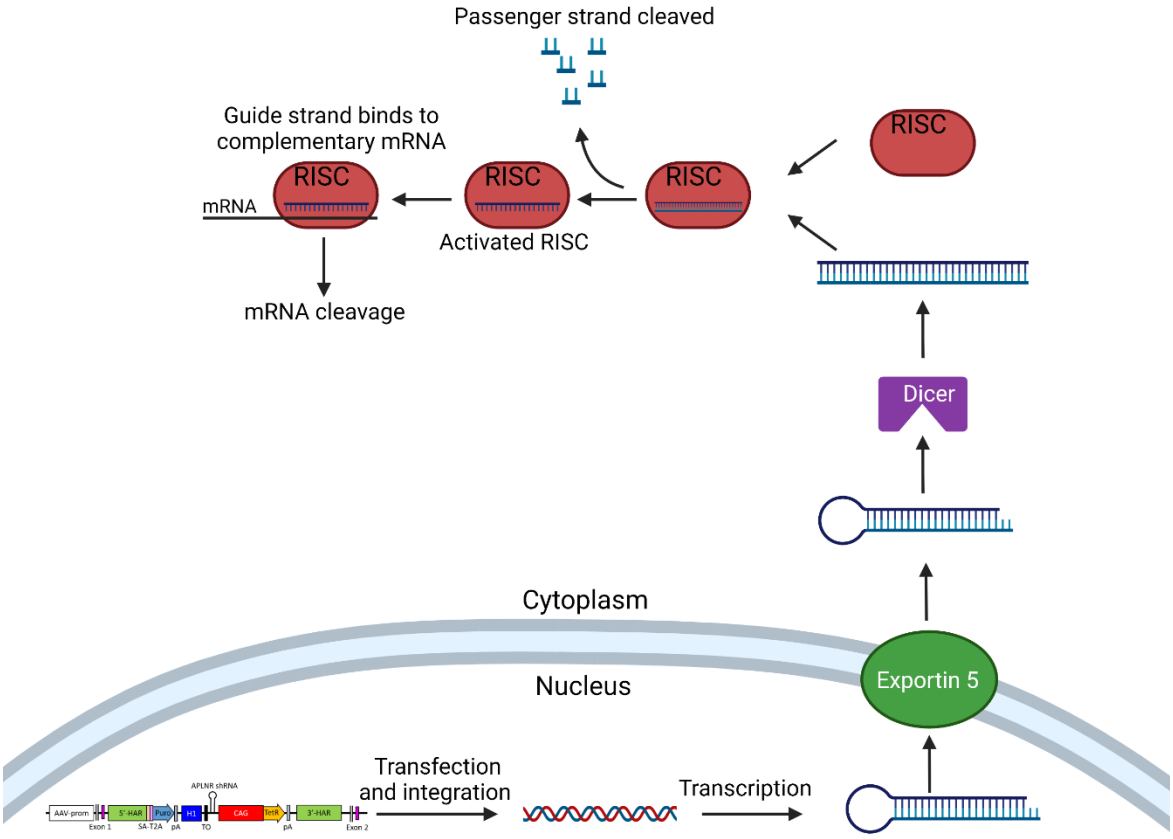

Figure 4.10: Processing of *APLNR* shRNA transgene to induce apelin receptor KD. Figure created using Biorender.com.

The sOPTiKD system is integrated into a genetic locus which ensures expression in the differentiated progeny of the hESCs. This is advantageous, as it is easier to achieve high transfection efficiency in hESCs when compared to hESC-CMs (Bodbin *et al.*, 2020). Additionally, because expression of the shRNA is under the control of a tetracycline response element, there is temporal control of *APLNR* KD, and knockdown can also be reversed by removing tetracycline (Bertero *et al.*, 2016). This is particularly beneficial here, as transgene expression is retained throughout differentiation from hESC to hESC-CM so *APLNR* KD can be induced at any stage throughout development simply by adding tetracycline to the culture medium. This is a powerful tool, allowing the exploration of the role of the apelin signalling system both throughout differentiation and in differentiated hESC-CMs, as well as in the differentiation and function of other cell types.

4.4.2.2 Differing levels of APLNR KD in two lines of shAPLNR hESC-CMs

When generating *APLNR* KD hESCs, a number of lines were identified with substantial knockdown, with two selected for further culture and study (2.2 and 5.3). When examining knockdown efficiency at the gene level in hESCs, level of *APLNR* KD was similar in the two lines following tetracycline treatment. Interestingly, however, in hESC-CMs treated with tetracycline, the 5.3 line displayed ~60% knockdown while 2.2 displayed ~90% knockdown. The reason for this divergence is unclear but it could be that the shRNA transgene is expressed at a lower level in the 5.3 hESC-CMs compared to 2.2. Alternatively, the tetracycline response element may be less accessible in the 5.3 line, or the tetracycline concentration is not reaching sufficient levels at the response element to induce as substantial *APLNR* KD as seen in 2.2.

Nevertheless, these fortuitous results are useful, as this provides another tool for investigation of apelin receptor function. By inducing knockdown in both 2.2 and 5.3, insights can be gained into the effect of level of apelin receptor KD on hESC-CM differentiation and function, allowing the determination of whether a 'threshold' of apelin receptor expression level is needed.

4.5 Conclusions

The apelin receptor was successfully knocked down at both gene and protein level in hESCs and hESC-CMs. Based on literature searches, not only is this the first use of the sOPTiKD system to knockdown the apelin receptor, but also the first application of this system to knockdown a GPCR in hESCs or hESC-CMs. This is of particular note as GPCRs are challenging to knockdown due to their low expression level.

This platform can be used to investigate the role of the apelin receptor in hESC-CM differentiation and function, by inducing knockdown at defined stages and characterising any resulting phenotype as described in the following sections.

5. Effect of Apelin Receptor Knockdown throughout hESC-Derived Cardiomyocyte Differentiation

5.1 Introduction

Having generated the apelin receptor inducible knockdown system, the next aim was to determine the effect of knocking down the apelin receptor throughout hESC-CM differentiation.

As described in Section 1, the apelin signalling system has previously been shown to have an important role in cardiovascular development. Apelin receptor KO mice are not born in Mendelian ratio, with the majority dying in utero displaying severe defects in heart formation (Kang *et al.*, 2013). The effects of apelin receptor activation in development are mainly dependent on ELA, as apelin peptide KO mice are normal, although do show defective cardiac contractility with age or stress (Kuba *et al.*, 2007; Charo *et al.*, 2009). In contrast, loss of function mutations in the zebrafish ELA gene resulted in a high proportion of embryonic lethality and only rudimentary heart formation (Chng *et al.*, 2013; Pauli *et al.*, 2014).

Despite this clear involvement of the apelin signalling system in heart formation, there is a lack of a suitable human *in vitro* model to investigate the contribution of the apelin receptor in human cardiomyocyte development.

This section describes the effect of *APLNR* KD on hESC-CM differentiation. The results show that loss of apelin receptor greatly reduces hESC-CM differentiation efficiency and increases the number of fibroblasts. Furthermore, *APLNR* KD throughout differentiation affects the function of resulting hESC-CMs, influencing cell adhesion properties, increasing apoptosis and disrupting voltage signalling.

5.2 Methods

The methods relevant to this section are listed in Table 5.1 and described in Section 2, with further detail for selected methods below.

Method	Section
Cell culture and hESC-CM differentiation	2.2 and 2.3
Troponin T and Thy1 flow cytometry co-stain	2.6
Analysis of stage specific marker gene expression by qRT-PCR	2.4
EthD-1 staining to quantify cell death	2.11
Binding of apelin fluorescent ligand	2.12
Peptide production determined by ELISA	2.8
RNA sequencing of apelin receptor KD hESC-CMs	2.13
hESC-CM adhesion assay	2.14
Measuring hESC-CM voltage signalling using FluoVolt	2.15
Measuring hESC-CM calcium signalling using Fluo-4, AM	2.16
Effect of apelin receptor ligands on hESC-CM differentiation	2.17
Data analysis and statistics	2.24

Table 5.1: Descriptions of the methods used in this section found can be found in the listed corresponding section.

5.2.1 Cell culture

hESCs were maintained as described in Section 2.2, cultured with or without tetracycline (1 µg/ml, daily refresh) for 4 days, and then plated for differentiation as described in Section 2.3. Tetracycline treatment was maintained throughout differentiation and hESC-CM culture, with refresh every second day. Cells were visualised with a brightfield microscope, and images acquired using an iPhone 7 mounted on a LabCam adaptor.

5.2.2 qRT-PCR for stage specific markers

At defined stages throughout differentiation, cells were lysed and RNA extracted. qRT-PCR for stage specific markers was performed using SYBR Green as described in Section 2.4, with *GAPDH* used as a housekeeping gene. Expression was normalised to housekeeping gene expression and relative expression compared to control cells with transgene targeting B2M cultured with tetracycline (B2M + Tet) calculated using the $2^{(-\Delta\Delta CT)}$ method (Schmittgen and Livak, 2008).

5.2.3 Effect of apelin receptor ligands on hESC-CM differentiation

To determine the effect of apelin receptor activation on hESC-CM differentiation, in Section 5.3.3, control or apelin receptor KD hESC-CMs were cultured in the presence of apelin receptor ligands throughout differentiation (Section 2.17). At day 14, cells were analysed by flow cytometry to determine TnT and Thy1 positive percentages (Section 2.6). The concentration of ligands used was higher than that seen physiologically. In Sections 5.3.1 and 5.3.2, no exogenous ligands were included and effects are dependent on endogenously produced ligands.

5.3 Results

In Section 4, significant knockdown of the apelin receptor was demonstrated in two lines of hESC-CMs, generated from hESCs cultured in the presence of tetracycline for 4 days and maintained in tetracycline throughout differentiation (early KD). 2.2 hESC-CMs displayed a greater decrease in apelin receptor expression (~90% KD at the gene level) compared to 5.3 hESC-CMs which had ~60% KD. I therefore aimed to determine the effects of loss of apelin receptor. Throughout Section 5, apelin receptor KD was induced in hESCs and maintained throughout differentiation and hESC-CM culture (early KD).

5.3.1 Effect of apelin receptor knockdown on hESC-CM differentiation

Throughout this section no exogenous apelin receptor ligands were added to cultures and effects are dependent on endogenous apelin receptor signalling.

5.3.1.1 Morphological changes in hESC-CMs with apelin receptor KD throughout differentiation

Looking firstly at cell morphology, brightfield microscopy revealed distinct differences between control and apelin receptor KD cells (Figure 5.1). Control lines formed homogenous sheets of beating cardiomyocytes, while 2.2 line *APLNR* KD cells grew as patches of clumped cardiomyocytes with areas of mesenchymal-like cells and fibroblasts interspersed in between. It should also be noted that there was variability in the outcome of distinct differentiations of the 2.2 line cultured with tetracycline, with different cardiomyocyte and fibroblast/mesenchymal-like cell density seen as shown

in the representative images displayed in Figure 5.1F. In contrast, there were no visual differences between control and *APLNR* KD 5.3 hESC-CMs.

Control cells (B2M ± Tet and shAPLNR – Tet) displayed strong, synchronous contraction. Again, in 5.3 hESC-CMs, no difference in contraction was seen between control and *APLNR* KD hESC-CMs. Conversely, *APLNR* KD in the 2.2 line also had marked consequences on spontaneous contraction, with variability seen in distinct differentiations as described above. In some differentiations, when focussing on areas of cardiomyocytes in 2.2 *APLNR* KD cells, contraction was weak and the hESC-CMs did not appear to function together, contracting asynchronously. Furthermore, in other differentiations there was no contraction observed in the whole field of view (Videos 5.1-5.3). These initial results suggest that the apelin receptor has an important role in cardiomyocyte development, with a certain threshold level needed to ensure proper differentiation.

Importantly, B2M line hESC-CMs looked similar regardless of tetracycline inclusion, suggesting that any effects seen in *APLNR* KD lines are dependent on loss of the apelin receptor, rather than tetracycline itself.

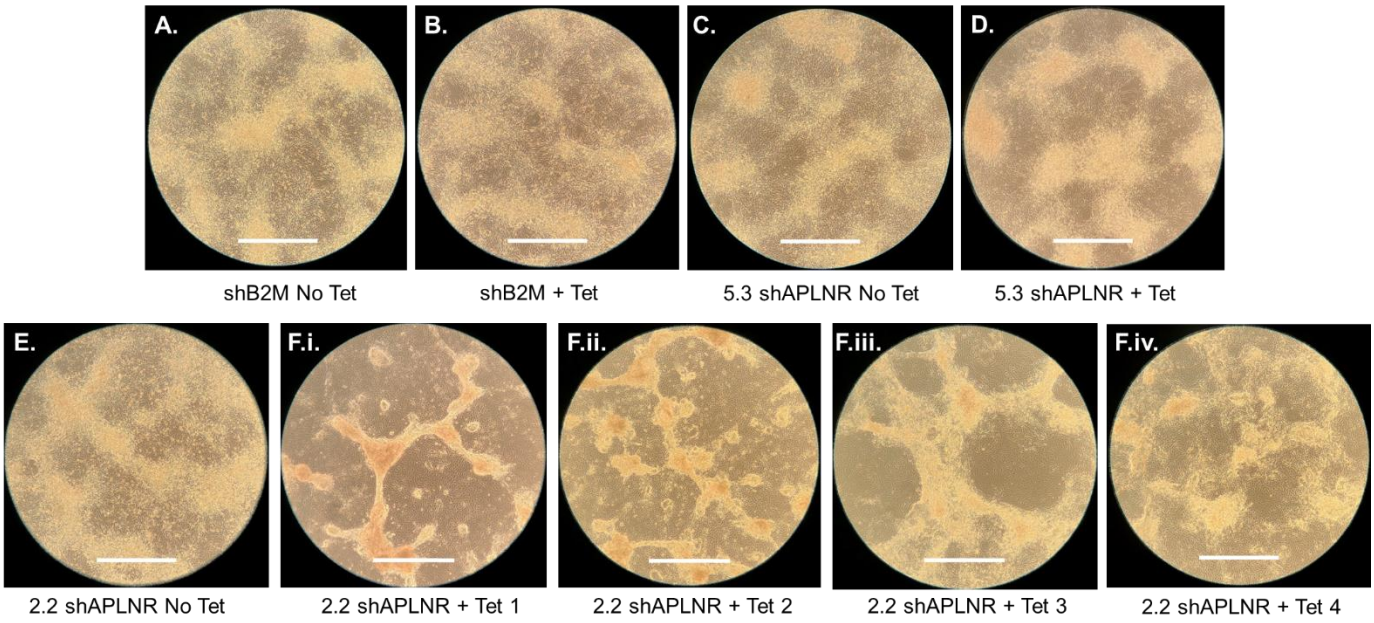

Figure 5.1: Representative brightfield images of control and *APLNR* KD hESC-CMs at day 14-17. shB2M control hESC-CMs cultured (A) without and (B) with tetracycline. 5.3 shAPLNR hESC-CMs cultured (C) without and (D) with tetracycline. 2.2 shAPLNR hESC-CMs cultured (E) without and (Fi-iv) with tetracycline treatment. Multiple images to show variability in differentiation. Scale bar = 200 µm.

5.3.1.2 Effect of APLNR KD on hESC-CM differentiation efficiency

Having visualised differences in cardiomyocyte differentiation with apelin receptor KD, it was important to quantify changes in differentiation efficiency. To do this, cells were co-stained for the cardiac marker troponin T (TnT) and fibroblast marker Thy1, and analysed by flow cytometry (Figure 5.2).

For 2.2, control cells were found to stain 58.1%±3.1 TnT positive and 32.5%±3.2 Thy1 positive. In *APLNR* KD, there was a significant increase in Thy1 positive cells to 67.7%±1.5. In tandem, there was a decrease in troponin positive percentage (13.8%±1.9), indicating a decrease in cardiomyocyte differentiation efficiency and an increase in the number of cells acquiring a fibroblast identity with apelin receptor knockdown.

In the 5.3 line, 67.1%±9.8 of control cells stained positively for troponin T, with 24.0%±2.0 staining positively for Thy1. For *APLNR* KD cells, there was a trend for a decrease in troponin positive (55.5%±11.0) and increase in Thy1 positive (31.6%±6.3) but this was small and did not reach significance.

There was a trend towards an increase in cardiomyocyte differentiation in B2M control cells cultured in the presence of tetracycline but this was not significant. Thy1 positive percentage was unaffected by tetracycline in the B2M line.

These results further support the hypothesis that a threshold level of apelin receptor expression is needed for efficient hESC-CM differentiation.

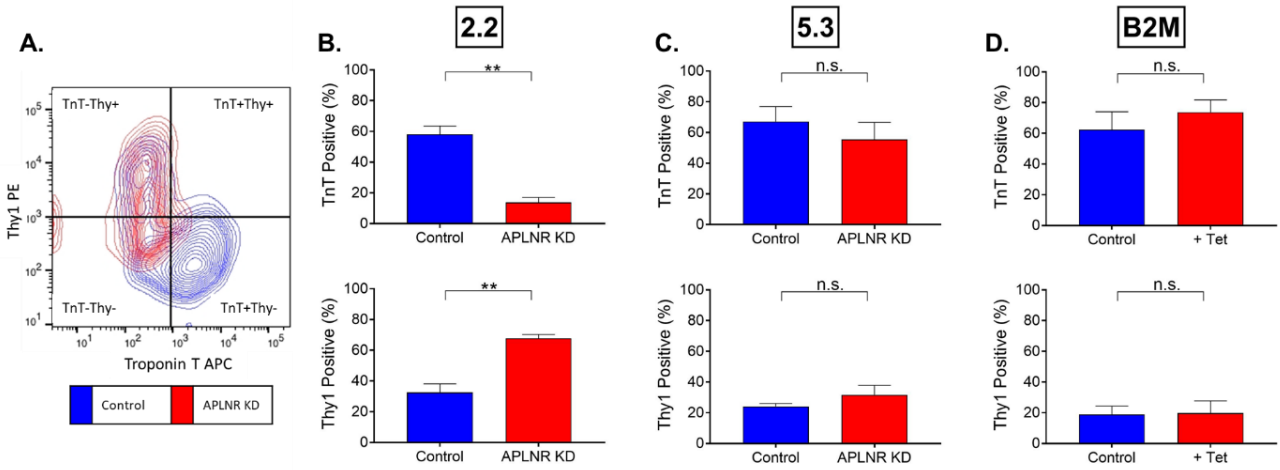

Figure 5.2: Flow cytometry staining to determine hESC-CM differentiation efficiency with *APLNR* KD. (A) Representative flow cytometry plot of control and *APLNR* KD hESC-CMs co-stained for troponin T (TnT, APC) and Thy1 (PE). Quantification of TnT (top) and Thy1 (bottom) positive percentages from flow cytomteric co-stain for (B) 2.2 control and *APLNR* KD hESC-CMs, (C) 5.3 control and *APLNR* KD hESC-CMs and (D) shB2M control and + tetracycline hESC-CMs. n = 3 for all, compared by unpaired, two-tailed Student's t-test,**p<0.01. Data represent mean±sem.

5.3.1.3 Effect of apelin receptor KD on cardiomyocyte differentiation stage specific markers

Following on from establishing the importance of apelin receptor in hESC-CM differentiation, the next aim was to identify if there is a particular differentiation stage at which loss of apelin receptor expression has its effects.

To determine if *APLNR* KD affects expression of cell stage specific markers, qRT-PCR using primers directed against characterised markers of differentiation stage was performed (Burridge *et al.*, 2014; Mendjan *et al.*, 2014). At the end of each stage of differentiation (Figure 3.1, FLyAB, FBRI, FB, Day 10 as described in Section 2.3), cells were collected and RNA was extracted. Table 5.2 describes the developmental stage for each sample.

Sample	Day of differentiation	Developmental stage
FLyAB	2	Mesoderm
FBRI	6	Cardiogenic mesoderm
FB	8	Cardiac progenitors
Day 10	10	Early cardiomyocytes

Table 5.2: Day of collection and developmental stage for samples analysed for cell stage markers. See Figure 3.1.

Initially, expression of *APLNR* gene was determined to ensure knockdown was seen throughout differentiation. As shown in Figure 5.3A, there was significant knockdown of *APLNR* across all stages of differentiation, with a higher level of knockdown seen in the 2.2 line, consistent with previous results.

Next, expression of various markers at each stage of differentiation was quantified in control (B2M + Tet) versus *APLNR* KD cells (Figure 5.3B-E). Across the differentiation stages, for the majority of markers examined no significant difference was found. After the FB stage (cardiac progenitors), there was a significant increase in *THY1* gene expression in the 2.2 line, however this increase was not significant at day 10. Expression of *THY1* at day 10 was however variable, correlating with what is seen in the images in Figure 5.1. A significant increase in expression of the gene encoding the ryanodine receptor was seen in the 2.2 line with *APLNR* KD, however reasons for this are unclear. It was therefore hypothesised that the apelin receptor may be involved in the late stages of cardiomyocyte differentiation, at the onset of contraction.

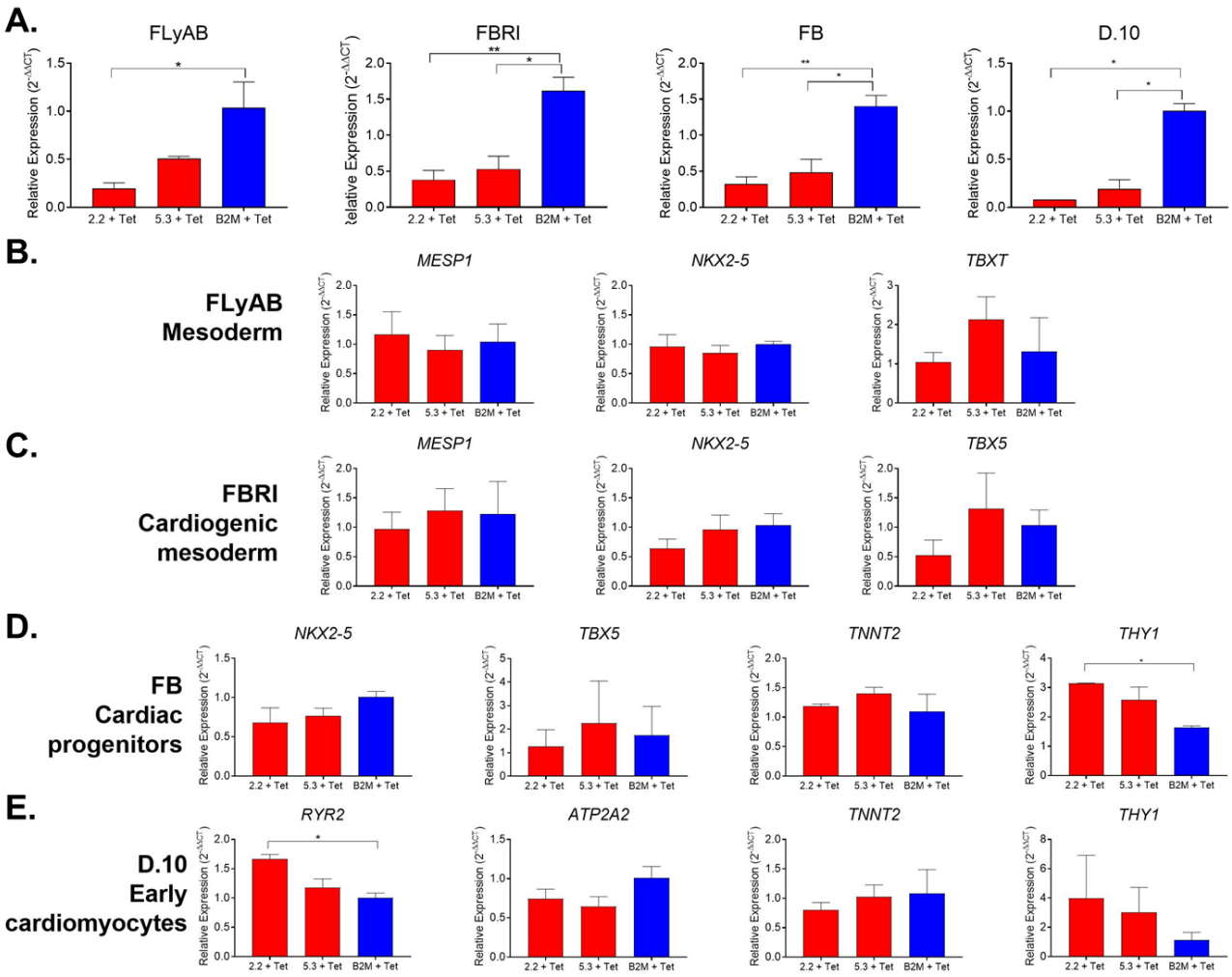

Figure 5.3: (A) Comparison of relative expression of *APLNR* gene across 4 stages of differentiation. Expression displayed relative to mean expression in B2M + Tet for each stage. n = 3, expression levels compared by unpaired, two-tailed Student's t-test, *p<0.05, **p<0.01. Comparison of relative expression of stage specific markers across 4 stages of differentiation, (B) FLyAB mesoderm, (C) FBRI cardiogenic mesoderm, (D) cardiac progenitors and (E) D.10 early cardiomyocytes. Expression displayed relative to mean expression in B2M + Tet for each gene. n = 3, expression levels compared by one way ANOVA followed by Tukey's post hoc test, *p<0.05. Data represent mean±sem.

Consistent with this hypothesis, when visualising the cells across differentiation stages, the morphology of control and *APLNR* KD is comparable in the 2.2 line until the late stages of differentiation, as shown in the image time course in Figure 5.4. As the effect on cardiomyocyte differentiation efficiency is not pronounced in the 5.3 line, only images of 2.2 are shown.

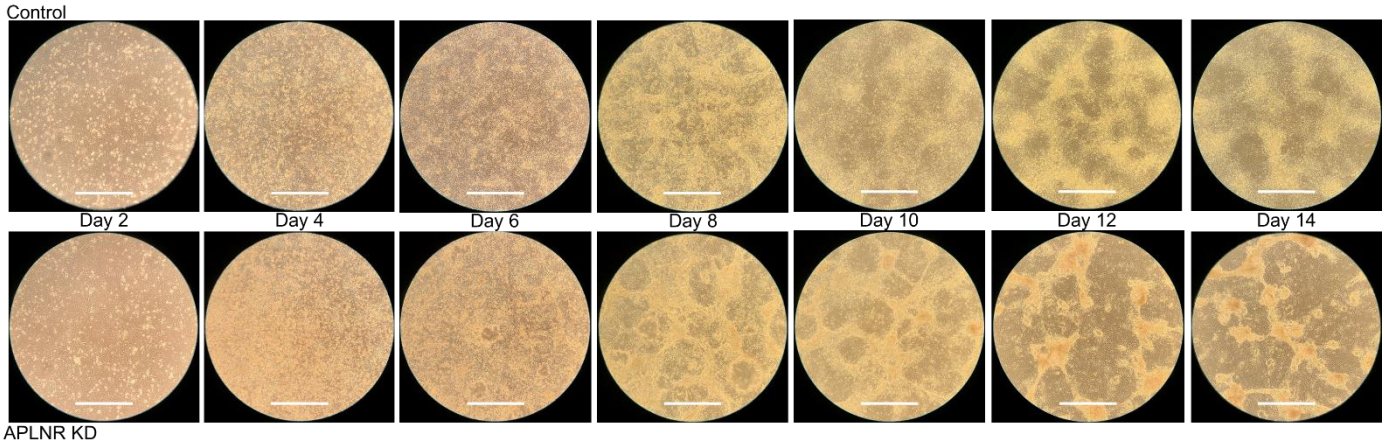

Figure 5.4: Representative time course images of control (top) and *APLNR* KD (bottom) 2.2 line throughout cardiomyocyte differentiation. Scale bar = 200 µm.

5.3.1.4 Effect of APLNR KD on cell death

Next, changes in apoptosis or cell death were investigated to determine if this underlies the differences seen in differentiation efficiency. To investigate this, at each differentiation stage (Figure 3.1) a live/dead assay was performed using a live cell nuclear stain (NucBlue) and cell impermeant Ethidium Homodimer-1 (EthD-1). Before media change at each stage, number of nuclei and number of EthD-1 positive cells were counted and expressed as a ratio for control and *APLNR* KD cells (Figure 5.5). At early stages, no change in cell death was seen in *APLNR* KD cells compared to B2M control line cultured with tetracycline. However, at both day 10 and day 12, a significant increase in the number of dead cells per number of nuclei was observed in the 2.2 *APLNR* KD line (Figures 5.5C and D), again supporting my proposal of a role for apelin receptor in the late stages of differentiation. As expected from previous results, no change was seen in the 5.3 line.

Taking these results together, I hypothesise that the apelin receptor promotes cell survival in late stage cardiomyocyte differentiation.

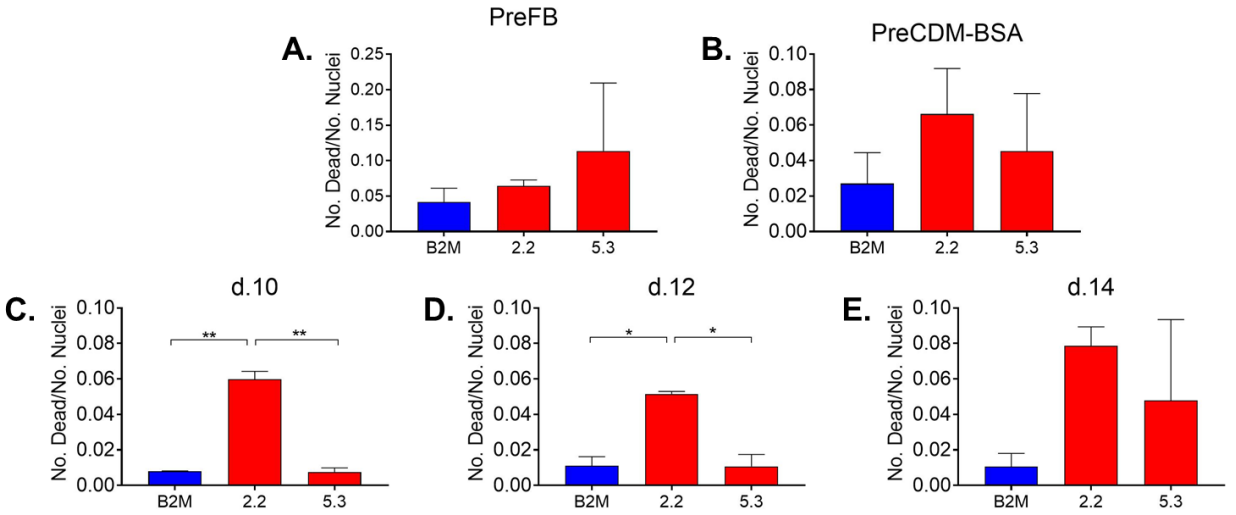

Figure 5.5: Number of dead cells per number of nuclei for *APLNR* KD (2.2 and 5.3) cells compared to control (B2M) at distinct stages of cardiomyocyte differentiation (see Figure 3.1). (A) PreFB = day 6, (B) PreCDM-BSA = day 8, (C) day 10, (D) day 12 and (E) day 14. n = 2 with 3 technical replicates for each, mean values compared by one way ANOVA followed by Tukey's post hoc test, *p<0.05, **p<0.01. Data represent mean±sem.

5.3.2 Effect of *APLNR* KD throughout differentiation on hESC-CM function

Having established an effect of *APLNR* KD on differentiation efficiency, the next aim was to determine if there were any functional consequences of *APLNR* KD on the resulting hESC-CMs if knockdown is maintained from hESC throughout differentiation to hESC-CM.

Throughout this section no exogenous apelin receptor ligands were added to cultures and effects are dependent on endogenous apelin receptor signalling.

5.3.2.1 Effect of APLNR KD on ability to bind apelin peptide

To investigate the effect of *APLNR* KD on ability of hESC-CMs to bind ligands, a fluorescently tagged version of the native [Pyr[1]]apelin-13 peptide (apelin647) was used (Figure 5.6). This assay was also used to visualise the *APLNR* KD and verify the saturation radioligand binding assay results shown in Section 4.3.4. Control and *APLNR* KD hESC-CMs were incubated with fluorescent ligand for 90 minutes before imaging. In the four control conditions (2.2 and 5.3 cultured without tetracycline and B2M ± tetracycline), punctate binding of apelin647 was seen. In both *APLNR* KD lines, apelin647 binding was drastically reduced as expected, with a greater reduction seen

in the 2.2 line. These results are in agreement with the saturation radioligand binding experiments described in Section 4.3.4.

Importantly, tetracycline itself had no effect on apelin647 binding as demonstrated by the comparable binding seen in B2M hESC-CMs regardless of tetracycline inclusion. Binding of apelin647 to apelin receptor was confirmed by incubating with a saturating concentration of [Pyr[1]]apelin-13 (10 µM).

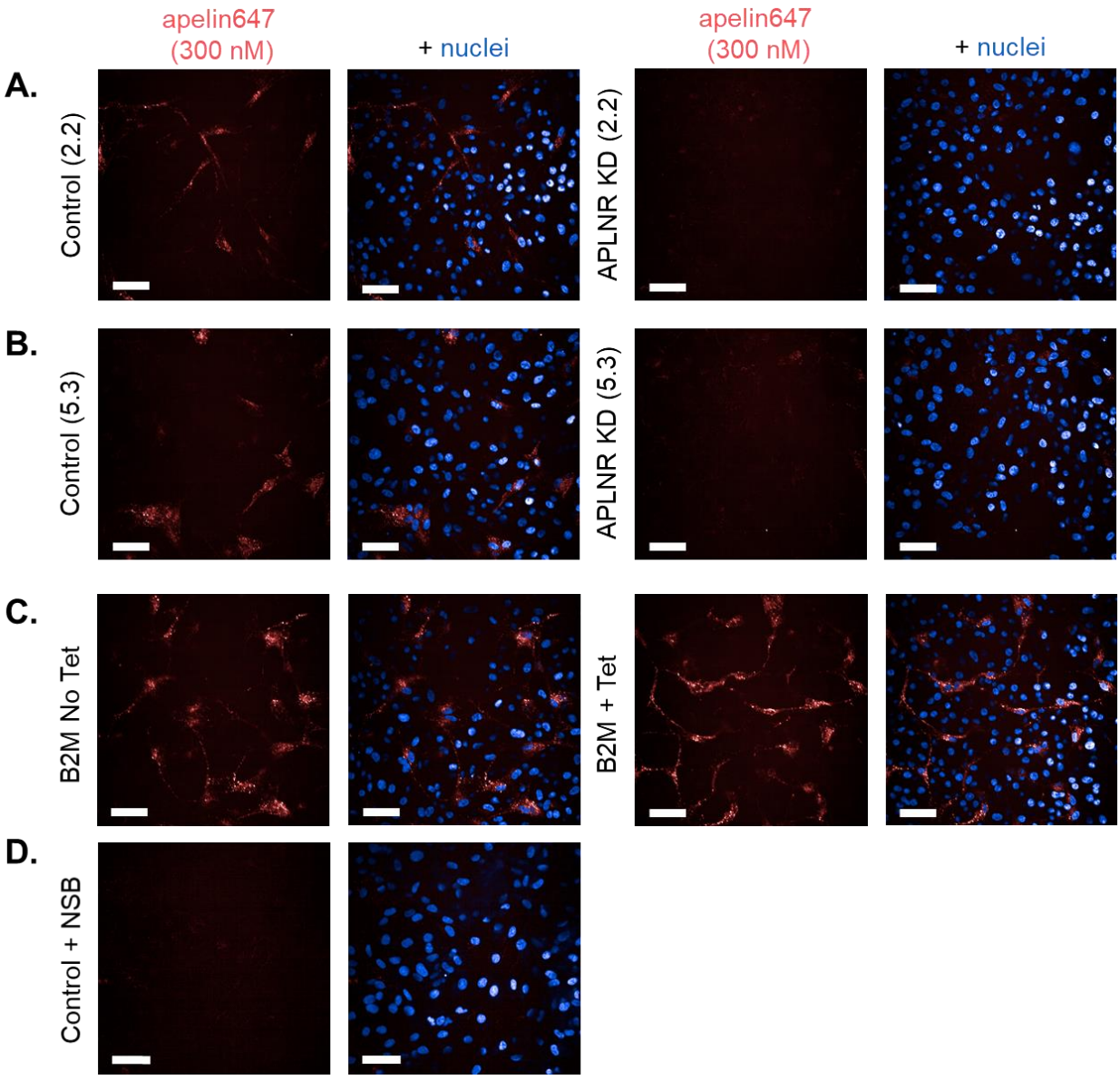

Figure 5.6: Representative images of hESC-CMs incubated with apelin647 fluorescent ligand and Hoechst 3342 nuclear dye. (A) 2.2 line control and *APLNR* KD hESCs, (B) 5.3 line control and *APLNR* KD hESCs and (C) B2M control line hESC-CMs cultured with and without tetracycline. (D) Non-specific binding (NSB) was determined by the inclusion of a saturating concentration of [Pyr[1]]apelin-13. Scale bar = 50 µm.

5.3.2.2 Effect of APLNR KD on hESC-CM peptide production

To quantify the effect of *APLNR* KD on ligand production, ELISAs for apelin and ELA using conditioned supernatant from control and *APLNR* KD hESC-CMs were performed (Figure 5.7). It was hypothesised that there may be an upregulation of ligand production to compensate for reduced signalling due to loss of apelin receptor. Interestingly, a decrease in apelin peptide production was seen in B2M hESC-CMs cultured with tetracycline, suggesting an effect of tetracycline itself (data not shown), hence here data for the two lines of *APLNR* KD hESC-CMs were compared to B2M + Tet hESC-CMs. In terms of ELA expression, no significant difference was seen between conditions. Similarly, for both *APLNR* KD lines, no significant difference in apelin peptide production was seen.

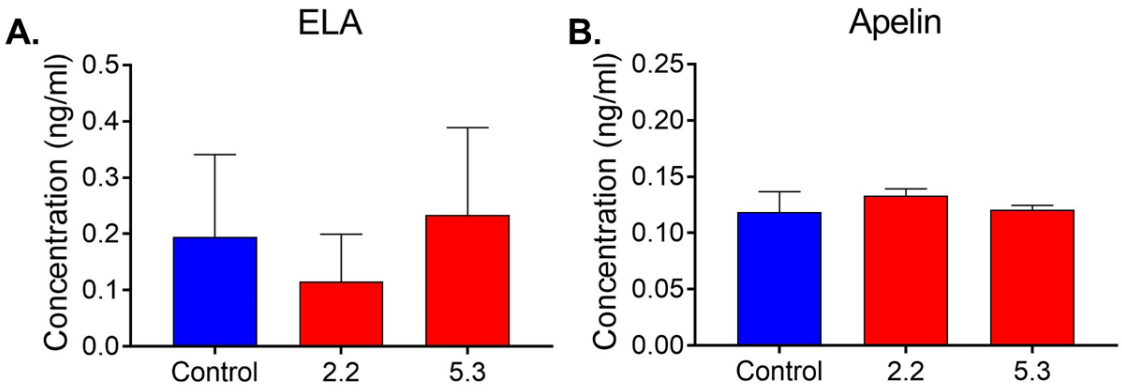

Figure 5.7: Comparison of concentration of (A) ELA and (B) apelin in conditioned supernatant from control (B2M + Tet) and *APLNR* KD (2.2 and 5.3) hESC-CMs. n = 4 for B2M ELA, n = 3 for 2.2 ELA, n = 2 for 5.3 ELA, n = 4 for B2M apelin, n = 4 for 2.2 apelin, n = 2 for 5.3 apelin. Means compared by one way ANOVA followed by Tukey's post hoc test. Data represent mean±sem.

5.3.2.3 RNA sequencing of APLNR KD hESC-CMs

RNA sequencing of control and *APLNR* KD hESC-CMs was performed to generate an unbiased view of the effect of *APLNR* KD. The aim here was to identify potential functional consequences of *APLNR* KD and inform the design of subsequent functional assays.

At day 15 of differentiation, control and *APLNR* KD hESC-CMs were collected for RNA extraction, quality control analysis performed and samples sent for next generation

bulk RNA sequencing (Figure 5.8A). Note that here the two lines of *APLNR* KD hESC-CMs (2.2 and 5.3) were analysed together and are referred to simply as *APLNR* KD throughout this section. Analysis was performed with assistance from E.L. Robinson (University of Colorado) and E.E. Davenport (Wellcome Sanger Institute).

Analysis of sequencing data identified 272 differentially expressed genes (DEGs) with *APLNR* KD, with approximately 50% downregulated and 50% upregulated compared to control (Figure 5.8B). XGR pathway analysis was performed, with a small number of significantly differentially expressed pathways identified, many of which were associated with adhesion and integrin signalling (Figure 5.8C), prompting the design of an assay to determine the effect of *APLNR* KD on hESC-CM adhesion as described in the following section.

Furthermore, of the DEGs identified with *APLNR* KD, *SCN5A,* the gene encoding the cardiac sodium channel $Na_{V1.5}$, was the third most significantly downregulated gene (Q value < 0.01, Figure 5.8D). This was chosen for further characterisation as the top druggable and physiologically relevant target (IUPHAR/BPS Guide to Pharmacology, https://www.guidetopharmacology.org/) (S. D. Harding *et al.*, 2021). $Na_{V1.5}$ is essential for cardiomyocyte depolarisation and conduction of the cardiac action potential (Abriel, 2010; Rook *et al.*, 2012). The pore forming α-subunit of the voltage-dependent cardiac sodium channel $Na_{V1.5}$ is encoded by the *SCN5A* gene, and mutations in this gene have been associated with a number of cardiac arrhythmic disorders such as Brugada syndrome (Rook *et al.*, 2012). Therefore the effect of *APLNR* KD on voltage signalling in hESC-CMs was investigated as described in Section 5.3.2.4.

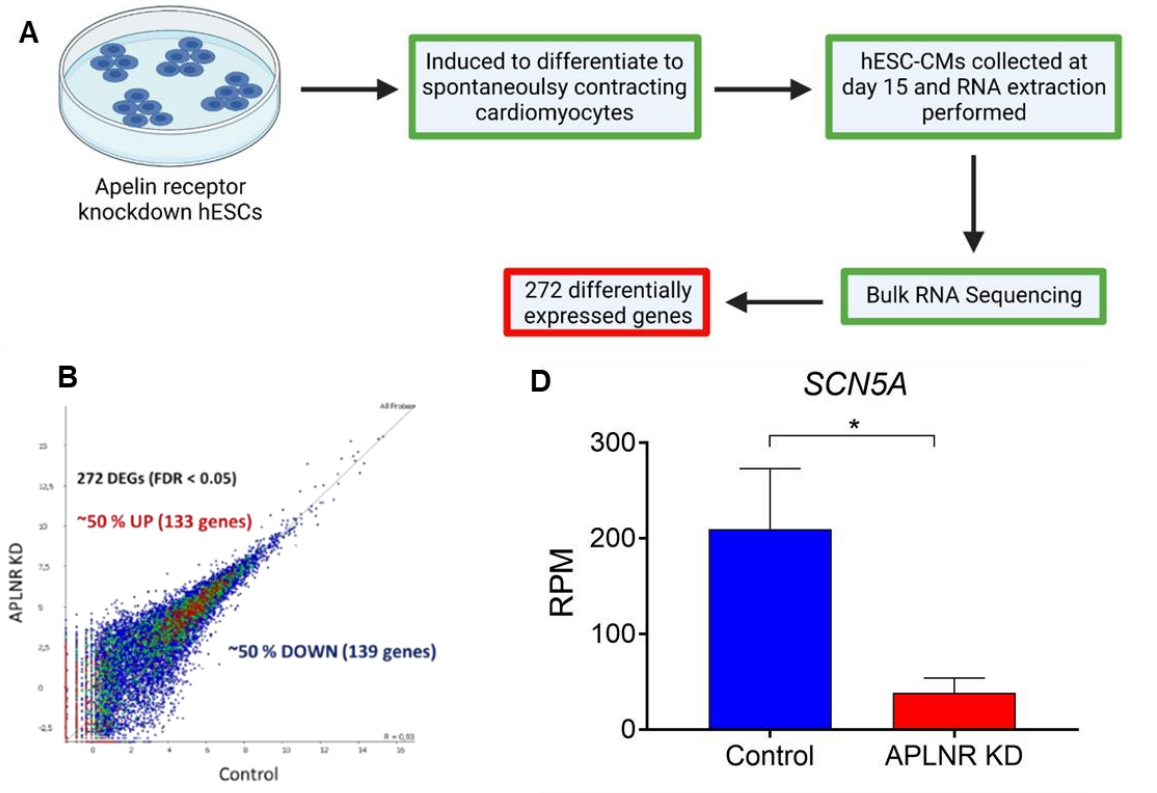

C

XGR Pathway	Z score	P value
Signalling events mediated by focal adhesion kinase	5.58	2.3E-05
Alpha4 beta1 integrin signaling events	4.31	0.00049
Beta3 integrin cell surface interactions	3.99	0.00078
Posttranslational regulation of adherens junction stability and dissassembly	3.02	0.0035
Beta1 integrin cell surface interactions	2.91	0.0041
Integrin Signaling Pathway	1.86	0.023

Figure 5.8: (A) Workflow for bulk RNA sequencing of *APLNR* KD hESC-CMs. This figure was created using Biorender.com. (B) Plot representing number of up- and downregulated differentially expressed genes (DEGs) in *APLNR* KD hESC-CMs compared to control. (C) Selected pathways identified from XGR pathway analysis. Of the small number of pathways identified, many were associated with adhesion and integrin signalling. (D) Expression of *SCN5A* gene encoding the cardiac sodium channel $Na_{v1.5}$ in *APLNR* KD hESC-CMs compared to control. Control n = 3, *APLNR* KD n = 4, means compared by two-tailed Student's t-test, *p<0.05. Data represent mean±sem.

5.3.2.3 Effect of APLNR KD on hESC-CM adhesion

Following on from the RNA sequencing results, an assay was designed to determine the effect of *APLNR* KD on hESC-CM adhesion. hESC-CMs were detached from the original culture plate, replated at a defined density and then fixed at three predetermined time points (3 hours, 12 hours and 24 hours). Cells were then stained

with DAPI nuclear stain to allow quantification of cell number, and phalloidin which binds to actin filaments, allowing visualisation and quantification of cell area and width/length ratio (Figure 5.9). For imaging and quantification, the Opera Phenix High-Content Screening System and Harmony image analysis software were used with assistance from T.L. Williams (University of Cambridge).

To control for any effects of tetracycline itself, all values for the two lines of *APLNR* KD hESC-CMs (2.2 and 5.3) were compared to B2M line hESC-CMs cultured with tetracycline (control). At all three time points, a trend for an increase in the number of cells was seen for 2.2 *APLNR* KD hESC-CMs, however this did not reach significance. In contrast, number of 5.3 hESC-CMs was comparable to that seen for control cells. For all three cell lines, no difference was seen in mean cell area at any time point. Cell width/length ratio was also quantified to give an indication of the effect of *APLNR* KD on hESC-CM shape – a lower width/length ratio indicates a more elongated cell, while a high value represents a rounder cell. 2.2 hESC-CMs were found to have a significantly lower width/length ratio at the three hour time point compared to control cells. At subsequent time points however, no difference was seen. For 5.3 hESC-CMs no difference was seen at any of the three time points.

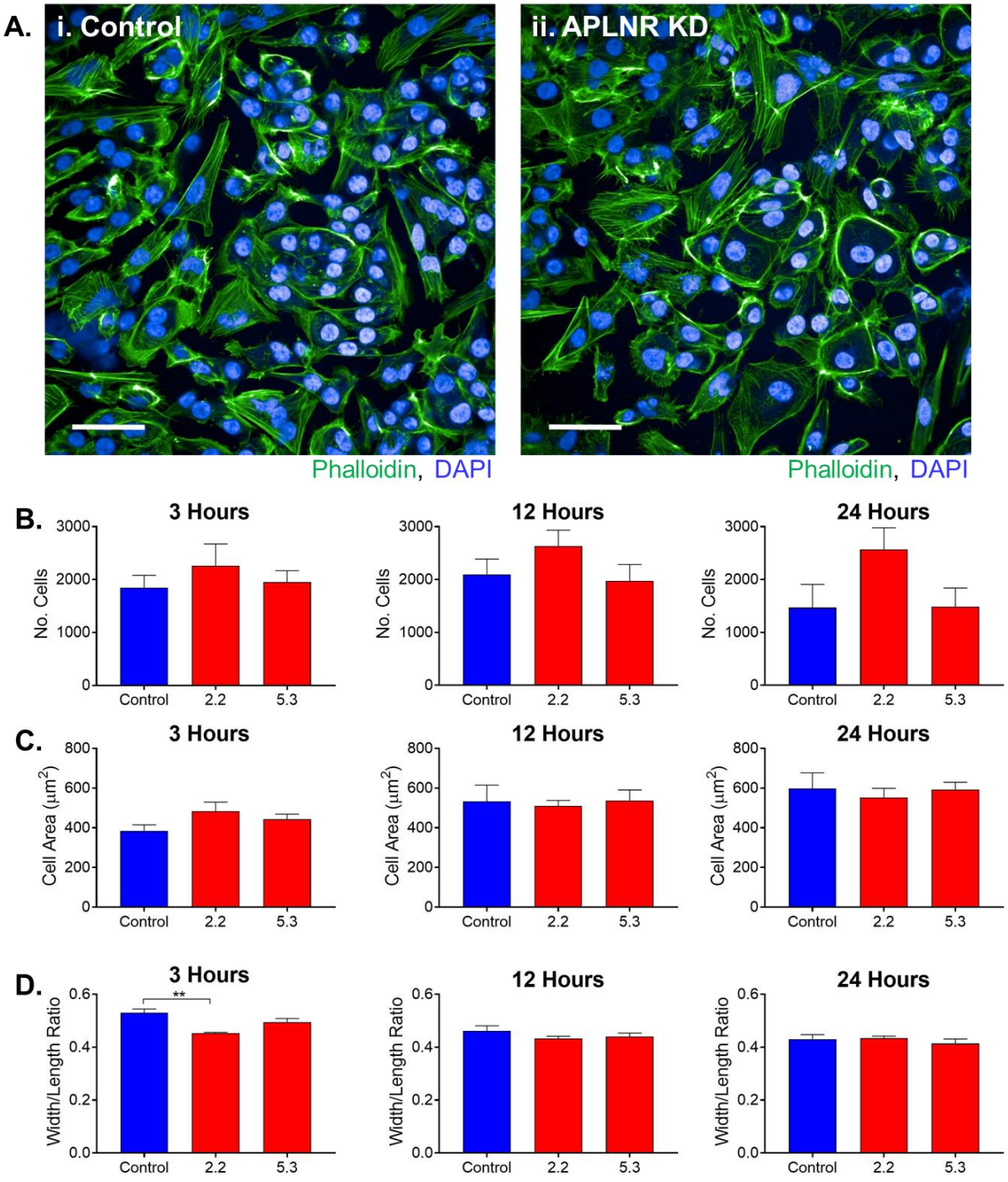

Figure 5.9: Effect of *APLNR* KD on hESC-CM adhesion properties. (A) Representative images of (i) control and (ii) *APLNR* KD hESC-CMs stained with phalloidin-488 (green) and DAPI nuclear stain blue) after 3 hours of culture. Scale bar = 50 µm. (B) Number of control and *APLNR* KD cells sticking at defined time points after replating. (C) Mean cell area of control and *APLNR* KD hESC-CMs at defined time points after replating. (D) Mean width/length ratio of control and *APLNR* KD hESC-CMs at defined time points after replating. n = 4 for all, mean values compared by one way ANOVA followed by Tukey's post hoc test, **p<0.01. Data represent mean±sem.

5.3.2.5 Effect of APLNR KD on hESC-CM voltage signalling

Following on from the identification of *SCN5A* as a significantly downregulated gene in *APLNR* KD hESC-CMs, the next aim was to investigate the effect of *APLNR* KD on voltage signalling. Previously the *APLNR* has been suggested to influence cardiac electrophysiology, and apelin peptide signalling has been shown to modulate cardiomyocyte sodium currents (Farkasfalvi *et al.*, 2007; Chamberland *et al.*, 2010). Additionally, in atrial fibrillation patients, plasma apelin levels are reduced and can be restored by cardiac resynchronisation therapy (Ellinor *et al.*, 2006; Francia *et al.*, 2007).

Here, the voltage sensitive FluoVolt Membrane Potential dye was used, with beating rate controlled by external electrical stimulation paced at 1 Hz. Videos of voltage transients were recorded, with an example recording shown in Video 5.4. A custom MATLAB code written by S. Bayraktar (University of Cambridge) was used to extract values for waveform time to peak (TTP) and time to 90% decay (T90). The code allows the user to select regions of interest, therefore here only regions containing cardiomyocytes (and not contaminating fibroblasts or mesenchymal cells) were selected. Analysis revealed differences between the B2M hESC-CMs cultured in the presence of tetracycline (data not shown), suggesting a tetracycline effect. Therefore results for 2.2 and 5.3 *APLNR* KD hESC-CMs were compared to B2M + Tet hESC-CMs (Figure 5.10). Representative traces are displayed for each condition. Three traces are shown for 2.2 *APLNR* KD hESC-CMs to indicate the variability seen in different differentiations. Observing the traces, the waveform appears different for the 2.2 line compared to control and 5.3 hESC-CMs, with smaller intervals in between spikes seen. The spike shapes themselves also appear different.

Interestingly, *APLNR* KD in 2.2 hESC-CMs was found to significantly increase both time to peak (TTP) and time to 90% decay (T90) compared to control (221.0 ± 18.3 ms *APLNR* KD vs 124.2 ± 10.1 ms control TTP, 119.7 ± 11.8 ms *APLNR* KD vs 51.0 ± 2.6 ms control T90, Figure 5.10). In agreement with previous results. *APLNR* KD in 5.3 line hESC-CMs had little effect on TTP or T90.

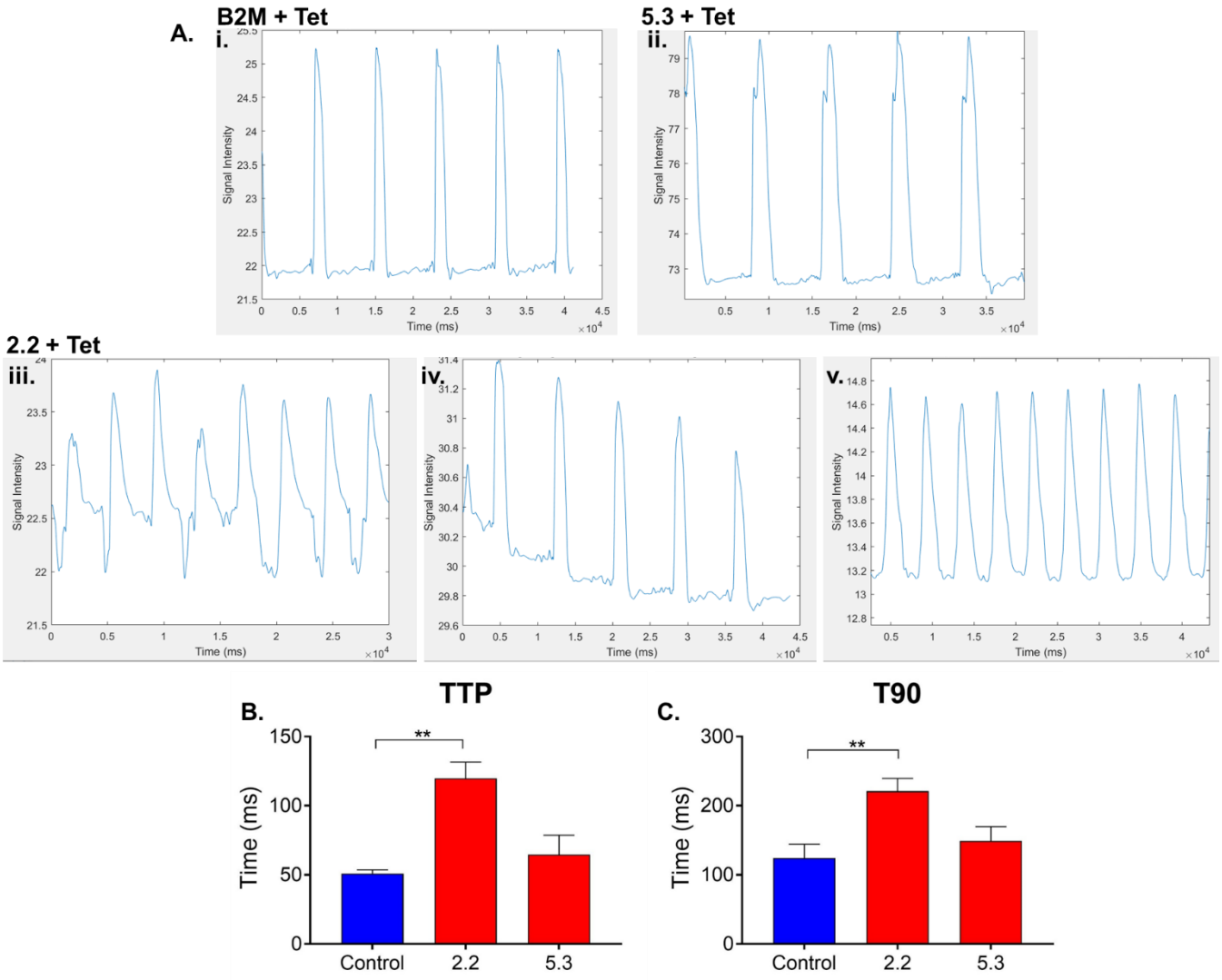

Figure 5.10: Effect of *APLNR* KD (2.2 and 5.3 lines) on hESC-CM voltage signalling. (A) Representative traces from MATLAB code output for (i) control, (ii) 5.3 + Tet and (iii-v) 2.2 + Tet hESC-CMs. Code designed and written by S. Bayraktar (University of Cambridge). (B) Time to peak (TTP) and (C) time to 90% decay (T90) compared to control. n = 6 for all, mean values compared by one way ANOVA followed by Tukey's post hoc test, **p<0.01. Data represent mean±sem.

In cardiomyocytes, tight regulation of voltage signalling, the associated ion fluxes and subsequent action potential are essential for contractility in a process known as excitation-contraction coupling. It was therefore hypothesised that the prolonged voltage sensing seen in 2.2 *APLNR* KD hESC-CMs may result in defective contractility, resulting from disruption to ion handling.

5.3.2.6 Effect of APLNR KD on hESC-CM calcium signalling

Tight regulation of changes in intracellular calcium, induced by changes in membrane potential, is also essential for cardiomyocyte excitation-contraction coupling. Following cardiac sodium channel induced depolarisation, intracellular calcium concentration increases, resulting in muscle contraction (Eisner *et al.*, 2017). Therefore, following on from the identification of an effect of *APLNR* KD on voltage signalling, effect on calcium signalling was also determined.

A similar approach to that described for voltage measurements was taken, making use of the calcium sensitive dye Fluo-4, AM (Video 5.5A), with hESC-CMs paced at 1 Hz and the same MATLAB code used for analysis. Again, a tetracycline effect was seen in B2M hESC-CMs (data not shown), therefore results for 2.2 and 5.3 *APLNR* KD hESC-CMs are compared to B2M + Tet hESC-CMs. Observing the traces, few differences in the shape of the waveforms were seen.

For both *APLNR* KD hESC-CM lines, no difference was seen in either TTP or T90 when compared to control cells (Figure 5.11), in contrast to what was seen for voltage signalling.

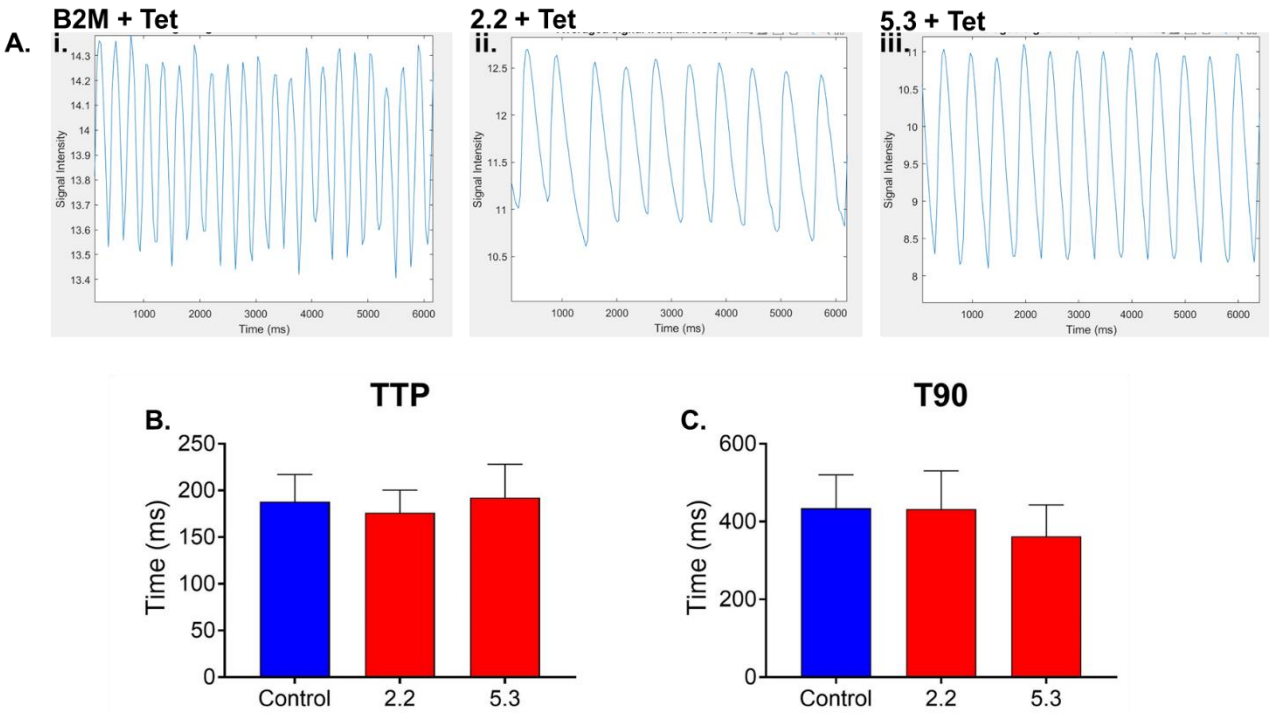

Figure 5.11: Effect of *APLNR* KD (2.2 and 5.3 lines) on hESC-CM calcium signalling. (A) Representative traces for (i) B2M + Tet, (ii) 2.2 + Tet and (iii) 5.3 + Tet hESC-CMs. (B) Time to peak (TTP) and (C) time to 90% decay (T90) compared to control. n = 6 for all, mean values compared by one way ANOVA followed by Tukey's post hoc test. Data represent mean±sem.

This is in agreement with previous studies using apelin receptor KO mice, in which no difference in calcium transients of isolated cardiomyocytes was seen compared to WT (Charo *et al.*, 2009).

For both voltage and calcium imagining, it should be noted that when observing signalling in the 2.2 *APLNR* KD cells, transients were not coordinated across the whole field of view as seen for control cells. Instead, flashing patches were observed, correlating with where contractile cardiomyocytes were present (Video 5.5B). This was variable, depending on the differentiation efficiency. For analysis, only areas containing cardiomyocytes were selected, therefore effects in hESC-CMs have been isolated.

Furthermore, for both fluorescent dyes, using the described experimental set-up it was not possible to quantify the magnitude of the signal. This is because the control and KD cells may not have taken up equal quantities of the dye or may have had different

fluorescent light exposures, leading to bleaching. This makes it inaccurate to quantify the magnitude of the signal. In the future, to overcome this a ratiometric dye such as Fura-2 may be used (Hwang *et al.*, 2015), or genetically encoded calcium sensors such as the previously described RGECO could be introduced (Kaestner *et al.*, 2014; Sparrow *et al.*, 2019).

5.3.3 Effect of apelin receptor ligands on hESC-CM differentiation

Significant reduction in expression of apelin receptor had effects on hESC-CM differentiation, suggesting an important role for apelin receptor in cardiomyocyte development. Therefore, the effect of apelin receptor stimulation on hESC-CM differentiation efficiency was investigated, by including physiologically high concentrations of exogenous apelin receptor ligands.

5.3.3.1 Effect of apelin receptor ligands on wild-type hESC-CM differentiation

It has previously been shown that apelin peptide can improve the differentiation efficiency of cardiomyocytes from hESCs, and increase the number of contractile cells in embryoid bodies formed using the hanging drop method (I.-N. E. Wang *et al.*, 2012). Therefore, the effect of inclusion of ligands targeting the apelin receptor on cardiomyocyte differentiation efficiency using a growth factor driven differentiation protocol was determined here.

Compound	**Concentration**	**Description**
[Pyr^{1}]apelin-13	10 nM or 1 µM	Equal activation of G-protein and β-arrestin. Naturally occurring peptide ligand.
MM07	1 µM	Preferentially activates G-protein signalling pathway. Synthetic peptide, improved stability compared to endogenous apelin.
26525	300 nM	Preferentially activates G-protein signalling pathway. Synthetic peptide, improved stability, high affinity.
31515	300 nM	Equal activation of G-protein and β-arrestin. Synthetic peptide, improved stability, high affinity.

Table 5.3: Apelin receptor ligands included in hESC-CM cultures throughout differentiation.

In a pilot experiment, several different apelin receptor ligands were used (Table 5.3). The ligands selected were either equal in their ability to activate G-protein and β-arrestin signalling pathways, or biased towards the G-protein signalling pathway compared to the β-arrestin pathway. This was in attempt to determine which molecular pathways are involved in the apelin receptor's role in hESC-CM differentiation. Ligands were included from day 0 of differentiation and maintained until collection for flow cytometry co-staining at day 14, with refresh every second day when media was changed.

Resulting cells were co-stained for TnT and Thy1 to determine differentiation efficiency. Across all compounds tested, little effect was seen on Thy1 positive percentage. As Thy1 staining was already low in control cells cultured without any ligand addition, it may not be possible to reduce this number any further. However, in all conditions, ligand inclusion promoted a trend towards an increase in TnT positive percentage (Figure 5.12A).

As little difference was seen between the different compounds, the experiment was repeated using only [Pyr^{1}]apelin-13 at a concentration of 10 nM. Here, inclusion of apelin peptide significantly improved cardiomyocyte differentiation efficiency, increasing TnT positive percentage from 71.7%±1.1 to 82.5%±0.9 (Figure 5.12B).

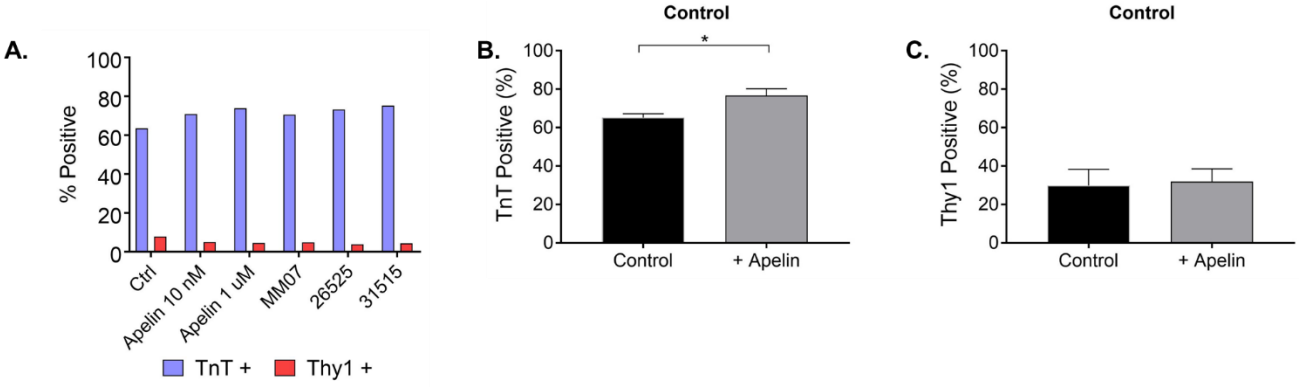

Figure 5.12: (A) Effect of inclusion of apelin receptor ligands throughout differentiation on troponin T positive (TnT +) and Thy1 positive (Thy1 +) percentage. n = 1. (B) TnT positive and (C) Thy1 positive percentage from flow cytometric analysis of control hESC-CMs and hESC-CMs cultured in the presence of 10nM [Pyr^{1}]apelin-13 throughout differentiation. n = 6. Means compared by unpaired, two-tailed Student's t-test, *p<0.05. Data represent mean±sem.

There was no effect on Thy1 positive percentage, but this was low in both control and ligand treated cultures (Figure 5.12C).

These results further support the key role of apelin receptor signalling in cardiomyocyte differentiation.

5.3.3.2 Effect of apelin receptor ligands on APLNR KD hESC-CM differentiation

In 2.2 *APLNR* KD hESC-CMs, around 90% knockdown of apelin receptor is seen, with a significant reduction in TnT positive percentage and cardiomyocyte differentiation efficiency. I therefore wanted to test the hypothesis that by stimulating the small amount of remaining apelin receptor protein, hESC-CM differentiation could be rescued.

2.2 line *APLNR* hESC-CMs were generated from hESCs cultured in the presence of tetracycline for 4 days prior to starting differentiation, with tetracycline treatment maintained throughout differentiation until collection at day 14. Additionally, cells were treated with 10 nM [Pyr^{1}]apelin-13 throughout.

Flow cytometry demonstrated an increase in TnT positive percentage from 31.0%±4.1 to 45.0%±3.2, with no difference seen in Thy1 positive percentage (Figure 5.13).

Although the increase in differentiation efficiency is small, given how little apelin receptor expression remains, the fact that any improvement is seen demonstrates the importance of apelin receptor signalling in cardiomyocyte differentiation.

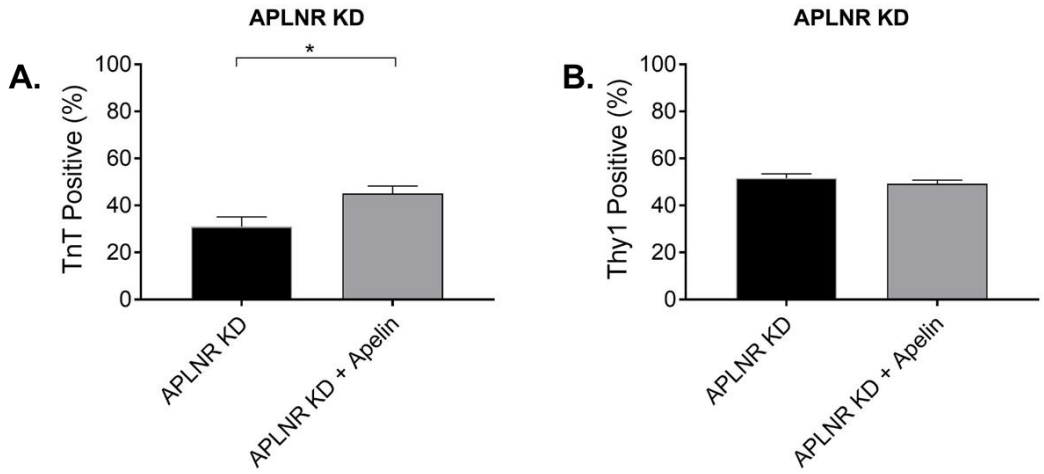

Figure 5.13: (A) TnT positive and (B) Thy1 positive percentage from flow cytometric analysis of control *APLNR* KD hESC-CMs and *APLNR* KD hESC-CMs cultured in the presence of 10nM [Pyr^{1}]apelin-13 throughout differentiation. n = 4. Means compared by unpaired, two-tailed Student's t-test. Data represent mean±sem.

5.4 Discussion

The aim of this section was to determine the effects of early *APLNR* KD on differentiation and function of the resulting hESC-CMs. By knocking down the apelin receptor prior to the initiation of differentiation, insights have been gained into an important role for the apelin receptor in the development of hESC-CMs.

This is the first time apelin receptor expression has been knocked down throughout the differentiation of human ESCs to cardiomyocytes. Furthermore, there are few published reports in which knockdown of any GPCR has been induced throughout differentiation of PSC to cardiomyocyte. In one study, knockdown of a cardiomyogenic cell-surface marker, latrophilin-2 in mouse ESCs was found to reduce the gene expression of cardiac markers and resulted in fewer contractile cells formed via embryoid body differentiation (C. S. Lee *et al.*, 2021). Interestingly, this reduction in cells with cardiomyocyte identity is similar to what was observed here with apelin receptor KD and using a better defined differentiation protocol.

5.4.1 The apelin receptor in cardiomyocyte development

APLNR KD had drastic effects on hESC-CM differentiation efficiency in the 2.2 line, which achieves a knockdown level of ~90% compared to control. These findings are consistent with previous studies, in which the apelin signalling system was identified as a critical regulator of heart development in both mice and zebrafish (Charo *et al.*, 2009; Chng *et al.*, 2013; Kang *et al.*, 2013; Pauli *et al.*, 2014)

Furthermore, a previous study has investigated the expression of the apelin receptor in mouse ESCs and in their differentiation to cardiomyocyte using the embryoid body method (D'Aniello *et al.*, 2013). This found that loss of apelin receptor expression resulted in defective cardiomyocyte differentiation, with *aplnr* overexpression increasing efficiency of differentiation. This study also showed that loss of apelin receptor affected the expression of key regulators of cardiomyogenesis (D'Aniello *et al.*, 2013).

In the 2.2 line, *APLNR* KD resulted in a significant increase in Thy1 positive staining, indicating an increase in the number of fibroblasts. This is consistent with the previously reported role of the apelin receptor in regulation of both physiological and pathophysiological fibrosis of a range of organs including the heart, lungs and liver (S. Huang *et al.*, 2016). Activation of the apelin signalling pathway has been shown to reduce cardiac fibrosis (S. Huang *et al.*, 2016), correlating with the results seen for *APLNR* KD.

It should be noted that the 2.2 hESC line cultured without tetracycline consistently differentiated with ~60% efficiency. This is lower than some reports, however differentiation efficiency is protocol and stem cell line dependent, and is likely dependent on some property of the stem cell line itself, or an effect of the introduced genetic manipulation. The hESC-CMs used here were not subjected to metabolic selection with lactate media – this normally necessary to increase differentiation efficiency to these high levels. Lactate selection was not used as in pilot experiments this caused all the apelin receptor knockdown cells to die due to the very low differentiation efficiencies. Despite the lower differentiation efficiency of the 2.2 line, it was still significantly reduced with apelin receptor knockdown.

Future studies inducing *APLNR* KD by tetracycline treatment at different stages throughout differentiation would be interesting in determining at which stage apelin

receptor signalling is important. From the current results, cells appear similar in early differentiation with differences appearing in the late stages, but it is unclear if these differences are because of events occurring earlier in differentiation.

5.4.1.1 Effect of APLNR KD on expression of markers of cardiac development

The effects of *APLNR* KD on cardiomyocyte differentiation cell stage marker expression have been investigated, but few significant effects were found, despite observing a clear phenotypic effect of *APLNR* KD in hESC-CMs.

An early study investigated the effects of zebrafish *grinch* mutation in the *agtrl1b* gene, an *APLNR* homolog (Scott *et al.*, 2007). Here, *grinch* mutants were found to have profound defects in cardiomyogenesis ranging in severity from reduction in heart size to complete absence of heart formation, and few cells staining positively for cardiac myosin. The effects of *grinch* mutations at different stages of heart development were investigated, examining stage specific markers similarly to Section 5.3.1.3. This study found that *nkx2-5* expression was greatly reduced in *grinch* mutants, suggesting a role for apelin receptor signalling in early development (Scott *et al.*, 2007). NKX2.5 is a transcription factor with a critical role in cardiomyocyte development, and mutations in this gene in humans are associated with a number of congenital heart diseases (Bouveret *et al.*, 2015). Therefore expression of the *NKX2-5* gene was quantified in the early stages of differentiation in the *APLNR* KD cells. However, no significant difference was seen compared to control, although there was a trend towards a decrease in expression in the 2.2 line at the cardiogenic mesoderm stage (Figure 5.3).

In performing qRT-PCR, expression of a number of standard genes has been quantified. However, although well characterised stage specific markers were selected, this method is biased. Having an unbiased view of the full transcriptome, such as that provided by RNA sequencing (S. Zhao *et al.*, 2014), at each stage of differentiation with *APLNR* KD would be beneficial. Here, the focus was not on the developmental stages but rather the effect on resulting hESC-CMs, therefore RNA sequencing was performed at day 15 of differentiation, which identified a number of pathways which could be explored with further assays. However, in the future it would be interesting to perform sequencing at each differentiation stage to identify DEGs between control and *APLNR* KD cells. This could provide further insight into the apelin

receptor mechanism of action and downstream signalling effects in its role in cardiomyocyte development.

5.4.1.2 Effect of APLNR KD on cell death in hESC-CM differentiation

The role of controlled cell death in mammalian heart development is widely accepted (van den Hoff *et al.*, 2000). As it is thought that tight regulation of apoptosis and cell death is needed for differentiation to proceed correctly, the effect of *APLNR* KD on cell death in hESC-CM differentiation was also examined. It has previously been shown that in order to initiate differentiation, a subset of ESCs undergo apoptosis to remove differentiation resistant cells which do not exit pluripotency (E. S. Wang *et al.*, 2015). Furthermore, in 3 week old embryoid bodies, stimulation with pre-apoptotic stimuli was found to increase cardiac differentiation, via caspase activation in cardiac progenitor cells (Bulatovic *et al.*, 2015). It has also been shown that WNT signalling acts to regulate caspase-dependent signalling which promotes cardiogenesis (Abdul-Ghani *et al.*, 2011). However, cellular stress can also cause unprogrammed cell death, which has detrimental consequences on hESC-CM function, and can affect intercellular communication and signalling (Saraf *et al.*, 2021).

APLNR KD was found to increase cell death in the 2.2 line at day 10 and 12 of differentiation. Generally at this stage, hESC-CMs have formed and relatively robust beating will have been established. As shown in the time course of images, the 2.2 *APLNR* KD cells start to show visual differences from around day 8. From day 6 onwards, a trend towards increased cell death is seen in 2.2 cells, reaching significance at day 10. Activation of the apelin receptor has previously been shown to be protective against endoplasmic reticulum (ER)-stress induced cardiomyocyte apoptosis in ischemia/reperfusion injury (Tao *et al.*, 2011), demonstrating a cardioprotective role, via regulation of autophagy (Jiao *et al.*, 2013). I therefore hypothesise that loss of apelin receptor results in cellular stress and disruption to intracellular signalling in developing cardiomyocytes, culminating in cell death. The reduced number of cardiomyocytes then leaves space for proliferation of cells with a fibroblast identity to overgrow, which appear to be less susceptible to *APLNR* KD.

To further test this hypothesis, a co-staining experiment for a cardiac marker (e.g. Troponin T, α-myosin heavy chain), fibroblast/mesenchymal marker (Thy1) and a cell death marker must be carried out in order to determine if the observed cell death is

restricted to cells with a cardiomyocyte identity. Additionally, the method used here for detecting cell death cannot distinguish between apoptosis and necrosis, hence it would also be beneficial to make use of an assay specific for apoptosis, such as Annexin V staining (Vermes *et al.*, 1995), to determine the contribution of the two processes to the *APLNR* KD phenotype.

5.4.2 *APLNR* KD in differentiation has functional effects on hESC-CMs

Along with the reduction in differentiation efficiency, *APLNR* KD throughout development had functional consequences on the resulting hESC-CMs. From RNA sequencing analysis, two areas were identified as differentially regulated in *APLNR* KD hESC-CMs and selected for further exploration – cell adhesion and voltage signalling.

5.4.2.1 The role of APLNR signalling in hESC-CM adhesion

From XGR analysis, a number of pathways associated with adhesion and integrin signalling were identified as differentially regulated in *APLNR* KD hESC-CMs compared to control. The apelin receptor has previously been shown to promote expression of adhesion molecules in endothelial cells (Lu *et al.*, 2012; Strohbach *et al.*, 2018), however its role in cardiomyocyte adhesion is not well established. Sequencing analysis revealed significant change in expression of genes involved in signalling events mediated by focal adhesion kinase (FAK). Consistent with this, in HEK cells, apelin treatment was found to induce FAK-mediated phosphorylation and resulted in increased F-actin staining indicating increased focal adhesion formation (Hashimoto *et al.*, 2005). Any relationship between the apelinergic system and integrin signalling molecules has not been well investigated in the published literature.

Taken together, the RNA sequencing results and the limited published data suggest a potential involvement of apelin receptor signalling in the adhesion properties of hESC-CMs. A simple assay was performed to determine the effect of *APLNR* KD on hESC-CM adhesion properties, however no significant differences were found. The design of this assay may not be optimal to capture any differences, and therefore could be further addressed. There are a number of techniques which have been used to examine the adhesion properties of a wide range of cell types which could be utilised here (Keselowsky and García, 2005; Khalili and Ahmad, 2015). It will also be

important to determine the effect of *APLNR* KD on cell-cell adhesion, as intercellular connections between cardiomyocytes are essential for function and contractility (Noorman *et al.*, 2009).

Furthermore, integrin signalling is also essential for cardiac development, with both FAK KO and integrin-β1 KO mice displaying cardiac developmental defects (Fassler *et al.*, 1996; Peng *et al.*, 2008). Hence the change in adhesion signalling in *APLNR* KD hESC-CMs may contribute to the poor differentiation efficiency. However, there are no drugs currently available to target molecules related to adhesion, hence no tool compounds are available to aid further study.

5.4.2.2 The role of apelin receptor in voltage signalling

RNA sequencing revealed a significant decrease in expression of the *SCN5A* gene in *APLNR* KD hESC-CMs, which encodes the cardiac voltage gated sodium channel, $Na_{V1.5}$. This channel is essential for the initiation and conduction of cardiac action potentials, with mutations in the *SCN5A* gene associated with a number of cardiac arrhythmic disorders (Rook *et al.*, 2012). Because of this, the effect of *APLNR* KD on voltage signalling in hESC-CMs was determined.

Previously, apelin signalling has been associated with regulation of voltage signalling. Firstly, in atrial fibrillation patients apelin peptide expression is reduced (Ellinor *et al.*, 2006), with expression levels returned to normal with long term resynchronisation therapy or electrical cardioversion (Francia *et al.*, 2007; Kallergis *et al.*, 2010). Furthermore, apelin treatment of isolated rat ventricular myocytes was shown to increase action potential conduction velocity (Farkasfalvi *et al.*, 2007), which was recapitulated in canine left ventricle (Chamberland *et al.*, 2010). This effect was found to be dependent on an increase in sodium current by decreasing the activation potential and modulating channel gating kinetics (Chamberland *et al.*, 2010). These results were recently confirmed in a mouse model of atrial fibrillation, in which treatment with apelin increased cardiomyocyte sodium current, resulting in decreased incidence of atrial arrhythmias (Y. M. Kim *et al.*, 2020).

In agreement with this, in *APLNR* KD hESC-CMs, voltage signalling was found to be prolonged, suggesting dysregulation of ion handling dynamics. The inotropic effects of apelin receptor activation have been proposed to be dependent on its effects on voltage signalling due to the tightly linked excitation-contraction coupling of

cardiomyocytes (Farkasfalvi *et al.*, 2007). In the analysis of voltage signalling, when using the MATLAB code for extracting values for TTP and T90, areas of culture containing contractile cardiomyocytes were selected. However, as shown in the image panels in Figure 5.1, the 2.2 line *APLNR* KD cultures form clumps of cardiomyocytes interspersed with variable numbers of fibroblast like cells. It is therefore difficult to interpret whether the effect on voltage signalling is a cell-autonomous effect due to disruption within the hESC-CMs themselves because of loss of apelin receptor signalling, or because the hESC-CMs are not able to form a homogenous sheet. Cell-cell adhesion of cardiomyocytes is essential for maintaining function and for electrophysiological regulation (J. Li *et al.*, 2006), hence the disruption of inter-cardiomyocyte contact by fibroblasts may have detrimental effects on voltage signalling. Furthermore, contact with other hESC-CMs has been shown to promote maturation (Karbassi *et al.*, 2020), which also effects electrophysiology. However, in the context of the heart, cardiac fibroblasts have been shown to secrete factors that promote cardiomyocyte maturation (Ieda *et al.*, 2009), therefore it is unclear what effect the fibroblast like cells seen in the *APLNR* KD cultures might have on electrophysiology. Ideally, metabolic selection would be performed for hESC-CMs as described in Section 2.3 to isolate cardiomyocytes to investigate functional consequences of *APLNR* KD specifically in hESC-CMs. However, when this was attempted, hESC-CM survival was very low, consistent with a previously published report that metabolic selection is ineffective in cardiomyocyte cultures with poor differentiation efficiency.

In the cardiac action potential, initial depolarisation caused by the opening of sodium channels promotes an influx of calcium ions (Ca^{2+}) through voltage gated Ca^{2+} channels, promoting calcium induced calcium release (CICR) from the sarcoplasmic reticulum. The Ca^{2+} ions then bind to myofilaments promoting contraction (Bers, 2002) (Figure 5.14).

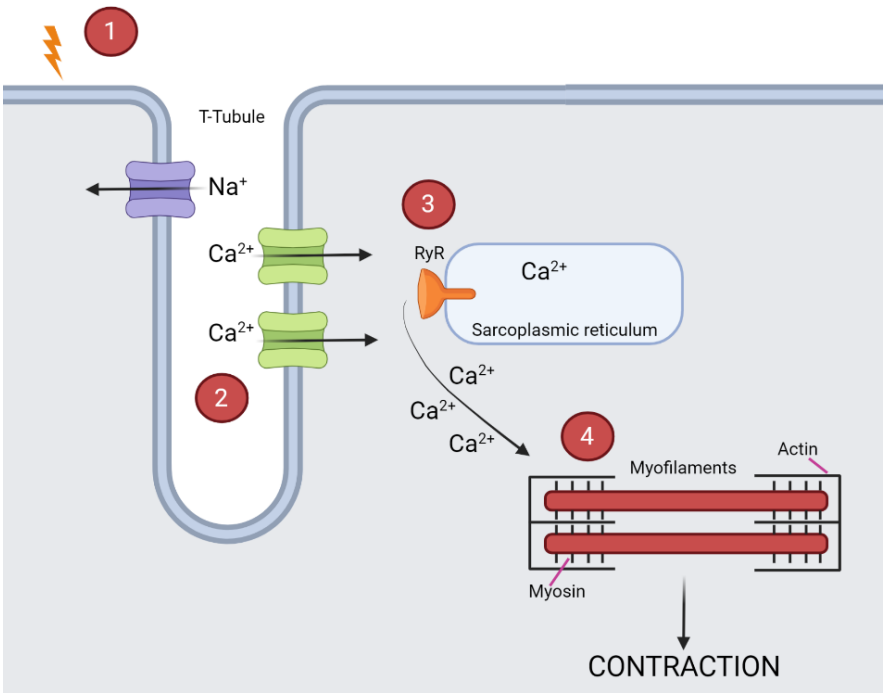

Figure 5.14: Excitation-contraction coupling in cardiomyocytes. (1) Action potential enters cell, promoting sodium ion entry and depolarisation. (2) Voltage gated calcium channels open and Ca^{2+} enters, (3) activating ryanodine receptors (RyR) and inducing calcium induced calcium release from the sarcoplasmic reticulum (SR). (4) Free Ca^{2+} from SR and extracellular entry binds to myofilaments promoting contraction. This figure was created using Biorender.com

Owing to the dysregulation of voltage signalling in *APLNR* KD hESC-CMs, it could be hypothesised that calcium signalling would also be affected. However, no difference in calcium signalling was found between control and KD hESC-CMs. This is consistent with previous reports, in which stimulation of rat cardiomyocytes with apelin increased voltage conduction velocity and cardiomyocyte contractility but had no effect on calcium transient amplitude (Farkasfalvi *et al.*, 2007). Furthermore, in cardiomyocytes isolated from *aplnr* KO mice, no changes in calcium transients were observed (Charo *et al.*, 2009).

My results therefore support the proposal that the positive inotropic effects of apelin receptor activation in cardiomyocytes are induced by an increase in conduction velocity and an increase in Ca^{2+} sensitivity of myofilaments (Farkasfalvi *et al.*, 2007; Charo *et al.*, 2009). In the future, it would also be beneficial to develop a protocol to simultaneously measure calcium and contractility (Ahola *et al.*, 2018), owing to the importance of calcium in controlling cardiomyocyte contraction.

Furthermore, patients with heart failure can be predisposed to developing arrhythmic conditions. As discussed in detail in Section 1, apelin receptor signalling is decreased in heart failure (K. S. Chong *et al.*, 2006) and atrial fibrillation patients have also been reported to have reduced apelin signalling (Ellinor *et al.*, 2006). Therefore there is potentially a previously overlooked link between apelin receptor activation, voltage signalling and development of heart failure.

It would be interesting to measure the effect of loss of apelin receptor on hESC-CM contraction. However, owing to the poor differentiation efficiency, early apelin receptor KD resulted in insufficient cardiomyocytes to be able to generate viable engineered heart tissues (EHTs) to measure force generation in 3D. Therefore, as described in Section 6, contractility of hESC-CMs with *APLNR* KD induced by tetracycline treatment post differentiation was measured.

5.4.2.3 Linking $Na_{V1.5}$ voltage sensing and adhesion

Returning to the specific downregulation of $Na_{V1.5}$ in *APLNR* KD hESC-CMs, it is important to note that this channel also has links to cell-adhesion. There is increasing evidence that the associated β1 subunits of $Na_{v1.5}$ act as adhesion molecules, including by forming trans homophillic interactions with other β1 subunits on neighbouring cells (Salvage *et al.*, 2020). This interaction is thought to facilitate ephaptic coupling, which is the transfer of action potentials between cells through the movement of sodium ions within narrow clefts (Veeraraghavan *et al.*, 2018). Hence, in the *APLNR* KD hESC-CMs the reduced *SCN5A* expression could be linked with the altered regulation of adhesion signalling also identified by RNA sequencing, both contributing to the functional dysregulation identified.

5.4.3 Apelin receptor activation enhances hESC-CM differentiation efficiency

Two previous studies have shown that inclusion of apelin peptide in the culture media of both mouse and human ESCs enhances the differentiation to cardiomyocyte using the hanging drop method (I.-N. E. Wang *et al.*, 2012; D'Aniello *et al.*, 2013). I have shown, for the first time, that this is also true for hESCs differentiated to cardiomyocytes in 2D, using a growth factor/small molecule inhibitor differentiation protocol. This improved differentiation efficiency further supports the importance of the role of the apelin receptor in cardiomyocyte differentiation.

In the pilot experiment, the effects of four different compounds on hESC-CM differentiation were tested. The endogenous ligand [Pyr^{1}]apelin-13 and three synthetic peptides were used. All the synthetic peptides have previously been shown to be highly potent *in vivo*, and have modifications resulting in increased stability and significantly longer half-lives compared to the native [Pyr^{1}]apelin-13. Bolus infusion of the synthetic peptides in rats resulted in a decrease in blood pressure, an effect which was maintained for a significantly prolonged time compared to that induced by [Pyr^{1}]apelin-13 (J.J. Maguire, University of Cambridge, unpublished,).

GPCRs signal through multiple pathways – namely heterotrimeric G-proteins and β-arrestins – resulting in different outcomes, in a concept known as biased signalling (P. Yang *et al.*, 2019). Here two G-protein biased compounds were used in an attempt to determine if the effects of apelin receptor activation in hESC-CM differentiation were G-protein or β-arrestin dependent. A G-protein biased agonist can be beneficial as prolonged stimulation of receptor leads to desensitisation and β-arrestin mediated internalisation (P. Yang *et al.*, 2019; Read *et al.*, 2020), as described in Section 1.7. Furthermore, a previous study has reported that the apelin receptor can act in a G-protein independent manner, signalling via β-arrestin in response to stretch promoting hypertrophy in a mouse model of chronic pressure overload, suggesting a G-protein biased agonist would be beneficial (Scimia *et al.*, 2012). Despite this, all ligands induced a similar increase in cardiomyocyte differentiation efficiency, hence the native [Pyr^{1}]apelin-13 peptide was selected for further experiments.

Following on from this, the possibility of rescuing hESC-CM differentiation with *APLNR* KD by including [Pyr^{1}]apelin-13 in the culture media was investigated. A small increase in TnT positive percentage was observed, which is perhaps expected, as in the 2.2 line ~90% of apelin receptor expression is lost, meaning there is little receptor available for receptor-ligand interaction. However, this is an exciting observation, and suggests that it may be possible to rescue differentiation with a modified ligand with higher stability and potency than [Pyr^{1}]apelin-13, such as that provided in the 26525 and 31515 ligands. Therefore in the future this experiment should be repeated using these ligands at different concentrations. It would also be interesting to start ligand inclusion in both control and *APLNR* KD at different points throughout differentiation to determine at what point apelin receptor activation is having an effect.

5.4.4 Differences in 2.2 and 5.3 *APLNR* KD hESC-CMs

As described in Section 4, two lines of apelin receptor inducible KD hESCs were generated, which display differing levels of *APLNR* KD when differentiated to hESC-CMs. Interestingly, in the 5.3 line which has around ~60% *APLNR* KD, few effects were seen on hESC-CM differentiation efficiency or function. In stark contrast, 2.2 hESC-CM differentiation efficiency was drastically reduced with ~90% *APLNR* KD, with functional consequences seen in resulting hESC-CMs. Interestingly, in RNA sequencing analysis both lines were analysed together, with 272 DEGs found. Together these results suggest that the apelin receptor has a complex role in hESC-CMs, and it may be that some of its functions can be performed even at a reduced expression level. There does, however, appear to be a threshold expression level needed for correct hESC-CM differentiation and function.

5.5 Conclusions

APLNR KD throughout differentiation of hESC-CMs has detrimental effects on differentiation efficiency. Furthermore, *APLNR* KD detrimentally prolongs voltage signalling which could have negative effects on cardiomyocyte contractility. Gene expression analysis showed that changes in voltage signalling could be linked to reduced expression of the cardiac sodium channel $Na_{V1.5}$, which may also be related to changes in regulation of pathways involved in cell adhesion.

My results are consistent with what has previously been reported in the literature for the role of the apelin receptor in cardiomyocyte development and function, but for the first time the effect of loss of apelin receptor in human ESC differentiation to cardiomyocyte has been examined. This provides a more clinically relevant system, hopefully generating more translatable results. These results have also revealed potentially underappreciated links between the apelin receptor and voltage signalling and adhesion properties, which are both key for correct cardiomyocyte contractility and function.

This also highlights the power of using hESCs for investigation of human cardiomyocyte development. Owing to the amenability of PSCs to genetic editing, and the ability to induce differentiation to cell type of interest, protein function can be

investigated in human cardiomyogenesis by manipulating gene expression. This can provide novel insights and highlight previously poorly studied links, such as the potential link between apelin receptor, voltage signalling and adhesion as seen here.

6. Effect of Apelin Receptor Knockdown in hESC-Derived Cardiomyocytes

6.1 Introduction

After establishing the effect of *APLNR* KD throughout differentiation of hESC-CMs, the next aim was to investigate the consequences of *APLNR* KD in differentiated hESC-CMs, which could give an indication of the consequences of loss of apelin signalling in the heart.

The apelin receptor has an important role in cardiac contractility, as discussed in detail in Section 1. Activation of the apelin receptor in the adult heart increases cardiac contractility, with apelin being one of the most potent inotropes identified to date in both rats and humans *ex vivo* (Szokodi *et al.*, 2002; Maguire *et al.*, 2009; Japp *et al.*, 2010; Murza *et al.*, 2016; Perjés *et al.*, 2016). Furthermore, adult *aplnr* and *apln* KO mice were found to have reduced capacity to respond to cardiac stress such as exercise (Charo *et al.*, 2009). Apelin KO mice also display reduced cardiac contractility with age and develop severe pressure overload induced heart failure (Kuba *et al.*, 2007). In human disease, apelin receptor signalling is downregulated (Iwanaga *et al.*, 2006; K. S. Chong *et al.*, 2006), with apelin or ELA infusion in animal models shown to improve systolic and diastolic function and also reduce detrimental cardiac remodelling and fibrosis (M. Wang *et al.*, 2013; Pang *et al.*, 2014).

It has therefore been proposed that targeting the apelin receptor for the treatment of heart failure may represent a novel therapeutic option. However, further study is needed to better understand the role and mechanism of action of the apelin receptor in the heart, and there is currently a lack of a suitable human *in vitro* model.

Therefore, in this section hESC-CMs were generated from the apelin receptor inducible knockdown hESCs. Upon completion of differentiation, *APLNR* KD was induced by 6-8 days of culture with tetracycline treatment. Following confirmation of successful *APLNR* KD, effect on cell morphology and identity, peptide production and calcium and voltage signalling was determined.

Using 3D engineered heart tissues offers a platform that more closely represents the heart *in vivo*. The heart responds to the Frank-Starling law, that increased ventricular filling and accompanied increase in stretch results in an increase in cardiac

contractility, and in turn an increase in cardiac output, which is essential for adapting to changes in demand, such as that induced by exercise (Asnes *et al.*, 2006). EHTs have been shown to respond to stretch following the Frank-Starling mechanism, offering a system to measure contractility (Asnes *et al.*, 2006). Therefore, to investigate the role of the apelin receptor in force generation, 3D engineered heart tissues were generated using *APLNR* KD hESC-CMs, with loss of apelin receptor found to have detrimental effects on cardiac contractility.

6.2 Methods

The methods relevant to this section are listed in Table 6.1 and described in Section 2, with further detail for selected methods below.

Method	**Section**
Cell culture and hESC-CM differentiation	2.2 and 2.3
Analysis of *APLNR* gene expression by qRT-PCR	2.4
Saturation radioligand binding	2.7
Troponin T and Thy1 flow cytometry co-stain	2.6
Peptide production determined by ELISA	2.8
Measuring hESC-CM voltage signalling using FluoVolt	2.15
Measuring hESC-CM calcium signalling using Fluo-4, AM	2.16
Generation of 3D engineered heart tissues (EHTs)	2.18
RNA extraction from EHTs	2.22
Measurement of voltage and calcium signalling in EHTs	2.19
Measurement of EHT force generation using Aurora myograph	2.20
Second-Harmonic Imaging Microscopy of EHTs	2.21
Data analysis and statistics	2.24

Table 6.1: Descriptions of the methods used in this section found can be found in the listed corresponding section.

6.2.1 Cell culture

hESCs were maintained as described in Section 2.2, before inducing to differentiate to hESC-CMs as described in Section 2.3. Tetracycline treatment was initiated at day 14-15 and maintained for 6-7 days, with refresh every second day.

In some assays, hESC-CMs were first subjected to metabolic selection using sodium-lactate containing media as described in Section 2.3. In this case, hESC-CMs were lactate selected, allowed to recover for 2 days in CDM-BSA and then subjected to tetracycline treatment for 6-8 days.

Throughout Section 6, no exogenous apelin receptor ligands were added to cultures.

6.2.2 qRT-PCR for determining *APLNR* KD efficiency

qRT-PCR was performed using TaqMan Gene Expression Assays, as detailed in Section 2.4, for *APLNR* gene expression using RNA isolated from hESC-CMs cultured with and without tetracycline. Human *18S* rRNA was used as a housekeeping gene. *APLNR* expression was normalised to housekeeping gene expression and relative expression compared to the corresponding cell line cultured without tetracycline calculated using the $2^{(-\Delta\Delta CT)}$ method (Schmittgen and Livak, 2008).

6.2.3 Generation of 3D EHTs

3D engineered heart tissues were generated as described in Section 2.18. A schematic representation of the workflow is shown in Figure 6.1. *APLNR* iKD hESCs were induced to differentiate to hESC-CMs, subjected to metabolic selection and then cast in constructs alongside a supportive fibroblast cell line, HS-27A, in a collagen gel. EHTs were cultured for 14 days, with or without tetracycline, to allow establishment of robust contraction and to induce *APLNR* KD, before performing functional assays.

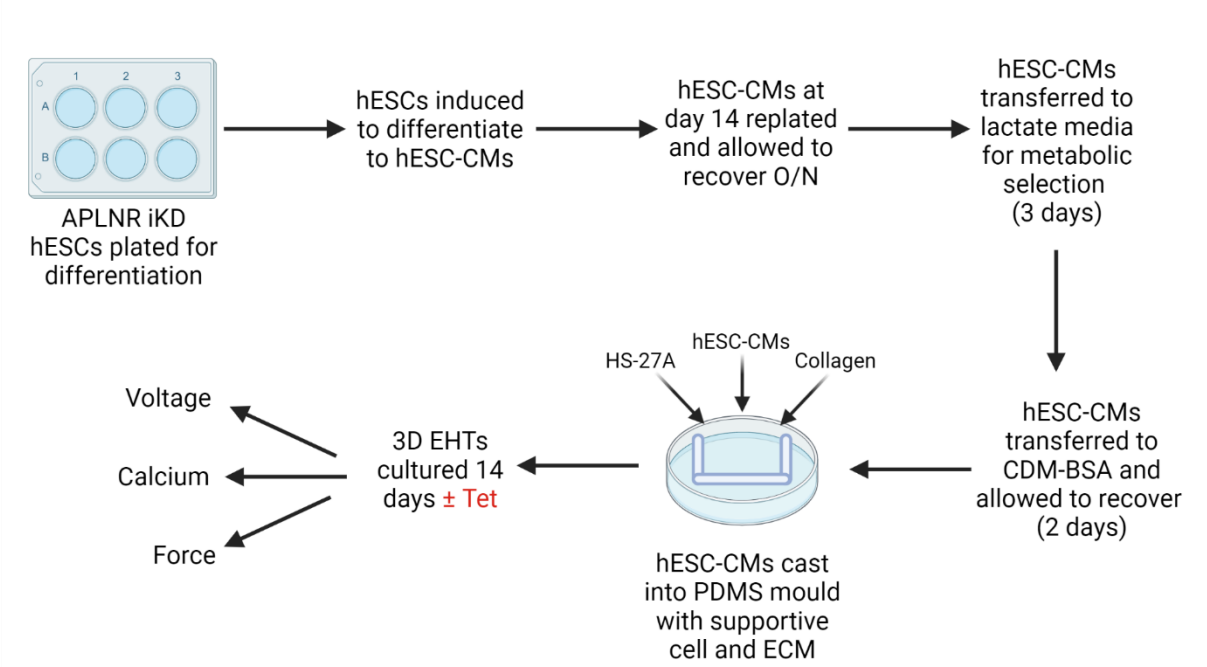

Figure 6.1: Workflow for the generation and measurement of 3D engineered heart tissues (EHTs). This figure was created using Biorender.com.

6.2.4 Gene expression analysis in EHTs

For the determination of *APLNR* gene expression in EHTs, constructs composed of hESC-CMs only were used, as HS27-A cells were also found to express the apelin receptor and hence may affect results. However, expression of the apelin receptor by HS-27A does not influence other results, as the focus is on investigating the effects of *APLNR* KD in hESC-CMs on cardiomyocyte function, hence supportive HS-27A cells were included in EHTs subjected to functional assays.

6.2.5 Measurement of EHT force generation using Aurora myograph

Following 14 days in culture, EHTs were transferred to a myograph and force generation measured as described in Section 2.20. At all pacing rates, differences in active and passive force were seen for *APLNR* KD hESC-CMs, therefore results are shown for pacing at 1 Hz only.

6.3 Results

In Section 5, the consequences of *APLNR* KD throughout differentiation on both hESC-CM differentiation efficiency and in resulting hESC-CMs were established, indicative of the role of the apelin receptor in development. Throughout Section 6, *APLNR* KD in hESC-CMs was induced post differentiation (referred to as late KD hESC-CMs), and the effects of KD characterised. This allows the modelling of apelin receptor function in adult cardiomyocytes.

6.3.1 Determination of *APLNR* KD efficiency induced in hESC-CMs

Before performing any assays, the efficiency of late *APLNR* KD was first established. Again, hESC-CMs were produced from the two shAPLNR hESC lines, 2.2 and 5.3, as well as the control B2M line. After 14-15 days of differentiation, when robust beating is consistently observed, tetracycline treatment was initiated for 6-7 days.

To achieve a pure population of hESC-CMs, for some assays metabolic selection was performed prior to the initiation of tetracycline treatment. This allows the investigation of the effect of *APLNR* KD in cardiomyocytes without influence from contaminating other cell types, such as fibroblasts.

6.3.1.1. APLNR KD efficiency at the gene level in differentiated hESC-CMs

hESC-CMs with and without tetracycline treatment were collected and *APLNR* gene expression determined by qRT-PCR (Figure 6.2). For the 2.2 line, significant KD was seen for both non-selected and lactate selected hESC-CMs (66% KD non-selected, 74% lactate selected). In contrast to what was seen in the early KD hESC-CMs, the level of KD in late hESC-CMs was comparable in the non-selected 5.3 and 2.2 lines (66% and 69%, respectively). Post lactate selection, KD in the 5.3 line was not as efficient (50%) and did not reach significance. Importantly, as seen in the early KD, expression of *APLNR* was unaffected in B2M hESC-CMs by tetracycline inclusion for both non-selected and selected cells.

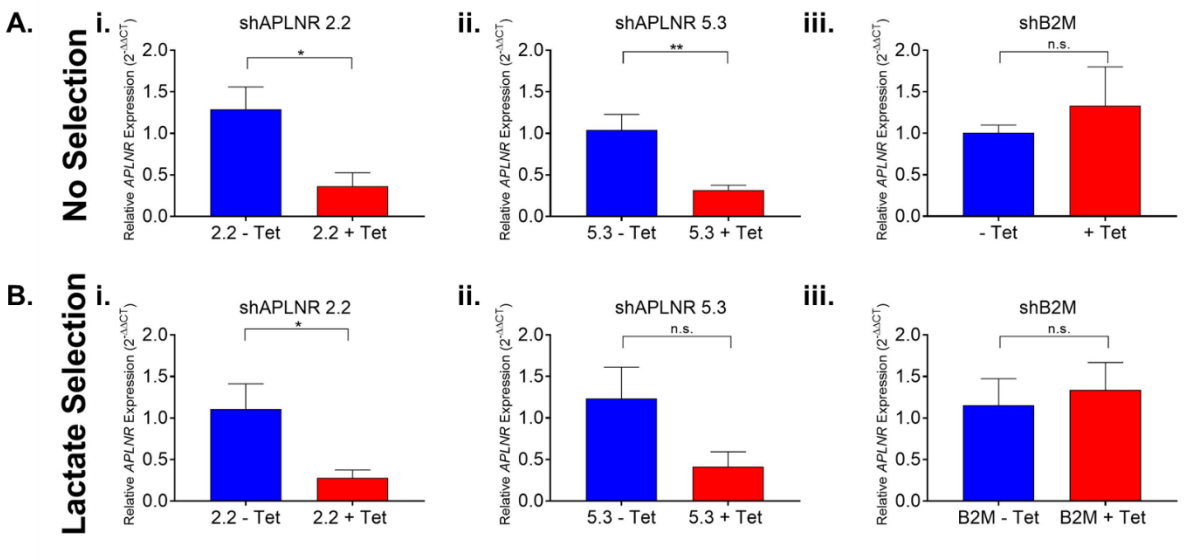

Figure 6.2: Comparison of relative expression of the apelin receptor gene (*APLNR*) in iKD (A) non-selected or (B) lactate selected hESC-CMs, with or without tetracycline treatment for 6-8 days post differentiation. Expression of *APLNR* in two lines of apelin receptor iKD hESCs, (i) 2.2 and (ii) 5.3. (iii) Expression of *APLNR* in B2M control line hESC-CMs cultured with or without tetracycline for 6-8 days. n = 3 for all. Relative expression compared to line – Tet mean expression. Expression compared by unpaired, two-tailed Student's t-test, *p<0.05, **p<0.01. Data represent mean±sem.

6.3.1.2 APLNR KD efficiency at the protein level in differentiated hESC-CMs

Having confirmed late KD at the gene level, the next aim was to determine the efficiency of KD at the protein level by performing saturation radioligand binding (Figure 6.3). Here, non-selected hESC-CMs were used, and as a very similar level of KD at the gene level was observed in the two shAPLNR lines, results have been pooled. As reported in previous sections, for control hESC-CMs binding of [^{125}I]apelin-13 was saturable, with a binding affinity of 1.6 x 10^{-10} M calculated. In hESC-CMs treated with tetracycline, specific binding was reduced substantially. In agreement with the reduction in gene expression as reported above, the reduction in binding was not as pronounced as that seen for the early KD 2.2 line. Again, binding of a fixed concentration of [^{125}I]apelin-13 in B2M hESC-CMs was similar irrespective of tetracycline treatment.

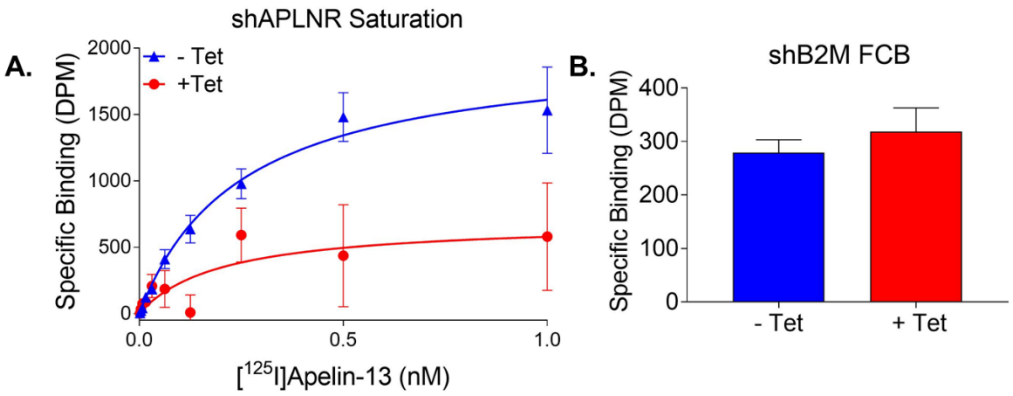

Figure 6.3: (A) Saturation specific [^{125}I]apelin-13 binding in shAPLNR hESC-CMs cultured with or without tetracycline for 6-7 days post differentiation. n = 3. (B) Binding of a fixed concentration of [^{125}I]apelin-13 in hESC-CMs expressing shB2M transgene cultured with or without tetracycline for 6-7 days post differentiation. Specific binding levels compared by unpaired, two-tailed Student's t-test. n = 3. Data represent mean±sem.

6.3.2 Effect of late *APLNR* KD in differentiated hESC-CMs

Having established robust *APLNR* KD at the gene and protein level in differentiated hESC-CMs, the next aim was to determine the effect of late KD on hESC-CM function. It is important to note, that although ~60% KD was seen, this is not as severe as the KD seen in the 2.2 early KD hESC-CMs.

6.3.2.1 Morphology and spontaneous contraction in late APLNR KD hESC-CMs

First, the effect of late *APLNR* KD on hESC-CM morphology was examined. As shown in Figure 6.4, hESC-CMs looked similar with and without *APLNR* KD for both 2.2 and 5.3 lines.

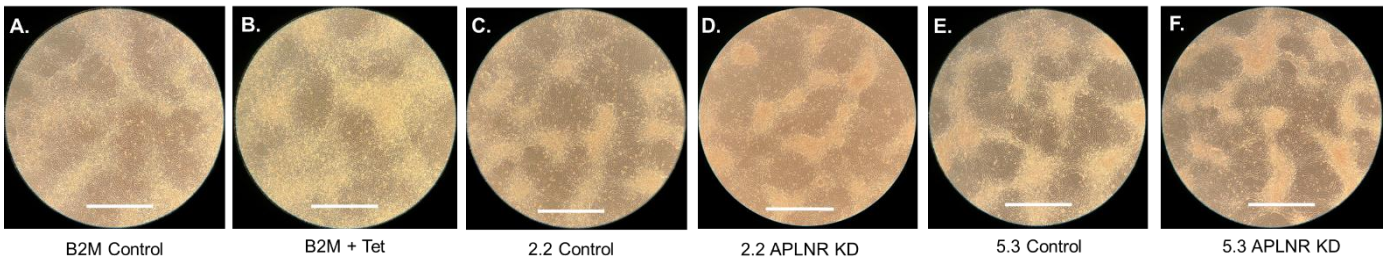

Figure 6.4: Representative brightfield images of control and late *APLNR* KD hESC-CMs at day 20-21 (after 6-7 days of tetracycline treatment). shB2M control hESC-CMs cultured (A) without and (B) with tetracycline. (C) Control and (D) late *APLNR* KD 2.2 shAPLNR hESC-CMs. (E) Control and (F) late *APLNR* KD 5.3 shAPLNR hESC-CMs. Scale bar = 200 µm.

Spontaneous contraction was also recorded, with no obvious differences observed regardless of *APLNR* KD (Videos 6.1-6.3).

6.3.2.2 Effect of late APLNR KD on cardiomyocyte identity in hESC-CMs

To determine if *APLNR* KD had effects on the proportion of cardiomyocytes, hESC-CMs were co-stained for the cardiac marker, TnT and the fibroblast marker, Thy1. In Section 5, *APLNR* KD throughout development was shown to significantly reduce TnT positive percentage and increase Thy1 positive percentage, indicating reduced differentiation efficiency. It was also hypothesised that the apelin receptor promoted cell survival in late stage differentiation. It was therefore important to determine if *APLNR* KD altered troponin positive percentage if induced upon completion of differentiation.

APLNR KD in both 2.2 and 5.3 hESC-CMs had no effect on either TnT positive percentage or Thy1 positive percentage (Figure 6.5). As expected, no changes were seen in B2M regardless of tetracycline inclusion. For all conditions, a troponin positive percentage of around 70-80% and a Thy1 positive percentage of less than 20% was recorded, indicating high efficiency differentiation. These results are consistent with the images shown in Figure 6.4, in which hESC-CM cultures looked comparable for all conditions.

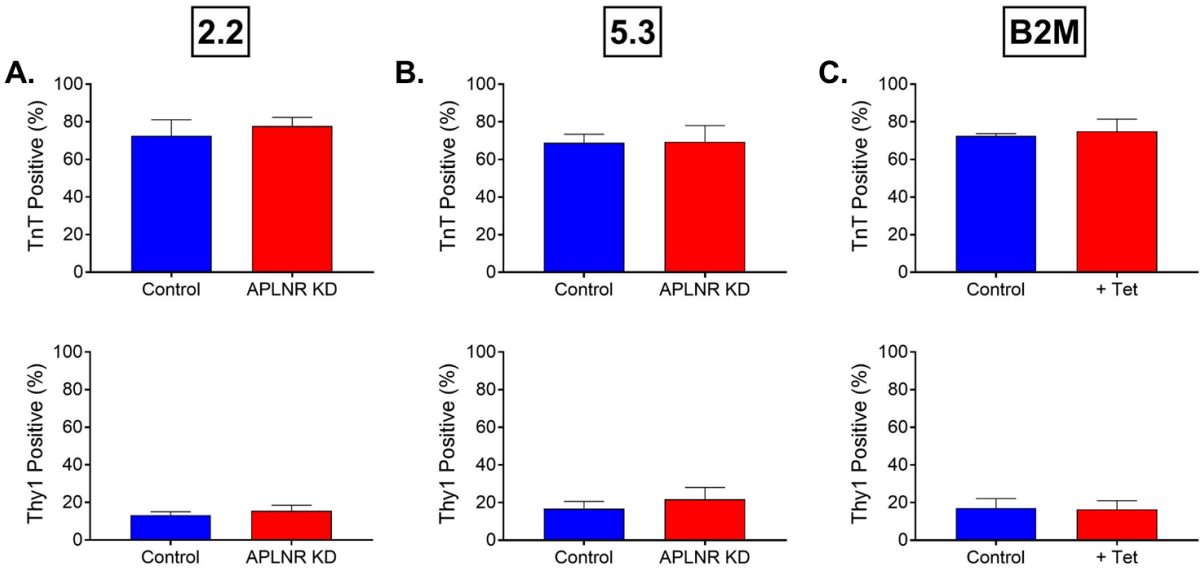

Figure 6.5: Quantification of TnT (top) and Thy1 (bottom) positive percentages from flow cytomteric co-stain for (A) 2.2 control and *APLNR* KD hESC-CMs, (B) 5.3 control and *APLNR* KD hESC-CMs and (C) shB2M control and with tetracycline treatment hESC-CMs. n = 3 for all, compared by unpaired, two-tailed Student's t-test. Data represent mean±sem.

These results suggest that loss of the apelin receptor does not cause hESC-CMs to lose their cardiomyocyte identity when cultured for 6-7 days. It would be interesting to repeat this experiment with tetracycline treatment maintained for a longer period. Although tetracycline treatment acts like a switch, with shRNA targeting the apelin receptor produced when tetracycline treatment is initiated, it may take time for the apelin receptor protein already present to be internalised or degraded. Furthermore, apelin receptor protein expression was found to be knocked down within the 6-7 days of tetracycline treatment used here, however it may take longer for an effect of this KD to be seen.

6.3.2.3 Effect of late APLNR KD in hESC-CMs on peptide production

As discussed in Section 5, ELISAs for ELA and apelin were performed using conditioned supernatant from control and *APLNR* KD hESC-CMs to determine if any change in ligand production was induced by reducing receptor expression. Data for 2.2 and 5.3 KD hESC-CMs are compared to B2M + Tet hESC-CMs here. For both lines, there was a trend towards an increase in production of both ligands, but only 5.3 ELA production reached a significant level of increased expression (Figure 6.6). It

could be suggested that under conditions of reduced apelin receptor expression, a feedback loop is formed to increase ligand production in a compensatory response.

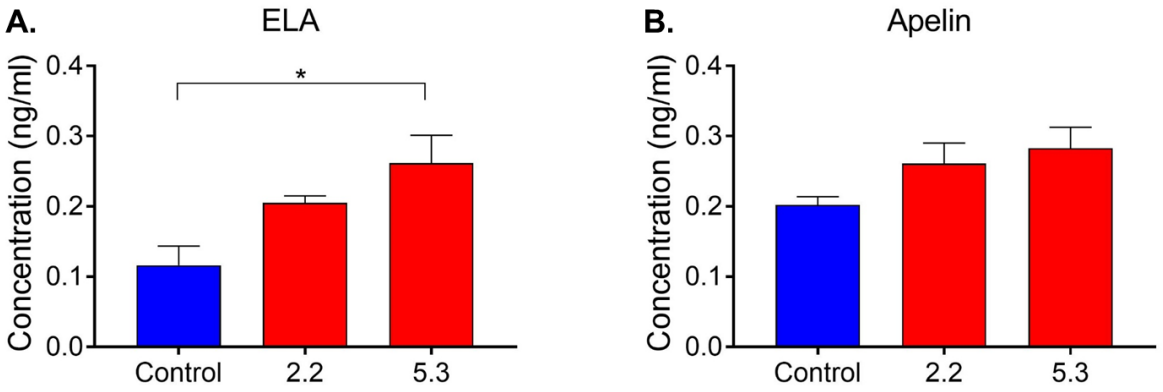

Figure 6.6: Comparison of concentration of (A) ELA and (B) apelin in conditioned supernatant from control (B2M + Tet) and late *APLNR* KD (2.2 and 5.3) hESC-CMs. n = 3 for all. Means compared by one way ANOVA followed by Tukey's post hoc test, *p<0.05. Data represent mean±sem.

Interestingly, apelin ligand production appears higher here than that seen in early KD hESC-CMs in Section 5.3. This may reflect the fact the hESC-CMs were cultured for a week longer and hence matured more.

6.3.2.4 Effect of late APLNR KD in hESC-CMs on voltage signalling

Having identified prolonged voltage signalling in hESC-CMs with *APLNR* KD throughout differentiation, the next aim was to determine if late *APLNR* KD had effects on hESC-CM voltage signalling. Here, FluoVolt voltage sensitive dye was used, with hESC-CMs paced at 1 Hz and waveform TTP and T90 measured. *APLNR* KD lines were compared to B2M hESC-CMs cultured with tetracycline to control for any effects of tetracycline treatment itself. In contrast to what was seen for 2.2 hESC-CMs with *APLNR* KD throughout differentiation, no difference in TTP or T90 was seen between either of the *APLNR* KD lines compared to control (Figure 6.7A).

Voltage signalling was also measured in hESC-CMs with *APLNR* KD induced after metabolic selection. Again, values for TTP and T90 were similar in both *APLNR* KD lines and control hESC-CMs (Figure 6.7B).

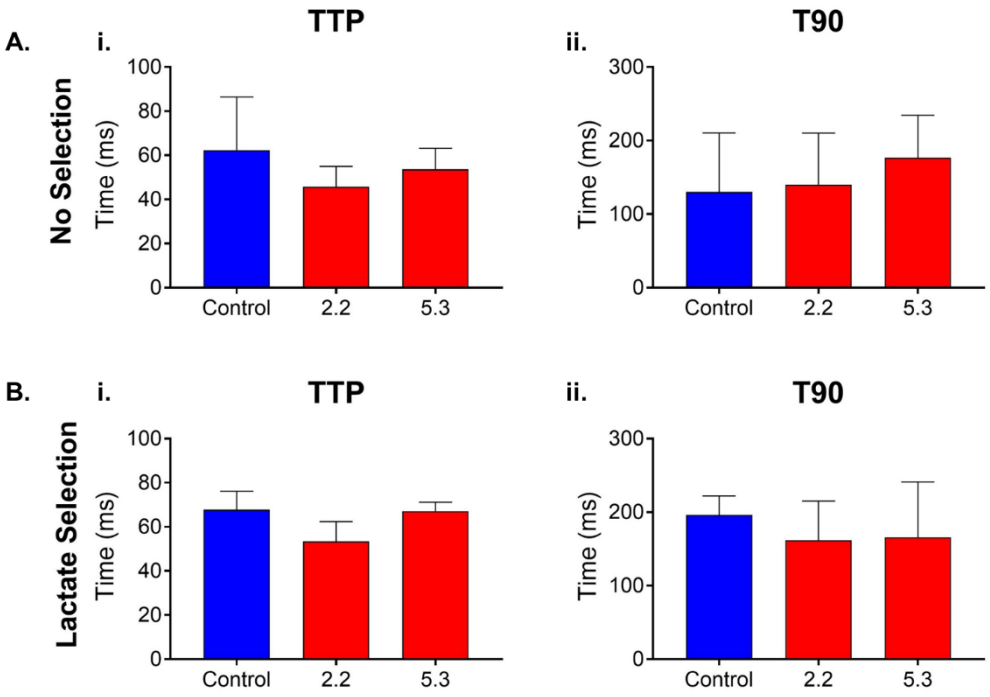

Figure 6.7: Effect of late *APLNR* KD (2.2 and 5.3 lines) on hESC-CM voltage signalling. (i) Time to peak (TTP) and (ii) time to 90% decay (T90) in *APLNR* KD compared to control for (A) non-selected and (B) lactate selected hESC-CMs. n = 3 for all, mean values compared by one way ANOVA followed by Tukey's post hoc test. Data represent mean±sem.

6.3.2.5 Effect of late APLNR KD in hESC-CMs on calcium signalling

Owing to the essential role of calcium signalling in cardiomyocyte contractility, the effect of late *APLNR* KD on calcium signalling was also measured. Calcium signalling in hESC-CMs paced at 1 Hz was measured using Fluo-4 calcium sensitive dye. As seen in hESC-CMs with *APLNR* KD throughout differentiation, loss of apelin receptor expression had no effect on calcium signalling (Figure 6.8A). This is, again, in agreement with previous studies which have suggested apelin receptor activation promotes calcium sensitisation rather than increase in calcium release (Farkasfalvi *et al.*, 2007; Charo *et al.*, 2009).

As seen for voltage signalling, performing lactate selection before inducing *APLNR* KD also had no effect on calcium signalling between control and KD hESC-CMs (Figure 6.8B).

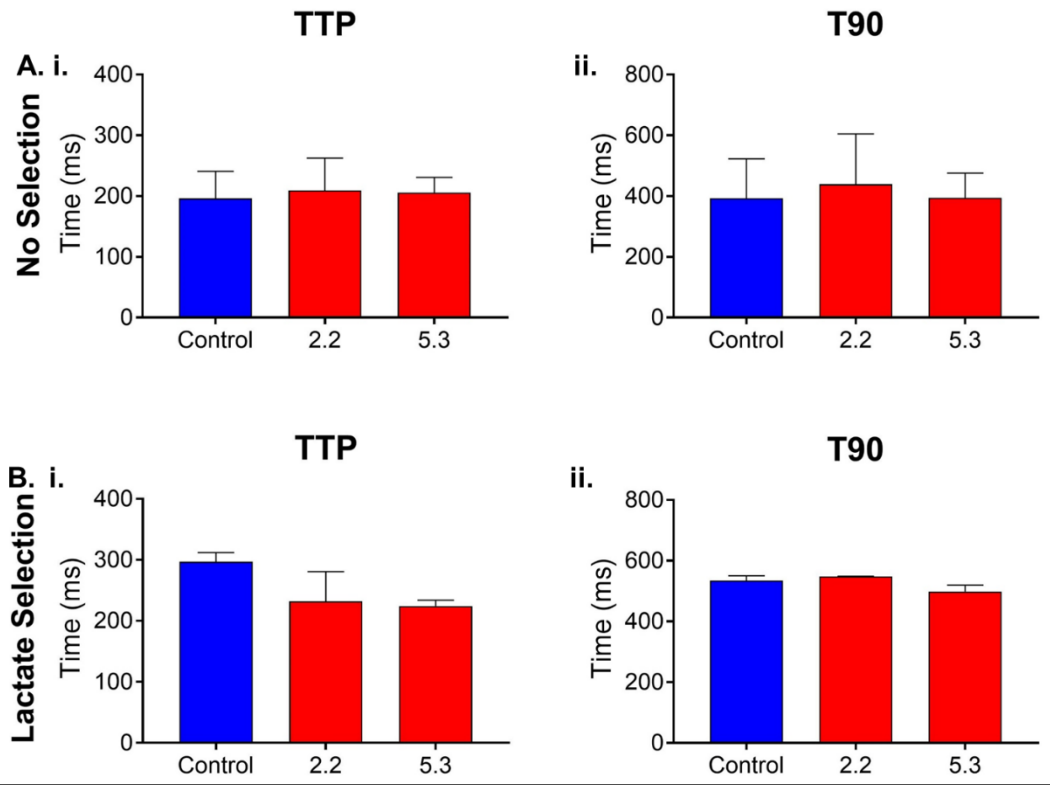

Figure 6.8: Effect of late *APLNR* KD (2.2 and 5.3 lines) on hESC-CM calcium signalling. (i) Time to peak (TTP) and (ii) time to 90% decay (T90) in *APLNR* KD compared to control for (A) non-selected and (B) lactate selected hESC-CMs. n = 3 for all, mean values compared by one way ANOVA followed by Tukey's post hoc test. Data represent mean±sem.

6.3.3 Effect of *APLNR* KD in 3D EHTs

Although effects on voltage and calcium signalling were not evident in hESC-CMs with late KD, because of the results generated in Section 5 relating to the effect of *APLNR* KD throughout differentiation, the effect of *APLNR* KD on the function of 3D EHTs was investigated. From previously published reports of the role of the apelin signalling system in heart contractility (Farkasfalvi *et al.*, 2007; Charo *et al.*, 2009; Maguire *et al.*, 2009; Japp *et al.*, 2010; Read *et al.*, 2019), the aim was to determine the effect of KD on voltage signalling, calcium signalling and force generation.

Taking account of the results generated up to this point, as the level of *APLNR* KD throughout differentiation in the 5.3 line was not sufficient to cause effect, and similar levels of KD were seen in both lines when induced post differentiation, I elected to

focus on the 2.2 line compared to B2M in 3D EHTs. In the subsequent section, *APLNR* KD 2.2 EHTs are simply referred to as *APLNR* KD.

6.3.3.1 Determination of APLNR KD efficiency in 3D EHTs

Before performing any functional assays, the ability to achieve sufficient *APLNR* KD in 3D EHTs was determined. hESC-CMs were generated, subjected to metabolic selection and then cast in moulds in a collagen matrix, where they were cultured for 14 days with or without tetracycline treatment. A representative video of an EHT in culture is shown in Video 6.4. At this point, RNA extraction and qRT-PCR were performed to determine *APLNR* gene expression. In the 2.2 line, tetracycline treatment was found to significantly reduce *APLNR* expression by ~71% compared to control cultured without tetracycline (Figure 6.9A).

In EHTs generated from the B2M line, when compared to B2M control cells, tetracycline appeared to increase *APLNR* expression, although this was variable and did not reach significance (Figure 6.9B). Therefore, to control for any tetracycline effect, expression of *APLNR* in 2.2 EHTs treated with tetracycline was compared to B2M + Tet EHTs, with expression found to be reduced by ~83% in *APLNR* KD (Figure 6.9C).

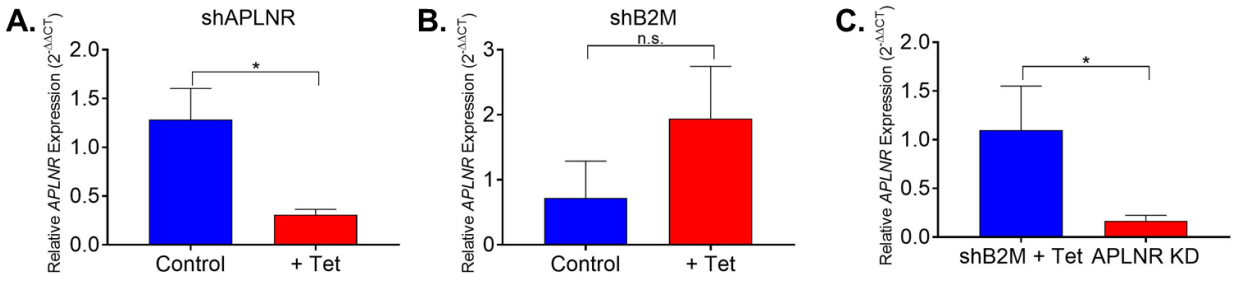

Figure 6.9: Comparison of relative expression of the apelin receptor gene (*APLNR*) in EHTs, with or without tetracycline treatment for 14 days. (A) Expression of *APLNR* in apelin receptor iKD EHTs treated with tetracycline compared to control cells cultured – Tet. (B) Expression of *APLNR* in B2M control line EHTs cultured with tetracycline for 14 days compared to control cells cultured - Tet. (C) Expression of *APLNR* in *APLNR* KD EHTs compared to relative expression in B2M control EHTs cultured + Tet for 14 days. n = 4 for shAPLNR line, n = 3 for shB2M line. Expression compared by unpaired, two-tailed Student's t-test, *p<0.05. Data represent mean±sem.

6.3.3.2 Effect of APLNR KD in 3D EHTs on voltage signalling

Next, effect of *APLNR* KD on voltage signalling in EHTs paced at 1 Hz was determined using voltage sensitive dye. Similar to what was seen in late KD hESC-CMs, *APLNR* KD had no effect on TTP or T90 (Figure 6.10). *APLNR* KD EHTs were compared to EHTs generated from B2M hESC-CMs cultured with tetracycline to control for effects of tetracycline itself.

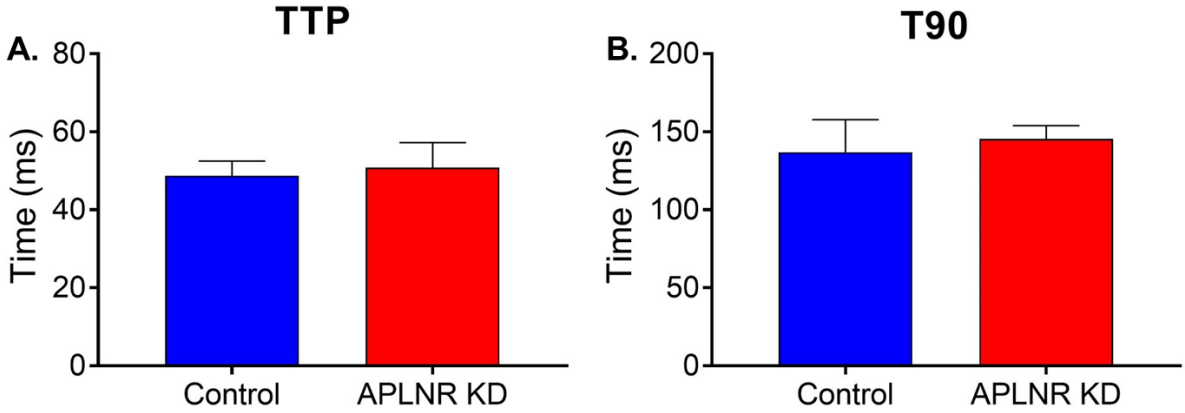

Figure 6.10: Effect of *APLNR* KD in 3D EHTs on voltage signalling (A) time to peak (TTP) and (B) time to 90% decay (T90) compared to control. n = 3 for all, mean values compared by unpaired, two-tailed Student's t-test. Data represent mean±sem.

6.3.3.3 Effect of APLNR KD in 3D EHTs on calcium signalling

The effect of *APLNR* KD on calcium signalling in EHTs was also examined. Consistent with previous results and published literature, *APLNR* KD had no effect on calcium signalling compared to control (Figure 6.11). Again, *APLNR* KD EHTs were compared to B2M EHTs cultured with tetracycline to control for tetracycline effect.

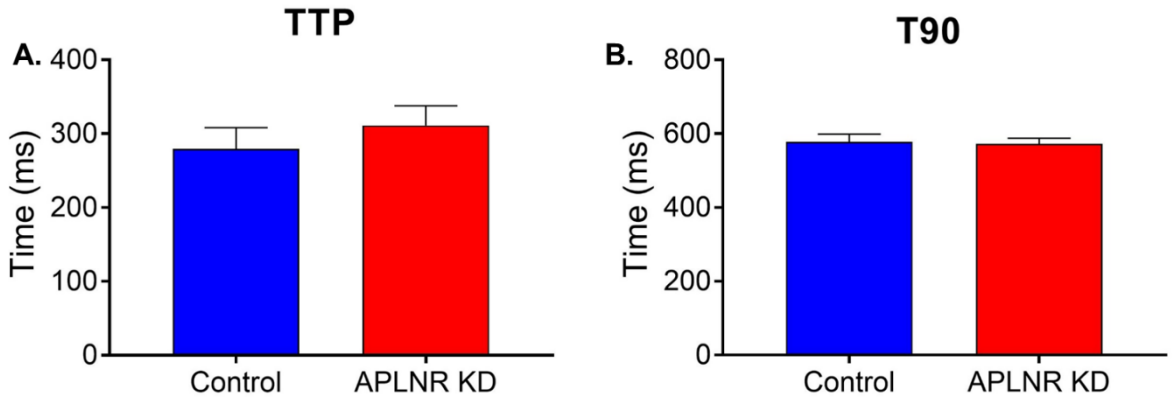

Figure 6.11: Effect of *APLNR* KD in 3D EHTs on calcium signalling (A) time to peak (TTP) and (B) time to 90% decay (T90) compared to control. n = 3 for all, mean values compared by unpaired, two-tailed Student's t-test. Data represent mean±sem.

6.3.3.4 Effect of APLNR KD in 3D EHTs on force generation

An advantage of producing EHTs is that they can be used to measure force of contraction. Previous studies have shown that EHTs generated using the protocol utilised here follow the Frank-Starling law, generating increased force of contraction in response to increasing strain (Ruan *et al.*, 2015; Bargehr *et al.*, 2019). Using an Aurora myograph and a custom stretch protocol, the effect of *APLNR* KD on EHT active and passive force was quantified. Active force is the force produced by the cardiomyocytes themselves as they beat, therefore indicating contractility, with a higher value representing better contractile performance. Passive force is a measure of how much force required to keep the EHT at a particular stretch. An increased passive force suggests that the tissue is stiffer, as more effort is required to keep it at that stretch level compared to a more elastic tissue which will stretch easily. Therefore a lower value here is generally better (Colomo *et al.*, 1997).

EHT force generation was measured on the myograph, with recordings analysed using a custom MATLAB code written by S. Bayraktar (University of Cambridge). A representative image of the recording output is shown in Figure 6.12A. EHTs were subject to a staircase of stretching, with 4% increases in length strain applied sequentially.

Tetracycline treatment was found to increase contractility in EHTs, as shown in the B2M line cultured with tetracycline (Figure 6.12B). Reasons for this are unclear, and

contractility reverted to the baseline level when tetracycline was removed. Therefore, the *APLNR* KD EHTs were compared to the B2M + Tet condition. EHTs were subjected to stretch and pacing at 1 Hz, and active and passive force was measured for *APLNR* KD compared to control (Figure 6.12C). Linear regression was performed to produce the Frank-Starling curve of force (Figure 6.12D), and slope of the resulting curve plotted (Figure 6.12E). Data points were normalised for slope calculations for each value by subtracting the mean value of recordings for all conditions at each stretch point, to centre the values around zero (Figure 6.12E).

Control EHTs responded to the Frank-Starling mechanism as expected, producing increased contraction in response to the applied stretch. Conversely, *APLNR* KD EHTs were less capable of responding to stretch and the slope of active force was significantly reduced, indicating reduced contractile ability. Furthermore, the slope of passive force was significantly increased for *APLNR* KD EHTs compared to control, indicative of increased tissue stiffness and decreased compliance.

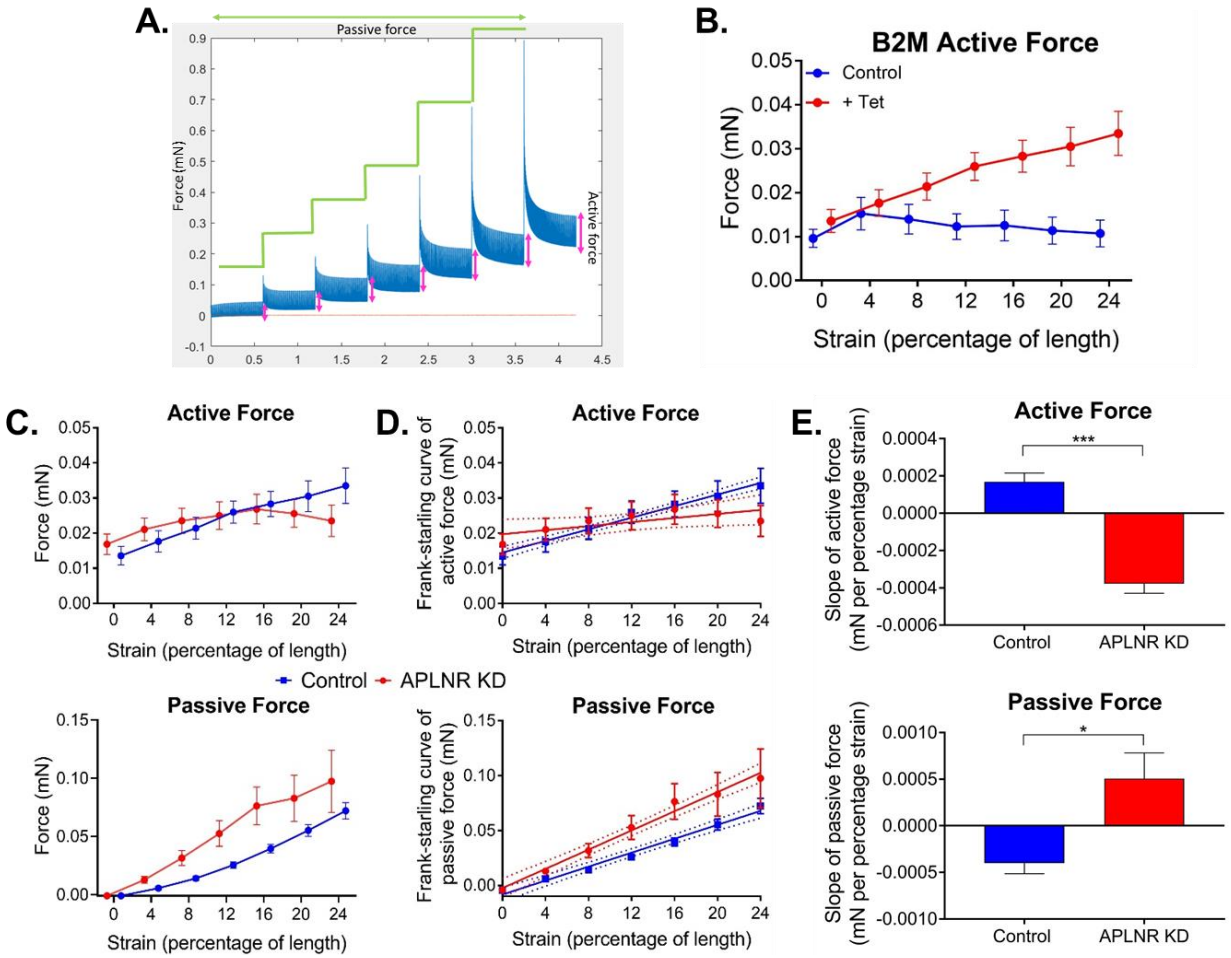

Figure 6.12: Effect of *APLNR* KD on force generation in EHTs. (A) Representative image of output from MATLAB code for analysis of force measurements generated by Aurora force transducer. (B) Active force generated by B2M EHTs cultured with and without tetracycline for 14 days. Tetracycline was found to increase contractility, therefore B2M + Tet EHTs were used as a control. (C) Active and passive force produced by control and *APLNR* KD EHTs as measured by force transducer in response to increasing strain. (D) Linear regression of force produced to generate Frank-Starling curve of active and passive force. (E) Normalised slope of generated Frank-Starling curve of active and passive force. n = 4, means compared by unpaired, two-tailed Student's t-test, ***p<0.001, *p<0.05. Data represent mean±sem.

6.3.3.5 Effect of APLNR KD in 3D EHTs on collagen expression

Having identified an increase in stiffness in the *APLNR* KD EHTs, second-harmonic imaging microscopy (SHIM) was performed to investigate the effects of *APLNR* KD on EHT collagen content. SHIM takes advantage of the natural properties of collagen, which interacts with light to produce intrinsic contrast which can be visualised without any exogenous staining (X. Chen *et al.*, 2012). Consistent with the increase in stiffness, by quantifying pixel intensity, *APLNR* KD EHTs were found to express increased collagen compared to control (Figure 6.13). This correlates with the previously reported anti-fibrotic action of apelin peptide in heart failure (Pchejetski *et al.*, 2012; X. Zhang *et al.*, 2016).

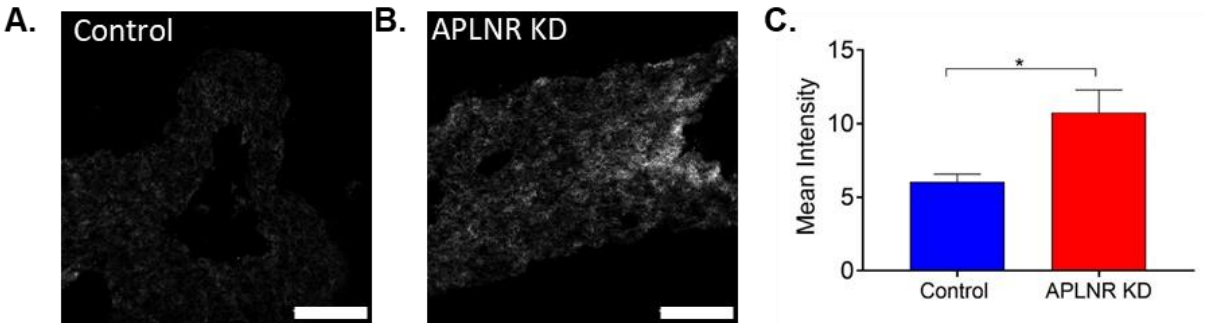

Figure 6.13: Effect of *APLNR* KD on collagen expression in EHTs. Representative images from second-harmonic imaging microscopy of (A) control and (B) *APLNR* KD EHTs to visualise collagen. (C) Quantification of mean pixel intensity of control and *APLNR* KD EHT collagen signal. n = 3, means compared by unpaired, two-tailed Student's t-test, *p<0.05. Data represent mean±sem.

Together, these results show that *APLNR* KD has negative consequences on force generation in EHTs, resulting in increased tissue stiffness, decreased contractile ability and increased collagen deposition. In previous studies, cardiomyocyte preparations isolated from heart failure patients show significantly increased passive force and decreased contractile force (Borbély *et al.*, 2005; Blair *et al.*, 2020). Therefore, the hESC-CM model recapitulates the phenotype of a failing cardiomyocyte, providing a potential platform for modelling heart failure in a human *in vitro* system.

Furthermore, *APLNR* KD appears to result in a failure of the Frank-Starling mechanism, with the EHTs less able to respond to increasing stretch compared to control EHTs.

6.4 Discussion

This section focussed on the role of the apelin receptor in differentiated hESC-CMs, by inducing KD after completion of differentiation, to gain insights into the role of the cardiac apelin receptor in cardiomyocyte function rather than development. By making use of both 2D and 3D culture methods, I have identified involvement of the apelin receptor in hESC-CM contractility.

This is the first time expression of the apelin receptor has been manipulated in hESC-CMs, likely owing to its low expression as discussed previously, making it difficult to induce knockdown. As only a low number of transcripts are present, it is harder for the processed shRNA targeting the mRNA to find and interact with its binding partner. Furthermore, literature searches indicate a lack of studies that have successfully knocked down any GPCR in PSC-CMs and characterised the effect.

6.4.1 Comparison of early and late *APLNR* KD in hESC-CMs

6.4.1.1 Effects of APLNR KD in hESC-CMs compared to APLNR KD throughout differentiation

Tetracycline treatment for 6-7 days was found to reduce apelin receptor expression by around 60-70% in hESC-CMs (late KD). Although significant, this reduction is less than that seen in the 2.2 line with tetracycline treatment throughout differentiation (~90%). The effects of this late *APLNR* KD were examined, performing similar assays to those used in Section 5, where the effect of *APLNR* KD throughout development (early KD) on resulting hESC-CM function was investigated. Some key similarities and differences in effects on hESC-CM function depending on when *APLNR* KD was induced were identified.

In early KD, loss of apelin receptor was found to decrease hESC-CM differentiation efficiency, with decreased number of cells with cardiomyocyte identity present and increased number with a fibroblast identity. Flow cytometry co-staining for a cardiomyocyte marker and a fibroblast marker in late KD cultures was performed, to determine if loss of apelin receptor promotes loss of cardiomyocytes, which could arise from death of hESC-CMs or de-differentiation to other cell types such as fibroblasts.

In contrast to what was seen for early KD, late *APLNR* KD had no effect on percentage of cells with cardiomyocyte identity.

Secondly, with early *APLNR* KD, there was no effect on hESC-CM ligand production as measured by assaying conditioned supernatant from hESC-CMs. In contrast, a trend towards an increase in both peptides was seen for both lines with late *APLNR* KD, with a significant increase in ELA expression found for the 5.3 *APLNR* KD hESC-CMs.

Furthermore, in contrast to what was found for early KD where voltage signalling was prolonged, in late KD hESC-CMs there was no effect on voltage signalling. Conversely, for both early and late KD, calcium signalling was unaffected.

6.4.1.2 Potential reasons for differences in effects of early and late APLNR KD in hESC-CMs

There are a number of potential explanations for these differences, both technical and biological.

The differences observed may be because the apelin receptor has a different role in development and in differentiated cardiomyocytes. The apelin receptor has been shown to have roles in both cardiac development and heart function in adults (Read *et al.*, 2019), however the differences in signalling pathways activated at the different life stages are poorly characterised. Hence, this is a powerful model system, and future studies will be able to investigate the molecular signalling involved in apelin receptor activation in a human system in both development and differentiated cardiomyocytes.

The differences in effects may also be dependent on the stages of the hESC-CMs themselves. Early KD hESC-CMs were assayed at day 14-17 of differentiation, whereas assays for late KD were performed at later stages of differentiation (Day 20-24). hESC-CMs are known to have an immature phenotype, with long-term culture shown to increase markers of maturation, including cell morphology, contractility, calcium handling and electrophysiology (Karbassi *et al.*, 2020). Although gradual increases in maturation continue to be observed when hPSC-CMs are cultured for up to 1 year (Kamakura *et al.*, 2013), many changes in maturation occur within the first 1-4 weeks of culture (Piccini *et al.*, 2015). Hence the difference in age of hESC-CMs

at the time of assaying may have effects on the results generated here. This could be investigated further by assaying the *APLNR* KD hESC-CMs at the same time point regardless of timing of inducing *APLNR* KD (e.g. assaying both early and late KD hESC-CMs at day 22).

Furthermore, in early KD, tetracycline treatment was maintained for 4 days prior to initiating differentiation, followed by 14-17 days of differentiation and maintenance culture (18-21 days total tetracycline treatment). In late KD, tetracycline was included in culture medium for only 6-7 days total. Although I established in Section 6.3.1 that this was sufficient time to induce robust KD at both the gene and protein level, it may not be sufficient time to allow functional consequences to manifest. The degradation and turnover rate of GPCRs is not well characterised and is highly variable depending on the receptor and cellular environment (Drake *et al.*, 2006; Kumagai *et al.*, 2015). For example, post-translational modification, such as phosphorylation, has been shown to affect protein turnover rate. Phosphorylation of the calcineruin regulator, calcipressin 1, significantly decreased its degradation time (Genescà *et al.*, 2003). The apelin receptor has been shown to undergo a variety of post-translational modifications including phosphorylation and glycosylation under different conditions (Y. Wu *et al.*, 2017), which may affect protein half-life. As discussed in Section 4, activation of a GPCR results in phosphorylation by GRKs and subsequent internalisation of receptor. Once internalised, the receptor can either be recycled back to the cell surface or sent for degradation (Penela *et al.*, 2006). Therefore, ligand exposure can also affect protein turnover. Furthermore, expression and rate of activity of GRKs can alter phosphorylation of GPCRs (Ribas *et al.*, 2007), therefore affecting internalisation and degradation rate. A point mutation induced at apelin receptor serine 348 abolished the recruitment of GRK and β-arrestins, and inhibited subsequent internalisation and degradation of ligand activated apelin receptor (X. Chen *et al.*, 2014), highlighting the importance of GRK expression in apelin receptor processing.

To investigate the length of time needed from initiation of tetracycline treatment to significant reduction in apelin receptor expression, a time course experiment could be carried out. By initiating tetracycline treatment and then collecting RNA and protein samples at regular intervals (e.g. every 24 hours), the time taken to achieve significant *APLNR* KD could be determined. A further experiment that could be performed is to

maintain tetracycline treatment in late KD for 18-21 days, as was done for the early KD hESC-CMs. However, this would mean the two conditions were at different stages of differentiation, which may cause further issues as described above. It is important to determine the time needed to achieve *APLNR* KD, so sufficient time is given to allow any effects of KD to manifest.

Finally, the efficiency of the tetracycline inducible system may be different across the differentiation stages. It has previously been shown that tetracycline-regulated gene expression was highly variable across differentiation of mouse haematopoietic cells, and also between cells within the same population indicating inconsistent expression of the tetracycline response element (Takiguchi *et al.*, 2013). However, for the system used here, this should not be the case as the transgene has been previously shown to be expressed stably and consistently across differentiation stages (Bertero *et al.*, 2016). It could be hypothesised that the tetracycline is less able to access the response element in hESC-CMs compared to hESCs. In attempt to induce similar levels of KD in late KD, a tetracycline titration curve could be performed to determine if a greater degree of KD can be induced by increasing tetracycline concentration.

Therefore, a number of experiments could be performed to further investigate the differences in results generated in early and late *APLNR* KD hESC-CMS. The technical differences should first be addressed. Depending on results generated here, biological differences in the role of the apelin receptor in development and in differentiated cardiomyocytes could then be investigated. It would be interesting to perform RNA sequencing analysis on late *APLNR* KD hESC-CMs to determine if similar DEGs and pathways are identified as those seen in early KD hESC-CMs.

6.4.2 *APLNR* KD in EHTs reduces cardiac contractility

From the results generated for early KD hESC-CMs and because of the previously reported role of the apelin receptor in cardiac contractility, it was important to investigate the effects of *APLNR* KD on hESC-CM force generation. To do this, 3D EHTs were generated, before inducing *APLNR* KD and measuring force generation using a myograph.

6.4.2.1 Measuring hESC-CM contractility in 2D

There are examples in the literature of systems which have been developed to measure PSC-CM contraction in 2D. These include a video analysis technique designed to extract information on cardiomyocyte beating dynamics and mechanobiology (Ahola *et al.*, 2014). This has further been combined with calcium signalling analysis to simultaneously measure PSC-CM contractility and calcium signalling (Ahola *et al.*, 2018). Furthermore, automated systems have been developed for simultaneously measuring contraction and calcium signalling in single isolated PSC-CMs (Pointon *et al.*, 2015).

Although it would be interesting to measure the effect of early *APLNR* KD on contractility, I have not made use of any of the aforementioned techniques here for the following reasons. Techniques used to investigate beating dynamics do not give information on the force of contraction generated by the hESC-CM, only on the motion of contraction (Ahola *et al.*, 2014). Automated systems for measuring single cell hESC-CMs were also not utilised, as measuring properties of single hESC-CMs is not representative of the *in vivo* environment, with cardiomyocyte contractility known to be dependent on interactions with neighbouring cardiomyocytes, other supportive cells types and the extracellular matrix (Karbassi *et al.*, 2020).

Recently, systems have been created to allow simultaneous measurement of action potentials, calcium signalling and contractility in 2D hPSC-CMs, utilising MUSCLEMOTION software (van Meer *et al.*, 2019). The imaging components needed for performing this assay are not easily available, however it would be interesting to measure early *APLNR* KD hESC-CMs in this system to determine if the voltage effects observed are linked to changes in contractility.

6.4.2.2 Measuring hESC-CM contractility in 3D

Owing to the lack of availability of a system to quantify force of contraction in 2D, it was not possible to examine effects of early *APLNR* KD on hESC-CM contractility. The Sinha group possesses the equipment and expertise to produce 3D EHTs and quantify force of contraction (Bargehr *et al.*, 2019), hence this method was used to investigate effects of *APLNR* KD on hESC-CM contractility. Furthermore, culturing in 3D has been shown to facilitate maturation of hESC-CMs, promoting interaction of hESC-CMs with neighbouring cells and extracellular matrix (Karbassi *et al.*, 2020).

Unfortunately, this technique needs a high number of hESC-CMs (Tulloch *et al.*, 2011; Ruan *et al.*, 2015). Because of the defects in cardiomyocyte differentiation seen in early *APLNR* KD hESC-CMs, it was not possible to generate EHTs from these cells. However, an advantage of the iKD system is that KD can be induced at any time, therefore hESC-CMs were generated, cast in moulds to produce EHTs and then *APLNR* KD induced by culturing with tetracycline throughout the 14 days culture period required for EHT maturation.

It should be noted, that for force measurements, *APLNR* KD hESC-CMs were cast as constructs alongside a supportive fibroblast cell (HS-27A). This is because it has previously been shown that tissues formed from hESC-CMs alone display poor contractility, with influence from fibroblast cells needed to promote extracellular matrix remodelling and tissue compaction (Tiburcy *et al.*, 2017). Bargehr *et al.* (2019) showed that inclusion of a supportive cell type can drastically increase the contractile force generated by resulting EHTs. These results were recapitulated in the system used in this project, in which force generation was minimal in hESC-CM only EHTs compared to EHTs also containing HS-27A cells (Figure 6.14).

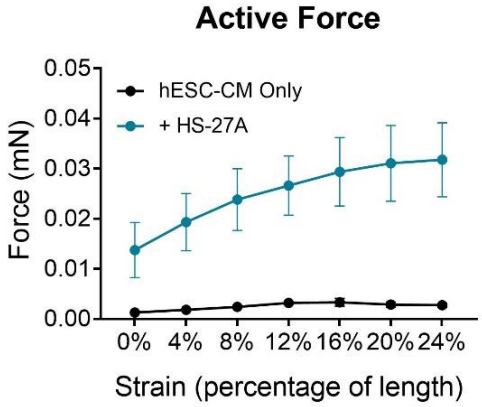

Figure 6.14: Active force generated by hESC-CM only EHTs compared to EHTs composed of hESC-CMs + HS-27A fibroblast cells cultured for 14 days. n = 2. Data represent mean±sem.

6.4.2.3 APLNR KD EHTs recapitulate the phenotype of a failing cardiomyocyte

The *APLNR* KD EHTs were found to produce reduced active force, indicating decreased contractility, and increased passive force, indicating increased stiffness. The *APLNR* KD EHTs did not respond to the Frank-Starling mechanism, similar to

what has previously been shown in isolated cardiomyocytes from apelin receptor KO mice (Parikh *et al.*, 2018). This is consistent with the previously proposed role of the apelin receptor as a stretch receptor (Scimia *et al.*, 2012) and suggests the apelin receptor may have a key role in the Frank-Starling response. Further work is needed here to ascertain whether there is mechanistic contribution from the apelin receptor or if the apelin receptor KD prevents integration and maturation of the hESC-CMs in the EHTs. Crucially, the observed changes are recapitulative of the phenotype of a failing cardiomyocyte. Previously, cardiomyocytes isolated from myocardial biopsies from human hearts with diastolic heart failure were found to generate twice as much passive force compared to cardiomyocytes isolated from control hearts (Borbély *et al.*, 2005).

There is controversy regarding the effect of heart failure on cardiomyocyte active force generation. In preparations of right and left ventricle from human failing heart, active force was significantly reduced by around 30% when subjected to increasing strain (Blair *et al.*, 2020). In contrast, another study reported that the maximum calcium activated force generated by control and heart failure isolated cardiomyocytes was comparable, and suggested that decline in force in heart failure is dependent on tissue remodelling (McDonald *et al.*, 2020). However, the results of this study were variable, likely reflecting the inherent variability associated with using samples from human patients, such as differences in age, sex and, perhaps most importantly, disease aetiology as there is large interpatient heterogeneity in heart failure presentation (McDonald *et al.*, 2020). In animal models, consistent decreases in active force generation are reported for heart failure cardiomyocytes. In a rat model of spontaneous hypertensive heart failure, force generation in isolated cardiomyocytes was significantly decreased, correlating with a marked decrease in left ventricular performance (Hanft *et al.*, 2017). Furthermore, in cardiomyocytes isolated from a mouse model of dilated cardiomyopathy, active force was significantly decreased while passive force increased, correlating with a decline in cardiac output (Édes *et al.*, 2008).

My results also recapitulate what has previously been seen in EHTs generated from PSC-CMs carrying mutations associated with heart failure. Firstly, one study investigated the effect of disease-associated phospholamban mutation on heart function by generating EHTs from iPSC-CMs derived from a patient suffering from dilated cardiomyopathy (DCM). Mutant EHTs were found to produce decreased active

force and increased passive force compared to control, indicating decreased contractility and increased stiffness. CRISPR/Cas9 correction of the mutation rescued the decreased contractility to a level similar to that recorded for control tissues (Stillitano *et al.*, 2016). In another study, iPSC-CMs were generated from DCM patients carrying truncating mutations in the sarcomere protein titin, which account for ~20% of familial and sporadic cases of DCM and are the most common genetic cause of DCM. Mutant iPSC-CMs incorporated into EHTs were found to generate less than 50% of the active force compared to control (Hinson *et al.*, 2015). Interestingly, EHTs generated from mouse cardiac cells with myosin-binding protein-C (cMyBP-C) KO produced increased maximal force output (Wijnker *et al.*, 2016). Mutations in the *MYBPC3* gene are the most common genetic cause of hypertrophic cardiomyopathy, which manifests differently to DCM. The hypercontractility of EHTs correlates with the phenotype seen in hypertrophic cardiomyopathy patients, however the reasons for the observed hypercontractility are unclear (Nag *et al.*, 2017).

In the *APLNR* KD EHT model, increased stiffness is observed. Myocardial stiffness is a hallmark of heart failure, with contributions from both increased collagen deposition and increased stiffness of the cardiomyocytes themselves (Borbély *et al.*, 2005). In the *APLNR* KD EHT model, it would be interesting to determine if the increased stiffness is due to an increase in collagen or because of an effect on the hESC-CMs themselves, or some combination of the two. The *APLNR* has previously been shown to regulate both physiological and pathophysiological organ fibrosis (S. Huang *et al.*, 2016), with apelin treatment in rats following myocardial infarction found to reduce fibrosis and associated collagen deposition, by inhibiting angiotensin II induced NF-κB activation (X. Zhang *et al.*, 2016). Furthermore, improved ventricular remodelling and function and attenuated fibrosis was observed in a model of surgically induced pressure overload with 14 days apelin administration (Pchejetski *et al.*, 2012). Here, *APLNR* KD EHTs were found to contain increased collagen compared to control, likely contributing to the increased stiffness and reduced contractility observed. This finding, in a human based system, supports the hypothesised anti-fibrotic properties of apelin receptor activation, highlighting the potential of therapeutically targeting the receptor to reduce the detrimental cardiac remodelling seen in heart failure.

Taken together, this work confirms that the *APLNR* KD EHTs recapitulate the contractile properties of a failing cardiomyocyte, with most similarity to the phenotype

of cardiomyocytes associated with DCM. Related to this, increased collagen deposition was seen, correlating with the increase in fibrosis observed in human diastolic dysfunction (Raman *et al.*, 2009). The results support a key role for apelin signalling in heart contractility and the Frank-Starling mechanism, and the link between reduced apelin signalling and decreased contractile performance observed in heart failure patients (K. S. Chong *et al.*, 2006). This offers a system to further investigate the signalling pathways in the apelin receptor's role in cardiac contractility. Moving forwards, it would be interesting to determine the effect of stimulating the EHTs with apelin receptor ligands (biased and non-biased). Furthermore, more generally, it is proposed that the *APLNR* KD EHTs could be used as a platform for modelling diastolic heart failure *in vitro* in a human system, and for screening compounds for potential novel treatments for heart failure.

Having demonstrated the effects of *APLNR* KD in EHTs, in the future EHTs carrying apelin receptor mutations associated with disease could also be produced to investigate functional consequences. EHTs can be generated from hiPSCs (Hinson *et al.*, 2015), therefore by isolating hiPSCs from patients carrying *APLNR* mutations, the contribution of the mutation to changes in contractility and disease could be assessed. Alternatively, genetic editing technology such as CRISPR/Cas9, could be used to introduce genetic variants before producing EHTs (Mosqueira *et al.*, 2018), to investigate the consequences of identified apelin receptor mutations.

6.4.2.4 Advantages of EHTs

There are a number of advantages of using EHTs. As mentioned above, incorporating hESC-CMs into EHTs promotes maturation, altering metabolism, cytoskeletal arrangement, calcium handling and electrophysiology (Greenberg *et al.*, 2018). For example, it was previously shown that hiPSC-CMs had $Na_{V1.5}$ subcellular distribution, sodium current density and action potential upstroke velocity more comparable to adult values when cultured in EHTs compared to 2D cultures (Lemoine *et al.*, 2017). The altered electrophysiological properties could potentially explain why effects on voltage signalling were observed in hESC-CMs with *APLNR* KD throughout development but not in EHTs with *APLNR* KD.

The increased maturation is thought to be in part dependent on the presence of non-cardiac cells within the EHT (e.g. fibroblasts), which are essential for cardiomyocyte

maturation *in vivo* through cell-cell signalling and interactions (Karbassi *et al.*, 2020). For example, in mouse embryonic heart development, cardiac fibroblasts regulate cardiomyocyte proliferation and ventricular chamber formation via β1-integrin signalling (Ieda *et al.*, 2009). The mechanical strain provided by the EHT mould itself can also promote maturation (Leonard *et al.*, 2018), which can be further increased by subjecting the EHTs to stretching, promoting cytoskeletal alignment to more closely recapitulate what is seen in the adult heart (Ruan *et al.*, 2016). Overall, the heart is a 3D organ with multiple cell types, in which cell-cell and extracellular matrix interaction and mechanical loading are essential for function. Hence, EHTs offer a more representative model to investigate heart physiology and pathophysiology, and also for drug screening (Greenberg *et al.*, 2018). In recent years, efforts have been made to increase throughput for drug screening using EHTs, with methods designed for producing 96-well micro arrays for EHT contractile force analysis (Thavandiran *et al.*, 2020).

6.5 Conclusions

The apelin receptor can be significantly knocked down at the gene and protein level in differentiated hESC-CMs by culturing with tetracycline over a period of 6-7 days, but over this time period, few functional consequences were seen in 2D cultures.

However, inducing *APLNR* KD in EHTs generated from hESC-CMs had significant detrimental effects on contractility, with *APLNR* KD EHTs displaying increased stiffness and decreased contractile force generation. The changes to contractility were associated with increased collagen deposition. This is consistent with previous studies reporting the positive inotropic and anti-fibrotic effects of apelin receptor activation, both *ex vivo* and *in vivo,* providing a platform for future investigation of the pathways activated by apelin receptor signalling. This is also recapitulative of the loss of apelin signalling seen in heart failure which correlates with reduced contractile performance. In the future, this system could be used for investigating the consequences of apelin receptor mutations associated with disease, by making use of genetic engineering to introduce mutations or by utilising hiPSCs isolated from patients carrying apelin receptor mutations.

Furthermore, the *APLNR* KD EHTs offer a potential novel model for diastolic heart failure, displaying the key characteristics of increased stiffness and decreased contractility which are seen in heart failure patients. This platform could therefore be used for screening novel treatments for heart failure in a human based system.

7. Generation of hESCs Carrying an Apelin Receptor Genetic Variant and Effect of the Apelin Receptor Genetic Variant in hESC-Derived Cardiomyocytes

7.1 Introduction

PSCs are amenable to genetic editing (Avior *et al.*, 2016). As shown in the previous sections, the expression of proteins of interest can be manipulated by introducing knockdown, knockout or over expression systems (Y. Chen *et al.*, 2015; Bertero *et al.*, 2016; Ma *et al.*, 2018). Going beyond this, PSCs can also be subjected to more precise genetic manipulation to introduce variants and mutations using technology such as CRISPR/Cas9 (González *et al.*, 2014; Gupta *et al.*, 2018). This could be used to introduce disease causing mutations in WT cells, or to correct disease causing mutations in hiPSCs derived from patients with genetic disease (Granata *et al.*, 2016; Gupta *et al.*, 2018).

The NIHR BioResource BRIDGE project is a sub-study of the ongoing 100,000 Genomes Project (Genomics England) (Turnbull *et al.*, 2018), aiming to identify sequence variants associated with poorly understood inherited rare diseases (Gräf *et al.*, 2018). The project has undertaken next generation sequencing of 13,000 patients with rare diseases, with the majority presenting with cardiovascular and bleeding disorders, and to date, performed case-control analysis of 7,423 patients (Gräf *et al.*, 2018). A strength of the BRIDGE project is the ability to provide phenotypic information on the patients, and it also offers the opportunity for patient recall in order to perform further investigations.

From the 7,423 patients screened so far, around 50 variants in the *APLNR* gene have been identified. The Davenport group has previously selected 11 variants of interest by using a predetermined exclusion criteria as shown in Table 7.1. The aim of the group is to determine the effects of the identified variants on apelin receptor binding, distribution and function.

Property	Criteria
Rare	Frequency < 1 in 10,000
Conservation	Sites conserved in the apelin receptor across 29 vertebrate species
Deleterious	Sites predicted to be deleterious by SIFT and Poly-Phen-2 (Flanagan *et al.*, 2010)
Impact on receptor function	Sites predicted to impact receptor function using GPCRdb (https://gpcrdb.org/) (Kooistra *et al.*, 2021)

Table 7.1: Predetermined exclusion criteria for selecting *APLNR* variants identified from the NIHR BioResource BRIDGE study for further investigation.

Rarity was included as part of the selection criteria because it is generally believed that rare variants contribute more to disease susceptibility than common variants. In relation to this, the "common disease-common variants" paradigm suggests that genetic diseases common in the population are dependent on genetic variants that are frequently found (Pierre and Génin, 2014).

Of the identified variants, preliminary work has characterised their effects on apelin receptor distribution and ligand binding in transfected CHO cells, which do not express the apelin receptor endogenously (Appendix I, T.L. Williams and R.E. Kuc, University of Cambridge, unpublished). This work has identified the R168H apelin receptor variant, in which a single point mutation results in the substitution of an arginine amino acid for a histidine at position 168 (Figure 7.1), as particularly interesting. R168 has previously been shown to form an important interaction with the G-protein biased small molecule CMF-019 (Read *et al.*, 2016). The patient that the R168H variant was identified in has a potentially associated rare bleeding disorder phenotype. Apelin signalling has previously been implicated in the regulation of platelet function and thrombosis (Adam *et al.*, 2016), however in this study apelin was found to be anti-thrombotic. Therefore, in the R168H individual, the bleeding disorder may be dependent the apelin receptor variant in cells other than platelets, on variants in other proteins or some combination of the two. Nevertheless, we sought to investigate the functional consequences of R168H in hESC-CMs.

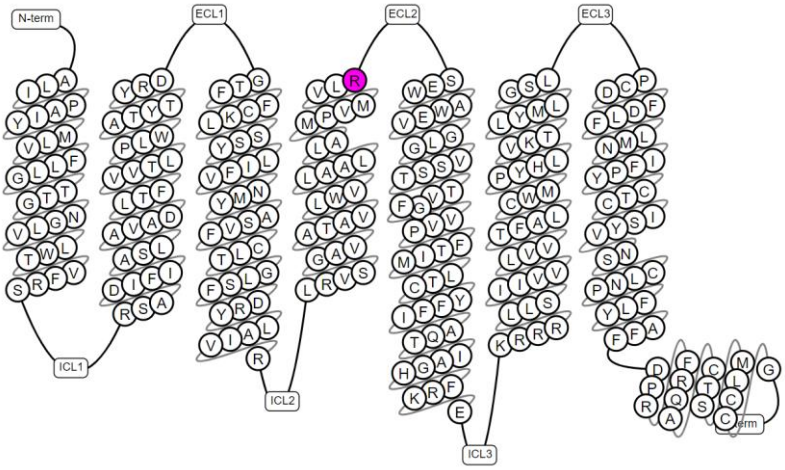

Figure 7.1: Representation of the apelin receptor amino acid sequence with R168 shown in purple. Plot generated from https://gpcrdb.org/protein/apj_human/

In CHO cells, R168H had no effect on apelin receptor expression or distribution, but abolished ligand binding in both radioligand binding and fluorescent ligand assays. Having identified the R168H variant as having effects on ligand binding, it would be beneficial to investigate its effects on the function of a clinically relevant cell type. Here therefore, base editing technology (Komor *et al.*, 2016) was used to introduce a single point mutation in hESCs, resulting in an amino acid change from arginine to histidine. By introducing the variant in hESCs, differentiation to cell types of interest (in this case, cardiomyocytes) can be induced and the consequences of the genetic change on cell function in a clinically relevant cell investigated.

Base editing is a modified form of CRISPR/Cas9 technology that introduces precise single base point mutations but does not introduce DSBs, and also does not rely on homology-directed repair (HDR) or require donor templates, in contrast to classic CRISPR/Cas techniques (Anzalone *et al.*, 2019). In genetic editing, DSBs can lead to generation of undesired genetic changes, such as indels and translocations (Kosicki *et al.*, 2018). Furthermore, relying on HDR to induce point mutations is inefficient due to competing cellular genetic repair mechanisms such as non-homologous end joining (NHEJ), again resulting in undesired genetic changes (Paquet *et al.*, 2016). Therefore, base editing offers a system that results in reduced indel generation and off target effects, and greatly increased editing efficiency (Molla and Yang, 2019). Base editors are made up of a catalytically inactive Cas9 and a base modifying enzyme, which can

induce a single nucleotide change on the target strand, whilst also generating a nick in the non-edited DNA strand, which is then repaired using the newly edited strand as a template (Rees and Liu, 2018). Here a cytosine base editor (CBE) was used, which induces a change from G-C to A-T (Komor *et al.*, 2016; Koblan *et al.*, 2018). Previously CBEs have been shown to have a 37% efficiency whilst generating an indel percentage of only 1.1%, in comparison to HDR with donor DNA which had a much higher indel rate (4.3%) and greatly reduced efficiency (0.5%) (Komor *et al.*, 2016). Therefore, base editing offers a powerful technology to introduce genetic variants of interest or to correct disease associated mutations not only in PSCs (Qi *et al.*, 2020), but in a wide range of cells. Base editing has the potential to be used *in vitro* for investigating genetic disease (Y. Zeng *et al.*, 2018) and also *in vivo* for gene therapy (Villiger *et al.*, 2018; Koblan *et al.*, 2021).

In this section the generation of hESCs carrying a heterozygous R168H apelin receptor variant using CBE is described. R168H hESCs were then induced to differentiate to hESC-CMs, and effects of the variant on apelin receptor expression and binding determined. In agreement with the Davenport group's previous work, R168H did not affect receptor expression but reduced apelin receptor ligand binding. The effects of R168H on hESC-CM differentiation were investigated, with the R168H variant found to reduce differentiation efficiency. hESC-CM function was also examined by investigating the effects on peptide production, voltage signalling and calcium signalling. The R168H variant also prolonged voltage sensing, similar to what was seen with *APLNR* KD.

7.2 Methods

The methods relevant to this section are listed in Table 7.2 and described in Section 2, with further detail for selected methods below.

Method	Section
Genome editing using base editor technology to generate hESCs with R168H *APLNR* variant	2.23
Cell culture and hESC-CM differentiation	2.2 and 2.3
Analysis of *APLNR* gene expression by qRT-PCR	2.4
Saturation radioligand binding	2.7
Binding of apelin fluorescent ligand	2.12
Immunocytochemistry for apelin receptor	2.5
Troponin T and Thy1 flow cytometry co-stain	2.6
Peptide production determined by ELISA	2.8
Measuring hESC-CM voltage signalling using FluoVolt	2.15
Measuring hESC-CM calcium signalling using Fluo-4, AM	2.16
Statistical analysis	2.24

Table 7.2: Descriptions of the methods used in this section found can be found in the listed corresponding section.

7.2.1 Genome editing using base editor technology to generate hESCs with R168H *APLNR* variant

hESCs carrying the R168H *APLNR* variant were generated as described in Section 2.23. gRNA was designed and inserted into an expression vector, and then nucleofected alongside the BE4max base editor plasmid into H9 hESCs. Cells were then subjected to puromycin selection and resistant colonies selected manually for clonal expansion.

Upon reaching sufficient confluence, genomic DNA was extracted from clonal cells for genotyping, to determine if successful genetic change had been induced. The required genetic change to induce a change from arginine to histidine at position 168 is shown in Table 7.3.

Amino acid change	Position	Base change	Position
Arg → His	168	CGC → CAC	812-814

Table 7.3: Base change needed to introduce R168H variant and associated position within the *APLNR* gene. Red = edited base.

The region of interest was amplified by PCR and samples sent for analysis by Sanger Sequencing. Generated sequencing traces were aligned to WT *APLNR* genetic sequence and examined to identify a change from a guanine (G) to adenine (A) at base position 813. From the clones sequenced, two separate clones (referred to as V1 and V2 subsequently) were found to have been successfully base edited, with a double peak for G and A visible at position 813, indicating heterozygous mutation (Figure 7.2).

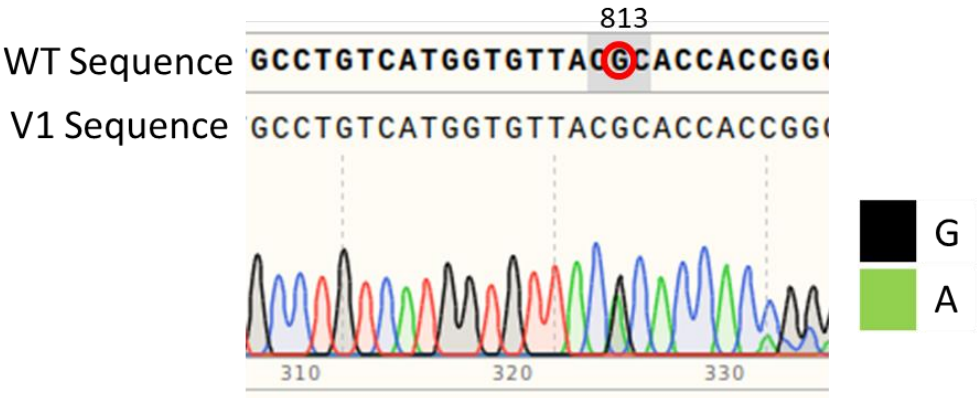

Figure 7.2: Representative sequencing trace of R168H V1 hESC clonal line showing a double peak at position 813 (red circle), indicating heterozygous point mutation with one allele containing G (black) and the other A (green), leading to a change in amino acid from arginine to histidine.

The patient in which the R168H variant was identified was heterozygous for the variant, hence the heterozygous base edit was deemed acceptable for further investigation. Interestingly, no homozygous clones were found in sequencing analysis of over 50 clones, therefore it was hypothesised that homozygous R168H mutation may be lethal.

The two heterozygous clones identified were expanded in culture and induced to differentiate to hESC-CMs.

7.2.2 Cell culture and hESC-CM differentiation

WT, V1 and V2 hESCs were maintained in E8 complete media as described in Section 2.2 on vitronectin coated plates. For differentiation to hESC-CMs, hESCs were plated

at a density of 1.2 x 10^6/well of a 6-well plate, with differentiation protocol followed as described in Section 2.3. Throughout Section 7, no exogenous apelin receptor ligands were added to cultures.

7.2.3 qRT-PCR for *APLNR* expression

qRT-PCR for *APLNR* gene expression was performed using TaqMan Gene Expression analysis as described in Section 2.4, with *18S* rRNA used as a housekeeping gene. Expression was normalised to housekeeping gene expression and relative expression compared to WT using the $2^{(-\Delta\Delta CT)}$ method (Schmittgen and Livak, 2008).

7.3 Results

7.3.1 Effect of R168H variant on apelin receptor expression

Following generation of the two hESC lines carrying the R168H variant, the first aim was to determine the effect of the introduced variant on expression of the apelin receptor. Previous work by the Davenport group has shown that in CHO cells transiently transfected with R168H apelin receptor, expression of the apelin receptor at the protein level is unchanged compared to control, but ligand binding is abolished, indicating a change in binding properties or an effect on the ligand binding site.

7.3.1.1 Effect of R168H variant on APLNR gene expression

First, *APLNR* gene expression was determined by qRT-PCR in both hESCs and hESC-CMs carrying the R168H variant and compared to WT. For both hESCs and hESC-CMs, no significant difference was seen between the two R168H lines (V1 and V2) and WT (Figure 7.3), supporting previous results that the R168H variant does not affect expression of the apelin receptor.

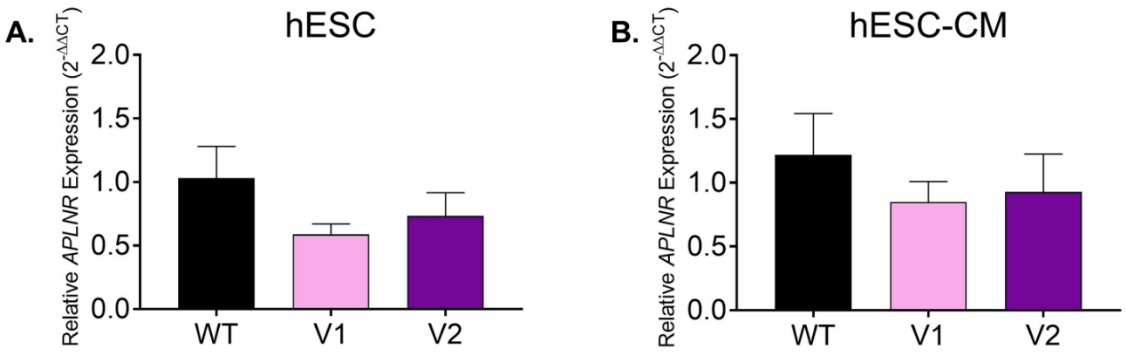

Figure 7.3: Comparison of relative expression of the apelin receptor gene (*APLNR*) in WT and R168H variant (V1 and V2) (A) hESCs (WT n = 2, V1 and V2 n = 4) and (B) hESC-CMs (n = 4 for all). Relative expression compared to WT mean expression. Expression compared by one way ANOVA followed by Tukey's post hoc test. Data represent mean±sem.

7.3.1.2 Effect of R168H variant on apelin receptor protein expression

Next, the effect of the R168H variant on apelin receptor protein expression was investigated. Saturation radioligand binding was performed using both hESCs and hESC-CMs and compared to WT (Figure 7.4). In hESCs, in both variant lines, binding of [^{125}I]apelin-13 was substantially reduced, with very low values for specific binding seen. Similarly, in R168H variant hESC-CMs, much reduced binding was observed. This suggests that the R168H variant is less able to bind the apelin ligand, in agreement with the Davenport group's previous work examining [^{125}I]apelin-13 binding in CHO cells transiently transfected with R168H apelin receptor.

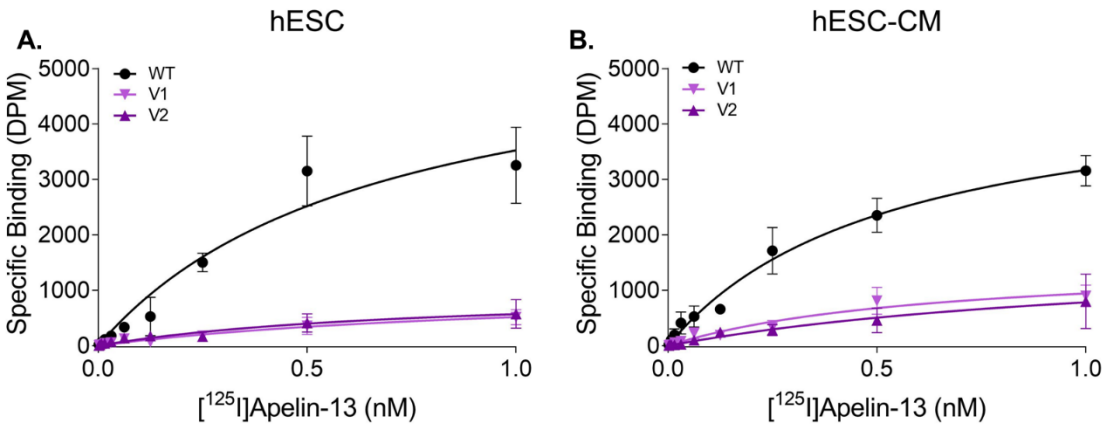

Figure 7.4: Saturation specific [^{125}I]apelin-13 binding in WT and R168H (A) hESCs and (B) hESC-CMs. n = 4 for WT, n = 3 for both V1 and V2 for hESCs and hESC-CMs. Data represent mean±sem.

Following on, hESC-CMs carrying the R168H variant were either incubated with apelin647 fluorescent ligand or stained using an antibody specific for the apelin receptor, in attempt to differentiate between effects on protein expression and protein function. Binding of fluorescent apelin647 was almost completely undetectable in both V1 and V2 R168H hESC-CMs (Figure 7.5). In contrast, binding of anti-apelin receptor antibody was similar in WT and both R168H variant line hESC-CMs (Figure 7.6). It should be noted that the morphology of the variant hESC-CMs was different to WT (as described further below), hence the number of cells per field of view was different. Despite this change in morphology, the apelin receptor antibody still bound to the variant hESC-CMs.

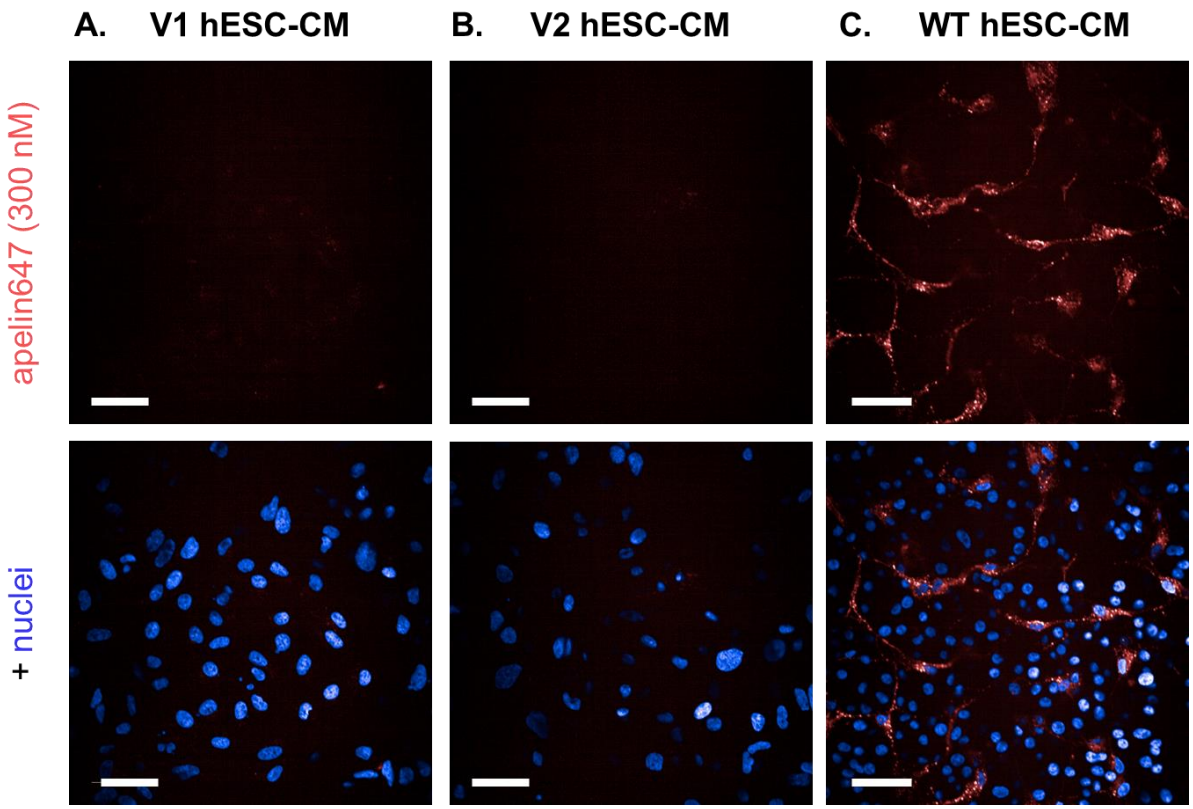

Figure 7.5: Representative images of (A) V1 R168H variant line, (B) V2 R168H variant line and (C) WT hESC-CMs incubated with apelin647 fluorescent ligand (300 nM, red) and Hoechst 3342 nuclear dye (blue). Non-specific binding (NSB) was determined by the inclusion of a saturating concentration of [Pyr^{1}]apelin-13 (shown in Figure 5.6). Scale bar = 50 µm.

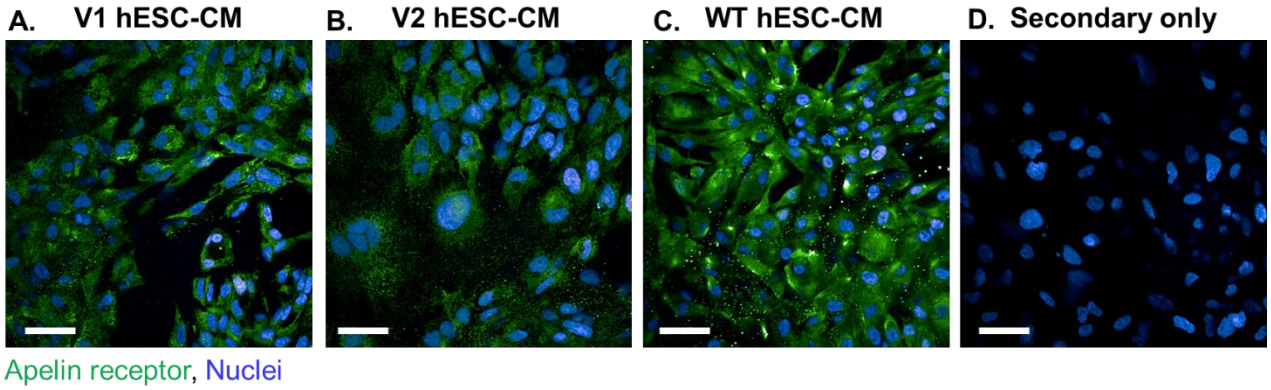

Figure 7.6: Representative images of (A) V1 R168H variant line, (B) V2 R168H variant line and (C) WT hESC-CMs stained with anti-apelin receptor antibody (green) and Hoechst 3342 nuclear dye (blue). (D) WT hESC-CMs incubated with secondary antibody alone. Scale bar = 50 µm.

Together, these data confirm previous work in CHO cells, that the R168H variant does not affect apelin receptor expression, but results in a substantial decrease in ligand binding. However, the hESC-CMs represent a more clinically relevant system. The R168H hESCs are heterozygous for the mutation, hence some functional apelin receptor expression is likely to remain, and therefore binding of either radiolabelled or fluorescently tagged ligand was not completely abolished.

7.3.2 Effect of R168H apelin receptor variant on hESC-CM differentiation

After confirming the effects of the R168H variant on apelin receptor expression and ligand binding, the effects of the variant on hESC-CM differentiation were examined.

7.3.2.1 Morphological changes in hESC-CMs with R168H apelin receptor variant

The morphology of R168H hESC-CMs appeared different to WT hESC-CMs. Beating hESC-CMs appeared in patches, with other cell types interspersed between clumps of cardiomyocytes (Figure 7.7). This phenotype is similar to that seen for hESC-CMs with *APLNR* KD throughout differentiation, although not as severe as seen for some differentiations of the 2.2 KD line. Again, there was variability in distinct differentiations with regard to how disrupted the hESC-CMs were. Interestingly, from observing the cells interspersed between the contractile cardiomyocytes, they did not appear to show a fibroblast-like morphology as seen in the *APLNR* KD cultures.

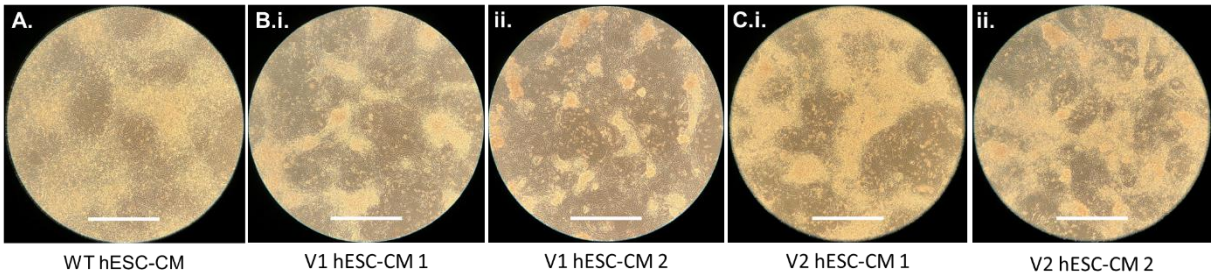

Figure 7.7: Representative brightfield images of (A) WT, (B) V1 and (C) V2 R168H hESC-CMs at day 14. Multiple images to show variability in differentiations. Scale bar = 200 µm.

The changes in differentiation are further exemplified in the recorded videos, in which clumps of hESC-CMs are seen to contract, with non-contractile areas found in-between. The contraction seen is more robust than that seen for *APLNR* KD hESC-

CMs, likely due to the less severe change in hESC-CM morphology. However, in many of the cultures, there was no regular beating rhythm and patches of cardiomyocytes contracted independently of other contractile areas (Videos 7.1 and 7.2).

7.3.2.2 Effect of R168H apelin receptor variant on hESC-CM differentiation efficiency

The effect of the R168H variant on hESC-CM differentiation was quantified by performing TnT/Thy-1 flow cytometry co-staining (Figure 7.8). As seen for *APLNR* KD, hESC-CM differentiation efficiency was significantly reduced in both R168H variant lines, as indicated by a decrease in TnT positive percentage (51.6±5.1% V1 and 58.9±3.4% V2 compared to 79.6±5.1 WT). However, there was no significant change in Thy1 positive percentage.

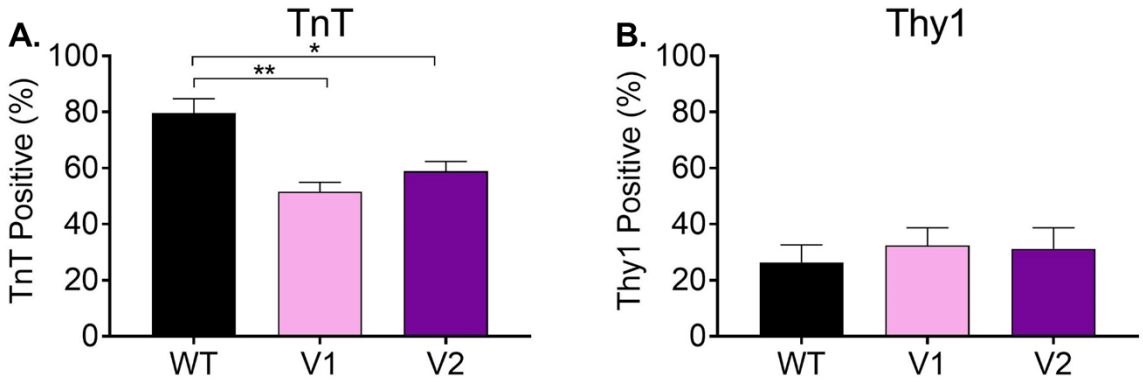

Figure 7.8: Quantification of (A) TnT and (B) Thy1 positive percentages from flow cytomteric co-stain for WT and R168H (V1 and V2) apelin receptor variant hESC-CMs. n = 3 for all, compared by one way ANOVA followed by Tukey's post hoc test, *p<0.05, **p<0.01. Data represent mean±sem.

Together these results show that the R168H apelin receptor variant decreases cardiomyocyte differentiation efficiency but does not increase the number of fibroblasts present in the culture, as reflected in the images displayed above (Figure 7.7). It is therefore unclear what the other cell types present in the culture are. Around 40-50% of cells do not stain positively for TnT, with ~30% staining positive for Thy1, leaving 20-30% unaccounted for. It could be suggested that the R168H heterozygosity results in a stalling of the differentiation process, generating cardiac progenitor cells that do

not express sufficient TnT to be detected in the staining protocol used here and hence stain as double negatives.

In the future, it would be interesting to determine if the differentiation efficiency can be rescued by application of exogenous ligand. To do this, a similar protocol to that used in Section 5.3.3 could be used. However, as it appears that the R168H apelin receptor is incapable of binding apelin ligand, it seems likely that there will be no effect of ligands targeting the apelin binding site and ligands targeting alternative sites may be needed.

7.3.3 Effect of R168H apelin receptor variant on hESC-CM function

Having established the effects of the R168H apelin receptor variant on hESC-CM differentiation, the effect of the variant on resulting hESC-CM function was also investigated. For all assays in this section, hESC-CMs were measured at day 14-16.

7.3.3.1 Effect of R168H apelin receptor variant on hESC and hESC-CM peptide production

First, the effects of R168H on apelin receptor ligand production were quantified by performing ELISAs using conditioned supernatant from WT and R168H V1 and V2 hESC-CMs (Figure 7.9). Comparing R168H hESC-CMs to WT, no differences in ELA production were seen. In contrast, both lines of R168H variant hESC-CMs were found to produce significantly increased levels of apelin peptide compared to WT control.

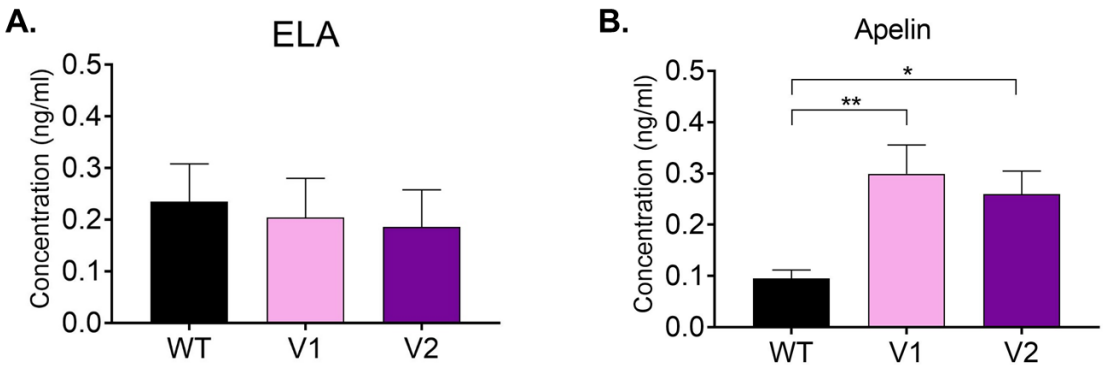

Figure 7.9: Comparison of concentration of (A) ELA and (B) apelin in conditioned supernatant from WT and R168H variant (V1 and V2) hESC-CMs. n = 6 for WT, n = 3 for both V1 and V2. Means compared by one way ANOVA followed by Tukey's post hoc test, *p<0.05, **p<0.01. Data represent mean±sem.

These results suggest that in the R168H hESC-CMs, where apelin receptor activation is reduced due to the R168H variant's lack of ability to bind peptide, there is a compensatory upregulation of apelin production, in attempt to increase apelin receptor signalling.

7.3.3.2 Effect of R168H apelin receptor variant on hESC-CM voltage signalling

Previously, *APLNR* KD throughout differentiation was found to significantly prolong voltage sensing in hESC-CMs. The effect of the R168H variant on hESC-CM voltage signalling was therefore investigated. As described previously, FluoVolt voltage sensitive dye was used to quantify TTP and T90 in WT and R168H hESC-CMs. Interestingly, TTP was significantly increased in both R168H variant lines compared to WT, however no effect was seen on T90 (Figure 7.10).

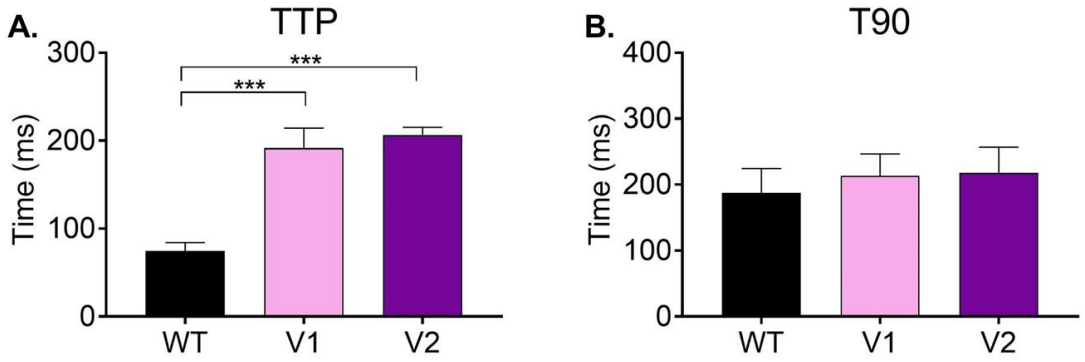

Figure 7.10: Effect of R168H variant on hESC-CM voltage signalling (A) time to peak (TTP) and (B) time to 90% decay (T90) compared to WT. n = 6 for WT, n = 3 for both V1 and V2. Mean values compared by one way ANOVA followed by Tukey's post hoc test, ***p<0.001. Data represent mean±sem.

This is different to what was seen in *APLNR* KD throughout differentiation, where both TTP and T90 were increased compared to control. This suggests that in the R168H hESC-CMs, there is dysregulation of depolarisation but not recovery. Nevertheless, this prolongation of voltage TTP could have detrimental effects on excitation-contraction coupling.

7.3.3.3 Effect of R168H apelin receptor variant on hESC-CM calcium signalling

The effect of R168H on hESC-CM calcium signalling was also investigated, utilising Fluo-4 calcium sensitive dye and MATLAB analysis. Consistent with what was

previously seen in hESC-CMs with *APLNR* KD, both throughout differentiation and post differentiation, no significant difference was seen between V1 and V2 hESC-CMs compared to WT control (Figure 7.11).

However, when performing this analysis, areas of visually beating cardiomyocytes are selected, meaning areas containing other cell types are not included. As shown in Figure 7.7, in both variant lines hESC-CMs are interspersed with other cell types which may influence contractility and signalling. Therefore surface plots of calcium signalling for the entire field of view for unpaced hESC-CMs were created using MATLAB. The plots show that R168H hESC-CM contraction and calcium signalling was asynchronous, with large non-contractile areas and patches of hESC-CMs firing calcium spikes randomly (Video 7.3).

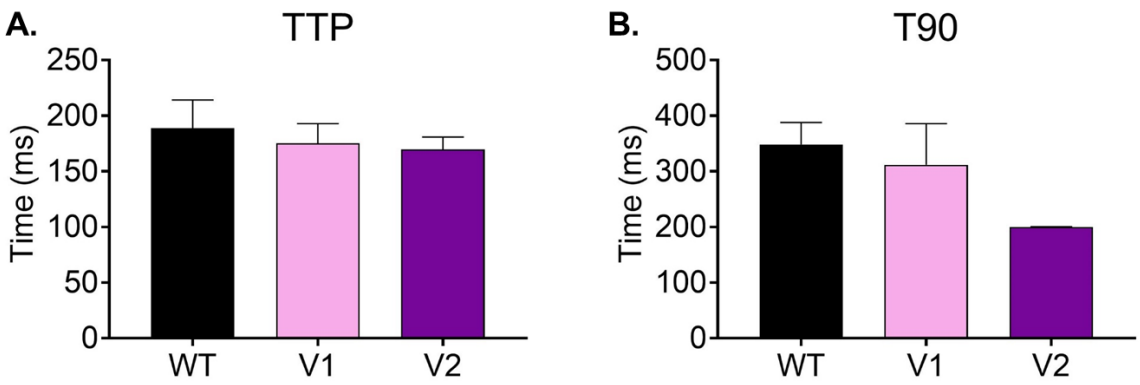

Figure 7.11: Effect of R168H variant on hESC-CM calcium signalling (A) time to peak (TTP) and (B) time to 90% decay (T90) compared to WT. n = 6 for WT, n = 3 for both V1 and V2. Mean values compared by one way ANOVA followed by Tukey's post hoc test. Data represent mean±sem.

7.4 Discussion

The aim of this section was to introduce an apelin receptor genetic variant R168H, previously identified to abolish ligand binding in CHO cells, into hESCs using base editing technology. By differentiating to hESC-CMs, the consequences of this variant in a clinically relevant cell type have been identified, and further insight has been gained into the role of the apelin receptor in both cardiomyocyte development and function. The work presented here is preliminary and further investigation and

characterisation are needed to fully understand the consequences of the R168H variant in hESC-CMs.

7.4.1 Generation of a novel apelin receptor variant hESC line using base editing

Two novel distinct clonal lines of hESCs carrying the R168H apelin receptor variant have been generated, with literature searches suggesting that this is the first use of base editing to target the apelin receptor.

Base editing is a relatively new technique, having first been demonstrated by the Liu lab in 2016 (Komor *et al.*, 2016). It presents a powerful tool for genetic editing, by introducing sequence changes without the need for DSBs, or relying on donor templates or error prone endogenous repair mechanisms. This means that efficiency is much increased and error rate much decreased compared to standard CRISPR/Cas9 genetic editing (Komor *et al.*, 2016; Anzalone *et al.*, 2019). Here a CBE was used to introduce a base change of G-C to A-T. CBE base editors are composed of a catalytically inactive Cas nuclease fused to a cytidine deaminase, which is an enzyme that deaminates cytosines (Anzalone *et al.*, 2020). BE4max was used as the base editor in this project, which is a modified version of the original CBEs, designed to have improved nuclear localisation. BE4max also contains a Cas nickase, designed to nick the non-deaminated strand, promoting more efficient repair and generating stable change of the base pair targeted (Koblan *et al.*, 2018).

Interestingly, although a large number of clones were selected and sequenced, only two heterozygous positive clones were found. Correlating with this, the R168H variant was identified in a patient who was heterozygous for the mutation. Hence it is hypothesised that homozygous R168H mutation is not viable, with those hESCs with homozygous base edit dying in culture.

The R168H variant in hESCs and hESC-CMs did not affect apelin receptor expression, but reduced ligand binding, consistent with previous results generated in CHO cells transfected with R168H apelin receptor. Structural studies within the Davenport group have shown that the R168H variant is found in the binding pocket of the apelin receptor (Read *et al.*, 2016), suggesting that mutation of this residue affects the conformation of the receptor, preventing ligand binding. Both arginine and histidine are basic side

chains, hence at neutral pH both will be positively charged, however the different side chains may affect receptor conformation. The site is also predicted to be important for G-protein coupling (Read *et al.*, 2016), but that has not been investigated here.

7.4.1.1 Heterozygous R168H variant reduced binding of apelin receptor ligands

The heterozygous R168H variant reduced binding of both fluorescent and radiolabelled apelin in hESC-CMs. However, intriguingly, the binding was reduced by more than the predicted 50% expected from the mutation of one allele, suggesting that either more variant receptor is expressed compared to WT, or variant receptor is having detrimental effects on WT receptor. To investigate this, two sets of qRT-PCR primers were designed to bind to the region containing the variant, which were identical apart from the single base change, with the last base of the primer binding at the genetic variant. Unfortunately, when these primers were tested on either WT or R168H apelin receptor plasmid DNA, equal amplification was seen for both primers regardless of which DNA was used. This suggests that the single base change was not sufficient to differentiate between the two alleles by qRT-PCR. In the future, it will be important to determine if there are differences in expression level between the variant and WT alleles.

It could be suggested that the R168H variant is having a dominant negative effect, having detrimental effects on WT receptor, perhaps affecting WT receptor localisation or binding ability (Dosil *et al.*, 1998). If the R168H variant influences WT ligand binding, that would explain the large reduction in binding of apelin ligands. However, if reduced ligand binding is dependent on dominant negative effects, this suggests that the apelin receptor is forming dimers or larger multimers (Dosil *et al.*, 1998). There is much controversy in the field of GPCRs surrounding oligomeric states of class-A GPCRs, and there is debate as to the existence or role of homodimerisation in GPCR function (Terrillon and Bouvier, 2004; Franco *et al.*, 2016; Kasai *et al.*, 2018). Nevertheless, there have been multiple studies suggesting the existence of GPCR homodimers. In one study, fluorescence correlation microscopy identified homodimer configuration of six different class-A GPCRs, including muscarinic and dopamine receptor families (Herrick-Davis *et al.*, 2013). Furthermore, crystal structure studies have revealed dimerization of the β1 adrenergic receptor in the ligand-free state (J. Huang *et al.*, 2013). Notably, one study found that ~60% of apelin receptor molecules were expressed as homodimers or oligomers, and dimerization was disrupted by

introducing mutations to the transmembrane domains (Cai *et al.*, 2017). Therefore, it could be hypothesised that R168H is affecting WT receptor function via the formation of homodimers. It will be necessary to investigate dimerisation in the future, for example by performing cross linking to bind interacting receptors followed by western blot using an antibody directed against the apelin receptor (Y. Yang *et al.*, 2007). This would provide insight into the role of dimerization in the function of the apelin receptor.

7.4.2 Effect of R168H apelin receptor variant on hESC-CM differentiation and function

Following generation of the R168H variant lines, hESCs were induced to differentiate to cardiomyocytes and the effects on differentiation and resulting hESC-CM function characterised.

7.4.2.1 R168H apelin receptor variant reduces hESC-CM differentiation efficiency

Cardiomyocyte differentiation efficiency of R168H hESCs was reduced compared to control, with a lower TnT positive percentage recorded. However, in contrast to what was observed with early *APLNR* KD (Section 5), there was no increase in the Thy1 positive percentage. Instead an increase in double negative stained cells was observed, suggesting that the cells have neither a cardiomyocyte or fibroblast identity. It could be hypothesised that introduction of the R168H variant results in a stalling of hESC-CM differentiation, resulting in the generation of cardiac progenitors which do not stain positively for TnT. To investigate this, a further stain could be carried out for a cell marker specific for early cardiac development such as Brachyury (mesoderm marker) or NKX2.5 (transcription factor regulating heart development) (Mendjan *et al.*, 2014). Alternatively, the R168H variant could result in induction of differentiation to a completely different lineage, hence stains for more diverse cell markers could also be used, such as CD31 (endothelial cell marker) (L. Liu and Shi, 2012).

7.4.2.2 R168H apelin receptor variant results in increased apelin peptide production

Conditioned supernatant collected from R168H variant hESC-CM cultures was found to contain increased apelin peptide, indicating increased cellular production. There are potentially multiple explanations for this increase. The WT hESC-CMs were found to produce apelin, suggesting an autocrine or paracrine mechanism of action on the apelin receptor. Negative feedback loops are essential for the control of ligand production in autocrine signalling pathways, with activation of the receptor signalling

to control the regulation of ligand production (Segers and De Keulenaer, 2021). In R168H hESC-CMs, receptor activation is reduced due to the reduced binding ability of the apelin receptor, which could result in upregulation of ligand production in attempt to compensate for the reduced receptor signalling (Figure 7.12).

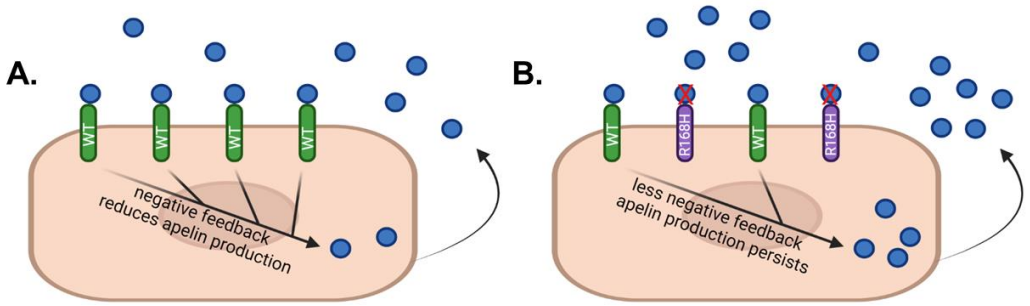

Figure 7.12: Simplified representation of the hypothesised effect of the R168H apelin receptor variant on apelin peptide production. (A) In WT hESC-CMs, apelin ligand (blue) binds to the apelin receptor, inducing a negative feedback mechanism to reduce apelin production. (B) In R168H hESC-CMs, there is reduced apelin receptor activation due to impaired ligand binding caused by the introduced variant, meaning the negative feedback loop is reduced and apelin production is therefore higher. Figure created using Biorender.com.

Another hypothesis is that the increased apelin production is coming from the other cell types present in the culture. As described above, the R168H variant resulted in decreased differentiation efficiency, with the identity of the other cell types present in the culture unclear. Depending on their cellular identity, their apelin ligand production will be different (Kleinz and Davenport, 2004; Read *et al.*, 2019). For example, if the cells are acquiring a more endothelial identity, apelin expression will be upregulated as these cells represent the main source of apelin ligand production *in vivo* (Kleinz and Davenport, 2004). This further highlights the importance of determining what the contaminating cell types are within the R168H cultures.

7.4.2.3 The effect of R168H apelin receptor variant on hESC-CM voltage and calcium signalling and contraction

The R168H variant was found to have effects on hESC-CM voltage signalling, prolonging TTP. However, in contrast to what was seen in the early KD hESC-CMs,

R168H did not affect T90. Reasons for this are unclear, but it suggests that the introduction of heterozygous R168H variant effects the action potential depolarisation stage but not the recovery phase (Grant, 2009). The depolarisation phase is dependent on cardiac sodium channels, including $Na_{V1.5}$ (Rook *et al.*, 2012), the gene for which was downregulated in early KD hESC-CMs. Therefore the reduction in apelin receptor signalling caused by the R168H variant could have consequential effects on sodium channel signalling, resulting in the prolongation of TTP. Apelin treatment has previously been shown to increase action potential conduction velocity in isolated rat cardiomyocytes and also increase sodium current (Farkasfalvi *et al.*, 2007; Chamberland *et al.*, 2010), supporting the hypothesis that apelin receptor activation is involved in the regulation of sodium channel kinetics and associated voltage signalling.

Consistent with previous sections, the R168H variant had no effect on hESC-CM calcium signalling TTP or T90. However, when examining the pattern of contraction and associated calcium signalling, compared to control the beating was uncoordinated, with patches of hESC-CMs contracting at different rates and calcium spikes firing asynchronously. This uncoordinated contraction may be due to defects in the hESC-CMs themselves, or it could be due to influence from the interfering cells found interspersed between the cardiomyocyte patches. Cell-cell contact between cardiomyocytes is crucial for electrophysiological signalling and regulation of contraction (J. Li *et al.*, 2006), as described previously. Hence it will be essential to isolate the effects of R168H in hESC-CMs on contractility. This could be done by performing metabolic selection to remove contaminating cell types, leaving a pure population of hESC-CMs. It is unclear how well metabolic selection will work in these cultures, as it resulted in high cell death in early KD hESC-CM cultures, but it should be attempted in the future.

7.4.3 Future experiments with apelin receptor variant hESCs

Here, the characterisation of the effects of the R168H apelin receptor variant has been initiated. The R168H hESC lines offer a powerful tool for investigating the functional consequences of the variant in a range of assays using hESC-CMs, but also in other differentiated progeny.

7.4.3.1 Investigating the effects of R168H apelin receptor variant on hESC-CM contractility

The next area that should be examined is the effect of the R168H apelin receptor variant on hESC-CM contractility. Here, 3D EHTs could be produced and force generation measured as described in Section 6 (Bargehr *et al.*, 2019). Given the reduced contractility and increased stiffness seen in *APLNR* KD hESC-CMs, and the established positive inotropic effects of apelin receptor activation (Maguire *et al.*, 2009; Japp *et al.*, 2010; Perjés *et al.*, 2016), it would be interesting to see if there were consequences of R168H on EHT contractile properties. As mentioned above however, this will be dependent on the successful metabolic selection of hESC-CMs carrying the variant.

7.4.3.2 Investigating the effects of R168H apelin receptor variant in other hESC-derived cell types

The focus of this project was to investigate the role of the apelin receptor in cardiomyocytes. However, hESCs are pluripotent and can be induced to differentiate to any cell type in the body (Thomson *et al.*, 1998). It would therefore be interesting to investigate the consequences of the R168H variant in other cell types. Of particular interest would be endothelial cells, as the patient from which the R168H variant was identified suffers from a genetic bleeding disorder. Endothelial cells form the lining of all blood vessels, influencing a range of process such as blood flow, vessel tone and permeability, cellular adhesion and inflammation, through the production of a range of signalling factors (Deanfield *et al.*, 2007). Hence, endothelial cell dysfunction can have drastic consequences on the whole organism.

Investigating the effect of R168H on vascular smooth muscle cells would also be interesting, as this cell type is exposed to various mechanical and biochemical signals in the blood vessels and contributes to physiological and pathological regulation of the vascular wall (Lacolley *et al.*, 2012).

The R168H apelin receptor variant hESC lines provide an ideal system for this further investigation, by inducing differentiation to cell type of interest and performing cell-specific assays to determine the consequences of the variant. Importantly, previous work identified that hESC-derived smooth muscle cells and endothelial cells produced

by the Sinha group express the apelin receptor at the gene and protein level (data not shown).

7.4.3.3 Investigating the effects of other apelin receptor variants

The work here provides a proof of principle that apelin receptor variants can be introduced into hESCs, and resulting hESC lines induced to differentiate to cell type of interest to characterise the effects of the variant. Hence, in the future, a similar approach could be used to investigate the effects of all 11 *APLNR* variants identified from the NIHR BioResource BRIDGE project. A further option for the investigation of the identified apelin receptor variants would be to recall the patients in which the variants were identified and to generate iPSCs. Genetic editing of iPSCs could then be used to correct the apelin receptor variant to provide a control cell line (Ryan *et al.*, 2013; Sterneckert *et al.*, 2014; Granata *et al.*, 2016). Both these approaches would provide isogenic control lines, allowing investigation of the effect of the variant in cells with identical genetic backgrounds apart from the single base change (Sterneckert *et al.*, 2014).

7.5 Conclusions

hESCs expressing the apelin receptor carrying the R168H variant identified from the BioResource BRIDGE project have been generated, utilising base editing technology for the first time to target the apelin receptor. Consistent with results in CHO cells, heterozygous expression of the R168H variant in hESCs and hESC-CMs had no effect on apelin receptor expression level, but decreased ligand binding.

The R168H variant reduced hESC-CM differentiation efficiency. Furthermore, R168H hESC-CMs formed patches of contractile cells with other as yet unidentified cell types interspersed. The contraction pattern was dysregulated, and voltage signalling in R168H hESCs was prolonged, consistent with previous results.

This system provides an excellent platform for further investigation into the effects of the R168H variant not only in hESC-CMs, but in other clinically relevant hESC-derived cell types such as endothelial cells. Furthermore, these results indicate that the other 10 *APLNR* variants identified from the BRIDGE project could be introduced into hESCs in a similar manner, and differentiated to cell types of interest to investigate their

consequences on cellular function. Together, these studies will provide insight into the role of the apelin receptor in disease, and highlight the importance of particular amino acid residues in receptor function.

8. Concluding Remarks

Since the discovery of the G-protein coupled apelin receptor (O'Dowd *et al.*, 1993) and its two endogenous peptide ligands, apelin (Tatemoto *et al.*, 1998) and ELA (Chng *et al.*, 2013; Pauli *et al.*, 2014), evidence has accumulated supporting a key role in the regulation of cardiovascular development, function and disease (Charo *et al.*, 2009; Kang *et al.*, 2013; P. Yang *et al.*, 2015; Read *et al.*, 2019). This study has focussed on the role of the apelin receptor in the heart, in cardiomyocytes specifically.

Loss of apelin receptor activation in developmental animal studies results in a high incidence of embryonic lethality, accompanied by severe cardiovascular defects, including rudimentary heart formation and poor vascularisation (Scott *et al.*, 2007; Chng *et al.*, 2013; Kang *et al.*, 2013; Pauli *et al.*, 2014). Furthermore, loss of apelin receptor in the differentiation of mouse ESCs resulted in severely reduced cardiomyocyte differentiation efficiency (D'Aniello *et al.*, 2013). Correspondingly, inclusion of apelin peptides in the culture media of mouse and human ESCs has been shown to enhance cardiomyocyte differentiation using embryoid body differentiation methods (I.-N. E. Wang *et al.*, 2012; D'Aniello *et al.*, 2013).

In the adult, apelin receptor activation promotes vasodilatation (Tatemoto *et al.*, 2001; Brame *et al.*, 2015) and positive inotropy (Szokodi *et al.*, 2002; Perjés *et al.*, 2014), with [Pyr^{1}]apelin-13 one of the most potent inotropic agent identified to date (Maguire *et al.*, 2009). Crucially, the positive inotropy induced by apelin receptor activation does not induce cardiac hypertrophy (Ashley *et al.*, 2005) and is also thought to be, at least in part, calcium independent (Seo *et al.*, 2020). Related to this, in cardiovascular disease states including heart failure and PAH, apelin receptor signalling is reduced (M. M. Chen *et al.*, 2003; K. S. Chong *et al.*, 2006; P. Yang *et al.*, 2017b), and hence targeting the apelin receptor has been proposed as a potentially novel therapeutic option.

Despite the growing evidence of the importance of the apelin receptor in cardiovascular physiology, there is a lack of a human *in vitro* system to investigate the cardiac apelin receptor. Human PSCs are a powerful tool, due to the potential to induce differentiation to any cell type and their amenability to genetic manipulation (Avior *et al.*, 2016). Furthermore, they can be used to generate a potentially unlimited supply of cardiomyocytes which can be maintained in culture (Paik *et al.*, 2020). This

study has therefore utilised hESCs differentiated to cardiomyocytes, in combination with genetic engineering, to assess the role of the apelin receptor in cardiomyocyte differentiation and function. This has identified a key role for the apelin receptor in the differentiation of hESC-CMs, and for the contractile function of differentiated hESC-CMs.

8.1 Strengths of using Pluripotent Stem Cells and Genetic Engineering for Investigating Protein Function

In this study, two genetic engineering approaches were used to investigate apelin receptor function. Firstly, an inducible knockdown system was generated, utilising the sOPTiKD technique (Bertero *et al.*, 2016), for the first time to target the apelin receptor. This novel inducible system generated significant apelin receptor knockdown at the gene and protein level in hESCs, hESC-CMs with knockdown induced throughout differentiation and hESC-CMs with knockdown induced post completion of differentiation. Not only is this the first time the sOPTiKD system has been used to target the apelin receptor, but literature searches indicate this is the first application of this system to a GPCR. This is likely due to the inherent difficulty of inducing GPCR knockdown, owing to their very low endogenous expression levels (Chakraborty *et al.*, 2015).

Apelin receptor knockdown throughout differentiation revealed a key role in cardiomyocyte differentiation, also highlighting poorly characterised roles of the apelin receptor in voltage signalling and adhesion. Using the inducible knockdown system has a number of advantages, which could be utilised to further investigate the involvement of the apelin receptor in cardiomyocyte differentiation. Firstly, apelin receptor knockdown could be induced at distinct stages of differentiation, in order to identify at what stage the apelin receptor has its effects. Furthermore, the apelin receptor KD can also be reversed, simply by removing tetracycline. There is therefore temporal control over apelin receptor expression, and by exploiting the Tet-on system, the key stages at which apelin receptor is needed can be defined. The ability to induce knockdown in differentiated hESC-CMs is also advantageous. It is well-known that transfection efficiency in hESC-CMs is often very low (Tan *et al.*, 2019), and therefore techniques such as transient transfection of siRNA to induce knockdown do not

generate reliable reduction in protein expression. As the transgene integrates into the host cell genome, expression of the shRNA targeting the apelin receptor can be induced at any stage (Bertero *et al.*, 2016), including in differentiated cardiomyocytes. As *APLNR* KD throughout differentiation significantly reduced hESC-CM differentiation efficiency, having the option to induce KD after completion of differentiation meant it was possible to investigate the effect of *APLNR* KD on hESC-CM function. It should also be noted that there is currently no selective antagonist targeting the apelin receptor available, meaning receptor activity cannot be inhibited pharmacologically. Hence the ability to reduce apelin receptor expression is advantageous for investigating its function.

Secondly, base editing technology (Anzalone *et al.*, 2019) was used to introduce an apelin receptor genetic variant (R168H) identified from the NIHR BioResourse BRIDGE project (Gräf *et al.*, 2018; Turnbull *et al.*, 2018) into hESCs. Literature searches indicate this is the first time base editing has been used to successfully target the apelin receptor. Introduction of the variant did not affect apelin receptor expression but significantly reduced ligand binding. This had detrimental effects, similar to that seen with *APLNR* KD, reducing differentiation efficiency, disrupting contractile coordination and prolonging voltage sensing. This highlights another strength of using PSCs – the ability to introduce genetic variants potentially associated with disease, differentiating to cell type of interest and characterising any phenotypic effects (Gupta *et al.*, 2018; Ma *et al.*, 2018). Additionally, when phenotypic drug screening is performed, often control cells expressing native protein are used. By utilising cell lines carrying a variant of interest, the effect of the variant on drug affinity and efficacy can be studied. The use of base editing technology generates isogenic lines for control and variant, meaning the genetic background is identical, allowing isolation of the effects of the variant itself (Avior *et al.*, 2016). An advantage of the BRIDGE project is the ability to recall patients from which interesting variants were identified. In the future, it could be possible to isolate iPSCs from the R168H patient, generate isogenic control lines by correcting the variant with genetic editing, and performing phenotypic characterisation. This may generate further insight, as the effect of any confounding variants or influence from the patient's genetic background could also be examined (Yamasaki *et al.*, 2017).

Finally, perhaps the biggest advantage of hESCs is the ability to differentiate to any cell type of interest (Thomson *et al.*, 1998), generating a potentially unlimited supply of cells for study. Although this project has focused on the role of the apelin receptor in cardiomyocytes, its expression is far more widespread (Medhurst *et al.*, 2003; Kleinz *et al.*, 2005), associated with a range of physiological and pathological effects. For example, in PAH apelin signalling is reduced (J. Kim *et al.*, 2013; P. Yang *et al.*, 2017b). As this condition is due to a combination of dysregulation of vascular endothelial and smooth muscle cells (Morrell *et al.*, 2009), it would be interesting to characterise the effects of *APLNR* KD both in the differentiation and function of these cell types. Furthermore, the R168H variant was identified in a patient suffering from a bleeding disorder. Hence it would be interesting to induce differentiation to endothelial cells to investigate any effect of the variant in this cell type.

Overall, these studies have shown proof of principle that it is possible to genetically manipulate the apelin receptor in hESCs and their differentiated progeny, to provide novel insights into its role and function. Moving forwards, the genetically manipulated lines generated here could be used to further investigate the role of the apelin receptor in the cardiovascular system and beyond. It also highlights the potential of introducing the various apelin receptor variants identified from the BRIDGE project into hESCs to characterise their effects in relevant cell types, in a human system. This will not only generate more clinically translatable results (Sterneckert *et al.*, 2014), but is easier and more high throughout than using animal models of disease (Giacomotto and Ségalat, 2010) or isolated human tissue (Avior *et al.*, 2016).

8.2 Limitations of the Project

PSCs represent powerful tools for development and disease modelling, however their inherent limitation is that their differentiated progeny often display a foetal phenotype (Sterneckert *et al.*, 2014). This means that the phenotypic characteristics are immature compared to their adult counterparts. For hPSC-CMs, it has previously been shown that their contractile force is significantly lower than that of adult cardiomyocytes, and they are also less responsive to inotropic stimuli (van Meer *et al.*, 2016). Furthermore, conditions such as heart failure generally have a mid to late age

onset, which is therefore difficult to model with immature hPSC-CMs (Parrotta *et al.*, 2020).

Cardiomyocyte cellular alignment and assembly of a syncytium with tightly regulated cell junctions is an essential step of heart development, which is difficult to mimic in an *in vitro* culture system, meaning PSC-CMs generally lack well-aligned myofibrils and T-tubules (Karbassi *et al.*, 2020). Furthermore, the cardiomyocytes generated tend to form a mixed population of atrial, ventricular and nodal cells (Weng *et al.*, 2014), which can make results more difficult to interpret. Together, this results in more foetal like properties, affecting contractility, voltage signalling, calcium handling and metabolism (Greenberg *et al.*, 2018).

A number of techniques have however been shown to induce maturation of PSC-CMs, resulting in changes to cardiomyocyte properties, making them more adult-like. For example, long term culture is a simple way to increase maturation (Kamakura *et al.*, 2013; Piccini *et al.*, 2015), however effects are limited and time consuming (Karbassi *et al.*, 2020). Altering media composition has also been shown to induce maturation. For example, by mimicking the switch to oxidative metabolism seen in embryogenesis (Malandraki-Miller *et al.*, 2018). Using a maturation media containing low glucose and high levels of substrates for oxidative metabolism resulted in increased hiPSC-CM maturation, with changes in electrophysiology and structural organisation observed (Feyen *et al.*, 2020). Manipulation of the hiPSC-CMs generated this way resulted in models for long QT syndrome and DCM which more faithfully recapitulated the human disease states (Feyen *et al.*, 2020).

Another effective method of inducing maturation is through the use of 3D culture methods, such as the EHTs used in this study (Ruan *et al.*, 2015; Mills *et al.*, 2017; Bargehr *et al.*, 2019). By combining PSC-CMs in an extracellular matrix with a supportive cell type, suspended between two pillars, cardiomyocyte maturation can be induced from the combination of intercell interaction, signalling between the supportive cell type and the mechanical load inferred from the culture posts (Ruan *et al.*, 2016; Leonard *et al.*, 2018). This maturation can be further increased by concurrently electrically stimulating the 3D tissues, as evidenced by the presence of T-tubules and organised myofibrils (Ronaldson-Bouchard *et al.*, 2018).

In this project, the effects of apelin receptor in cardiomyocyte differentiation have been investigated, because of the previously proposed role of the apelin receptor in heart development. Therefore, for this part of the study, the immaturity of the hESC-CMs should not influence results. However, when examining the calcium handling and voltage sensing in the resulting hESC-CMs, the immaturity may affect results. The same is true for the hESC-CMs with apelin receptor KD induced post completion of differentiation. However, the effect of *APLNR* KD on contractility, voltage and calcium signalling was investigated in 3D EHTs, therefore this will have induced some maturation of the hESC-CMs.

Furthermore, the expression of the apelin receptor at the gene and protein level has been compared to the expression in the adult heart. From a combination of qRT-PCR, RNA sequencing and saturation radioligand binding, a comparable level of apelin receptor expression was found in hESC-CMs as that seen in human adult heart. Therefore, the system is suitable. When interpreting results however, when extrapolating to the human heart, it is important to consider the potential differences arising from hESC-CM immaturity. In future studies, further techniques could be employed to enhance maturation as needed.

It should also be noted that only a single line of hESCs has been used throughout this thesis. As each hESC line is isolated from a single embryo, this genetic background represents only one individual. It would therefore be interesting in the future to introduce apelin receptor knockdown and the apelin receptor variant into further lines of hESCs. Furthermore, it would be interesting to look at the effects in iPSCs (of introduced variants or from donors carrying apelin receptor variants inherently).

8.3 Conclusions

The studies presented here have made use of a hESC-derived cardiomyocyte model to reveal key roles of the apelin receptor in cardiomyocyte differentiation and function. This is the first time detailed characterisation of apelin receptor function in hESC-CMs has been carried out.

Importantly, expression of the apelin receptor in hESC-CMs was quantified and found to be comparable at both the gene and protein level to that seen in adult human heart.

hESC-CMs were also found to produce both apelin and ELA peptides, providing a ligand source in the cell culture system. Furthermore, expression of apelin receptor gene and protein was also seen in hESCs, in contrast to previous reports. This observation is crucial, as the existence of a second, unidentified receptor for ELA in development has been proposed – the search for which has been unsuccessful thus far. The data here supports the action of both apelin and ELA through a single receptor.

To investigate the role of the apelin receptor, a novel inducible knockdown system was generated in hESCs. This is the first time the apelin receptor has been successfully knocked down in hESC-CMs, and the first time the sOPTiKD system has been used to target a GPCR. This provided a powerful platform to manipulate apelin receptor expression throughout differentiation to characterise apelin receptor function in cardiomyocytes.

The apelin receptor has previously been shown to be important for cardiovascular development. Here, knockdown of the apelin receptor throughout differentiation to cardiomyocyte resulted in significantly reduced cardiomyocyte differentiation efficiency and an increase in the number of fibroblasts. Consistent with this, inclusion of apelin in the culture media increased cardiomyocyte differentiation efficiency. Together these results support the key signalling role of the apelin receptor in cardiomyocyte differentiation, in a human relevant system. The resulting hESC-CMs produced with apelin receptor knockdown throughout differentiation displayed prolonged voltage sensing, consistent with previous studies suggesting that voltage signalling is an important regulator of the positive inotropic effects of apelin receptor activation. Furthermore, loss of apelin receptor was associated with changes in adhesion properties, which has not been studied previously.

The apelin receptor also has important effects in the adult heart, acting as a positive inotrope, with decreased apelin receptor signalling observed in heart failure patients. In 3D EHTs, knockdown of apelin receptor resulted in decreased force generation and increased stiffness, associated with increased collagen deposition. This is recapitulative of animal knockout studies, in which loss of apelin signalling results in decreased contractility and ability to respond to cardiovascular stress. Furthermore, it is similar to the phenotype seen in heart failure patients which have an associated

reduction in apelin receptor signalling. More generally, the characteristics of the *APLNR* KD EHTs are reminiscent of the phenotype of cardiomyocytes isolated from dilated cardiomyopathy patients, indicating this system could be used more generally as a model of heart failure. In the future, this platform could be used for screening novel treatments for heart failure, targeting both the apelin receptor and other pharmacological targets.

It would be interesting to determine if the effects of apelin receptor knockdown both throughout differentiation and in EHTs are mediated through ligand-dependent signalling, as the apelin receptor has previously been shown to also function in a ligand-independent manner as discussed above (Scimia *et al.*, 2012; Seo *et al.*, 2020). The hESC-CMs were found to produce both apelin and ELA peptides, however it would be beneficial to determine whether the previously described stretch responsive function is involved in the phenotype observed here. I have begun to investigate this, through the use of biased compounds which preferentially activate the G-protein signalling pathway, but further work is needed. An apelin receptor antagonist would help elucidate the contribution of ligand-dependent versus independent effects, however a selective compound is not currently available.

A second genetic manipulation technique was used to introduce a genetic variant identified from the NIHR BioResource BRIDGE project into hESCs. hESC-CMs carrying the R168H variant had reduced apelin receptor ligand binding and also displayed reduced differentiation efficiency and prolonged voltage sensing. This further supports the role of the apelin receptor in cardiomyocyte differentiation and function.

The two approaches used in this study highlight the power of using hESC-derived cell types in combination with genetic manipulation to investigate protein function in a human based system. Roles for the apelin receptor in cardiomyocyte development and function have been identified which have previously not been well characterised, and a potential novel model for investigating heart failure has been produced. In the future, the apelin receptor cell lines generated here could be used for further investigation into the identified cardiomyocyte roles, and also for screening novel compounds which have the potential for treating heart failure and other cardiovascular diseases. Furthermore, effects in other hESC-derived cell types could be investigated

to gain insights into the role of the apelin receptor throughout the body. Finally, by introducing apelin receptor genetic variants associated with disease, the contribution of the apelin receptor to disease aetiology could be determined and improved treatments developed, contributing to the implementation of precision medicine.

References

100000 Genomes Project Pilot Investigators (2021). 100,000 Genomes Pilot on Rare-Disease Diagnosis in Health Care - Preliminary Report. *The New England Journal of Medicine* **385**(20):1868–1880.

Abdul-Ghani M, Dufort D, Stiles R, Repentigny Y De, Kothary R and Megeney LA (2011). Wnt11 Promotes Cardiomyocyte Development by Caspase-Mediated Suppression of Canonical Wnt Signals. *Molecular and Cellular Biology* **31**(1):163–178.

Abriel H (2010). Cardiac sodium channel Nav1.5 and interacting proteins: Physiology and pathophysiology. *Journal of Molecular and Cellular Cardiology* **48**(1):2–11.

Adam F, Khatib AM, Lopez JJ, Vatier C, Turpin S, Muscat A, Soulet F, Aries A, Jardin I, Bobe R, Stepanian A, De Prost D, Dray Ć, Rosado JA, Valet P, Feve B and Siegfried G (2016). Apelin: an antithrombotic factor that inhibits platelet function. *Blood* **127**(7):908–920.

Ahola A, Kiviaho AL, Larsson K, Honkanen M, Aalto-Setälä K and Hyttinen J (2014). Video image-based analysis of single human induced pluripotent stem cell derived cardiomyocyte beating dynamics using digital image correlation. *BioMedical Engineering* **13**(1):1–18.

Ahola A, Pölönen R-P, Aalto-Setälä K and Hyttinen J (2018). Simultaneous Measurement of Contraction and Calcium Transients in Stem Cell Derived Cardiomyocytes. *Annals of Biomedical Engineering* **46**(1):148–158.

Akyea RK, Kai J, Qureshi N, Iyen B and Weng SF (2019). Sub-optimal cholesterol response to initiation of statins and future risk of cardiovascular disease. *Heart* **105**(13):975–981.

del Álamo JC, Lemons D, Serrano R, Savchenko A, Cerignoli F, Bodmer R and Mercola M (2016). High throughput physiological screening of iPSC-derived cardiomyocytes for drug development. *Biochimica et Biophysica Acta - Molecular Cell Research* **1863**(7):1717–1727.

Alqahtani MS, Kazi M, Alsenaidy MA and Ahmad MZ (2021). Advances in Oral Drug Delivery. *Frontiers in Pharmacology* **12**:618411.

Anisuzzaman ASM, Morishima S, Suzuki F, Tanaka T, Yoshiki H, Sultana Sathi Z, Akino H, Yokoyama O and Muramatsu I (2008). Assessment of Muscarinic Receptor Subtypes in Human and Rat Lower Urinary Tract by Tissue Segment Binding Assay. *Journal of Pharmacological Sciences J Pharmacol Sci* **106**(2):271–279.

Anzalone A V., Koblan LW and Liu DR (2020). Genome editing with CRISPR–Cas nucleases, base editors, transposases and prime editors. *Nature Biotechnology* **38**(7):824–844.

Anzalone A V., Randolph PB, Davis JR, Sousa AA, Koblan LW, Levy JM, Chen PJ, Wilson C, Newby GA, Raguram A and Liu DR (2019). Search-and-replace genome editing without double-strand breaks or donor DNA. *Nature* **576**:149–157.

Ashley EA, Powers J, Chen M, Kundu R, Finsterbach T, Caffarelli A, Deng A, Eichhorn J, Mahajan R, Agrawal R, Greve J, Robbins R, Patterson AJ, Bernstein D and Quertermous T (2005). The endogenous peptide apelin potently improves cardiac contractility and reduces cardiac loading in vivo. *Cardiovascular Research* **65**(1):73–82.

Asnes CF, Marquez JP, Elson EL and Wakatsuki T (2006). Reconstitution of the Frank-Starling Mechanism in Engineered Heart Tissues. *Biophysical Journal* **91**(5):1800–1810.

Ason B, Chen Y, Guo Q, Hoagland KM, Chui RW, Fielden M, Sutherland W, Chen R, Zhang Y, Mihardja S, Ma X, Li X, Sun Y, Liu D, Nguyen K, Wang J, Li N, Rajamani S, Qu Y, Gao BX, Boden A, Chintalgattu V, Turk JR, Chan J, Hu LA, Dransfield P, Houze J, Wong J, Ma J, Pattaropong V, Véniant MM, Vargas HM, Swaminath G and Khakoo AY (2020). Cardiovascular response to small-molecule APJ activation. *JCI Insight* **5**(8):1–16.

Atluri P, Morine K, Liao G, Panlilio C, Berry M, Hsu V, Hiesinger W, Cohen J and Joseph Woo Y (2007). Ischemic heart failure enhances endogenous myocardial apelin and APJ receptor expression. *Cellular and Molecular Biology Letters* **12**(1):127–138.

Avior Y, Sagi I and Benvenisty N (2016). Pluripotent stem cells in disease modelling and drug discovery. *Nature Reviews Molecular Cell Biology* **17**(3):170–182.

Bar-Nur O, Russ HA, Efrat S and Benvenisty N (2011). Epigenetic memory and

preferential lineage-specific differentiation in induced pluripotent stem cells derived from human pancreatic islet beta cells. *Cell Stem Cell* **9**(1):17–23.

Bargehr J, Ong LP, Colzani M, Davaapil H, Hofsteen P, Bhandari S, Gambardella L, Le Novère N, Iyer D, Sampaziotis F, Weinberger F, Bertero A, Leonard A, Bernard WG, Martinson A, Figg N, Regnier M, Bennett MR, Murry CE and Sinha S (2019). Epicardial cells derived from human embryonic stem cells augment cardiomyocyte-driven heart regeneration. *Nature Biotechnology* **37**(8):895–906.

Barmada SJ, Serio A, Arjun A, Bilican B, Daub A, Ando DM, Tsvetkov A, Pleiss M, Li X, Peisach D, Shaw C, Chandran S and Finkbeiner S (2014). Autophagy induction enhances TDP43 turnover and survival in neuronal ALS models. *Nature Chemical Biology* **10**(8):677–685.

Barnes GD, Alam S, Carter G, Pedersen CM, Lee KM, Hubbard TJ, Veitch S, Jeong H, White A, Cruden NL, Huson L, Japp AG and Newby DE (2013). Sustained cardiovascular actions of APJ agonism during renin-angiotensin system activation and in patients with heart failure. *Circulation: Heart Failure* **6**(3):482–491.

Bedut S, Seminatore-Nole C, Lamamy V, Caignard S, Boutin JA, Nosjean O, Stephan J-P and Coge F (2016). High-throughput drug profiling with voltage- and calcium-sensitive fluorescent probes in human iPSC-derived cardiomyocytes. *American Journal of Physiology-Heart and Circulatory Physiology* **311**(1):H44–H53.

Berry MF, Pirolli TJ, Jayasankar V, Burdick J, Morine KJ, Gardner TJ and Woo YJ (2004). Apelin has in vivo inotropic effects on normal and failing hearts. *Circulation* **110**(11):II187-93.

Bers DM (2002). Cardiac excitation–contraction coupling. *Nature* **415**:198–205.

Bertero A, Pawlowski M, Ortmann D, Snijders K, Yiangou L, Brito MC de, Brown S, Bernard WG, Cooper JD, Giacomelli E, Gambardella L, Hannan NRF, Iyer D, Sampaziotis F, Serrano F, Zonneveld MCF, Sinha S, Kotter M and Vallier L (2016). Optimized inducible shRNA and CRISPR/Cas9 platforms for in vitro studies of human development using hPSCs. *Development* **143**(23):4405–4418.

Blair CA, Brundage EA, Thompson KL, Stromberg A, Guglin M, Biesiadecki BJ and Campbell KS (2020). Heart Failure in Humans Reduces Contractile Force in

Myocardium From Both Ventricles. *JACC: Basic to Translational Science* **5**(8):786–798.

Bodbin SE, Denning C and Mosqueira D (2020). Transfection of hPSC-Cardiomyocytes Using Viafect™ Transfection Reagent. *Methods and Protocols* **3**(3):1–10.

Bogaard HJ, Legchenko E, Ackermann M, Kühnel MP, Jonigk DD, Chaudhary KR, Sun X, Stewart DJ and Hansmann G (2020). The adult sprague-dawley sugen-hypoxia rat is still 'the One:' A model of group 1 pulmonary hypertension: Reply to le cras and abman. *American Journal of Respiratory and Critical Care Medicine* **201**(5):621–624.

Borbély A, Velden J van der, Papp Z, Bronzwaer JGF, Edes I, Stienen GJM and Paulus WJ (2005). Cardiomyocyte Stiffness in Diastolic Heart Failure. *Circulation* **111**(6):774–781.

Bouveret R, Waardenberg AJ, Schonrock N, Ramialison M, Doan T, de jong D, Bondue A, Kaur G, Mohamed S, Fonoudi H, Chen CM, Wouters MA, Bhattacharya S, Plachta N, Dunwoodie SL, Chapman G, Blanpain C and Harvey RP (2015). NKX2-5 mutations causative for congenital heart disease retain functionality and are directed to hundreds of targets. *eLife* **4**:e06942.

Boycott KM, Rath A, Chong JX, Hartley T, Alkuraya FS, Baynam G, Brookes AJ, Brudno M, Carracedo A, den Dunnen JT, Dyke SOM, Estivill X, Goldblatt J, Gonthier C, Groft SC, Gut I, Hamosh A, Hieter P, Höhn S, Hurles ME, Kaufmann P, Knoppers BM, Krischer JP, Macek M, Matthijs G, Olry A, Parker S, Paschall J, Philippakis AA, Rehm HL, Robinson PN, Sham PC, Stefanov R, Taruscio D, Unni D, Vanstone MR, Zhang F, Brunner H, Bamshad MJ and Lochmüller H (2017). International Cooperation to Enable the Diagnosis of All Rare Genetic Diseases. *The American Journal of Human Genetics* **100**(5):695–705.

Braam SR, Tertoolen L, van de Stolpe A, Meyer T, Passier R and Mummery CL (2010). Prediction of drug-induced cardiotoxicity using human embryonic stem cell-derived cardiomyocytes. *Stem Cell Research* **4**(2):107–116.

Brame AL, Maguire JJ, Yang P, Dyson A, Torella R, Cheriyan J, Singer M, Glen RC, Wilkinson IB and Davenport AP (2015). Design, characterization, and first-in-human

study of the vascular actions of a novel biased apelin receptor agonist. *Hypertension* **65**(4):834–40.

Brash L, Barnes GD, Brewis MJ, Church AC, Gibbs SJ, Howard LSGE, Jayasekera G, Johnson MK, McGlinchey N, Onorato J, Simpson J, Stirrat C, Thomson S, Watson G, Wilkins MR, Xu C, Welsh DJ, Newby DE and Peacock AJ (2018). Short-Term Hemodynamic Effects of Apelin in Patients With Pulmonary Arterial Hypertension. *JACC: Basic to Translational Science* **3**(2):176–186.

Breckwoldt K, Letuffe-Brenière D, Mannhardt I, Schulze T, Ulmer B, Werner T, Benzin A, Klampe B, Reinsch MC, Laufer S, Shibamiya A, Prondzynski M, Mearini G, Schade D, Fuchs S, Neuber C, Krämer E, Saleem U, Schulze ML, Rodriguez ML, Eschenhagen T and Hansen A (2017). Differentiation of cardiomyocytes and generation of human engineered heart tissue. *Nature Protocols* **12**(6):1177–1197.

Briganti F, Sun H, Wei W, Wu J, Zhu C, Liss M, Karakikes I, Rego S, Cipriano A, Snyder M, Meder B, Xu Z, Millat G, Gotthardt M, Mercola M and Steinmetz LM (2020). iPSC Modeling of RBM20-Deficient DCM Identifies Upregulation of RBM20 as a Therapeutic Strategy. *Cell Reports* **32**(10):108117.

Bruno BJ, Miller GD and Lim CS (2013). Basics and recent advances in peptide and protein drug delivery. *Therapeutic Delivery* **4**(11):1443.

Buddeke J, Bots ML, Van Dis I, Visseren FLJ, Hollander M, Schellevis FG and Vaartjes I (2019). Comorbidity in patients with cardiovascular disease in primary care: A cohort study with routine healthcare data. *British Journal of General Practice* **69**(683):E398–E406.

Bulatovic I, Ibarra C, Österholm C, Wang H, Beltrán-Rodríguez A, Varas-Godoy M, Månsson-Broberg A, Uhlén P, Simon A and Grinnemo K-H (2015). Sublethal Caspase Activation Promotes Generation of Cardiomyocytes from Embryonic Stem Cells. *PLoS ONE* **10**(3):e0120176.

Burridge PW, Matsa E, Shukla P, Lin ZC, Churko JM, Ebert AD, Lan F, Diecke S, Huber B, Mordwinkin NM, Plews JR, Abilez OJ, Cui B, Gold JD and Wu JC (2014). Chemically defined generation of human cardiomyocytes. *Nature Methods* **11**(8):855–860.

Cai X, Bai B, Zhang R, Wang C and Chen J (2017). Apelin receptor homodimer-oligomers revealed by single-molecule imaging and novel G protein-dependent signaling. *Scientific Reports* **7**:40335.

Calejo MT, Saari J, Vuorenpää H, Vuorimaa-Laukkanen E, Kallio P, Aalto-Setälä K, Miettinen S, Skottman H, Kellomäki M and Juuti-Uusitalo K (2020). Co-culture of human induced pluripotent stem cell-derived retinal pigment epithelial cells and endothelial cells on double collagen-coated honeycomb films. *Acta Biomaterialia* **101**:327–343.

Caspi O, Huber I, Kehat I, Habib M, Arbel G, Gepstein A, Yankelson L, Aronson D, Beyar R and Gepstein L (2007). Transplantation of Human Embryonic Stem Cell-Derived Cardiomyocytes Improves Myocardial Performance in Infarcted Rat Hearts. *Journal of the American College of Cardiology* **50**(19):1884–1893.

Caulfield M, Davies J, Dennys M, Elbahy L, Fowler T, Hill S, Hubbard T, Jostins L, Maltby N, Mahon-Pearson J, McVean G, Nevin-Ridley K, Parker M, Parry V, Rendon A, Riley L, Turnbull C and Woods K (2017). The 100,000 Genomes Project Protocol.

Chakraborty R, Xu B, Bhullar RP and Chelikani P (2015). Expression of G Protein-Coupled Receptors in Mammalian Cells. *Methods in Enzymology* **556**:267–281.

Chamberland C, Barajas-Martinez H, Haufe V, Fecteau M-H, Delabre J-F, Burashnikov A, Antzelevitch C, Lesur O, Chraibi A, Sarret P and Dumaine R (2010). Modulation of canine cardiac sodium current by Apelin. *Journal of Molecular and Cellular Cardiology* **48**(4):694–701.

Chandra SM, Razavi H, Kim J, Agrawal R, Kundu RK, de Jesus Perez V, Zamanian RT, Quertermous T and Chun HJ (2011). Disruption of the apelin-APJ system worsens hypoxia-induced pulmonary hypertension. *Arteriosclerosis, Thrombosis and Vascular Biology* **31**(4):814–20.

Charo DN, Ho M, Fajardo G, Kawana M, Kundu RK, Sheikh AY, Finsterbach TP, Leeper NJ, Ernst K V, Chen MM, Ho YD, Chun HJ, Bernstein D, Ashley EA and Quertermous T (2009). Endogenous regulation of cardiovascular function by apelin-APJ. *American Journal of Physiology - Heart and Circulatory Physiology* **297**(5):H1904-13.

Chen MM, Ashley EA, Deng DXF, Tsalenko A, Deng A, Tabibiazar R, Ben-Dor A, Fenster B, Yang E, King JY, Fowler M, Robbins R, Johnson FL, Bruhn L, McDonagh T, Dargie H, Yakhini Z, Tsao PS and Quertermous T (2003). Novel role for the potent endogenous inotrope apelin in human cardiac dysfunction. *Circulation* **108**(12):1432–9.

Chen X, Bai B, Tian Y, Du H and Chen J (2014). Identification of serine 348 on the apelin receptor as a novel regulatory phosphorylation site in apelin-13-induced G protein-independent biased signaling. *The Journal of Biological Chemistry* **289**(45):31173–87.

Chen X, Nadiarynkh O, Plotnikov S and Campagnola PJ (2012). Second harmonic generation microscopy for quantitative analysis of collagen fibrillar structure. *Nature Protocols* **7**(4):654–669.

Chen Y, Cao J, Xiong M, Petersen AJ, Dong Y, Tao Y, Huang CTL, Du Z and Zhang SC (2015). Engineering Human Stem Cell Lines with Inducible Gene Knockout using CRISPR/Cas9. *Cell Stem Cell* **17**(2):233–244.

Chester N, Kuo F, Kozak C, O'Hara CD and Leder P (1998). Stage-specific apoptosis, developmental delay, and embryonic lethality in mice homozygous for a targeted disruption in the murine Bloom's syndrome gene. *Genes and Development* **12**(21):3382–3393.

Chirikian O, Goodyer WR, Dzilic E, Serpooshan V, Buikema JW, McKeithan W, Wu H Di, Li G, Lee S, Merk M, Galdos F, Beck A, Ribeiro AJS, Paige S, Mercola M, Wu JC, Pruitt BL and Wu SM (2021). CRISPR/Cas9-based targeting of fluorescent reporters to human iPSCs to isolate atrial and ventricular-specific cardiomyocytes. *Scientific Reports* **11**(1):1–10.

Chng SC, Ho L, Tian J and Reversade B (2013). ELABELA: A hormone essential for heart development signals via the apelin receptor. *Developmental Cell* **27**(6):672–680.

Choi SM, Kim Y, Shim JS, Park JT, Wang RH, Leach SD, Liu JO, Deng C, Ye Z and Jang YY (2013). Efficient drug screening and gene correction for treating liver disease using patient-specific stem cells. *Hepatology* **57**(6):2458–2468.

Chong JJH, Yang X, Don CW, Minami E, Liu YW, Weyers JJ, Mahoney WM, Van Biber

B, Cook SM, Palpant NJ, Gantz JA, Fugate JA, Muskheli V, Gough GM, Vogel KW, Astley CA, Hotchkiss CE, Baldessari A, Pabon L, Reinecke H, Gill EA, Nelson V, Kiem HP, Laflamme MA and Murry CE (2014). Human embryonic-stem-cell-derived cardiomyocytes regenerate non-human primate hearts. *Nature* **510**:273–277.

Chong KS, Gardner RS, Morton JJ, Ashley EA and McDonagh TA (2006). Plasma concentrations of the novel peptide apelin are decreased in patients with chronic heart failure. *European Journal of Heart Failure* **8**(4):355–360.

Colomo F, Piroddi N, Poggesi C, Kronnie G te and Tesi C (1997). Active and passive forces of isolated myofibrils from cardiac and fast skeletal muscle of the frog. *The Journal of Physiology* **500**:535.

D'Aniello C, Fiorenzano A, Iaconis S, Liguori GL, Andolfi G, Cobellis G, Fico A and Minchiotti G (2013). The G-protein-coupled receptor APJ is expressed in the second heart field and regulates Cerberus–Baf60c axis in embryonic stem cell cardiomyogenesis. *Cardiovascular Research* **100**(1):95–104.

Dai T, Ramirez-Correa G and Gao WD (2006). Apelin increases contractility in failing cardiac muscle. *European Journal of Pharmacology* **553**(1–3):222–228.

Das M, Fessel J, Tang H and West J (2012). A Process-Based Review of Mouse Models of Pulmonary Hypertension. *Pulmonary Circulation* **2**(4):415–433.

Deanfield JE, Halcox JP and Rabelink TJ (2007). Endothelial function and dysfunction: Testing and clinical relevance. *Circulation* **115**(10):1285–1295.

DeKelver RC, Choi VM, Moehle EA, Paschon DE, Hockemeyer D, Meijsing SH, Sancak Y, Cui X, Steine EJ, Miller JC, Tam P, Bartsevich V V., Meng X, Rupniewski I, Gopalan SM, Sun HC, Pitz KJ, Rock JM, Zhang L, Davis GD, Rebar EJ, Cheeseman IM, Yamamoto KR, Sabatini DM, Jaenisch R, Gregory PD and Urnov FD (2010). Functional genomics, proteomics, and regulatory DNA analysis in isogenic settings using zinc finger nuclease-driven transgenesis into a safe harbor locus in the human genome. *Genome Research* **20**(8):1133–1142.

DiMasi JA, Grabowski HG and Hansen RW (2016). Innovation in the pharmaceutical industry: New estimates of R&D costs. *Journal of Health Economics* **47**:20–33.

Ding Q, Lee YK, Schaefer EAK, Peters DT, Veres A, Kim K, Kuperwasser N, Motola DL, Meissner TB, Hendriks WT, Trevisan M, Gupta RM, Moisan A, Banks E, Friesen M, Schinzel RT, Xia F, Tang A, Xia Y, Figueroa E, Wann A, Ahfeldt T, Daheron L, Zhang F, Rubin LL, Peng LF, Chung RT, Musunuru K and Cowan CA (2013). A TALEN genome-editing system for generating human stem cell-based disease models. *Cell Stem Cell* **12**(2):238–251.

Dosil M, Giot L, Davis C and Konopka JB (1998). Dominant-Negative Mutations in the G-Protein-Coupled α-Factor Receptor Map to the Extracellular Ends of the Transmembrane Segments. *Molecular and Cellular Biology* **18**(10):5981.

Drake MT, Shenoy SK and Lefkowitz RJ (2006). Trafficking of G Protein–Coupled Receptors. *Circulation Research* **99**(6):570–582.

Ebert AD, Liang P and Wu JC (2012). Induced pluripotent stem cells as a disease modeling and drug screening platform. *Journal of Cardiovascular Pharmacology* 408–416.

Édes IF, Tóth A, Csányi G, Lomnicka M, Chłopicki S, Édes I and Papp Z (2008). Late-stage alterations in myofibrillar contractile function in a transgenic mouse model of dilated cardiomyopathy (Tgαq*44). *Journal of Molecular and Cellular Cardiology* **45**(3):363–372.

Edinger AL, Hoffman TL, Sharron M, Lee B, Yi Y, Choe W, Kolson DL, Mitrovic B, Zhou Y, Faulds D, Collman RG, Hesselgesser J, Horuk R and Doms RW (1998). An Orphan Seven-Transmembrane Domain Receptor Expressed Widely in the Brain Functions as a Coreceptor for Human Immunodeficiency Virus Type 1 and Simian Immunodeficiency Virus. *Journal of Virology* **72**(10):7934–7940.

Eichberg DG, Slepak TI, Pascoini AL, Komotar RJ and Ivan ME (2021). Genetic manipulation of adhesion GPCR CD97/ADGRE5 modulates invasion in patient-derived glioma stem cells. *Journal of Neuro-Oncology* **153**(3):383–391.

Eisner DA, Caldwell JL, Kistamás K and Trafford AW (2017). Calcium and Excitation-Contraction Coupling in the Heart. *Circulation Research* **121**(2):181–195.

Ellinor PT, Low AF and MacRae CA (2006). Reduced apelin levels in lone atrial fibrillation. *European Heart Journal* **27**:222–226.

Ervin E-H, Pook M, Teino I, Kasuk V, Trei A, Pooga M and Maimets T (2019). Targeted gene silencing in human embryonic stem cells using cell-penetrating peptide PepFect 14. *Stem Cell Research & Therapy 2019 10:1* **10**(1):1–14.

Evans MJ and Kaufman MH (1981). Establishment in culture of pluripotential cells from mouse embryos. *Nature* **292**:154–156.

Evans SM, Yelon D, Conlon FL and Kirby ML (2010). Myocardial lineage development. *Circulation Research* **107**(12):1428–1444.

Falcão-Pires I, Gonçalves N, Henriques-Coelho T, Moreira-Gonçalves D, Roncon-Albuquerque R and Leite-Moreira AF (2009). Apelin decreases myocardial injury and improves right ventricular function in monocrotaline-induced pulmonary hypertension. *American Journal of Physiology-Heart and Circulatory Physiology* **296**(6):H2007–H2014.

Fang H, Knezevic B, Burnham KL and Knight JC (2016). XGR software for enhanced interpretation of genomic summary data, illustrated by application to immunological traits. *Genome Medicine* **8**(1):1–20.

Farkasfalvi K, Stagg MA, Coppen SR, Siedlecka U, Lee J, Soppa GK, Marczin N, Szokodi I, Yacoub MH and Terracciano CMN (2007). Direct effects of apelin on cardiomyocyte contractility and electrophysiology. *Biochemical and Biophysical Research Communications* **357**(4):889–895.

Fassler R, Rohwedel J, Maltsev V, Bloch W, Lentini S, Guan K, Gullberg D, Hescheler J, Addicks K and Wobus AM (1996). Differentiation and integrity of cardiac muscle cells are impaired in the absence of beta 1 integrin. *Journal of Cell Science* **109**(13):2989–2999.

Feyen DAM, McKeithan WL, Bruyneel AAN, Spiering S, Hörmann L, Ulmer B, Zhang H, Briganti F, Schweizer M, Hegyi B, Liao Z, Pölönen RP, Ginsburg KS, Lam CK, Serrano R, Wahlquist C, Kreymerman A, Vu M, Amatya PL, Behrens CS, Ranjbarvaziri S, Maas RGC, Greenhaw M, Bernstein D, Wu JC, Bers DM, Eschenhagen T, Metallo CM and Mercola M (2020). Metabolic Maturation Media Improve Physiological Function of Human iPSC-Derived Cardiomyocytes. *Cell Reports* **32**(3):107925.

Flanagan SE, Patch AM and Ellard S (2010). Using SIFT and PolyPhen to predict loss-

of-function and gain-of-function mutations. *Genetic Testing and Molecular Biomarkers* **14**(4):533–537.

Földes G, Mioulane M, Wright JS, Liu AQ, Novak P, Merkely B, Gorelik J, Schneider MD, Ali NN and Harding SE (2011). Modulation of human embryonic stem cell-derived cardiomyocyte growth: A testbed for studying human cardiac hypertrophy? *Journal of Molecular and Cellular Cardiology* **50**:367–376.

Foord SM, Bonner TI, Neubig RR, Rosser EM, Pin JP, Davenport AP, Spedding M and Harmar AJ (2005). International Union of Pharmacology. XLVI. G protein-coupled receptor list. *Pharmacological Reviews* **57**(2):279–288.

Francia P, Salvati A, Balla C, De Paolis P, Pagannone E, Borro M, Gentile G, Simmaco M, De Biase L and Volpe M (2007). Cardiac resynchronization therapy increases plasma levels of the endogenous inotrope apelin. *European Journal of Heart Failure* **9**(3):306–309.

Franco R, Martínez-Pinilla E, Lanciego JL and Navarro G (2016). Basic Pharmacological and Structural Evidence for Class A G-Protein-Coupled Receptor Heteromerization. *Frontiers in Pharmacology* **7**:76.

Freyer L, Hsu C-W, Nowotschin S, Pauli A, Ishida J, Kuba K, Fukamizu A, Schier AF, Hoodless PA, Dickinson ME and Hadjantonakis A-K (2017). Loss of Apela Peptide in Mice Causes Low Penetrance Embryonic Lethality and Defects in Early Mesodermal Derivatives. *Cell Reports* **20**(9):2116–2130.

Gargalovic P, Wong P, Onorato J, Finlay H, Wang T, Yan M, Crain E, St-Onge S, Héroux M, Bouvier M, Xu C, Chen XQ, Generaux C, Lawrence M, Wexler R and Gordon D (2021). In Vitro and In Vivo Evaluation of a Small-Molecule APJ (Apelin Receptor) Agonist, BMS-986224, as a Potential Treatment for Heart Failure. *Circulation. Heart Failure* **14**(3):e007351.

Genescà L, Aubareda A, Fuentes J, Estivill X, De La Luna S and Pérez-Riba M (2003). Phosphorylation of calcipressin 1 increases its ability to inhibit calcineurin and decreases calcipressin half-life. *The Biochemical Journal* **374**:567–575.

Giacomotto J and Ségalat L (2010). High-throughput screening and small animal models, where are we? *British Journal of Pharmacology* **160**(2):204–216.

González F, Zhu Z, Shi ZD, Lelli K, Verma N, Li Q V. and Huangfu D (2014). An iCRISPR platform for rapid, multiplexable, and inducible genome editing in human pluripotent stem cells. *Cell Stem Cell* **15**(2):215–226.

Goodman O., Krupnick JG, Santini F, Gurevich V V., Penn RB, Gagnon AW, Keen JH and Benovic JL (1996). β-Arrestin acts as a clathrin adaptor in endocytosis of the β2-adrenergic receptor. *Nature* **383**:447–450.

Gräf S, Haimel M, Bleda M, Hadinnapola C, Southgate L, Li W, Hodgson J, Liu B, Salmon RM, Southwood M, Machado RD, Martin JM, Treacy CM, Yates K, Daugherty LC, Shamardina O, Whitehorn D, Holden S, Aldred M, Bogaard HJ, Church C, Coghlan G, Condliffe R, Corris PA, Danesino C, Eyries M, Gall H, Ghio S, Ghofrani H-A, Gibbs JSR, Girerd B, Houweling AC, Howard L, Humbert M, Kiely DG, Kovacs G, MacKenzie Ross R V., Moledina S, Montani D, Newnham M, Olschewski A, Olschewski H, Peacock AJ, Pepke-Zaba J, Prokopenko I, Rhodes CJ, Scelsi L, Seeger W, Soubrier F, Stein DF, Suntharalingam J, Swietlik EM, Toshner MR, van Heel DA, Vonk Noordegraaf A, Waisfisz Q, Wharton J, Wort SJ, Ouwehand WH, Soranzo N, Lawrie A, Upton PD, Wilkins MR, Trembath RC and Morrell NW (2018). Identification of rare sequence variation underlying heritable pulmonary arterial hypertension. *Nature Communications* **9**(1):1416.

Granata A, Serrano F, Bernard WG, McNamara M, Low L, Sastry P and Sinha S (2016). An iPSC-derived vascular model of Marfan syndrome identifies key mediators of smooth muscle cell death. *Nature Genetics* **49**(1):97–109.

Grant AO (2009). Cardiac ion channels. *Circulation: Arrhythmia and Electrophysiology* **2**(2):185–194.

Greenberg MJ, Daily NJ, Wang A, Conway MK and Wakatsuki T (2018). Genetic and Tissue Engineering Approaches to Modeling the Mechanics of Human Heart Failure for Drug Discovery. *Frontiers in Cardiovascular Medicine* **5**:120.

Guhr A, Kobold S, Seltmann S, Seiler Wulczyn AEM, Kurtz A and Löser P (2018). Stem Cell Reports Article Recent Trends in Research with Human Pluripotent Stem Cells: Impact of Research and Use of Cell Lines in Experimental Research and Clinical Trials. *Stem Cell Reports* **11**:485–496.

Gupta N, Susa K, Yoda Y, Bonventre J V., Valerius MT and Morizane R (2018). CRISPR/Cas9-based Targeted Genome Editing for the Development of Monogenic Diseases Models with Human Pluripotent Stem Cells. *Current Protocols in Stem Cell Biology* **45**(1):e50.

Habata Y, Fujii R, Hosoya M, Fukusumi S, Kawamata Y, Hinuma S, Kitada C, Nishizawa N, Murosaki S, Kurokawa T, Onda H, Tatemoto K and Fujino M (1999). Apelin, the natural ligand of the orphan receptor APJ, is abundantly secreted in the colostrum. *Biochimica et Biophysica Acta* **1452**(1):25–35.

Hanft LM, Emter CA and McDonald KS (2017). Cardiac myofibrillar contractile properties during the progression from hypertension to decompensated heart failure. *American Journal of Physiology - Heart and Circulatory Physiology* **313**:H103–H113.

Harding SD, Armstrong JF, Faccenda E, Southan C, Alexander SPH, Davenport AP, Pawson AJ, Spedding M, Davies JA and NC-IUPHAR (2021). The IUPHAR/BPS guide to PHARMACOLOGY in 2022: curating pharmacology for COVID-19, malaria and antibacterials. *Nucleic Acids Research*.

Harding SE, Ali NN, Brito-Martins M and Gorelik J (2007). The human embryonic stem cell-derived cardiomyocyte as a pharmacological model. *Pharmacology & Therapeutics* **113**(2):341–353.

Hashimoto Y, Ishida J, Yamamoto R, Fujiwara K, Asada S, Kasuya Y, Mochizuki N and Fukamizu A (2005). G protein-coupled APJ receptor signaling induces focal adhesion formation and cell motility. *International Journal of Molecular Medicine* **16**(5):787–792.

Hauser AS, Attwood MM, Rask-Andersen M, Schiöth HB and Gloriam DE (2017). Trends in GPCR drug discovery: New agents, targets and indications. *Nature Reviews Drug Discovery* **16**(12):829–842.

He J-Q, Ma Y, Lee Y, Thomson JA and Kamp TJ (2003). Human Embryonic Stem Cells Develop Into Multiple Types of Cardiac Myocytes - Action Potential Characterization Cellular Biology. *Circulation Research* **93**(1):32–39.

Herrick-Davis K, Grinde E, Cowan A and Mazurkiewicz JE (2013). Fluorescence Correlation Spectroscopy Analysis of Serotonin, Adrenergic, Muscarinic, and

Dopamine Receptor Dimerization: The Oligomer Number Puzzle. *Molecular Pharmacology* **84**(4):630.

Hershberger RE, Hedges DJ and Morales A (2013). Dilated cardiomyopathy: The complexity of a diverse genetic architecture. *Nature Reviews Cardiology* **10**(9):531–547.

Hinson JT, Chopra A, Nafissi N, Polacheck WJ, Benson CC, Swist S, Gorham J, Yang L, Schafer S, Sheng CC, Haghighi A, Homsy J, Hubner N, Church G, Cook SA, Linke WA, Chen CS, Seidman JG and Seidman CE (2015). Titin mutations in iPS cells define sarcomere insufficiency as a cause of dilated cardiomyopathy. *Science* **349**(6251):982–986.

Hnatiuk AP, Briganti F, Staudt DW and Mercola M (2021). Human iPSC modeling of heart disease for drug development. *Cell Chemical Biology* **28**(3):271–282.

Ho L, Van Dijk M, Chye STJ, Messerschmidt DM, Chng SC, Ong S, Yi LK, Boussata S, Goh GHY, Afink GB, Lim CY, Dunn NR, Solter D, Knowles BB and Reversade B (2017). ELABELA deficiency promotes preeclampsia and cardiovascular malformations in mice. *Science* **357**(6352):707–713.

Ho L, Tan SYX, Wee S, Wu Y, Tan SJC, Ramakrishna NB, Chng SC, Nama S, Szczerbinska I, Chan YS, Avery S, Tsuneyoshi N, Ng HH, Gunaratne J, Dunn NR and Reversade B (2015). ELABELA Is an Endogenous Growth Factor that Sustains hESC Self-Renewal via the PI3K/AKT Pathway. *Cell Stem Cell* **17**(4):435–447.

van den Hoff MJ., van den Eijnde SM, Virágh S and Moorman AF. (2000). Programmed cell death in the developing heart. *Cardiovascular Research* **45**(3):603–620.

Hong SW, Jiang Y, Kim S, Li CJ and Lee D (2014). Target Gene Abundance Contributes to the Efficiency of siRNA-Mediated Gene Silencing. *Nucleic Acid Therapeutics* **24**(3):192.

Hosoya M, Kawamata Y, Fukusumi S, Fujii R, Habata Y, Hinuma S, Kitada C, Honda S, Kurokawa T, Onda H, Nishimura O and Fujino M (2000). Molecular and functional characteristics of APJ. Tissue distribution of mRNA and interaction with the endogenous ligand apelin. *The Journal of Biological Chemistry* **275**(28):21061–7.

Hsu MN, Chang YH, Truong VA, Lai PL, Nguyen TKN and Hu YC (2019). CRISPR technologies for stem cell engineering and regenerative medicine. *Biotechnology Advances* **37**(8):107447.

Hu BY, Weick JP, Yu J, Ma LX, Zhang XQ, Thomson JA and Zhang SC (2010). Neural differentiation of human induced pluripotent stem cells follows developmental principles but with variable potency. *Proceedings of the National Academy of Sciences of the United States of America* **107**(9):4335–4340.

Huang J, Chen S, Zhang JJ and Huang XY (2013). Crystal structure of oligomeric β1-adrenergic G protein–coupled receptors in ligand-free basal state. *Nature Structural & Molecular Biology 2013 20:4* **20**(4):419–425.

Huang S, Chen L, Lu L and Li L (2016). The apelin–APJ axis: A novel potential therapeutic target for organ fibrosis. *Clinica Chimica Acta* **456**:81–88.

Hulme EC and Trevethick MA (2010). Ligand binding assays at equilibrium: validation and interpretation. *British Journal of Pharmacology* **161**(6):1219–37.

Huynh J, Thomas WG, Aguilar MI and Pattenden LK (2009). Role of helix 8 in G protein-coupled receptors based on structure-function studies on the type 1 angiotensin receptor. *Molecular and Cellular Endocrinology* 118–127.

Hwang HS, Kryshtal DO, Feaster TK, Sánchez-Freire V, Zhang J, Kamp TJ, Hong CC, Wu JC and Knollmann BC (2015). Comparable calcium handling of human iPSC-derived cardiomyocytes generated by multiple laboratories. *Journal of Molecular and Cellular Cardiology* **85**:79–88.

Ieda M, Tsuchihashi T, Ivey KN, Ross RS, Hong T-T, Shaw RM and Srivastava D (2009). Cardiac Fibroblasts Regulate Myocardial Proliferation through β1 Integrin Signaling. *Developmental cell* **16**(2):233.

Insel PA, Wilderman A, Zambon AC, Snead AN, Murray F, Aroonsakool N, McDonald DS, Zhou S, McCann T, Zhang L, Sriram K, Chinn AM, Michkov A V., Lynch RM, Overland AC and Corriden R (2015). G Protein–Coupled Receptor (GPCR) Expression in Native Cells: 'Novel' endoGPCRs as Physiologic Regulators and Therapeutic Targets. *Molecular Pharmacology* **88**(1):181.

Ishida J, Hashimoto T, Hashimoto Y, Nishiwaki S, Iguchi T, Harada S, Sugaya T, Matsuzaki H, Yamamoto R, Shiota N, Okunishi H, Kihara M, Umemura S, Sugiyama F, Yagami K-I, Kasuya Y, Mochizuki N and Fukamizu A (2004). Regulatory roles for APJ, a seven-transmembrane receptor related to angiotensin-type 1 receptor in blood pressure in vivo. *The Journal of Biological Chemistry* **279**(25):26274–9.

Itzhaki I, Rapoport S, Huber I, Mizrahi I, Zwi-Dantsis L, Arbel G, Schiller J and Gepstein L (2011). Calcium handling in human induced pluripotent stem cell derived cardiomyocytes. *PloS ONE* **6**(4):e18037.

Iwanaga Y, Kihara Y, Takenaka H and Kita T (2006). Down-regulation of cardiac apelin system in hypertrophied and failing hearts: Possible role of angiotensin II-angiotensin type 1 receptor system. *Journal of Molecular and Cellular Cardiology* **41**(5):798–806.

Japp AG, Cruden NL, Amer DAB, Li VKY, Goudie EB, Johnston NR, Sharma S, Neilson I, Webb DJ, Megson IL, Flapan AD and Newby DE (2008). Vascular Effects of Apelin In Vivo in Man. *Journal of the American College of Cardiology* **52**(11):908–913.

Japp AG, Cruden NL, Barnes G, van Gemeren N, Mathews J, Adamson J, Johnston NR, Denvir MA, Megson IL, Flapan AD and Newby DE (2010). Acute Cardiovascular Effects of Apelin in Humans: Potential Role in Patients With Chronic Heart Failure. *Circulation* **121**(16):1818–1827.

Japp AG and Newby DE (2008). The apelin–APJ system in heart failure: Pathophysiologic relevance and therapeutic potential. *Biochemical Pharmacology* **75**(10):1882–1892.

Jhoti H, Rees S and Solari R (2013). High-throughput screening and structure-based approaches to hit discovery: Is there a clear winner? *Expert Opinion on Drug Discovery* **8**(12):1449–1453.

Jia Y-X, Pan C-S, Zhang J, Geng B, Zhao J, Gerns H, Yang J, Chang J-K, Tang C-S and Qi Y-F (2006). Apelin protects myocardial injury induced by isoproterenol in rats. *Regulatory Peptides* **133**(1–3):147–154.

Jia ZQ, Hou L, Leger A, Wu I, Kudej AB, Stefano J, Jiang C, Pan CQ and Akita GY (2012). Cardiovascular effects of a PEGylated apelin. *Peptides* **38**(1):181–188.

Jiao H, Zhang Z, Ma Q, Fu W and Liu Z (2013). Mechanism underlying the inhibitory effect of Apelin-13 on glucose deprivation-induced autophagy in rat cardiomyocytes. *Experimental and Therapeutic Medicine* **5**(3):797–802.

Kaestner L, Scholz A, Tian Q, Ruppenthal S, Tabellion W, Wiesen K, Katus HA, Müller OJ, Kotlikoff MI and Lipp P (2014). Genetically encoded Ca2+ indicators in cardiac myocytes. *Circulation Research* 1623–1639.

Kallergis EM, Manios EG, Kanoupakis EM, Mavrakis HE, Goudis CA, Maliaraki NE, Saloustros IG, Milathianaki ME, Chlouverakis GI and Vardas PE (2010). Effect of Sinus Rhythm Restoration After Electrical Cardioversion on Apelin and Brain Natriuretic Peptide Prohormone Levels in Patients With Persistent Atrial Fibrillation. *American Journal of Cardiology* **105**(1):90–94.

Kamakura T, Makiyama T, Sasaki K, Yoshida Y, Wuriyanghai Y, Chen J, Hattori T, Ohno S, Kita T, Horie M, Yamanaka S and Kimura T (2013). Ultrastructural Maturation of Human-Induced Pluripotent Stem Cell-Derived Cardiomyocytes in a Long-Term Culture. *Circulation Journal* **77**(5):1307–1314.

Kang Y, Kim J, Anderson JP, Wu J, Gleim SR, Kundu RK, McLean DL, Kim J, Park H, Jin S, Hwa J, Quertermous T and Chun HJ (2013). Apelin-APJ signaling is a critical regulator of endothelial MEF2 activation in cardiovascular development. *Circulation Research* **113**(1):22–31.

Karabekian Z, Idrees S, Ding H, Jamshidi A, Posnack NG and Sarvazyan N (2015). Downregulation of beta-microglobulin to diminish T-lymphocyte lysis of non-syngeneic cell sources of engineered heart tissue constructs. *Biomedical Materials* **10**(3):034101.

Karakikes I, Senyei GD, Hansen J, Kong C-W, Azeloglu EU, Stillitano F, Lieu DK, Wang J, Ren L, Hulot J-S, Iyengar R, Li RA and Hajjar RJ (2014). Small Molecule-Mediated Directed Differentiation of Human Embryonic Stem Cells Toward Ventricular Cardiomyocytes. *Stem Cells Translational Medicine* **3**(1):18–31.

Karbassi E, Fenix A, Marchiano S, Muraoka N, Nakamura K, Yang X and Murry CE (2020). Cardiomyocyte maturation: advances in knowledge and implications for regenerative medicine. *Nature Reviews Cardiology* **17**(6):341.

Kasai RS, Ito S V., Awane RM, Fujiwara TK and Kusumi A (2018). The Class-A GPCR Dopamine D2 Receptor Forms Transient Dimers Stabilized by Agonists: Detection by Single-Molecule Tracking. *Cell Biochemistry and Biophysics* **76**(1):29.

Kattman SJ, Witty AD, Gagliardi M, Dubois NC, Niapour M, Hotta A, Ellis J and Keller G (2011). Stage-Specific Optimization of Activin/Nodal and BMP Signaling Promotes Cardiac Differentiation of Mouse and Human Pluripotent Stem Cell Lines. *Cell Stem Cell* **8**(2):228–240.

Katugampola SD, Maguire JJ, Matthewson SR and Davenport a P (2001). [(125)I]-(Pyr(1))Apelin-13 is a novel radioligand for localizing the APJ orphan receptor in human and rat tissues with evidence for a vasoconstrictor role in man. *British Journal of Pharmacology* **132**(6):1255–1260.

Kawamata Y, Habata Y, Fukusumi S, Hosoya M, Fujii R, Hinuma S, Nishizawa N, Kitada C, Onda H, Nishimura O and Fujino M (2001). Molecular properties of apelin: Tissue distribution and receptor binding. *Biochimica et Biophysica Acta- Molecular Cell Research* **1538**:162–171.

Kazemi-Bajestani SMR, Patel VB, Wang W and Oudit GY (2012). Targeting the ACE2 and Apelin Pathways Are Novel Therapies for Heart Failure: Opportunities and Challenges. *Cardiology Research and Practice* **2012**(1):823193.

Kehat I, Kenyagin-Karsenti D, Snir M, Segev H, Amit M, Gepstein A, Livne E, Binah O, Itskovitz-Eldor J and Gepstein L (2001). Human embryonic stem cells can differentiate into myocytes with structural and functional properties of cardiomyocytes. *The Journal of Clinical Investigation* **108**(3):407–14.

Kelly E, Bailey CP and Henderson G (2008). Agonist-selective mechanisms of GPCR desensitization. *British Journal of Pharmacology* **153**:S379-88.

Kelly OG, Chan MY, Martinson LA, Kadoya K, Ostertag TM, Ross KG, Richardson M, Carpenter MK, D'Amour KA, Kroon E, Moorman M, Baetge EE and Bang AG (2011). Cell-surface markers for the isolation of pancreatic cell types derived from human embryonic stem cells. *Nature Biotechnology* **29**(8):750–756.

Keselowsky BG and García AJ (2005). Quantitative methods for analysis of integrin binding and focal adhesion formation on biomaterial surfaces. *Biomaterials* **26**(4):413–

418.

Khalili AA and Ahmad MR (2015). A Review of Cell Adhesion Studies for Biomedical and Biological Applications. *International Journal of Molecular Sciences* **16**(8):18149.

Kidoya H, Ueno M, Yamada Y, Mochizuki N, Nakata M, Yano T, Fujii R and Takakura N (2008). Spatial and temporal role of the apelin/APJ system in the caliber size regulation of blood vessels during angiogenesis. *EMBO Journal* **27**(3):522–534.

Kim J, Kang Y, Kojima Y, Lighthouse JK, Hu X, Aldred MA, McLean DL, Park H, Comhair SA, Greif DM, Erzurum SC and Chun HJ (2013). An endothelial apelin-FGF link mediated by miR-424 and miR-503 is disrupted in pulmonary arterial hypertension. *Nature Medicine* **19**(1):74–82.

Kim TK and Eberwine JH (2010). Mammalian cell transfection: the present and the future. *Analytical and Bioanalytical Chemistry* **397**(8):3173–3178.

Kim YM, Lakin R, Zhang H, Liu J, Sachedina A, Singh M, Wilson E, Perez M, Verma S, Quertermous T, Olgin J, Backx PH and Ashley EA (2020). Apelin increases atrial conduction velocity, refractoriness, and prevents inducibility of atrial fibrillation. *JCI Insight* **5**(17):e126525.

Kishino Y, Fujita J, Tohyama S, Okada M, Tanosaki S, Someya S and Fukuda K (2020). Toward the realization of cardiac regenerative medicine using pluripotent stem cells. *Inflammation and Regeneration* **40**(1):1.

Kleinz MJ and Davenport AP (2004). Immunocytochemical localization of the endogenous vasoactive peptide apelin to human vascular and endocardial endothelial cells. *Regulatory Peptides* **118**(3):119–125.

Kleinz MJ, Skepper JN and Davenport AP (2005). Immunocytochemical localisation of the apelin receptor, APJ, to human cardiomyocytes, vascular smooth muscle and endothelial cells. *Regulatory Peptides* **126**(3):233–240.

Koblan LW, Doman JL, Wilson C, Levy JM, Tay T, Newby GA, Maianti JP, Raguram A and Liu DR (2018). Improving cytidine and adenine base editors by expression optimization and ancestral reconstruction. *Nature Biotechnology* **36**(9):843–848.

Koblan LW, Erdos MR, Wilson C, Cabral WA, Levy JM, Xiong ZM, Tavarez UL,

Davison LM, Gete YG, Mao X, Newby GA, Doherty SP, Narisu N, Sheng Q, Krilow C, Lin CY, Gordon LB, Cao K, Collins FS, Brown JD and Liu DR (2021). In vivo base editing rescues Hutchinson–Gilford progeria syndrome in mice. *Nature* **589**:608–614.

Kodama M, Furutani K, Kimura R, Ando T, Sakamoto K, Nagamori S, Ashihara T, Kurachi Y, Sekino Y, Furukawa T, Kanda Y and Kurokawa J (2019). Systematic expression analysis of genes related to generation of action potentials in human iPS cell-derived cardiomyocytes. *Journal of Pharmacological Sciences* **140**(4):325–330.

Koguchi W, Kobayashi N, Takeshima H, Ishikawa M, Sugiyama F and Ishimitsu T (2012). Cardioprotective Effect of Apelin-13 on Cardiac Performance and Remodeling in End-Stage Heart Failure. *Circulation Journal* **76**(1):137–144.

Komor AC, Kim YB, Packer MS, Zuris JA and Liu DR (2016). Programmable editing of a target base in genomic DNA without double-stranded DNA cleavage. *Nature* **533**:420–424.

Kooistra AJ, Mordalski S, Pándy-Szekeres G, Esguerra M, Mamyrbekov A, Munk C, Keserű GM and Gloriam DE (2021). GPCRdb in 2021: integrating GPCR sequence, structure and function. *Nucleic Acids Research* **49**(D1):D335–D343.

Koplan BA and Stevenson WG (2007). Sudden arrhythmic death syndrome. *Heart* **93**(5):547.

Kopljar I, Lu HR, Van Ammel K, Otava M, Tekle F, Teisman A and Gallacher DJ (2018). Development of a Human iPSC Cardiomyocyte-Based Scoring System for Cardiac Hazard Identification in Early Drug Safety De-risking. *Stem Cell Reports* **11**(6):1365–1377.

Kosicki M, Tomberg K and Bradley A (2018). Repair of double-strand breaks induced by CRISPR–Cas9 leads to large deletions and complex rearrangements. *Nature Biotechnology* **36**(8):765–771.

Kraushaar U, Meyer T, Hess D, Gepstein L, L Mummery C, R Braam S and Guenther E (2012). Cardiac safety pharmacology: From human ether-a-gogo related gene channel block towards induced pluripotent stem cell based disease models. *Expert Opinion on Drug Safety* **11**(2):285–298.

Kuba K, Zhang L, Imai Y, Arab S, Chen M, Maekawa Y, Leschnik M, Leibbrandt A, Markovic M, Makovic M, Schwaighofer J, Beetz N, Musialek R, Neely GG, Komnenovic V, Kolm U, Metzler B, Ricci R, Hara H, Meixner A, Nghiem M, Chen X, Dawood F, Wong KM, Sarao R, Cukerman E, Kimura A, Hein L, Thalhammer J, Liu PP and Penninger JM (2007). Impaired heart contractility in Apelin gene-deficient mice associated with aging and pressure overload. *Circulation Research* **101**(4):e32-42.

Kumagai H, Ikeda Y, Motozawa Y, Fujishiro M, Okamura T, Fujio K, Okazaki H, Nomura S, Takeda N, Harada M, Toko H, Takimoto E, Akazawa H, Morita H, Suzuki JI, Yamazaki T, Yamamoto K, Komuro I and Yanagisawa M (2015). Quantitative measurement of GPCR endocytosis via pulse-chase covalent labeling. *PLoS ONE* **10**(5):e0129394.

Lacolley P, Regnault V, Nicoletti A, Li Z and Michel JB (2012). The vascular smooth muscle cell in arterial pathology: a cell that can take on multiple roles. *Cardiovascular Research* **95**(2):194–204.

Lagerström MC and Schiöth HB (2008). Structural diversity of g proteincoupled receptors and significance for drug discovery. *Nature Reviews Drug Discovery* **7**(4):339–357.

Lam CK, Tian L, Belbachir N, Wnorowski A, Shrestha R, Ma N, Kitani T, Rhee J-W and Wu JC (2019). Identifying the Transcriptome Signatures of Calcium Channel Blockers in Human Induced Pluripotent Stem Cell-Derived Cardiomyocytes. *Circulation Research* **125**(2):212–222.

Lam JKW, Chow MYT, Zhang Y and Leung SWS (2015). siRNA Versus miRNA as Therapeutics for Gene Silencing. *Molecular Therapy - Nucleic Acids* **4**(9):e252.

Lee CS, Cho HJ, Lee JW, Son HJ, Chai J and Kim HS (2021). Adhesion GPCR Latrophilin-2 Specifies Cardiac Lineage Commitment through CDK5, Src, and P38MAPK. *Stem Cell Reports* **16**(4):868–882.

Lee DK, Cheng R, Nguyen T, Fan T, Kariyawasam AP, Liu Y, Osmond DH, George SR and O'Dowd BF (2001). Characterization of Apelin, the Ligand for the APJ Receptor. *Journal of Neurochemistry* **74**(1):34–41.

Lee J, Termglinchan V, Diecke S, Itzhaki I, Lam CK, Garg P, Lau E, Greenhaw M,

Seeger T, Wu H, Zhang JZ, Chen X, Gil IP, Ameen M, Sallam K, Rhee JW, Churko JM, Chaudhary R, Chour T, Wang PJ, Snyder MP, Chang HY, Karakikes I and Wu JC (2019). Activation of PDGF pathway links LMNA mutation to dilated cardiomyopathy. *Nature* **572**:335–340.

Lemoine MD, Mannhardt I, Breckwoldt K, Prondzynski M, Flenner F, Ulmer B, Hirt MN, Neuber C, Horváth A, Kloth B, Reichenspurner H, Willems S, Hansen A, Eschenhagen T and Christ T (2017). Human iPSC-derived cardiomyocytes cultured in 3D engineered heart tissue show physiological upstroke velocity and sodium current density. *Scientific Reports* **7**(1):1–11.

Leonard A, Bertero A, Powers JD, Beussman KM, Bhandari S, Regnier M, Murry CE and Sniadecki NJ (2018). Afterload promotes maturation of human induced pluripotent stem cell derived cardiomyocytes in engineered heart tissues. *Journal of Molecular and Cellular Cardiology* **118**:147–158.

Li C, Ding L, Sun CW, Wu LC, Zhou D, Pawlik KM, Khodadadi-Jamayran A, Westin E, Goldman FD and Townes TM (2016). Novel HDAd/EBV Reprogramming Vector and Highly Efficient Ad/CRISPR-Cas Sickle Cell Disease Gene Correction. *Scientific Reports* **6**(1):1–10.

Li HL, Fujimoto N, Sasakawa N, Shirai S, Ohkame T, Sakuma T, Tanaka M, Amano N, Watanabe A, Sakurai H, Yamamoto T, Yamanaka S and Hotta A (2015). Precise correction of the dystrophin gene in duchenne muscular dystrophy patient induced pluripotent stem cells by TALEN and CRISPR-Cas9. *Stem Cell Reports* **4**(1):143–54.

Li J, Patel V V. and Radice GL (2006). Dysregulation of Cell Adhesion Proteins and Cardiac Arrhythmogenesis. *Clinical Medicine & Research* **4**(1):42–52.

Li L, Dong M and Wang X-G (2016). The Implication and Significance of Beta 2 Microglobulin: A Conservative Multifunctional Regulator. *Chinese Medical Journal* **129**(4):448–455.

Li M, Gou H, Tripathi BK, Huang J, Jiang S, Dubois W, Waybright T, Lei M, Shi J, Zhou M and Huang J (2015). An Apela RNA-Containing Negative Feedback Loop Regulates p53-Mediated Apoptosis in Embryonic Stem Cells. *Cell Stem Cell* **16**(6):669–683.

Lian X, Zhang J, Azarin SM, Zhu K, Hazeltine LB, Bao X, Hsiao C, Kamp TJ and

Palecek SP (2013). Directed cardiomyocyte differentiation from human pluripotent stem cells by modulating Wnt/β-catenin signaling under fully defined conditions. *Nature Protocols* **8**(1):162–175.

Liang P, Lan F, Lee AS, Gong T, Sanchez-Freire V, Wang Y, Diecke S, Sallam K, Knowles JW, Wang PJ, Nguyen PK, Bers DM, Robbins RC and Wu JC (2013). Drug screening using a library of human induced pluripotent stem cell-derived cardiomyocytes reveals disease-specific patterns of cardiotoxicity. *Circulation* **127**(16):1677–91.

Liao BY and Zhang J (2008). Null mutations in human and mouse orthologs frequently result in different phenotypes. *Proceedings of the National Academy of Sciences of the United States of America* **105**(19):6987–6992.

Libby P (2015). Murine 'model' monotheism: an iconoclast at the altar of mouse. *Circulation Research* **117**(11):921–5.

Liu G, Han J, Profirovic J, Strekalova E and Voyno-Yasenetskaya TA (2009). Gα13 regulates MEF2-dependent gene transcription in endothelial cells: Role in angiogenesis. *Angiogenesis* **12**(1):1–15.

Liu L and Shi GP (2012). CD31: beyond a marker for endothelial cells. *Cardiovascular Research* **94**(1):3–5.

Liu T, Song D, Dong J, Zhu P, Liu J, Liu W, Ma X, Zhao L and Ling S (2017). Current understanding of the pathophysiology of myocardial fibrosis and its quantitative assessment in heart failure. *Frontiers in Physiology* **8**:238.

Lodish H, Berk A, Zipursky S, Matsudaira P, Baltimore D and Darnell J (2000). *Processing of rRNA and tRNA*. *Molecular Biology*. W.H. Freeman, New York.

Love MI, Huber W and Anders S (2014). Moderated estimation of fold change and dispersion for RNA-seq data with DESeq2. *Genome Biology* **15**(12):550.

Lu Y, Zhu X, Liang G-X, Cui R-R, Liu Y, Wu S-S, Liang Q-H, Liu G-Y, Jiang Y, Liao X-B, Xie H, Zhou H-D, Wu X-P, Yuan L-Q and Liao E-Y (2012). Apelin–APJ induces ICAM-1, VCAM-1 and MCP-1 expression via NF-κB/JNK signal pathway in human umbilical vein endothelial cells. *Amino Acids 2012 43:5* **43**(5):2125–2136.

Lundstrom K (2009). An overview on GPCRs and drug discovery: structure-based drug design and structural biology on GPCRs. *Methods in Molecular Biology* **552**:51–66.

Ma X, Chen X, Jin Y, Ge W, Wang W, Kong L, Ji J, Guo X, Huang J, Feng XH, Fu J and Zhu S (2018). Small molecules promote CRISPR-Cpf1-mediated genome editing in human pluripotent stem cells. *Nature Communications* **9**(1):1–7.

Maarman G, Lecour S, Butrous G, Thienemann F and Sliwa K (2013). A comprehensive review: the evolution of animal models in pulmonary hypertension research; are we there yet? *Pulmonary Circulation* **3**(4):739–56.

Maguire JJ, Kleinz MJ, Pitkin SL and Davenport AP (2009). [Pyr1]apelin-13 identified as the predominant apelin isoform in the human heart: vasoactive mechanisms and inotropic action in disease. *Hypertension* **54**(3):598–604.

Maguire JJ, Kuc RE and Davenport AP (2012). *Radioligand Binding Assays and Their Analysis*. *Receptor Binding Techniques. Methods in Molecular Biology*. Humana Press, Totowa, NJ.

Malandraki-Miller S, Lopez CA, Al-Siddiqi H and Carr CA (2018). Changing Metabolism in Differentiating Cardiac Progenitor Cells—Can Stem Cells Become Metabolically Flexible Cardiomyocytes? *Frontiers in Cardiovascular Medicine* **5**:119.

Maqsood MI, Matin MM, Bahrami AR and Ghasroldasht MM (2013). Immortality of cell lines: challenges and advantages of establishment. *Cell Biology International* **37**(10):1038–1045.

Marsault E, Llorens-Cortes C, Iturrioz X, Chun HJ, Lesur O, Oudit GY and Auger-Messier M (2019). The apelinergic system: a perspective on challenges and opportunities in cardiovascular and metabolic disorders. *Annals of the New York Academy of Sciences* **1455**(1):12–33.

Matin MM, Walsh JR, Gokhale PJ, Draper JS, Bahrami AR, Morton I, Moore HD and Andrews PW (2004). Specific Knockdown of Oct4 and β2-microglobulin Expression by RNA Interference in Human Embryonic Stem Cells and Embryonic Carcinoma Cells. *Stem Cells* **22**(5):659–668.

Matsa E, Burridge PW, Yu K-H, Ahrens JH, Termglinchan V, Wu H, Liu C, Shukla P, Sayed N, Churko JM, Shao N, Woo NA, Chao AS, Gold JD, Karakikes I, Snyder MP and Wu JC (2016). Transcriptome Profiling of Patient-Specific Human iPSC-Cardiomyocytes Predicts Individual Drug Safety and Efficacy Responses In Vitro. *Cell Stem Cell* **19**(3):311–25.

Matsumoto M, Hidaka K, Akiho H, Tada S, Okada M and Yamaguchi T (1996). Low stringency hybridization study of the dopamine D4 receptor revealed D4-like mRNA distribution of the orphan seven-transmembrane receptor, APJ, in human brain. *Neuroscience Letters* **219**(2):119–122.

McDonald KS, Hanft LM, Robinett JC, Guglin M and Campbell KS (2020). Regulation of Myofilament Contractile Function in Human Donor and Failing Hearts. *Frontiers in Physiology* **11**:468.

McKeithan WL, Feyen DAM, Bruyneel AAN, Okolotowicz KJ, Ryan DA, Sampson KJ, Potet F, Savchenko A, Gómez-Galeno J, Vu M, Serrano R, George AL, Kass RS, Cashman JR and Mercola M (2020). Reengineering an Antiarrhythmic Drug Using Patient hiPSC Cardiomyocytes to Improve Therapeutic Potential and Reduce Toxicity. *Cell Stem Cell* **27**(5):813–821.

McKinnie SMK, Wang W, Fischer C, McDonald T, Kalin KR, Iturrioz X, Llorens-Cortes C, Oudit GY and Vederas JC (2017). Synthetic Modification within the ‘rPRL’ Region of Apelin Peptides: Impact on Cardiovascular Activity and Stability to Neprilysin and Plasma Degradation. *Journal of Medicinal Chemistry* **60**(14):6408–6427.

McPherson GA (1985). Analysis of radioligand binding experiments: A collection of computer programs for the IBM PC. *Journal of Pharmacological Methods* **14**(3):213–228.

Medhurst AD, Jennings CA, Robbins MJ, Davis RP, Ellis C, Winborn KY, Lawrie KWM, Hervieu G, Riley G, Bolaky JE, Herrity NC, Murdock P and Darker JG (2003). Pharmacological and immunohistochemical characterization of the APJ receptor and its endogenous ligand apelin. *Journal of Neurochemistry* **84**(5):1162–1172.

van Meer BJ, Krotenberg A, Sala L, Davis RP, Eschenhagen T, Denning C, Tertoolen LGJ and Mummery CL (2019). Simultaneous measurement of excitation-contraction

coupling parameters identifies mechanisms underlying contractile responses of hiPSC-derived cardiomyocytes. *Nature Communications* **10**(1):1–9.

van Meer BJ, Tertoolen LGJ and Mummery CL (2016). Concise Review: Measuring Physiological Responses of Human Pluripotent Stem Cell Derived Cardiomyocytes to Drugs and Disease. *STEM CELLS* **34**(8):2008–2015.

Mendjan S, Mascetti VL, Ortmann D, Ortiz M, Karjosukarso DW, Ng Y, Moreau T and Pedersen RA (2014). NANOG and CDX2 Pattern Distinct Subtypes of Human Mesoderm during Exit from Pluripotency. *Cell Stem Cell* **15**(3):310–325.

Mercola M, Colas A and Willems E (2013). Induced pluripotent stem cells in cardiovascular drug discovery. *Circulation Research* **112**(3):534–548.

Mills RJ, Titmarsh DM, Koenig X, Parker BL, Ryall JG, Quaife-Ryan GA, Voges HK, Hodson MP, Ferguson C, Drowley L, Plowright AT, Needham EJ, Wang Q-D, Gregorevic P, Xin M, Thomas WG, Parton RG, Nielsen LK, Launikonis BS, James DE, Elliott DA, Porrello ER and Hudson JE (2017). Functional screening in human cardiac organoids reveals a metabolic mechanism for cardiomyocyte cell cycle arrest. *Proceedings of the National Academy of Sciences of the United States of America* **114**(40):E8372–E8381.

Min J-Y, Yang Y, Sullivan MF, Ke Q, Converso KL, Chen Y, Morgan JP and Xiao Y-F (2003). Long-term improvement of cardiac function in rats after infarction by transplantation of embryonic stem cells. *The Journal of Thoracic and Cardiovascular Surgery* **125**(2):361–369.

Molenaar P, O'Reilly G, Sharkey A, Kuc RE, Harding DP, Plumpton C, Gresham GA and Davenport AP (1993). Characterization and localization of endothelin receptor subtypes in the human atrioventricular conducting system and myocardium. *Circulation Research* **72**(3):526–538.

Molla KA and Yang Y (2019). CRISPR/Cas-Mediated Base Editing: Technical Considerations and Practical Applications. *Trends in Biotechnology* **37**(10):1121–1142.

Moradi S, Mahdizadeh H, Šarić T, Kim J, Harati J, Shahsavarani H, Greber B and Moore JB (2019). Research and therapy with induced pluripotent stem cells (iPSCs):

Social, legal, and ethical considerations. *Stem Cell Research and Therapy* **10**:341.

Morrell NW, Adnot S, Archer SL, Dupuis J, Jones PL, MacLean MR, McMurtry IF, Stenmark KR, Thistlethwaite PA, Weissmann N, Yuan JX-J and Weir EK (2009). Cellular and Molecular Basis of Pulmonary Arterial Hypertension. *Journal of the American College of Cardiology* **54**(1):S20–S31.

Mosqueira D, Mannhardt I, Bhagwan JR, Lis-Slimak K, Katili P, Scott E, Hassan M, Prondzynski M, Harmer SC, Tinker A, Smith JGW, Carrier L, Williams PM, Gaffney D, Eschenhagen T, Hansen A and Denning C (2018). CRISPR/Cas9 editing in human pluripotent stem cell-cardiomyocytes highlights arrhythmias, hypocontractility, and energy depletion as potential therapeutic targets for hypertrophic cardiomyopathy. *European Heart Journal* **39**(43):3879–3892.

Mummery CL, Ward D, van den Brink CE, Bird SD, Doevendans PA, Opthof T, Brutel de la Riviere A, Tertoolen L, van der Heyden M and Pera M (2002). Cardiomyocyte differentiation of mouse and human embryonic stem cells. *Journal of Anatomy* **200**:233–42.

Mummery CL, Zhang J, Ng ES, Elliott DA, Elefanty AG and Kamp TJ (2012). Differentiation of human embryonic stem cells and induced pluripotent stem cells to cardiomyocytes: A methods overview. *Circulation Research* **111**(3):344–358.

Murata K, Ishida J, Ishimaru T, Mizukami H, Hamada J, Saito C and Fukamizu A (2016). Lactation Is a Risk Factor of Postpartum Heart Failure in Mice with Cardiomyocyte-specific Apelin Receptor (APJ) Overexpression. *The Journal of Biological Chemistry* **291**(21):11241–11251.

Murza A, Sainsily X, Coquerel D, Côté J, Marx P, Besserer-Offroy É, Longpré J-M, Lainé J, Reversade B, Salvail D, Leduc R, Dumaine R, Lesur O, Auger-Messier M, Sarret P and Marsault É (2016). Discovery and Structure–Activity Relationship of a Bioactive Fragment of ELABELA that Modulates Vascular and Cardiac Functions. *Journal of Medicinal Chemistry* **59**(7):2962–2972.

Nag S, Trivedi D V, Sarkar SS, Adhikari AS, Sunitha MS, Sutton S, Ruppel KM and Spudich JA (2017). The myosin mesa and the basis of hypercontractility caused by hypertrophic cardiomyopathy mutations. *Nature Structural & Molecular Biology*

24(6):525–533.

Narayanan S, Maitra R, Deschamps JR, Bortoff K, Thomas JB, Zhang Y, Warner K, Vasukuttan V, Decker A and Runyon SP (2016). Discovery of a Novel Small Molecule Agonist Scaffold for the APJ Receptor. *Bioorganic & Medicinal Chemistry* **24**(16):3758.

Noorman M, van der Heyden MAG, van Veen TAB, Cox MGPJ, Hauer RNW, de Bakker JMT and van Rijen HVM (2009). Cardiac cell–cell junctions in health and disease: Electrical versus mechanical coupling. *Journal of Molecular and Cellular Cardiology* **47**(1):23–31.

Nostro MC, Sarangi F, Ogawa S, Holtzinger A, Corneo B, Li X, Micallef SJ, Park IH, Basford C, Wheeler MB, Daley GQ, Elefanty AG, Stanley EG and Keller G (2011). Stage-specific signaling through TGFβ family members and WNT regulates patterning and pancreatic specification of human pluripotent stem cells. *Development* **138**(5):861–871.

O'Dowd BF, Heiber M, Chan A, Heng HHQ, Tsui L-C, Kennedy JL, Shi X, Petronis A, George SR and Nguyen T (1993). A human gene that shows identity with the gene encoding the angiotensin receptor is located on chromosome 11. *Gene* **136**:355–360.

Oldham WM and Hamm HE (2008). Heterotrimeric G protein activation by G-protein-coupled receptors. *Nature Reviews Molecular Cell Biology* **9**(1):60–71.

Onakpoya IJ, Heneghan CJ and Aronson JK (2016). Post-marketing withdrawal of 462 medicinal products because of adverse drug reactions: a systematic review of the world literature. *BMC Medicine* **14**(1):10.

Osafune K, Caron L, Borowiak M, Martinez RJ, Fitz-Gerald CS, Sato Y, Cowan CA, Chien KR and Melton DA (2008). Marked differences in differentiation propensity among human embryonic stem cell lines. *Nature Biotechnology* **26**(3):313–315.

Paik DT, Chandy M and Wu JC (2020). Patient and disease–specific induced pluripotent stem cells for discovery of personalized cardiovascular drugs and therapeutics. *Pharmacological Reviews* **72**(1):320–342.

Pang H, Han B, Yu T and Zong Z (2014). Effect of apelin on the cardiac hemodynamics in hypertensive rats with heart failure. *International Journal of Molecular Medicine*

34(3):756–764.

Papapetrou EP and Schambach A (2016). Gene insertion into genomic safe harbors for human gene therapy. *Molecular Therapy* **24**(4):678–684.

Paquet D, Kwart D, Chen A, Sproul A, Jacob S, Teo S, Olsen KM, Gregg A, Noggle S and Tessier-Lavigne M (2016). Efficient introduction of specific homozygous and heterozygous mutations using CRISPR/Cas9. *Nature* **533**:125–129.

Parikh VN, Liu J, Shang C, Woods C, Chang AC, Zhao M, Charo DN, Grunwald Z, Huang Y, Seo K, Tsao PS, Bernstein D, Ruiz-Lozano P, Quertermous T and Ashley EA (2018). Integrative Cardiovascular Physiology and Pathophysiology: Apelin and APJ orchestrate complex tissue-specific control of cardiomyocyte hypertrophy and contractility in the hypertrophy-heart failure transition. *American Journal of Physiology - Heart and Circulatory Physiology* **315**(2):H348.

Parrotta EI, Lucchino V, Scaramuzzino L, Scalise S and Cuda G (2020). Modeling Cardiac Disease Mechanisms Using Induced Pluripotent Stem Cell-Derived Cardiomyocytes: Progress, Promises and Challenges. *International Journal of Molecular Sciences* **21**(12):1–30.

Pauli A, Norris ML, Valen E, Chew GL, Gagnon JA, Zimmerman S, Mitchell A, Ma J, Dubrulle J, Reyon D, Tsai SQ, Joung JK, Saghatelian A and Schier AF (2014). Toddler: An embryonic signal that promotes cell movement via apelin receptors. *Science* **343**:1248636.

Pchejetski D, Foussal C, Alfarano C, Lairez O, Calise D, Guilbeau-Frugier C, Schaak S, Seguelas M-H, Wanecq E, Valet P, Parini A and Kunduzova O (2012). Apelin prevents cardiac fibroblast activation and collagen production through inhibition of sphingosine kinase 1. *European Heart Journal* **33**(18):2360–2369.

Penela P, Murga C, Ribas C, Tutor AS, Peregrín S and Mayor F (2006). Mechanisms of regulation of G protein-coupled receptor kinases (GRKs) and cardiovascular disease. *Cardiovascular Research* **69**(1):46–56.

Peng X, Wu X, Druso JE, Wei H, Park AY-J, Kraus MS, Alcaraz A, Chen J, Chien S, Cerione RA and Guan J-L (2008). Cardiac developmental defects and eccentric right ventricular hypertrophy in cardiomyocyte focal adhesion kinase (FAK) conditional

knockout mice. *Proceedings of the National Academy of Sciences* **105**(18):6638–6643.

Perjés Á, Kilpiö T, Ulvila J, Magga J, Alakoski T, Szabó Z, Vainio L, Halmetoja E, Vuolteenaho O, Petäjä-Repo U, Szokodi I and Kerkelä R (2016). Characterization of apela, a novel endogenous ligand of apelin receptor, in the adult heart. *Basic Research in Cardiology* **111**:2.

Perjés Á, Skoumal R, Tenhunen O, Kónyi A, Simon M, Horváth IG, Kerkelä R, Ruskoaho H and Szokodi I (2014). Apelin Increases Cardiac Contractility via Protein Kinase Cε- and Extracellular Signal-Regulated Kinase-Dependent Mechanisms. *PLoS ONE* **9**(4).

Phan J-A, Landau AM, Jakobsen S, Wong DF and Gjedde A (2017). Radioligand binding analysis of α2 adrenoceptors with [11C]yohimbine in brain in vivo: Extended Inhibition Plot correction for plasma protein binding. *Scientific Reports* **7**(1):1–17.

Piccini I, Rao J, Seebohm G and Greber B (2015). Human pluripotent stem cell-derived cardiomyocytes: Genome-wide expression profiling of long-term in vitro maturation in comparison to human heart tissue. *Genomics Data* **4**:69.

Pierre A Saint and Génin E (2014). How important are rare variants in common disease? *Briefings in Functional Genomics* **13**(5):353–361.

Pinho S and Frenette PS (2019). Haematopoietic stem cell activity and interactions with the niche. *Nature Reviews Molecular Cell Biology* **20**(5):303–320.

Pitkin SL, Maguire JJ, Bonner TI and Davenport AP (2010). International Union of Basic and Clinical Pharmacology. LXXIV. Apelin receptor nomenclature, distribution, pharmacology, and function. *Pharmacological Reviews* **62**(3):331–42.

Pointon A, Harmer AR, Dale IL, Abi-Gerges N, Bowes J, Pollard C and Garside H (2015). Assessment of Cardiomyocyte Contraction in Human-Induced Pluripotent Stem Cell-Derived Cardiomyocytes. *Toxicological Sciences* **144**(2):227–237.

Priest BT and McDermott JS (2015). Cardiac ion channels. *Channels* **9**(6):352–359.

Qi T, Wu F, Xie Y, Gao S, Li M, Pu J, Li D, Lan F and Wang Y (2020). Base Editing Mediated Generation of Point Mutations Into Human Pluripotent Stem Cells for

Modeling Disease. *Frontiers in Cell and Developmental Biology* **8**:590581.

Raman S V., Moreo A, Ambrosio G, Chiara B De, Pu M, Tran T and Mauri F (2009). Influence of myocardial fibrosis on left ventricular diastolic function noninvasive assessment by cardiac magnetic resonance and echo. *Circulation: Cardiovascular Imaging* **2**(6):437–443.

Ramirez-Correa GA, Cortassa S, Stanley B, Gao WD and Murphy AM (2010). Calcium Sensitivity, Force Frequency Relationship and Cardiac Troponin I: Critical Role of PKA and PKC Phosphorylation Sites. *Journal of Molecular and Cellular Cardiology* **48**(5):943.

Rao DD, Vorhies JS, Senzer N and Nemunaitis J (2009). siRNA vs. shRNA: Similarities and differences. *Advanced Drug Delivery Reviews* **61**(9):746–759.

Rask-Andersen M, Masuram S and Schiöth HB (2014). The Druggable Genome: Evaluation of Drug Targets in Clinical Trials Suggests Major Shifts in Molecular Class and Indication. *Annual Review of Pharmacology and Toxicology* **54**(1):9–26.

Read C, Fitzpatrick CM, Yang P, Kuc RE, Maguire JJ, Glen RC, Foster RE and Davenport AP (2016). Cardiac action of the first G protein biased small molecule apelin agonist. *Biochemical Pharmacology* **116**:63–72.

Read C, Nyimanu D, Williams TL, Huggins DJ, Sulentic P, Macrae RGC, Yang P, Glen RC, Maguire JJ and Davenport AP (2019). International Union of Basic and Clinical Pharmacology. CVII. Structure and Pharmacology of the Apelin Receptor with a Recommendation that Elabela/Toddler Is a Second Endogenous Peptide Ligand. *Pharmacological Reviews* **71**(4):467–502.

Read C, Nyimanu D, Yang P, Kuc RE, Williams TL, Fitzpatrick CM, Foster R, Glen RC, Maguire JJ and Davenport AP (2020). The G Protein Biased Small Molecule Apelin Agonist CMF-019 is Disease Modifying in Endothelial Cell Apoptosis In Vitro and Induces Vasodilatation Without Desensitisation In Vivo. *Frontiers in Pharmacology* **11**:588669.

Rees HA and Liu DR (2018). Base editing: precision chemistry on the genome and transcriptome of living cells. *Nature Reviews Genetics* **19**(12):770.

Relling M V. and Evans WE (2015). Pharmacogenomics in the clinic. *Nature* **526**:343–350.

Ren Y, Lee MY, Schliffke S, Paavola J, Amos PJ, Ge X, Ye M, Zhu S, Senyei G, Lum L, Ehrlich BE and Qyang Y (2011). Small molecule Wnt inhibitors enhance the efficiency of BMP-4-directed cardiac differentiation of human pluripotent stem cells. *Journal of Molecular and Cellular Cardiology* **51**(3):280–7.

Reppel M, Boettinger C and Hescheler J (2004). Beta-adrenergic and Muscarinic Modulation of Human Embryonic Stem Cell-derived Cardio-myocytes. *Cellular Physiology and Biochemistry* **14**(4–6):187–196.

Reppel M, Pillekamp F, Brockmeier K, Matzkies M, Bekcioglu A, Lipke T, Nguemo F, Bonnemeier H and Hescheler J (2005). The electrocardiogram of human embryonic stem cell-derived cardiomyocytes. *Journal of Electrocardiology* **38**(4):166–170.

Ribas C, Penela P, Murga C, Salcedo A, García-Hoz C, Jurado-Pueyo M, Aymerich I and Mayor F (2007). The G protein-coupled receptor kinase (GRK) interactome: Role of GRKs in GPCR regulation and signaling. *Biochimica et Biophysica Acta (BBA) - Biomembranes* **1768**(4):913–922.

Riehle C and Bauersachs J (2019). Small animal models of heart failure. *Cardiovascular Research* **115**:1838–1849.

Romagnuolo R, Masoudpour H, Porta-Sánchez A, Qiang B, Barry J, Laskary A, Qi X, Massé S, Magtibay K, Kawajiri H, Wu J, Valdman Sadikov T, Rothberg J, Panchalingam KM, Titus E, Li RK, Zandstra PW, Wright GA, Nanthakumar K, Ghugre NR, Keller G and Laflamme MA (2019). Human Embryonic Stem Cell-Derived Cardiomyocytes Regenerate the Infarcted Pig Heart but Induce Ventricular Tachyarrhythmias. *Stem Cell Reports* **12**(5):967–981.

Ronaldson-Bouchard K, Ma SP, Yeager K, Chen T, Song L, Sirabella D, Morikawa K, Teles D, Yazawa M and Gordana Vunjak-Novakovic & (2018). Advanced maturation of human cardiac tissue grown from pluripotent stem cells. *Nature* **556**:239–243.

Rook MB, Evers MM, Vos MA and Bierhuizen MFA (2012). Biology of cardiac sodium channel Na v 1.5 expression. *Cardiovascular Research* **93**:12–23.

Rosenbaum DM, Rasmussen SGF and Kobilka BK (2009). The structure and function of G-protein-coupled receptors. *Nature* **459**:356–363.

Ross EM (2014). G Protein-coupled receptors: Multi-turnover GDP/GTP exchange catalysis on heterotrimeric G proteins. *Cellular Logistics* **4**(2):29391.

Roy A, Fields WC, Rocha-Resende C, Resende RR, Guatimosim S, Prado VF, Gros R and Prado MAM (2013). Cardiomyocyte-secreted acetylcholine is required for maintenance of homeostasis in the heart. *The FASEB Journal* **27**(12):5072.

Ruan J-L, Tulloch NL, Razumova M V., Saiget M, Muskheli V, Pabon L, Reinecke H, Regnier M and Murry CE (2016). Mechanical Stress Conditioning and Electrical Stimulation Promote Contractility and Force Maturation of Induced Pluripotent Stem Cell-Derived Human Cardiac Tissue. *Circulation* **134**(20):1557–1567.

Ruan J-L, Tulloch NL, Saiget M, Paige SL, Razumova M V, Regnier M, Tung KC, Keller G, Pabon L, Reinecke H and Murry CE (2015). Mechanical Stress Promotes Maturation of Human Myocardium From Pluripotent Stem Cell-Derived Progenitors. *Stem Cells* **33**(7):2148–57.

Ryan SD, Dolatabadi N, Chan SF, Zhang X, Akhtar MW, Parker J, Soldner F, Sunico CR, Nagar S, Talantova M, Lee B, Lopez K, Nutter A, Shan B, Molokanova E, Zhang Y, Han X, Nakamura T, Masliah E, Yates JR, Nakanishi N, Andreyev AY, Okamoto SI, Jaenisch R, Ambasudhan R and Lipton SA (2013). Isogenic Human iPSC Parkinson's Model Shows Nitrosative Stress-Induced Dysfunction in MEF2-PGC1α Transcription. *Cell* **155**(6):1351.

Sadelain M, Papapetrou EP and Bushman FD (2012). Safe harbours for the integration of new DNA in the human genome. *Nature Reviews Cancer* **12**(1):51–58.

Salcedo A, Garijo J, Monge L, Fernández N, Luis García-Villalón A, Sánchez Turrión V, Cuervas-Mons V and Diéguez G (2007). Apelin effects in human splanchnic arteries. Role of nitric oxide and prostanoids. *Regulatory Peptides* **144**(1–3):50–5.

Salvage SC, Huang CL-H and Jackson AP (2020). Cell-Adhesion Properties of β-Subunits in the Regulation of Cardiomyocyte Sodium Channels. *Biomolecules* **10**(7):1–22.

Saraf A, Rampoldi A, Chao M, Li D, Armand L, Hwang H, Liu R, Jha R, Fu H, Maxwell JT and Xu C (2021). Functional and molecular effects of TNF-α on human iPSC-derived cardiomyocytes. *Stem Cell Research* **52**:102218.

Sato T, Sato C, Kadowaki A, Watanabe H, Ho L, Ishida J, Yamaguchi T, Kimura A, Fukamizu A, Penninger JM, Reversade B, Ito H, Imai Y and Kuba K (2017). ELABELA-APJ axis protects from pressure overload heart failure and angiotensin II-induced cardiac damage. *Cardiovascular Research* **113**(7):760–769.

Schmittgen TD and Livak KJ (2008). Analyzing real-time PCR data by the comparative CT method. *Nature Protocols* **3**(6):1101–1108.

Schroeder A, Mueller O, Stocker S, Salowsky R, Leiber M, Gassmann M, Lightfoot S, Menzel W, Granzow M and Ragg T (2006). The RIN: An RNA integrity number for assigning integrity values to RNA measurements. *BMC Molecular Biology* **7**(1):1–14.

Scimia MC, Hurtado C, Ray S, Metzler S, Wei K, Wang J, Woods CE, Purcell NH, Catalucci D, Akasaka T, Bueno OF, Vlasuk GP, Kaliman P, Bodmer R, Smith LH, Ashley E, Mercola M, Brown JH and Ruiz-Lozano P (2012). APJ acts as a dual receptor in cardiac hypertrophy. *Nature* **488**:394–398.

Scott IC, Masri B, D'Amico LA, Jin S-W, Jungblut B, Wehman AM, Baier H, Audigier Y and Stainier DYR (2007). The G Protein-Coupled Receptor Agtrl1b Regulates Early Development of Myocardial Progenitors. *Developmental Cell* **12**(3):403–413.

Segers VFM and De Keulenaer GW (2021). Autocrine signaling in cardiac remodeling: A rich source of therapeutic targets. *Journal of the American Heart Association* **10**(3):1–28.

Seo K, Parikh VN and Ashley EA (2020). Stretch-Induced Biased Signaling in Angiotensin II Type 1 and Apelin Receptors for the Mediation of Cardiac Contractility and Hypertrophy. *Frontiers in Physiology* **11**:181.

Sharma A, Burridge PW, McKeithan WL, Serrano R, Shukla P, Sayed N, Churko JM, Kitani T, Wu H, Holmström A, Matsa E, Zhang Y, Kumar A, Fan AC, Del Álamo JC, Wu SM, Moslehi JJ, Mercola M and Wu JC (2017). High-Throughput Screening of Tyrosine Kinase Inhibitor Cardiotoxicity with Human Induced Pluripotent Stem Cells. *Science Translational Medicine* **9**(377):2584.

Shen B, Zhang W, Zhang J, Zhou J, Wang J, Chen L, Wang L, Hodgkins A, Iyer V, Huang X and Skarnes WC (2014). Efficient genome modification by CRISPR-Cas9 nickase with minimal off-target effects. *Nature Methods* **11**(4):399–402.

Sheng P, Flood KA and Xie M (2020). Short Hairpin RNAs for Strand-Specific Small Interfering RNA Production. *Frontiers in Bioengineering and Biotechnology* **8**:940.

Siddiquee K, Hampton J, Khan S, Zadory D, Gleaves L, Vaughan DE and Smith LH (2011). Apelin Protects Against Angiotensin II-Induced Cardiovascular Fibrosis and Decreases PAI-1 Production. *Journal of Hypertension* **29**(4):724–731.

Siddiquee K, Hampton J, McAnally D, May LT and Smith LH (2013). The apelin receptor inhibits the angiotensin II type 1 receptor via allosteric trans-inhibition. *British Journal of Pharmacology* **168**(5):1104–1117.

Silverman M, Zeidifard E, Paterson JW and Godfrey S (1973). The effect of isoprenaline on the cardiac and respiratory responses to exercise. *Quarterly Journal of Experimental Physiology and Cognate Medical Sciences* **58**(1):7–17.

Singh VK, Saini A, Kalsan M, Kumar N and Chandra R (2016). Describing the stem cell potency: The various methods of functional assessment and in silico diagnostics. *Frontiers in Cell and Developmental Biology* **4**:134.

Sirenko O, Hesley J, Rusyn I and Cromwell EF (2014). High-content assays for hepatotoxicity using induced pluripotent stem cell-derived cells. *Assay and Drug Development Technologies* **12**(1):43–54.

Smith JR, Maguire S, Davis LA, Alexander M, Yang F, Chandran S, ffrench-Constant C and Pedersen RA (2008). Robust, Persistent Transgene Expression in Human Embryonic Stem Cells Is Achieved with AAVS1-Targeted Integration. *Stem Cells* **26**(2):496–504.

Sparrow AJ, Sievert K, Patel S, Chang Y-F, Broyles CN, Brook FA, Watkins H, Geeves MA, Redwood CS, Robinson P and Daniels MJ (2019). Measurement of Myofilament-Localised Calcium Dynamics in Adult Cardiomyocytes and the Effect of Hypertrophic Cardiomyopathy Mutations. *Circulation Research* **124**(8):1228–1239.

Splinter K, Adams DR, Bacino CA, Bellen HJ, Bernstein JA, Cheatle-Jarvela AM, Eng

CM, Esteves C, Gahl WA, Hamid R, Jacob HJ, Kikani B, Koeller DM, Kohane IS, Lee BH, Loscalzo J, Luo X, McCray AT, Metz TO, Mulvihill JJ, Nelson SF, Palmer CGS, Phillips JA, Pick L, Postlethwait JH, Reuter C, Shashi V, Sweetser DA, Tifft CJ, Walley NM, Wangler MF, Westerfield M, Wheeler MT, Wise AL, Worthey EA, Yamamoto S and Ashley EA (2018). Effect of Genetic Diagnosis on Patients with Previously Undiagnosed Disease. *New England Journal of Medicine* **379**(22):2131–2139.

Sterneckert JL, Reinhardt P and Schöler HR (2014). Investigating human disease using stem cell models. *Nature Reviews Genetics* **15**(9):625–639.

Stillitano F, Turnbull IC, Karakikes I, Nonnenmacher M, Backeris P, Hulot J-S, Kranias EG, Hajjar RJ and Costa KD (2016). Genomic correction of familial cardiomyopathy in human engineered cardiac tissues. *European Heart Journal* **37**(43):3282–3284.

Stone NJ, Robinson JG, Lichtenstein AH, Bairey Merz CN, Blum CB, Eckel RH, Goldberg AC, Gordon D, Levy D, Lloyd-Jones DM, McBride P, Schwartz JS, Shero ST, Smith SC, Watson K and Wilson PWF (2014). 2013 ACC/AHA guideline on the treatment of blood cholesterol to reduce atherosclerotic cardiovascular risk in adults: A report of the american college of cardiology/american heart association task force on practice guidelines. *Circulation* **129**(25):S1–S45.

Strohbach A, Pennewitz M, Glaubitz M, Palankar R, Groß S, Lorenz F, Materzok I, Rong A, Busch MC, Felix SB, Delcea M and Busch R (2018). The apelin receptor influences biomechanical and morphological properties of endothelial cells. *Journal of Cellular Physiology* **233**(8):6250–6261.

Szokodi I, Tavi P, Földes G, Voutilainen-Myllylä S, Ilves M, Tokola H, Pikkarainen S, Piuhola J, Rysä J, Tóth M and Ruskoaho H (2002). Apelin, the novel endogenous ligand of the orphan receptor APJ, regulates cardiac contractility. *Circulation Research* **91**(5):434–40.

Takahashi K, Tanabe K, Ohnuki M, Narita M, Ichisaka T, Tomoda K and Yamanaka S (2007). Induction of Pluripotent Stem Cells from Adult Human Fibroblasts by Defined Factors. *Cell* **131**(5):861–872.

Takiguchi M, Dow LE, Prier JE, Carmichael CL, Kile BT, Turner SJ, Lowe SW, Huang DCS and Dickins RA (2013). Variability of Inducible Expression across the

Hematopoietic System of Tetracycline Transactivator Transgenic Mice. *PLoS ONE* **8**(1):e54009.

Tan S, Tao Z, Loo S, Su L, Chen X and Ye L (2019). Non-viral vector based gene transfection with human induced pluripotent stem cells derived cardiomyocytes. *Scientific Reports* **9**:14404.

Tao J, Zhu W, Li Y, Xin P, Li J, Liu M, Li J, Redington AN and Wei M (2011). Apelin-13 protects the heart against ischemia-reperfusion injury through inhibition of ER-dependent apoptotic pathways in a time-dependent fashion. *American Journal of Physiology - Heart and Circulatory Physiology* **301**(4):H1471-1486.

Tatemoto K, Hosoya M, Habata Y, Fujii R, Kakegawa T, Zou M-X, Kawamata Y, Fukusumi S, Hinuma S, Kitada C, Kurokawa T, Onda H and Fujino M (1998). Isolation and Characterization of a Novel Endogenous Peptide Ligand for the Human APJ Receptor. *Biochemical and Biophysical Research Communications* **251**(2):471–476.

Tatemoto K, Takayama K, Zou M-X, Kumaki I, Zhang W, Kumano K and Fujimiya M (2001). The novel peptide apelin lowers blood pressure via a nitric oxide-dependent mechanism. *Regulatory Peptides* **99**:87–92.

Terrillon S and Bouvier M (2004). Roles of G-protein-coupled receptor dimerization: From ontogeny to signalling regulation. *EMBO Reports* **5**(1):30–34.

Thavandiran N, Hale C, Blit P, Sandberg ML, McElvain ME, Gagliardi M, Sun B, Witty A, Graham G, Do VTH, Bakooshli MA, Le H, Ostblom J, McEwen S, Chau E, Prowse A, Fernandes I, Norman A, Gilbert PM, Keller G, Tagari P, Xu H, Radisic M and Zandstra PW (2020). Functional arrays of human pluripotent stem cell-derived cardiac microtissues. *Scientific Reports* **10**:6919.

Thiel C, Cordes H, Fabbri L, Aschmann HE, Baier V, Smit I, Atkinson F, Blank LM and Kuepfer L (2017). A Comparative Analysis of Drug-Induced Hepatotoxicity in Clinically Relevant Situations. *PLoS Computational Biology* **13**(2):e1005280.

Thomson JA, Itskovitz-Eldor J, Shapiro SS, Waknitz MA, Swiergiel JJ, Marshall VS and Jones JM (1998). Embryonic stem cell lines derived from human blastocysts. *Science* **282**(5391):1145–1147.

Tiburcy M, Hudson JE, Balfanz P, Schlick S, Meyer T, Liao M-LC, Levent E, Raad F, Zeidler S, Wingender E, Riegler J, Wang M, Gold JD, Kehat I, Wettwer E, Ravens U, Dierickx P, Laake LW van, Goumans MJ, Khadjeh S, Toischer K, Hasenfuss G, Couture LA, Unger A, Linke WA, Araki T, Neel B, Keller G, Gepstein L, Wu JC and Zimmermann W-H (2017). Defined Engineered Human Myocardium With Advanced Maturation for Applications in Heart Failure Modeling and Repair. *Circulation* **135**(19):1832–1847.

Tohyama S, Hattori F, Sano M, Hishiki T, Nagahata Y, Matsuura T, Hashimoto H, Suzuki T, Yamashita H, Satoh Y, Egashira T, Seki T, Muraoka N, Yamakawa H, Ohgino Y, Tanaka T, Yoichi M, Yuasa S, Murata M, Suematsu M and Fukuda K (2013). Distinct metabolic flow enables large-scale purification of mouse and human pluripotent stem cell-derived cardiomyocytes. *Cell Stem Cell* **12**(1):127–137.

Tse G (2016). Mechanisms of cardiac arrhythmias. *Journal of Arrhythmia* **32**(2):75–81.

Tulloch NL, Muskheli V, Razumova M V., Korte FS, Regnier M, Hauch KD, Pabon L, Reinecke H and Murry CE (2011). Growth of engineered human myocardium with mechanical loading and vascular coculture. *Circulation Research* **109**(1):47–59.

Turnbull C, Scott RH, Thomas E, Jones L, Murugaesu N, Pretty FB, Halai D, Baple E, Craig C, Hamblin A, Henderson S, Patch C, O'Neill A, Devereaux A, Smith K, Martin AR, Sosinsky A, McDonagh EM, Sultana R, Mueller M, Smedley D, Toms A, Dinh L, Fowler T, Bale M, Hubbard T, Rendon A, Hill S and Caulfield MJ (2018). The 100 000 Genomes Project: bringing whole genome sequencing to the NHS. *BMJ* **2018**:361.

Turro E, Astle WJ, Megy K, Gräf S, Greene D, Shamardina O, Allen HL, Sanchis-Juan A, Frontini M, Thys C, Stephens J, Mapeta R, Burren OS, Downes K, Haimel M, Tuna S, Deevi SVV, Aitman TJ, Bennett DL, Calleja P, Carss K, Caulfield MJ, Chinnery PF, Dixon PH, Gale DP, James R, Koziell A, Laffan MA, Levine AP, Maher ER, Markus HS, Morales J, Morrell NW, Mumford AD, Ormondroyd E, Rankin S, Rendon A, Richardson S, Roberts I, Roy NBA, Saleem MA, Smith KGC, Stark H, Tan RYY, Themistocleous AC, Thrasher AJ, Watkins H, Webster AR, Wilkins MR, Williamson C, Whitworth J, Humphray S, Bentley DR, Abbs S, Abulhoul L, Adlard J, Ahmed M, Alachkar H, Allsup DJ, Almeida-King J, Ancliff P, Antrobus R, Armstrong R, Arno G,

Ashford S, Attwood A, Aurora P, Babbs C, Bacchelli C, Bakchoul T, Banka S, Bariana T, Barwell J, Batista J, Baxendale HE, Beales PL, Bentley DR, Bierzynska A, Biss T, Bitner-Glindzicz MAK, Black GC, Bleda M, Blesneac I, Bockenhauer D, Bogaard H, Bourne CJ, Boyce S, Bradley JR, Bragin E, Breen G, Brennan P, Brewer C, Brown M, Browning AC, Browning MJ, Buchan RJ, Buckland MS, Bueser T, Diz CB, Burn J, Burns SO, Burren OS, Burrows N, Campbell C, Carr-White G, Carss K, Casey R, Chambers J, Chambers J, Chan MMY, Cheah C, Cheng F, Chinnery PF, Chitre M, Christian MT, Church C, Clayton-Smith J, Cleary M, Brod NC, Coghlan G, Colby E, Cole TRP, Collins J, Collins PW, Colombo C, Compton CJ, Condliffe R, Cook S, Cook HT, Cooper N, Corris PAA, Furnell A, Cunningham F, Curry NS, Cutler AJ, Daniels MJ, Dattani M, Daugherty LC, Davis J, De Soyza A, Deevi SVV, Dent T, Deshpande C, Dewhurst EF, Dixon PH, Douzgou S, Downes K, Drazyk AM, Drewe E, Duarte D, Dutt T, Edgar JDM, Edwards K, Egner W, Ekani MN, Elliott P, Erber WN, Erwood M, Estiu MC, Evans DG, Evans G, Everington T, Eyries M, Fassihi H, Favier R, Findhammer J, Fletcher D, Flinter FA, Floto RA, Fowler T, Fox J, Frary AJ, French CE, Freson K, Frontini M, Gale DP, Gall H, Ganesan V, Gattens M, Geoghegan C, Gerighty TSA, Gharavi AG, Ghio S, Ghofrani HA, Gibbs JSR, Gibson K, Gilmour KC, Girerd B, Gleadall NS, Goddard S, Goldstein DB, Gomez K, Gordins P, Gosal D, Gräf S, Graham J, Grassi L, Greene D, Greenhalgh L, Greinacher A, Gresele P, Griffiths P, Grigoriadou S, Grocock RJ, Grozeva D, Gurnell M, Hackett S, Hadinnapola C, Hague WM, Hague R, Haimel M, Hall M, Hanson HL, Haque E, Harkness K, Harper AR, Harris CLL, Hart D, Hassan A, Hayman G, Henderson A, Herwadkar A, Hoffman J, Holden S, Horvath R, Houlden H, Houweling ACC, Howard LS, Hu F, Hudson G, Hughes J, Huissoon AP, Humbert M, Humphray S, Hunter S, Hurles M, Irving M, Izatt L, James R, Johnson SA, Jolles S, Jolley J, Josifova D, Jurkute N, Karten T, Karten J, Kasanicki MA, Kazkaz H, Kazmi R, Kelleher P, Kelly AM, Kelsall W, Kempster C, Kiely DG, Kingston N, Klima R, Koelling N, Kostadima M, Kovacs G, Koziell A, Kreuzhuber R, Kuijpers TW, Kumar A, Kumararatne D, Kurian MA, Laffan MA, Lalloo F, Lambert M, Lawrie A, Layton DM, Lench N, Lentaigne C, Lester T, Levine AP, Linger R, Longhurst H, Lorenzo LE, Louka E, Lyons PA, Machado RD, MacKenzie Ross R V., Madan B, Maher ER, Maimaris J, Malka S, Mangles S, Mapeta R, Marchbank KJ, Marks S, Markus HS, Marschall HU, Marshall A, Martin J, Mathias M, Matthews E, Maxwell H, McAlinden P, McCarthy MI, McKinney H, McMahon A, Meacham S, Mead AJ, Castello IM, Megy K, Mehta SGG, Michaelides M, Millar C, Mohammed SN,

Moledina S, Montani D, Moore AT, Morales J, Morrell NW, Mozere M, Muir KW, Mumford AD, Nemeth AH, Newman WG, Newnham M, Noorani S, Nurden P, O'Sullivan J, Obaji S, Odhams C, Okoli S, Olschewski A, Olschewski H, Ong KR, Oram SH, Ormondroyd E, Ouwehand WH, Palles C, Papadia S, Park SM, Parry D, Patel S, Paterson J, Peacock A, Pearce SHH, Peden J, Peerlinck K, Penkett CJ, Pepke-Zaba J, Petersen R, Pilkington C, Poole KES, Prathalingam R, Psaila B, Pyle A, Quinton R, Rahman S, Rankin S, Rao A, Raymond FL, Rayner-Matthews PJ, Rees C, Rendon A, Renton T, Rhodes CJ, Rice ASC, Richardson S, Richter A, Robert L, Roberts I, Rogers A, Rose SJ, Ross-Russell R, Roughley C, Roy NBA, Ruddy DM, Sadeghi-Alavijeh O, Saleem MA, Samani N, Samarghitean C, Sanchis-Juan A, Sargur RB, Sarkany RN, Satchell S, Savic S, Sayer JA, Sayer G, Scelsi L, Schaefer AM, Schulman S, Scott R, Scully M, Searle C, Seeger W, Sen A, Sewell WAC, Seyres D, Shah N, Shamardina O, Shapiro SE, Shaw AC, Short PJ, Sibson K, Side L, Simeoni I, Simpson MAA, Sims MC, Sivapalaratnam S, Smedley D, Smith KR, Smith KGC, Snape K, Soranzo N, Soubrier F, Southgate L, Spasic-Boskovic O, Staines S, Staples E, Stark H, Stephens J, Steward C, Stirrups KE, Stuckey A, Suntharalingam J, Swietlik EM, Syrris P, Tait RC, Talks K, Tan RYY, Tate K, Taylor JM, Taylor JC, Thaventhiran JE, Themistocleous AC, Thomas E, Thomas D, Thomas MJ, Thomas P, Thomson K, Thrasher AJ, Threadgold G, Thys C, Tilly T, Tischkowitz M, Titterton C, Todd JA, Toh CH, Tolhuis B, Tomlinson IP, Toshner M, Traylor M, Treacy C, Treadaway P, Trembath R, Tuna S, Turek W, Turro E, Twiss P, Vale T, Geet C Van, Zuydam N van, Vandekuilen M, Vandersteen AM, Vazquez-Lopez M, von Ziegenweidt J, Noordegraaf AV, Wagner A, Waisfisz Q, Walker SM, Walker N, Walter K, Ware JS, Watkins H, Watt C, Webster AR, Wedderburn L, Wei W, Welch SB, Wessels J, Westbury SK, Westwood JP, Wharton J, Whitehorn D, Whitworth J, Wilkie AOM, Wilkins MR, Williamson C, Wilson BT, Wong EKS, Wood N, Wood Y, Woods CG, Woodward ERR, Wort SJ, Worth A, Wright M, Yates K, Yong PFK, Young T, Yu P, Yu-Wai-Man P, Zlamalova E, Kingston N, Walker N, Penkett CJ, Freson K, Stirrups KE and Raymond FL (2020). Whole-genome sequencing of patients with rare diseases in a national health system. *Nature* **583**:96–102.

Urbach A, Schuldiner M and Benvenisty N (2004). Modeling for Lesch-Nyhan Disease by Gene Targeting in Human Embryonic Stem Cells. *Stem Cells* **22**(4):635–641.

Uzun AU, Mannhardt I, Breckwoldt K, Horváth A, Johannsen SS, Hansen A,

Eschenhagen T and Christ T (2016). Ca2+-Currents in Human Induced Pluripotent Stem Cell-Derived Cardiomyocytes Effects of Two Different Culture Conditions. *Frontiers in Pharmacology* **7**:300.

Vandesompele J, De Preter K, Pattyn F, Poppe B, Van Roy N, De Paepe A and Speleman F (2002). Accurate normalization of real-time quantitative RT-PCR data by geometric averaging of multiple internal control genes. *Genome Biology* **3**(7):1–12.

Veeraraghavan R, Hoeker GS, Alvarez-Laviada A, Hoagland D, Wan X, King DR, Sanchez-Alonso J, Chen C, Jourdan J, Isom LL, Deschenes I, Smyth JW, Gorelik J, Poelzing S and Gourdie RG (2018). The adhesion function of the sodium channel beta subunit (β1) contributes to cardiac action potential propagation. *eLife* **7**.

Vermes I, Haanen C, Steffens-Nakken H and Reutellingsperger C (1995). A novel assay for apoptosis Flow cytometric detection of phosphatidylserine expression on early apoptotic cells using fluorescein labelled Annexin V. *Journal of Immunological Methods* **184**(1):39–51.

Villiger L, Grisch-Chan HM, Lindsay H, Ringnalda F, Pogliano CB, Allegri G, Fingerhut R, Häberle J, Matos J, Robinson MD, Thöny B and Schwank G (2018). Treatment of a metabolic liver disease by in vivo genome base editing in adult mice. *Nature Medicine* **24**(10):1519–1525.

Wang C, Du J-F, Wu F and Wang H-C (2008). Apelin decreases the SR Ca^{2+} content but enhances the amplitude of $[Ca^{2+}]_i$ transient and contractions during twitches in isolated rat cardiac myocytes. *American Journal of Physiology-Heart and Circulatory Physiology* **294**(6):H2540–H2546.

Wang D, Quan Y, Yan Q, Morales JE and Wetsel RA (2015). Targeted Disruption of the β2-Microglobulin Gene Minimizes the Immunogenicity of Human Embryonic Stem Cells. *Stem Cells Translational Medicine* **4**(10):1234.

Wang ES, Reyes NA, Melton C, Huskey NE, Momcilovic O, Goga A, Blelloch R and Oakes SA (2015). Fas-Activated Mitochondrial Apoptosis Culls Stalled Embryonic Stem Cells to Promote Differentiation. *Current Biology* **25**(23):3110–3118.

Wang I-NE, Wang X, Ge X, Anderson J, Ho M, Ashley E, Liu J, Butte MJ, Yazawa M, Dolmetsch RE, Quertermous T and Yang PC (2012). Apelin Enhances Directed

Cardiac Differentiation of Mouse and Human Embryonic Stem Cells. *PLoS ONE* **7**(6):e38328.

Wang M, Gupta RC, Rastogi S, Kohli S, Sabbah MS, Zhang K, Mohyi P, Hogie M, Fischer Y and Sabbah HN (2013). Effects of acute intravenous infusion of apelin on left ventricular function in dogs with advanced heart failure. *Journal of Cardiac Failure* **19**(7):509–16.

Wang Q, Dong X, Lu J, Hu T and Pei G (2020). Constitutive activity of a G protein-coupled receptor, DRD1, contributes to human cerebral organoid formation. *Stem Cells* **38**(5):653.

Wang Q, Yang H, Bai A, Jiang W, Li X, Wang X, Mao Y, Lu C, Qian R, Guo F, Ding T, Chen H, Chen S, Zhang J, Liu C and Sun N (2016). Functional engineered human cardiac patches prepared from nature's platform improve heart function after acute myocardial infarction. *Biomaterials* **105**:52–65.

Wang W, McKinnie SMK, Farhan M, Paul M, McDonald T, McLean B, Llorens-Cortes C, Hazra S, Murray AG, Vederas JC and Oudit GY (2016). Angiotensin-Converting Enzyme 2 Metabolizes and Partially Inactivates Pyr-Apelin-13 and Apelin-17: Physiological Effects in the Cardiovascular System. *Hypertension* **68**(2):365–377.

Wang Z, Yu D, Wang M, Wang Q, Kouznetsova J, Yang R, Qian K, Wu W, Shuldiner A, Sztalryd C, Zou M, Zheng W and Gong D-W (2015). Elabela-Apelin Receptor Signaling Pathway is Functional in Mammalian Systems. *Scientific Reports* **5**(1):8170.

Weinberger F, Mannhardt I and Eschenhagen T (2017). Engineering Cardiac Muscle Tissue: A Maturating Field of Research. *Circulation Research* **120**(9):1487–1500.

Weng Z, Kong CW, Ren L, Karakikes I, Geng L, He J, Chow MZY, Mok CF, Harvey C, Sarah W, Keung W, Chow H, Andrew M, Leung AYH, Hajjar RJ, Li RA and Chan CW (2014). A Simple, Cost-Effective but Highly Efficient System for Deriving Ventricular Cardiomyocytes from Human Pluripotent Stem Cells. *Stem Cells and Development* **23**(14):1704.

Wheatley M and Hawtin SR (1999). Glycosylation of G-protein-coupled receptors for hormones central to normal reproductive functioning: its occurrence and role. *Human Reproduction Update* **5**(4):356–364.

Wijnker PJM, Friedrich FW, Dutsch A, Reischmann S, Eder A, Mannhardt I, Mearini G, Eschenhagen T, van der Velden J and Carrier L (2016). Comparison of the effects of a truncating and a missense MYBPC3 mutation on contractile parameters of engineered heart tissue. *Journal of Molecular and Cellular Cardiology* **97**:82–92.

Williams LA, Davis-Dusenbery BN and Eggan KC (2012). SnapShot: Directed Differentiation of Pluripotent Stem Cells. *Cell* **149**:1174-1174.e1.

Wu M, Liu S, Gao Y, Bai H, Machairaki V, Li G, Chen T and Cheng L (2018). Conditional gene knockout and reconstitution in human iPSCs with an inducible Cas9 system. *Stem Cell Research* **29**:6–14.

Wu Y, Wang X, Zhou X, Cheng B, Li G and Bai B (2017). Temporal Expression of Apelin/Apelin Receptor in Ischemic Stroke and its Therapeutic Potential. *Frontiers in Molecular Neuroscience* **10**:1.

Yamasaki AE, Panopoulos AD and Belmonte JCI (2017). Understanding the genetics behind complex human disease with large-scale iPSC collections. *Genome Biology* **18**(1):1–3.

Yamoah MA, Moshref M, Sharma J, Chen WC, Ledford HA, Lee JH, Chavez KS, Wang W, López JE, Lieu DK, Sirish P and Zhang X-D (2018). Highly efficient transfection of human induced pluripotent stem cells using magnetic nanoparticles. *International Journal of Nanomedicine* **13**:6073–6078.

Yang P, Kuc RE, Brame AL, Dyson A, Singer M, Glen RC, Cheriyan J, Wilkinson IB, Davenport AP and Maguire JJ (2017a). [Pyr1]apelin-13(1-12) is a biologically active ACE2 metabolite of the endogenous cardiovascular peptide [Pyr1]apelin-13. *Frontiers in Neuroscience* **11**:92.

Yang P, Maguire JJ and Davenport AP (2015). Apelin, Elabela/Toddler, and biased agonists as novel therapeutic agents in the cardiovascular system. *Trends in Pharmacological Sciences* **36**(9):560–7.

Yang P, Read C, Kuc RE, Buonincontri G, Southwood M, Torella R, Upton PD, Crosby A, Sawiak SJ, Carpenter TA, Glen RC, Morrell NW, Maguire JJ and Davenport AP (2017b). Elabela/toddler is an endogenous agonist of the apelin APJ receptor in the adult cardiovascular system, and exogenous administration of the peptide

compensates for the downregulation of its expression in pulmonary arterial hypertension. *Circulation* **135**(12):1160–1173.

Yang P, Read C, Kuc RE, Nyimanu D, Williams TL, Crosby A, Buonincontri G, Southwood M, Sawiak SJ, Morrell NW, Davenport AP and Maguire JJ (2019). A novel cyclic biased agonist of the apelin receptor, MM07, is disease modifying in the rat monocrotaline model of pulmonary arterial hypertension. *British Journal of Pharmacology* **176**(9):1206–1221.

Yang Y, Liu Y, Dong Z, Xu J, Peng H, Liu Z and Zhang J-T (2007). Regulation of Function by Dimerization through the Amino-terminal Membrane-spanning Domain of Human ABCC1/MRP1. *The Journal of Biological Chemistry* **282**(12):8821–8830.

Ye L, Chang Y-H, Xiong Q, Zhang P, Zhang L, Somasundaram P, Lepley M, Swingen C, Su L, Wendel JS, Guo J, Jang A, Rosenbush D, Greder L, Dutton JR, Zhang J, Kamp TJ, Kaufman DS, Ge Y and Zhang J (2014). Cardiac Repair in a Porcine Model of Acute Myocardial Infarction with Human Induced Pluripotent Stem Cell-Derived Cardiovascular Cells. *Cell Stem Cell* **15**(6):750–761.

Yokoo N, Baba S, Kaichi S, Niwa A, Mima T, Doi H, Yamanaka S, Nakahata T and Heike T (2009). The effects of cardioactive drugs on cardiomyocytes derived from human induced pluripotent stem cells. *Biochemical and Biophysical Research Communications* **387**(3):482–488.

Yu QC, Hirst CE, Costa M, Ng ES, Schiesser J V, Gertow K, Stanley EG and Elefanty AG (2012). Apelin promotes hematopoiesis from human embryonic stem cells. *Blood* **119**(26):6243–54.

Zakrzewski W, Dobrzyński M, Szymonowicz M and Rybak Z (2019). Stem cells: Past, present, and future. *Stem Cell Research and Therapy* **10**(1):68.

Zeng XXI, Wilm TP, Sepich DS and Solnica-Krezel L (2007). Apelin and Its Receptor Control Heart Field Formation during Zebrafish Gastrulation. *Developmental Cell* **12**(3):391–402.

Zeng Y, Li J, Li G, Huang S, Yu W, Zhang Y, Chen D, Chen J, Liu J and Huang X (2018). Correction of the Marfan Syndrome Pathogenic FBN1 Mutation by Base Editing in Human Cells and Heterozygous Embryos. *Molecular Therapy* **26**(11):2631–

2637.

Zhang J, Wilson GF, Soerens AG, Koonce CH, Yu J, Palecek SP, Thomson JA and Kamp TJ (2009). Functional cardiomyocytes derived from human induced pluripotent stem cells. *Circulation Research* **104**(4):e30-41.

Zhang Q, Jiang J, Han P, Yuan Q, Zhang J, Zhang X, Xu Y, Cao H, Meng Q, Chen L, Tian T, Wang X, Li P, Hescheler J, Ji G and Ma Y (2011). Direct differentiation of atrial and ventricular myocytes from human embryonic stem cells by alternating retinoid signals. *Cell Research* **21**(4):579–587.

Zhang X, Hu W, Feng F, Xu J and Wu F (2016). Apelin-13 protects against myocardial infarction-induced myocardial fibrosis. *Molecular Medicine Reports* **13**(6):5262–5268.

Zhao Q, Wang X, Wang S, Song Z, Wang J and Ma J (2017). Cardiotoxicity evaluation using human embryonic stem cells and induced pluripotent stem cell-derived cardiomyocytes. *Stem Cell Research and Therapy* **8**(1):54.

Zhao S, Fung-Leung W-P, Bittner A, Ngo K and Liu X (2014). Comparison of RNA-Seq and Microarray in Transcriptome Profiling of Activated T Cells. *PLoS ONE* **9**(1):e78644.

Zhao Y, Rafatian N, Feric NT, Broeckel U, Backx PH and Radisic M (2019). A Platform for Generation of Chamber-Specific Cardiac Tissues and Disease Modeling. *Cell* **176**:913-927.e18.

Zhen EY, Higgs RE and Gutierrez JA (2013). Pyroglutamyl apelin-13 identified as the major apelin isoform in human plasma. *Analytical Biochemistry* **442**(1):1–9.

Zhong JC, Zhang ZZ, Wang W, McKinnie SMK, Vederas JC and Oudit GY (2017). Targeting the apelin pathway as a novel therapeutic approach for cardiovascular diseases. *Biochimica et Biophysica Acta (BBA) - Molecular Basis of Disease* **1863**(8):1942–1950.

Zhu Z and Huangfu D (2013). Human pluripotent stem cells: An emerging model in developmental biology. *Development* **140**(4):705–717.

Zwi L, Caspi O, Arbel G, Huber I, Gepstein A, Park I-H and Gepstein L (2009).

Cardiomyocyte Differentiation of Human Induced Pluripotent Stem Cells. *Circulation* **120**(15):1513–1523.

Appendix I. Preliminary Work Characterising the Effects of R168H Apelin Receptor Genetic Variant

The work in this section is unpublished and was performed by T.L. Williams and R.E. Kuc (both University of Cambridge) and relates to the results displayed in Section 7. From the NIHR BioResource Bridge Project, ~50 apelin receptor genetic variants were identified. The Davenport group selected 11 variants of interest based on predetermined selection criteria (as described in Section 7) to perform preliminary characterisation in transiently transfected CHO cells. From this initial work, variant 9 was identified as particularly interesting (indicated with red arrow or circle throughout this section), as it completely abolished both radiolabelled and fluorescent ligand binding. It was also found to drastically reduce G-protein signalling in response to [Pyr^{1}]apelin-13. However, it did not affect receptor membrane expression. This variant was decoded as R168H, meaning an arginine residue at position 168 is substituted for a histidine. This site has previously been predicted to be important for ligand binding and G-protein signalling (Read *et al.*, 2016).

First, saturation radioligand binding was performed to determine effects on receptor affinity and density, while dynamic mass redistribution was performed to give an indication of effect on G-protein dependent functional activity (Figure A.1).

B.

	Code	K_D (nM)	B_{max} (fmol/mg protein)	Hill slope (*nH*)
	U	ND	ND	ND
WT	1	2.14 ± 0.36	813 ± 133	1.03 ± 0.04
Apelin receptor mutation	2	2.35 ± 0.85	175 ± 91*	1.03 ± 0.02
	3	ND	ND	ND
	4	1.64 ± 0.56	445 ± 106	1.06 ± 0.05
	5	5.33 ± 3.20	1630 ± 325	1.08 ± 0.07
	6	5.63 ± 4.00	4920 ± 3520	1.15 ± 0.07
	7	1.61 ± 0.35	562 ± 250	0.99 ± 0.06
	8	1.37 ± 0.76	64.3 ± 19.4**	0.95 ± 0.03
	9	ND	ND	ND
	10	ND	ND	ND
	11	3.57 ± 1.93	1340 ± 775	1.04 ± 0.04
	12	3.48 ± 1.81	1370 ± 351	1.02 ± 0.03

WT = wild-type receptor; U = untransfected; ND = no binding determined

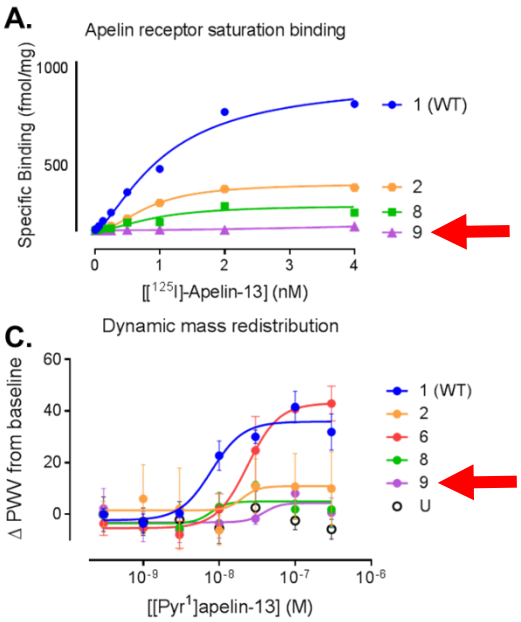

Figure A.1: Effect of identified apelin receptor variants on (A) saturation specific binding of [^{125}I]apelin-13 and (B) calculated affinity (K_D), receptor density (B_{max}) and Hill slope. (C) Effect of apelin receptor variants on dynamic mass redistribution, indicative of effects on G-protein interaction and signalling. Data represent mean±sem. Data for R168H highlighted with red arrows/circle.

Next, effect of the apelin receptor variants on subcellular distribution was investigated, by transfecting either WT or variant eGFP tagged apelin receptor into CHO cells, and visualising membrane expression by co-staining with a membrane marker and nuclei stain (Figure A.2). The Opera Phenix High Content Screening system was used in combination with Harmony image analysis software to quantify eGFP membrane intensity.

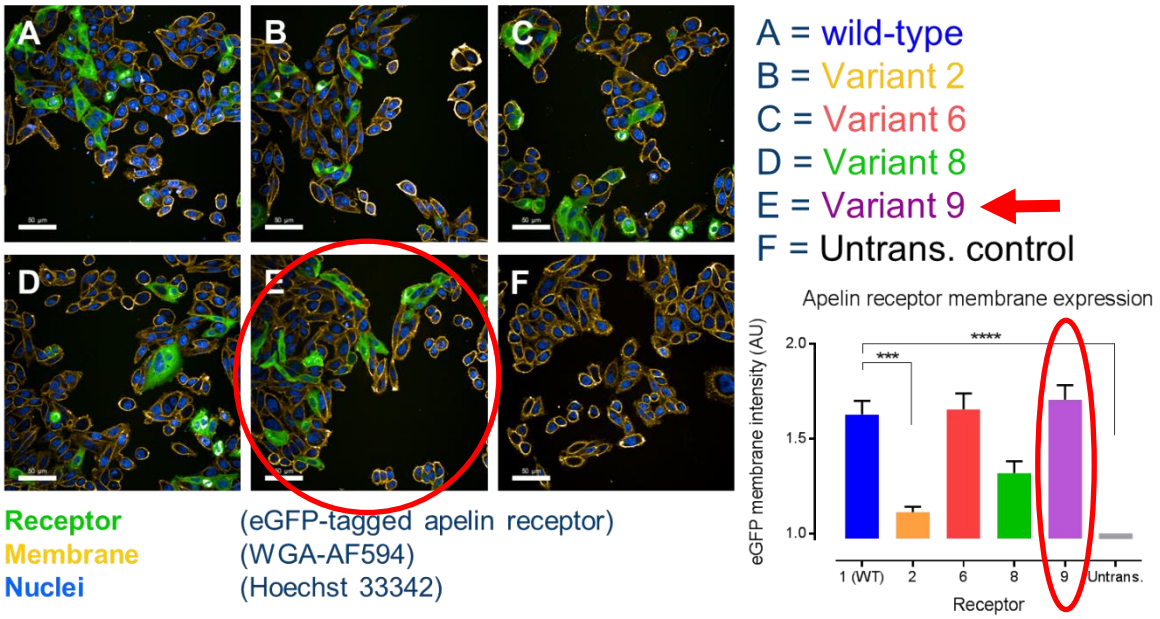

Figure A.2: Effect of identified apelin receptor variants on receptor subcellular distribution, with representative images from Opera Phenix High Content Screening system and associated quantification of eGFP membrane intensity. Scale bar = 50 µm. Data represent mean±sem, compared by one way ANOVA with Dunnet's post hoc test. ***p<0.001, ****p<0.0001. Data for R168H highlighted with red arrows/circles.

Finally, the effect of the apelin receptor variants on binding of fluorescently tagged apelin647 was determined by incubating CHO cells transfected with either WT or variant eGFP tagged apelin receptor with saturating concentrations of fluorescent apelin647. Visualisation was again performed using the Opera Phenix High Content Screening system and mean 647 fluorescence quantified in the whole cell and at the membrane (Figure A.3).

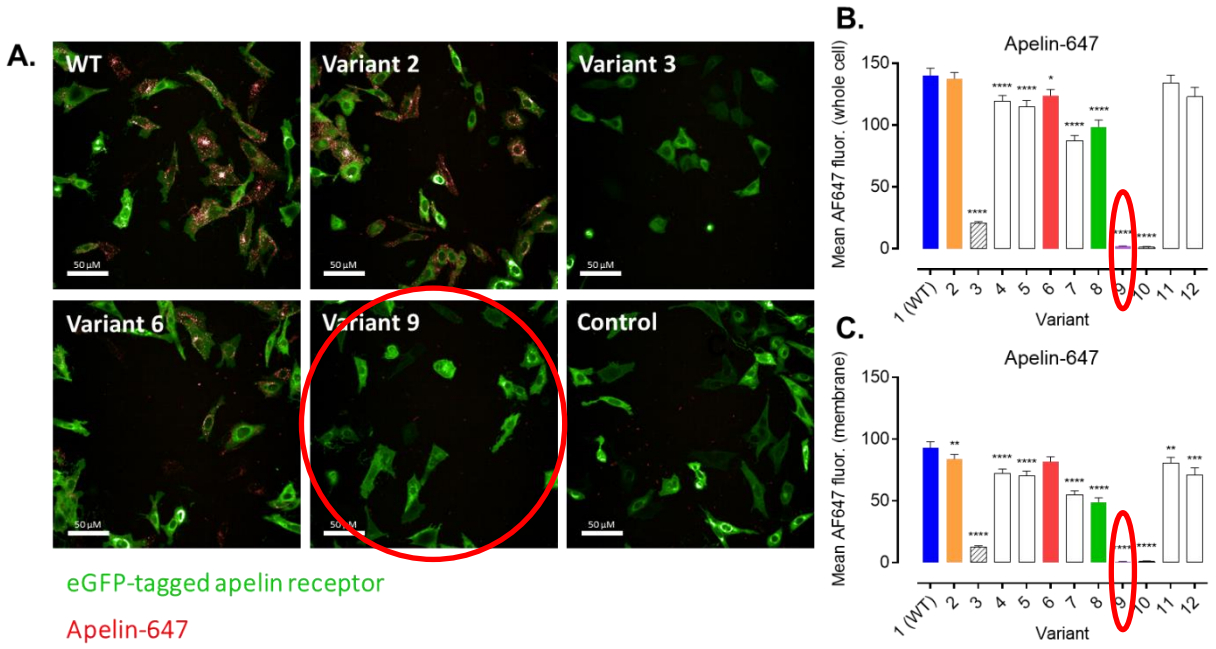

Figure A.3: Effect of identified apelin receptor variants on apelin647 binding, with (A) representative images from Opera Phenix High Content Screening system (scale bar = 50 µm) and associated quantification of mean 647 fluorescence in (B) the whole cell and (C) at the membrane. Data represent mean±sem, compared by one way ANOVA with Dunnet's post hoc test. *p<0.05, **p<0.01, ***p<0.001, ****p<0.0001. Data for R168H highlighted with red circles.